The University of Nottingham

UNITED KINGDOM · CHINA · MALAYSIA

Managing engine thermal state to reduce friction losses during warm-up

Jean-Paul Zammit

Thesis submitted to The University of Nottingham
for the degree of Doctor of Philosophy

September 2012

Contents

Abstract

The thermal behaviour of a 2.4 l direct injection diesel engine has been investigated to identify how the fuel consumption penalty associated with operation during warm–up can be minimised. A version of PROMETS (Programme for Modelling Engine Thermal Systems) was developed to support the investigations. The developments improved the representation of thermal-friction conditions in the oil circuit, extended the piston heat transfer sub-model to account for the effects of piston cooling jets and introduced a main bearing thermal-friction model to predict friction and oil film temperatures. Computational studies were complemented by an experimental investigation of the effectiveness of pre-heating the oil feed to the bearings. Results show that heat transfer from the oil film to the bearings shells and crankshaft journal reduces the benefit in friction savings. Other measures considered were exhaust gas heat recovery, repositioning of the oil main gallery within the block, thermal energy storage, reductions in engine thermal capacity and a novel split-EGR cooler able to cool the EGR gases and heat either the coolant or oil streams. All of the above measures were investigated in isolation, but where appropriate different measures were adopted in conjunction to achieve even greater fuel savings.

During warm-up the energy available to raise fluid temperatures is small. As a result, over the New European Drive Cycle, thermal energy storage showed the greatest benefits. Given an available source of thermal energy which can be transferred to the oil over a chosen time, simulations indicate that a higher power input over a shorter period is most beneficial. This reflects the increased sensitivity of oil viscosity to temperature changes at colder temperatures which in turn means that the potential to reduce friction is highest in the first minutes after engine start up but drops rapidly hereafter. Results also show how the balance of energy transfers out of the oil changes as the engine warms up and point to the importance of oil interaction with components in the lower parts of the engine which have a large thermal capacity, such as elements supporting the main bearings, the crankshaft and the lower liner which limit the rate of temperature rise of the oil. A combination of supplementary heat introduction into the oil circuit from a thermal store and an elimination of heat losses from the oil to the lower parts of the engine resulted in a fuel consumption

saving close to that achieved by starting the engine fully warm, which equates to around 6% improvement.

Acknowledgements

I am of course deeply indebted to Professor Paul Shayler and Dr Antonino La Rocca, for their help and guidance throughout the duration of my research and writing of this thesis.

I would also like to thank the technical staff of Nottingham University Engine Research Group, Geoff Fryer, John Clark, Paul Haywood, John McGhee, Paul Johns and Dave Smith and my fellow research colleagues, in particular Ben 'Greg' Waters, Richard Gardiner, Theo Law and Mike McGhee.

This research was supported by Ford Motor Company, and I would particularly like to thank Ian Pegg, Rob Helle Lorentzen, Roland Stark and Andy Scarisbrick for their assistance. Thanks are also due to Dr Chris Brace and Dr Richard Burke from Bath University for their assistance during the TSB program.

Most of all I'd like to thank my fiancé Luisa and all my family for their love and support.

Nomenclature

A	Area	(m^2)
B	Bore	(m)
Bi	Biot Number	(-)
C_{cb}	Constant for main bearing term	(-)
C_{cs}	Constant for crankshaft oil seal term	(-)
C_{ps}	Constant for piston skirt term	(-)
C_{pr}	Constant for piston ring term	(-)
C_{pb}	Constant for big-end bearing term	(-)
C_{vb}	Constant for camshaft bearing term	(-)
C_{vs}	Constant for camshaft oil seal term	(-)
$C_{v,ff}$	Constant for cam/ flat follower term	(-)
$C_{v,rf}$	Constant for cam/ roller follower term	(-)
$C_{v,oh}$	Constant for oscillating hydrodynamic term	(-)
$C_{v,om}$	Constant for oscillating mixed term	(-)
C_p	Specific Heat Capacity	(J/kg K)
C_v	Specific Heat Capacity	(J/kg K)
C1, C2	Equation Constants	
D	Diameter	(m)
D_b	Bearing Diameter	(m)
k	Thermal Conductivity	(W/ m K)
h	Heat Transfer Coefficient	(W/ m^2K)
Δh	Latent Heat of Vaporisation	(J)
ρ	Density	(kg/ m^3)

μ	Dynamic Viscosity	(kg/ m s)
υ	Kinematic Viscosity	(m^2/ s)
$\dot{m}$	Mass Flow Rate	(kg/ s)
N	Engine Speed	(rev/ min)
n_b	Number of bearings	(-)
n_c	Number of cylinders	(-)
n_v	Number of valves	(-)
η	Efficiency	(-)
S	Stroke	(m)
ΔS	Degree of Superheat	(°C)
t	Time	(s)
Δt	Time Step	(s)
V_s	Swept Volume	(m^3)
V	Velocity	(m/ s)
V_p	Mean piston speed	(m/ s)
$\dot{\mathbf{Q}}$	Heat Transfer	(W)
R_{th}	Thermal Resistance	(K/ W)

Subscripts

amb	Ambient
comb	Combustion
conv	Convective
cool	Coolant
cyl	Of the Cylinder
eff	Effective

ex	Exhaust
f	Fuel
fric	Friction
fw	Fully-warm
g	Gas Value
g,a	Effective Average Gas Value
gr	Gross
h	Hydrodynamic
i	Of Element i
in	Property of the Variable When Entering Heat Exchanger
ind	Indicated
man	Manifold
max	Maximum Value
min	Minimum Value
nucl, boiling	Nucleate Boiling
oc	Oil Cooler
oil	Oil
out	Property of the Variable When Exiting Heat Exchanger
p	Pressure
pt	Of the Exhaust Port
r	Radial
rings	Of the Rings
s	Of the Surface

Dimensionless Groups

Re	Reynolds Number	$\mathbf{Re} = \frac{\rho \mathbf{VD}}{\mu}$
Pr	Prandtl Number	$\mathbf{Pr} = \frac{\mathbf{c}_p \mu}{\mathbf{k}}$
Nu	Nusselt Number	$\mathbf{Nu} = \frac{\mathbf{hD}}{\mathbf{k}}$
Bi	Biot Number	$\mathbf{Bi} = \frac{\mathbf{hV}}{\mathbf{kA}}$

Abbreviations

1-D	One Dimensional
3-D	Three Dimensional
ACEA	European Automobile Manufacturers Association
AFR	Air Fuel Ratio
BDC	Bottom Dead Centre
BMEP	Brake Mean Effective Pressure
BSFC	Brake Specific Fuel Consumption
DI	Direct Injection
DOC	Diesel Oxidation Catalyst
DPF	Diesel Particulate Filter
ECE	Economic Commission of Europe
EGR	Exhaust Gas Recirculation
FCA	Filter Cooler Assembly
FE	Finite Element
FMEP	Friction Mean Effective Pressure

FTP	Federal Test Procedure
HC	Hydrocarbons
HTC	Heat Transfer Coefficient
IMEP	Indicated Mean Effective Pressure
JAMA	Japan Automobile Manufacturers Association
KAMA	Korean Automobile Manufacturers Association
LHV	Lower Heating Value
MAF	Mass Air Flow
Mpg	Miles per gallon
NTU	Number of Transfer Units
NEDC	New European Driving Cycle
NVH	Noise Vibration Harshness
OFT	Oil Film Thickness
PCJ	Piston Cooling Jet
PNH	Patton Nitschke Heywood
PRT	Pressure Regulating Thermostat
SAE	Society of Automotive Engineers
SHC	Specific Heat Capacity
TDC	Top Dead Centre
THD	Thermo hydrodynamic
WOT	Wide Open Throttle

Chapter 1 - Introduction

The direction of this research has been set up by the desire to reduce the cold start fuel consumption penalty of a modern 2.4l direct injection (DI) diesel engine through improved engine thermal management. An engine thermal model has been used in conjunction with experimental studies to investigate the main heat flow mechanisms between the oil, coolant and engine structure. Specifically, the aim has been to understand if and how these can be manipulated to shorten the oil warm-up period and hence reduce frictional losses over the New European Drive Cycle (NEDC) [1].

The thermal and mechanical conversion efficiencies of an internal combustion engine mean that typically for a modern day diesel engine operating at rated power, only 34-38% [2] of the energy released from fuel combustion is converted into 'useful' brake power output. The mechanical efficiency is a function of the engine's friction losses which in turn are strongly dependent on the lubricant temperature [3]. Shayler et al. [4] examined engine friction during warm-up and observed that after the early seconds of engine operation, the variation followed a simple power law dependence on oil viscosity evaluated at oil temperature in the main gallery or sump. Farrant et al. [5] used a similar viscosity-based correction to predict the instantaneous fuel consumption during warm-up, further suggesting that increased fuel consumption on engine start up can be mainly attributed to increased oil viscosity at low temperatures.

Over the NEDC, frictional losses account for between 25 to 30% of the total fuel consumption of a diesel engine but significantly less if the engine is fully-warm at the start of the cycle [6] [7]. Andre [8] recorded the use of 58 vehicles in three European countries over a period of 1580 days. The study revealed that 20-22% of the trips recorded were less than 1 km in length, while approximately 50% of trips were less than 3 km long. Approximately 30% of the trips were completed before engine coolant temperature reached 80 ºC and on 42% of the trips completed, engine oil temperature was below 60 ºC. This suggests that in Europe the mean travel length is relatively short with engines spending considerable time in a transient thermal state (i.e. not fully warm). Shortening the engine warm-up phase can hence offer

significant fuel consumption benefits, with proportionate reductions in CO_2 emissions.

This chapter provides a background into the motivation for this research while introducing some of the key areas of interest. The first part, in particular, covers the legislation imposed by the European Union (EU) on car makers to reduce vehicle fuel consumption and the feasibility of achieving these goals. A brief review of some of the latest engine technology being developed to improve power-train efficiency is included. The aim of this is to compare the fuel consumption benefit offered by improved engine thermal management to that achievable from other technologies. The majority of this research is carried out using an in-house developed CAE tool called PROMETS (Program for Modelling Engine Thermal Systems) [9]. A brief overview of the model is therefore given in this chapter, with a more detailed explanation of the theory of PROMETS provided in Chapter 3. An introduction to some of the fundamentals of engine heat transfer is also presented and finally the thesis layout is explained.

Part of the work presented in this thesis was undertaken in connection with the Low Carbon Vehicle (LCV) research programme led by the Technology Strategy Board (TSB). Participant members were Ford Motor Company, Bath University, Imperial College London, BP Lubricants and Mahle. The project was focussed on reducing engine parasitic losses, with investigations ranging from tribological modification of friction surfaces to do the re-design of the engine's auxiliary drive. The simulation work carried out at Nottingham University and reported in this thesis was complemented by experimental investigations performed at Bath University [10]. The experimental measurements provided both validation data and also various model inputs; this source of data is acknowledged in references in the thesis as appropriate. The main findings reported in Chapter 7 have been published and presented at the VTMS 10 conference [11] while the model developments and investigations of Chapters 5 and 6 were published and presented at the SAE World Congress 2012 [12].

1.1. Background: CO_2 emissions and the automotive industry

1.1.1. Legislation

The ACEA's (European Automobile Manufacturer's Association) continuous effort to improve vehicle fuel economy is partly driven by the EU's commitment at the Kyoto Protocol of the United Nations Convention on Climate Change to reduce its greenhouse gas emissions [13]. Road transport represents the second biggest source of EU carbon dioxide (CO_2) emissions, with passenger cars and vans in particular accounting for 12% of the total emissions [14]. A vehicle's CO_2 emissions are directly related to its fuel consumption. Approximately every kg of diesel fuel combusted releases just over 3kg of CO_2.

The original target set by the EU in 1995 was to reduce average new car CO_2 emissions to 120 g/km by 2005 [15]. However, this target has been postponed numerous times. In 1998 the ACEA agreed to 140 g/km by 2008, equivalent to an average fuel consumption of 6 l/100km for gasoline cars and 5.3l/100km for diesel cars. Figure 1 illustrates the trend in CO_2 emissions reduction over the last decade together with the originally proposed targets. This reduction has been mainly due to a greater penetration of diesel engines into the market [16] [17]. In 2007, a legally-binding target of 120 g/km was set for 2012, with the requirement to achieve 130g/ km through technical development and the remainder through use of lower carbon or carbon-neutral fuels. In effect, each manufacturer has an individual annual target which is based on the average mass of all its new cars registered in the EU, according to what is referred to as the limit-value curve, Figure 2. As it is the fleet average that is regulated, manufacturers are still able to produce vehicles with emissions above their indicative targets as long as these are offset by other vehicles below the target. The limit-value curve ensures that a fleet average of 130 g of CO_2 per km is achieved for the EU as a whole and is also set in such a way that emissions reductions from heavier cars must still be greater than those from lighter cars. As of 2012, 65% of the new cars registered in the EU each year must comply with the average emissions target of the respective manufacturer. The percentage rises to 75% in 2013, 80% in 2014 and 100% in 2015. Vehicle manufacturers will have to pay an excess emissions premium for each car registered of €5 for the first g/km over their target, €15 for the second g/km, €25 for the third g/km, and €95 for each subsequent g/km [14].

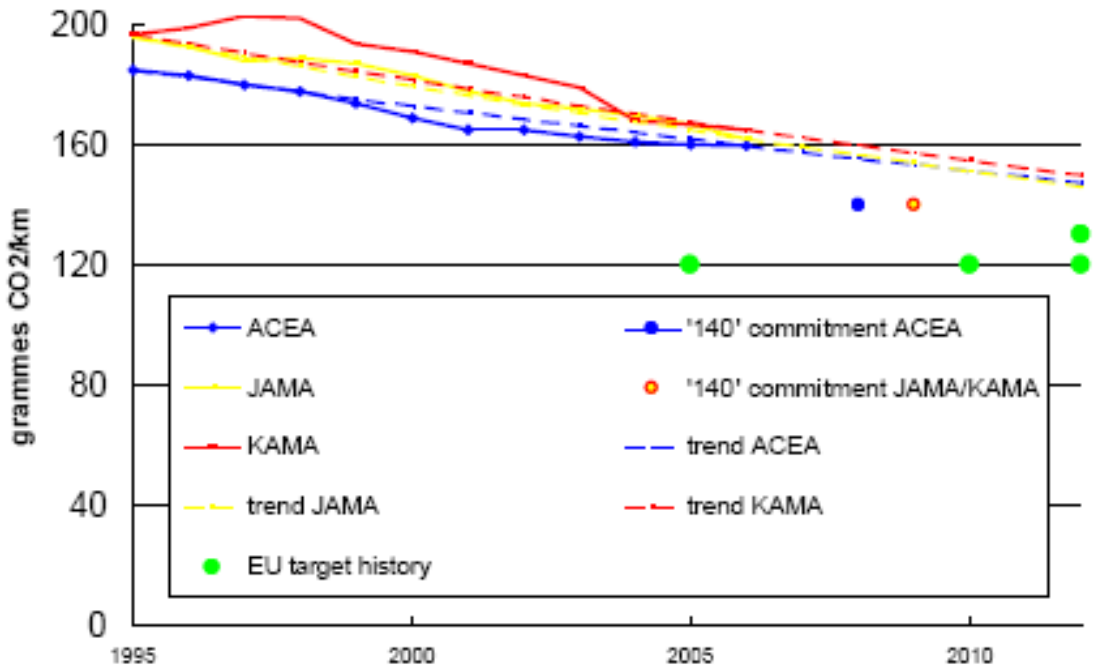

Figure 1 CO_2 emissions trend and industry commitments between 1995 and 2011. JAMA – Japanese Automobile Manufacturers Association, KAMA – Korean Automobile Manufacturers Association [15]

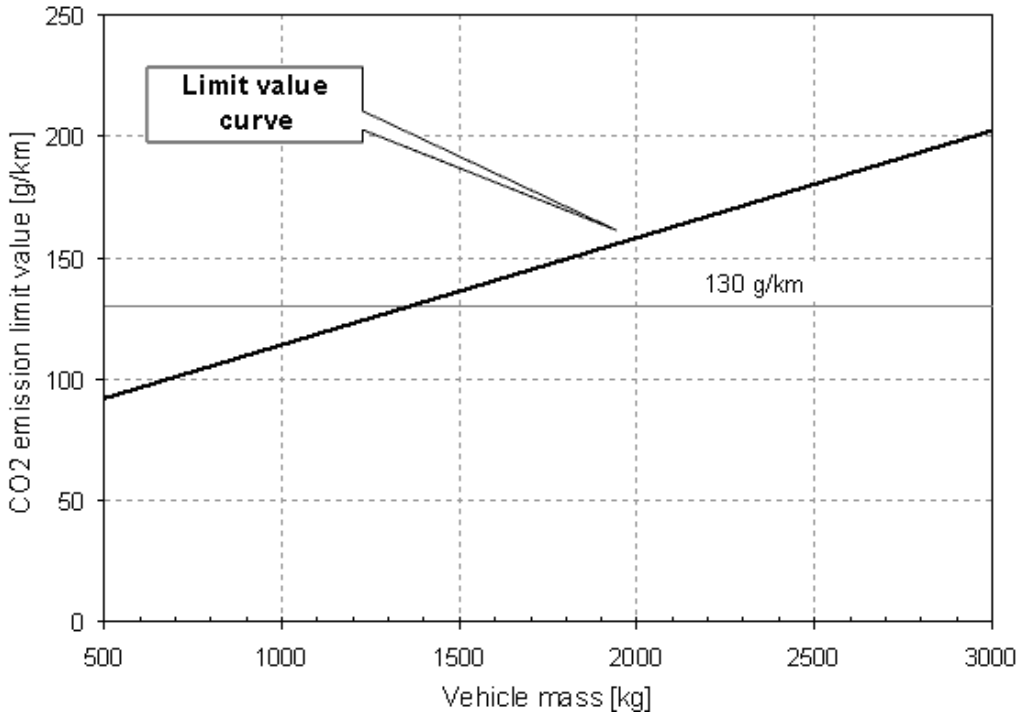

Figure 2 According to the limit value curve, heavier cars are allowed higher emissions than lighter cars while preserving the overall fleet average [14].

Passenger car CO_2 emissions and specific fuel consumption (in litres per 100 km) are defined from measurements of performance over the New European Drive Cycle (NEDC). The NEDC is designed to represent the typical usage of a car in Europe and consists of four repeated Economic Commission of Europe (ECE-15) driving cycles and an Extra-Urban driving cycle (EUDC). This is illustrated in Figure 3. The ECE-15 drive cycle is representative of low speed, low load city driving, while the EUDC is more representative of motorway driving. Before the test, the vehicle is allowed to soak for at least 6 hours at a test temperature of 20-30 °C.

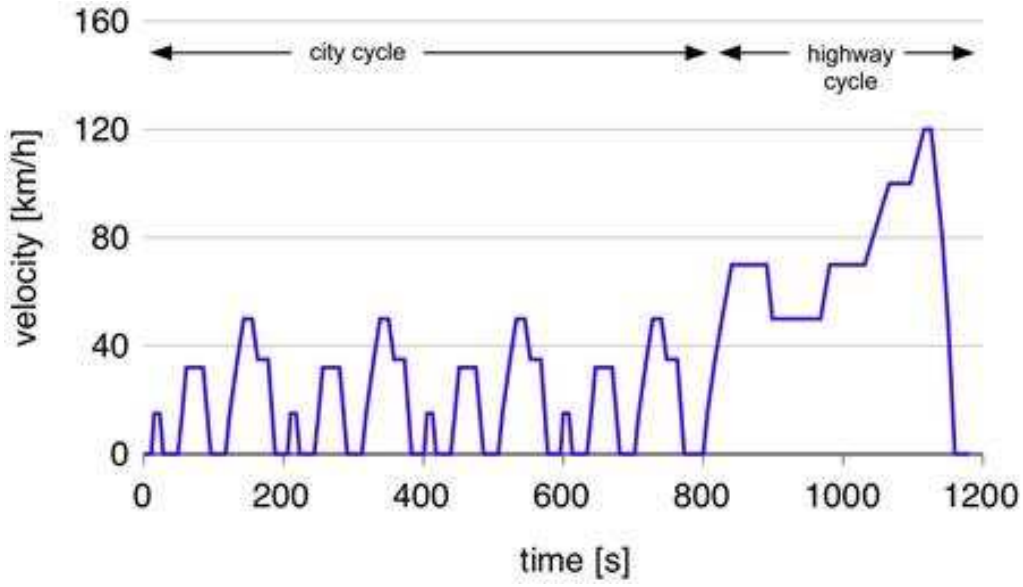

Figure 3 New European Drive Cycle (NEDC). The city cycle (first 780s) is made up of four repeated ECE-15 drive cycles. From 780-1180s it is referred to as the Extra-Urban driving cycle (EUDC) [1]

1.1.2. Reaching the Target: Role of engine thermal management

Currently a wide range of cars is available on the market that meets the 130 g/km standard as illustrated by Table 1. Furthermore, most vehicles in the range of 140-160 g/km can be brought to meet the 130g/km standard by relatively inexpensive modifications, such as a reprogrammed ECU and the addition of technologies like stop-start systems [18]. However, the above is only true for small to medium sized cars. Larger cars will require more expensive technologies possibly reducing their

competitiveness on the market and hence their demand, which would help to reduce CO_2 emissions further. Different studies [19] have compared the potential reduction in fuel consumption provided by various technologies particularly suited to gasoline engines operating under lightly loaded conditions. Depending on the specific variation used, variable valve timing (VVT) systems were reported to offer a 6-16 % reduction in fuel consumption over the NEDC, achieved by de-throttling the engine, improved mixture formation and cylinder de-activation. Improvements of over 20% were predicted with turbo-charging, engine downsizing and variable compression ratio [19]. The maximum theoretical benefit from shortening the engine warm-up phase is the difference in fuel used over the drive cycle between a cold and hot started engine, typically around 7-12 % [20] [21]. This is significant and equivalent to the fuel saving of the cold started engine with 25-30 % lower friction. Furthermore, as engines become more fuel efficient the role of thermal management becomes even more important as the available heat energy is reduced. Integration of stop-start systems and vehicle hybridisation [22] for example, offer substantial fuel savings, but lead to intermittent engine operation which has a detrimental effect on engine and cabin warm-up. As engines take longer to reach their fully-warm operating condition, the opportunity to reduce fuel consumption from raising the temperature of the engine fluids faster, becomes greater. While a number of technological developments are only applicable to gasoline engines, many of the measures encompassed by thermal management can be applied to any engine type and combined with other technologies to provide even greater fuel savings than those provided by that technology in isolation.

Make	Models < 120g/km	Models 120-130g/km	Models 130-140g/km
BMW	MINI 1.4d	118d, 120d	118i, MINI 1.4, 1.6
Chevrolet		Matiz 0.8	Matiz 1.0, 0.8auto
Citroën	C1, C2 diesel, C3 diesel	C4 1.6d	C2 1.4 stopstart
Daihatsu	Charade, Sirion 1.0		Sirion 1.3
Fiat	Panda 1.3 Multijet; Grande Punto 1.3 Multijet 75	Grande Punto Multijet 90	Panda 1.1,1.2, Punto 1.2; Stilo 1.9 Multijet 90 3d
Ford	Fiesta 1.4 tdci, 1.6tdci	Focus 1.6 tdci; C-Max1.6tdci	Focus 1.8tdci
Honda	Civic 1.3 hybrid	Jazz 1.2dsi-s	Jazz 1.4dsi; Civic 1.4, 2.2cdti
Hyundai		Amica 1.1gsi; Getz 1.1, 1.5d	Amica 1.1cdx
Kia		Picanto 1.0, 1.1; Rio 1.5d; Cerato 1.5d	
Mazda		2 1.4d; 3 1.6d	
Mercedes-Benz		A160 cdi	A180 cdi
MINI			Cooper 1.6
Mitsubishi		Colt 1.1, 1.5d	
Nissan		Micra 1.5d	Note 1.5d
Perodua		Kelisa1.0	Myvi 1.3sxi; Kenari 1.0
Peugeot	107 1.0 urban; 206 1.4hdi	1007 1.4hdi; 207 1.4hdi, 1.6hdi; 206 1.6hdi; 206cc 1.6hdi; 307 1.6hdi 3d	307 1.6 hdi 5d
Proton			Savvy 1.2 street
Renault	Clio Campus 1.5dci; Clio 1.5 dci 86	Modus 1.5dci; Clio 1.5dci; Megane 1.5dci 86 & 106	Scenic 1.5dci 86 & 106; Grand Scenic 1.5dci 106 Privilege
SEAT		Ibiza 1.4tdi	Ibiza 1.9tdi 100; Leon 1.9tdi
Škoda		Fabia 1.4tdi pd	Fabia 1.9tdi; Roomster 1.4tdi pd
Smart	ForTwo Pure; all For Two diesels	ForTwo Pulse & Brabus; ForFour 1.0, 1.5cdi; Roadster, Roadster Brabus	
Suzuki		Swift 1.3d	
Toyota	Aygo; Prius	Yaris 1.0, 1.4d	Auris 1.4d
Vauxhall		Corsa 1.3 cdti; Tigra 1.3cdti	Agila 1.0; Corsa 1.0, 1.2 (some); Meriva 1.3 cdti; Astra 1.7cdti
Volkswagen		Polo 1.4tdi	Polo 1.9tdi
Volvo		C30 1.6d; S40 1.6d	C30

Table 1 EU available cars with <140g/km emissions [15]

1.2. Engine Heat Transfer and Thermal Management Fundamentals

Engine thermal management serves a variety of needs. The most basic is to control the thermal state of the engine under different engine operating conditions and limit the temperature of thermally loaded components to within safe working limits. Peak in-cylinder gas temperatures are in the order of 2200 ºC [2], while metal temperatures must generally be kept below 400 ºC in the case of cast iron and 300 ºC for aluminium alloys to ensure satisfactory strength. The gas-side surface of the cylinder liner must be kept below 180 ºC to prevent thermal degradation of the lubricating oil film. Air cooling has been used in the past in automotive applications and is still commonplace on small capacity motorcycle/ moped engines. However, the increase in engine specific power output has meant that in recent times liquid-cooled systems have become the industry standard. The cooling medium is generally a 50:50 mixture by volume of water and ethylene glycol formulated to widen the temperature range in which the fluid can operate without change of phase. Freezing temperature is -57 ºC, while the boiling temperature depends on the coolant system pressure, but is typically in the region of 125 ºC [23]. Coolant flow, driven by a centrifugal pump, generally enters the block and circulates through the block and head before exiting from the head. Different flow paths can be arranged and can be generally classified as series, parallel or cross-flow cooling circuits [23]. A typical engine coolant circuit is illustrated in Figure 4. When the engine is cold, coolant only flows through the inner circuit and by-pass branch. This is to minimise heat losses from the coolant while still providing cabin heat. The thermostat will start to open when the coolant reaches a pre-fixed temperature, usually around 90 ºC. A portion of the coolant flow is then diverted through the radiator rejecting heat to ambient. As illustrated in Figure 5, for a fully-warm engine the coolant load typically accounts for a third of the fuel energy liberated during combustion. The greatest heat input to the coolant is from gas-side heat transfer in the cylinder and exhaust ports. The remainder is from friction dissipation at the rubbing surfaces and heat transfer in exhaust gas recirculation (EGR) coolers if these are used.

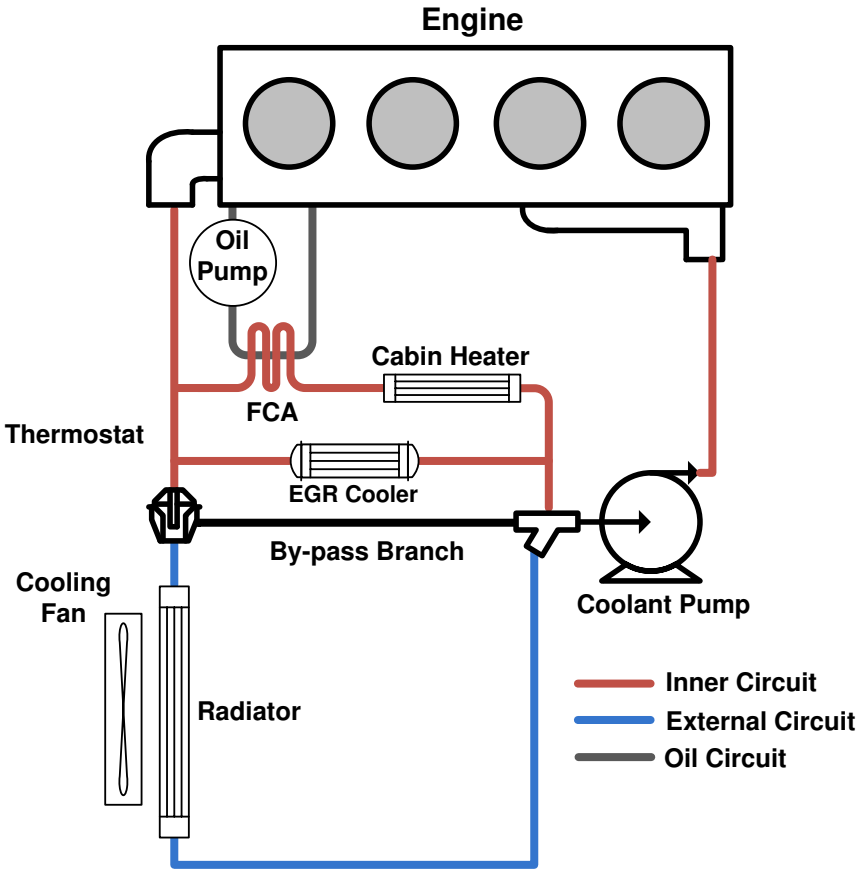

Figure 4 Typical layout of automotive coolant circuit (FCA – Filter Cooler Assembly).

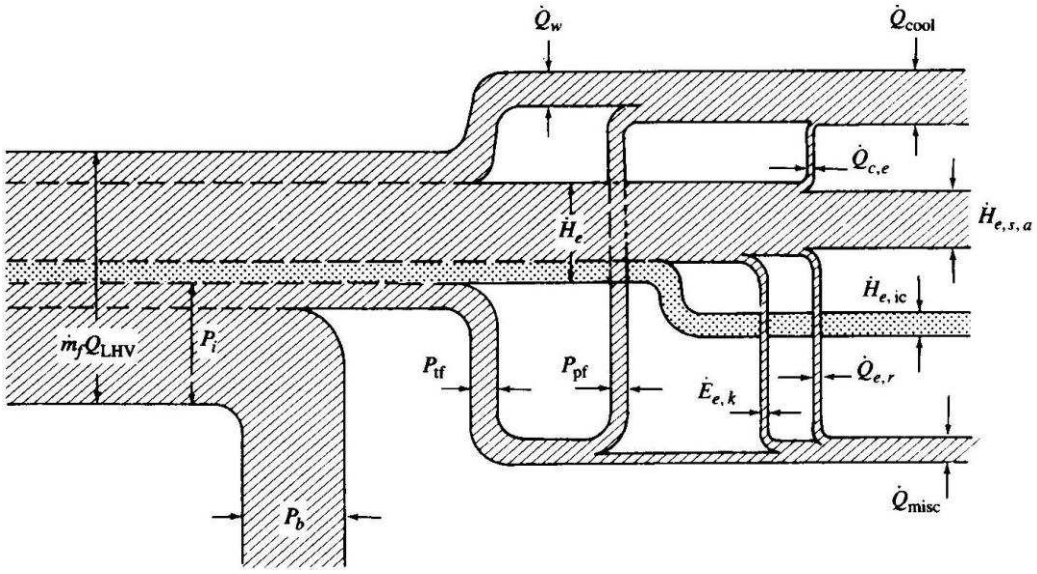

Figure 5 Energy flow diagram for IC engine under fully-warm conditions [2]. ($\dot{m}_f Q_{LHV}$)= fuel flow rate x lower heating value, $\dot{Q}_w$= heat transfer rate to combustion chamber wall, $\dot{H}_e$= exhaust gas enthalpy flux, P_b= brake power, P_{tf} = total friction power, P_i = indicated power, P_{pf} = piston friction power, $\dot{Q}_{cool}$ = heat rejection rate to coolant, $\dot{Q}_{c,e}$ = heat transfer rate to coolant in exhaust ports, $\dot{H}_{e,s,a}$ = exhaust sensible enthalpy flux entering atmosphere, $\dot{H}_{e,ic}$ = exhaust chemical enthalpy flux due to incomplete combustion, $\dot{Q}_{e,r}$ = heat flux radiated from exhaust system, $\dot{E}_{e,k}$ = exhaust kinetic energy flux, $\dot{Q}_{misc}$ = sum of remaining energy fluxes and transfers.

In recent years greater focus has been placed on the role of thermal management in increasing power-train efficiency through an improved utilisation/ redistribution of the engine's waste thermal energy. As an introduction to the lines of the investigations pursued in this thesis, the major heat flow interactions taking place within an engine system are illustrated in Figure 6 to highlight the key areas of interest and changes that could promote faster oil warm-up rates and hence reduced frictional losses following a cold engine start.

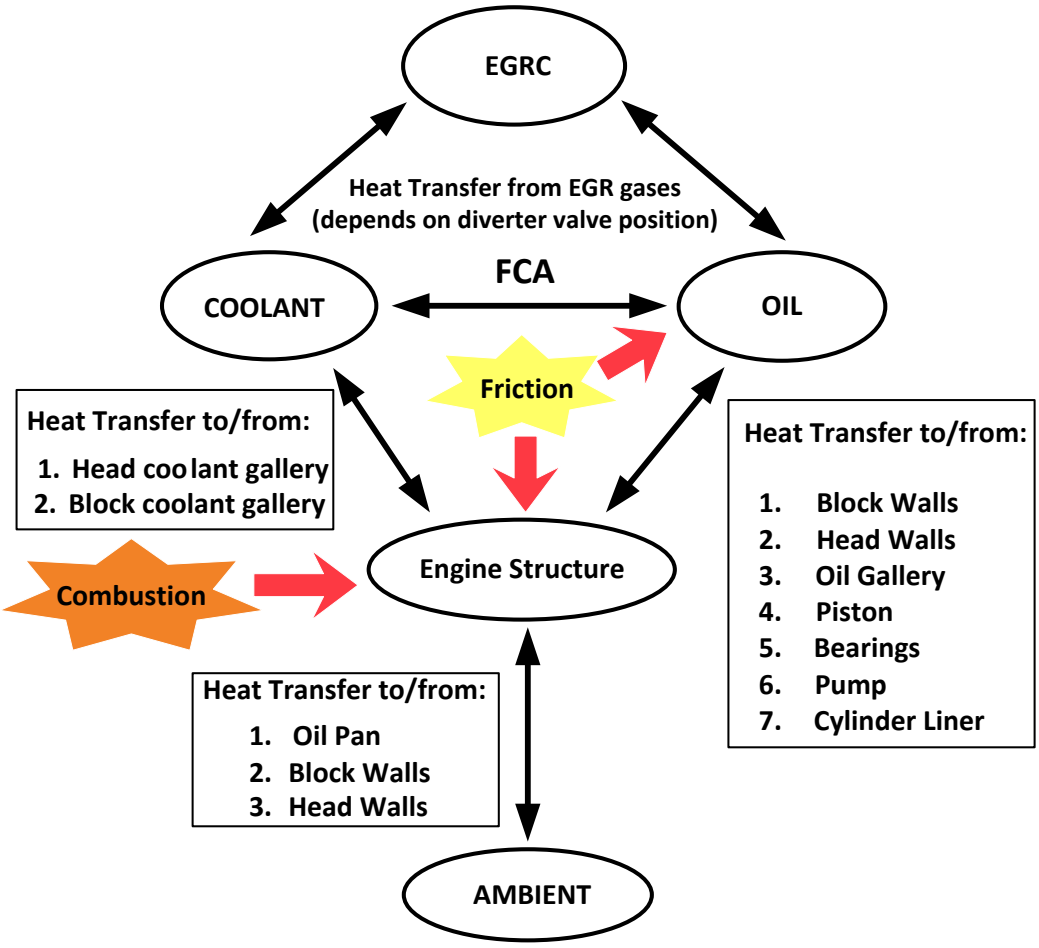

Figure 6 Basic Engine Heat Flow Schematic.

Two strategies to shorten the oil warm-up phase have been investigated. The first is to introduce more heat into the oil system predominantly by the re-direction of heat from the coolant to the oil circuit. While fast coolant warm-up is advantageous for better cabin heater performance, this has not been considered as a constraint in the

current study. Recovery of energy from EGR heat is one area where such a compromise can be made. Re-circulated exhaust gases are cooled prior to their introduction into the engine intake system. Generally on production systems this is done using a tube-in-shell heat exchanger in which the re-circulated gas is cooled by a coolant flow. A novel split-EGR cooler setup was modelled to make a direct comparison between EGR cooling with either coolant or oil and the effect of each on oil and coolant warm-up rates.

For medium speed, light load engine operation, typical of the urban section of the NEDC, gas-side heat transfer to the engine structure is larger than, but comparable to friction dissipation. Gas-side heat losses are mainly transferred to the coolant from the cylinder head and block. When the engine structure is cold the majority of friction losses are also conducted to the rubbing surfaces while the proportion retained in the oil flow is small. Due to the above reasons, coolant temperature generally leads that of the oil throughout the majority of the warm-up phase. Heat transfer from the coolant to the oil can be one way of accelerating the rate of temperature rise of the oil. A degree of thermal coupling between the two fluids is inherently provided through the engine structure. Further to that, the engine used in this study was equipped with a Filter Cooler Assembly (FCA). The latter is an oil filter unit integral with an oil-to-coolant heat exchanger. The flow of coolant in the heat exchanger can be controlled to vary the thermal coupling between the two fluids. The effect of this has been investigated and shown to have a significant impact on the predicted improvements in engine friction.

Piston Cooling Jets (PCJs) provide a further means of re-directing combustion heat from the coolant to the oil circuit. Enabling the PCJs reduces piston temperatures and heat conducted from the rings into the cylinder liner while heat transfer to the oil jets results in shorter oil warm-up times with small benefits in friction. The effect of the PCJs on the warm-up and heat rejection characteristics of the engine was therefore modelled.

The second strategy is to reduce or inhibit heat losses from the oil circuit. Oil interacts with the engine structure at various locations. Maintaining high metal temperatures at the rubbing surfaces is important as they govern oil film temperatures

which in turn dictate frictional losses. This is particularly true for engine components operating in the hydrodynamic lubrication regime. However, regions of the engine structure remote from the rubbing surfaces act as heat sinks to the oil limiting its rate of temperature rise. The crankcase structure is one such area. The major heat losses from the oil circuit are in the form of heat transfer from oil flowing in the main gallery and from the oil mist to the crankcase surfaces. Reducing such interactions is shown to have an important influence on oil warm up. While thermal isolation of oil flowing in the main gallery may be hard to achieve, relocation of the gallery to a different position within the engine block was shown to be one possible way of reducing and even reversing the heat losses from oil flowing in the main gallery.

Crankshaft main bearings represent one area where a strong thermal coupling between the oil film and rubbing surfaces (bearings shells and crankshaft journal) is observed. This restricts the oil film temperature rise and increases the cold start friction penalty. Investigations in this thesis show that it also limits the effectiveness of supplying pre-heated oil to the bearings as a way of reducing main bearing friction. The effect of different extents of thermal isolation of the film from the rubbing surfaces was therefore simulated and the benefits in friction predicted.

As for the coolant, exhaust enthalpy flow accounts for ~30 % of fuel energy released [2]. Heat recovery from the exhaust is therefore one obvious way of increasing engine thermal efficiency. However, during warm-up the thermal inertia of the after-treatment system and heat recovery device itself, limits the ‘surplus’ energy available to raise engine fluid temperatures. Different heat exchanger setups have been simulated to explore the trade-off between heat recovered and the additional thermal inertia incurred by the heat exchanger installation.

1.3. CAE Modeling: PROMETS Overview

A variety of software packages is available to assist in the development of engine and vehicle thermal systems. These vary from 3-D computational fluid dynamics (CFD) [24] and finite element (FE) packages [25] to 1-D fluid flow solvers [26] [27]. They can either be used in isolation or coupled together in a co-simulation [28]. In the investigations described in this thesis, PROMETS has been used.

PROMETS (**PRO**GRAM for **M**ODELLING **E**NGINE **T**HERMAL **S**YSTEMS) is an assembly of models describing engine friction, thermal behaviour and thermodynamic performance. At its core is a lumped capacity engine structure representation, with various sub-models to provide the appropriate boundary conditions [29]. It has been developed at the University of Nottingham in collaboration with Ford Motor Company. Work on the project was started in 1989 by Christian [30] and developed through several PhD investigations, notably Yuen [31], Chick [32] and Baylis [33]. PROMETS can be used in a variety of engine thermal management roles. These range from the prediction of fully-warm engine temperature fields and heat flows, to the assessment of technology and measures aimed at shortening engine warm-up times. The lumped capacity approach (as used in PROMETS) offers a number of advantages over some of the simulation techniques described above. Simulation times are considerably shorter when compared to 3-D model counterparts. Setting up of the model is also generally simpler. Unlike 3-D models they do not rely on detailed engine geometry which is rarely available early in the concept phase. Finally, a high flexibility to amend the core software also means that various changes can be implemented relatively easily in the model.

Recent versions of the PROMETS package have been developed in Matlab Simulink. It is composed of two programs run in series, Figure 7. The first is PROGEN (**Pro**gram for creating **Gen**eric engine representations), used to generate the lumped capacity elemental representation of the engine structure together with details of the thermal connections between them. PROGEN requires only a very basic engine specification to generate the engine build information. This includes a number of key dimensions, such as bore and stroke, together with information such as valve – train type, engine cylinder arrangement and coolant and lubrication circuit layouts. PROMETS solves the governing equations generated by PROGEN using an explicit time-marching method. It is composed of seven main sections: the engine structure representation, fuel flow prediction, gas-side heat transfer calculation, friction model, engine-out exhaust gas temperature calculation, and finally the coolant (external) and lubrication circuit representations. Each section is in turn composed of various sub-models, such as the oil and EGR cooler sub-models in the case of the coolant circuit. The analysis can either be based on a ‘single-cylinder’ or a ‘multi-cylinder’ engine representation. In the latter, inboard cylinders are assigned adiabatic interfaces on

both sides whereas outboard cylinders are assigned adiabatic interfaces on sides adjacent to neighbouring cylinders while their outer surfaces are exposed to ambient. While a ‘single-cylinder’ model is more computationally efficient, it neglects the thermal variation between cylinders which is generally small anyhow. Morgan [34] reports that for a 4-cylinder 1.6 l gasoline engine running at a medium speed and load condition, a maximum temperature difference of 10 K was predicted between different cylinder liner elements. A ‘multi-cylinder’ model can assess the impact of coolant circuit design on the thermal state of different cylinders and can provide useful information for engine structural analyses. However, for most studies where the bulk heat flow through the engine structure and into the oil and coolant circuits is of interest, the small variation in thermal state of different cylinders has little effect on the accuracy of the analysis. A single-cylinder model was hence adopted here.

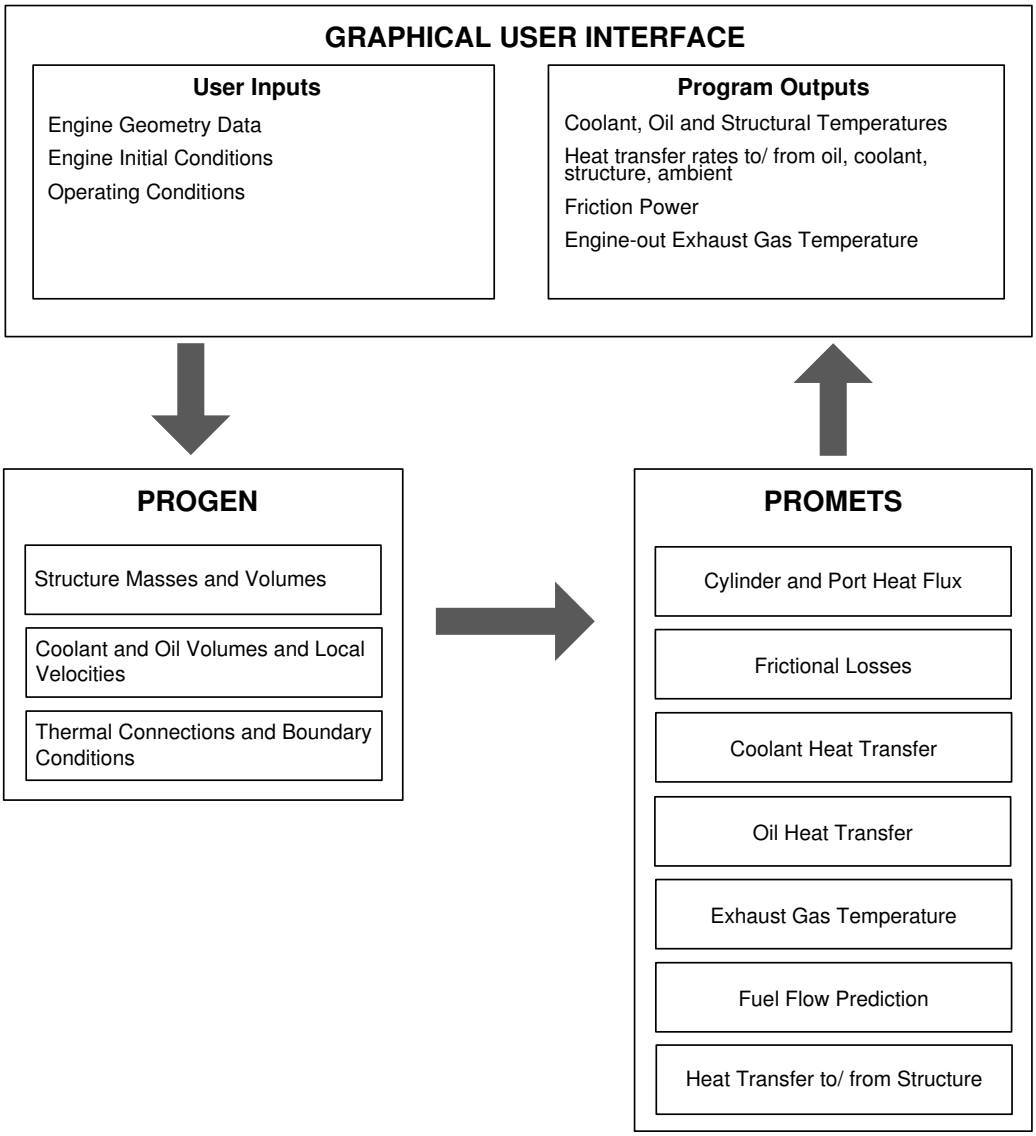

Figure 7 Basic structure of PROMETS [34]

The engine structure elemental representation used in PROMETS is illustrated in Figure 8. This is constructed around generic engine templates. While engine performance, efficiency and refinement have improved significantly throughout the years, the basic design has remained relatively unchanged [35]. The degree of variation in engine design is greatly limited by practical considerations of durability, compactness, balance and so on. The generic engine form used in PROMETS is based on a number of these engine design constraints and commonly used dimensionless ratios. Wall thicknesses in castings for example are generally uniform with a typical value of 7 mm [32]. The stroke and connecting rod length determine the position of the crankshaft relative to the top of the cylinder block. Required clearances for reciprocating and rotating components then fix the basic shape of the

crankcase. Valve head sizes are generally a ratio of the bore dimension, while the position of the camshafts in the cylinder head is fixed according to the typical values of valve angle and length. The number and size of elements used in the model was based on comparisons of predicted temperature fields with those generated from a proprietary FE code (PAFEC) running similar boundary conditions [30]. Accuracy criteria, as discussed further in Section 3.3, are also met. For a more complete review on the exploitation of the generic engine design concept the reader is referred to Chick [32].

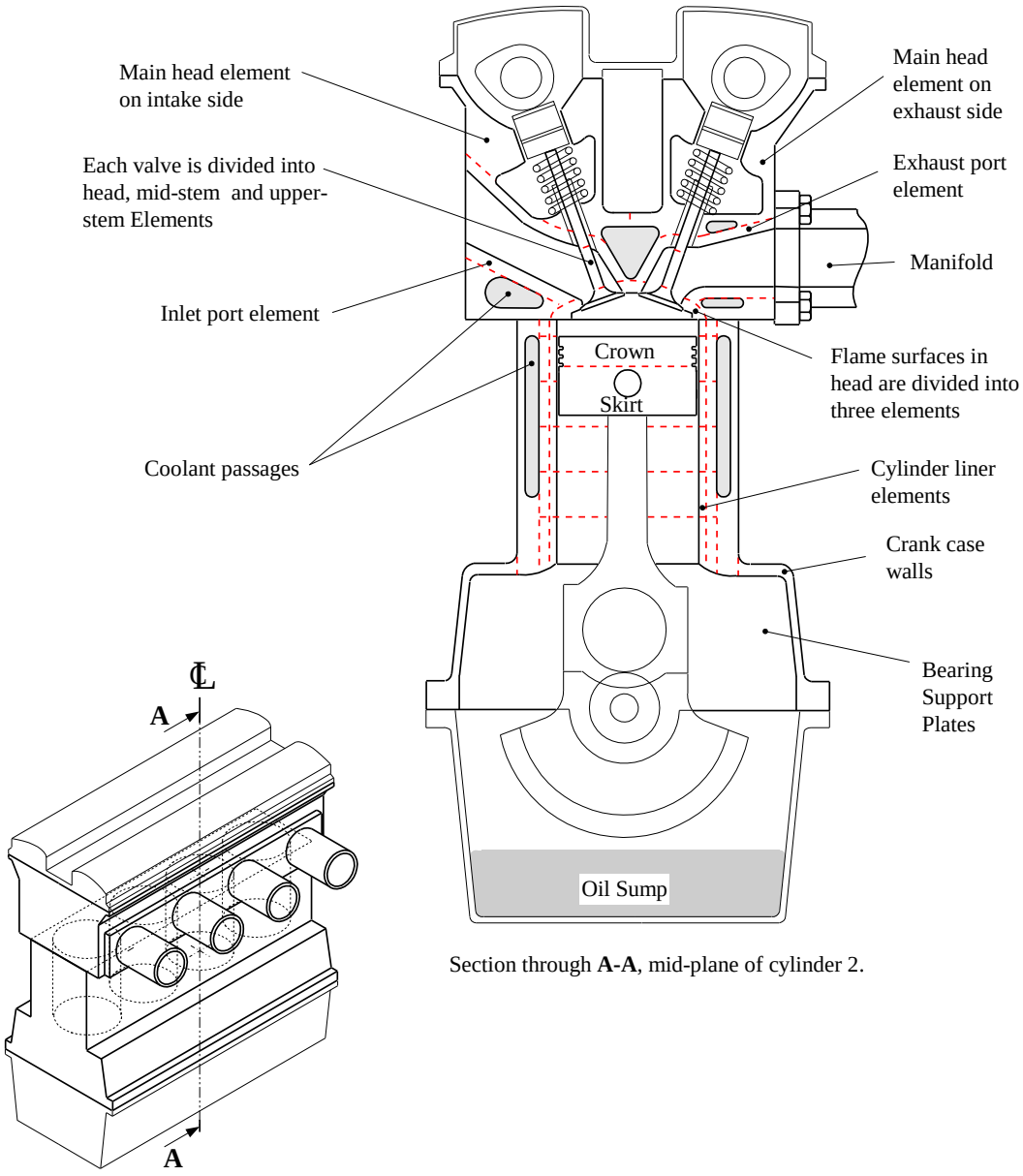

Section through **A-A**, mid-plane of cylinder 2.

Figure 8 Core engine structure elemental representation in PROMETS [32]

1.4. Thesis Layout

This thesis describes sub-model developments undertaken in PROMETS and exploitation of the model to investigate the minimisation of the cold start fuel consumption penalty by improvements to the engine warm-up characteristic.

A literature review is introduced in Chapter 2 with particular focus on engine thermal and friction modelling. A variety of technology, from exhaust heat recovery, coolant heat stores to a 'split-sump' design, is described, all aimed at optimising different aspects of engine thermal management. A summary is also provided at the end of the chapter, where a number of concepts particularly relevant to this project have been identified.

Chapter 3 introduces parts of the fundamental theory and formulations used in PROMETS, from the lumped capacity calculations to the major sub-models. The gas-side heat transfer, friction and fuel consumption calculations are all described together with the layout of the oil and coolant circuits.

Chapter 4 describes the extension of the piston heat transfer sub-model. Experimental measurements from a specially modified 2.4l Puma engine were used to extend the piston heat transfer model in PROMETS to account for the effect of PCJs. The heat flow through the piston rings to the cylinder liner, the interaction of the oil jet with the piston cooling cavity and heat transfer from the piston skirt to the crankcase oil mist are all described. The effect of enabling the PCJs on heat rejection to the oil and coolant circuits together with the main model assumptions and limitations are also discussed.

The development of a main bearing thermal-friction model is the focus of Chapter 5. The basic theory of the model is introduced together with the revisions carried out to the crankcase elemental representation in PROMETS required to allow the integration of the bearing sub-model. Comparisons of model predictions with experimental data are presented as is the sensitivity of predictions to the main model uncertainties.

Chapter 6 reviews the exploitation of the bearing model in exploring ways of raising the film temperature following a cold start. The effects of reducing the oil flow rate through the bearings and feeding pre-heated oil to the bearings were simulated. The model was used to show that de-coupling the oil film from the bearing rubbing surfaces (shells and journal) is crucial to maximise the benefits of such measures.

Chapter 7 looks at the application of PROMETS in evaluating the potential benefits in fuel consumption from different measures: modifications to the internal heat flows within the engine structure and re-distribution of waste heat from the coolant and exhaust to the oil circuit. Simulations are conducted over the New European Drive Cycle (NEDC) from ambient temperature starts of ~26 °C.

The main findings and implications from Chapters 4-7 are discussed in Chapter 8. Some avenues for further research are also recommended.

Chapter 2 - Literature Review

2.1. Introduction

The material presented in this chapter provides an insight into past and current work on improving vehicle fuel economy by means of shortening warm-up times and minimising engine parasitic losses. The automotive industry is relying more on computer simulation to develop new engines because of the time and cost benefits over purely experimental methods. For this reason, and because the majority of this research is based on modelling investigations, particular attention is given to published work on the development of thermal models. The modelling of engine friction is an essential part of this work and a brief review of the different types of friction models developed throughout the years is therefore presented first. Various aspects of engine thermal management are then explored in significant detail, looking at different concepts, covering split-cooling, energy stores and exhaust heat recovery devices. A brief discussion is also included to help identify technology relevant to this project while highlighting some of the gaps in the current body of knowledge.

2.2. Engine Friction

2.2.1. Fundamentals

Engine friction and ancillaries' power consumption accounts for the difference between the net indicated and brake power output of an internal combustion engine. This varies from typically around 10% of the indicated work output at full load, to 100% at idle or no-load conditions [2]. Engine friction is usually divided into three main components: rubbing friction, pumping (or gas exchange) losses and ancillary losses. Ancillary losses originate from driving engine ancillaries such as water, oil and fuel pumps. The major component and of major concern in this study is the rubbing or mechanical friction. Rubbing friction occurs at the interface between surfaces with a relative speed; shafts rotating in bearings, piston liner relative motion, cam shaft/ follower interaction etc. Strip down motored tests have been used extensively by researchers [36] to measure the contribution of each of these components to total engine friction. Generally 40-50 % of the mechanical/ rubbing loss is attributed to the piston assembly (which includes friction due to the ring pack,

piston skirt and big end bearings), 30% to the crankshaft assembly (main bearings and seals) and the remaining 20% to the valve train assembly [2].

The three friction regimes can be characterised on a Stribeck plot, as in Figure 9 [37]. The friction coefficient between two sliding surfaces can be plotted against the duty parameter (or Stribeck variable), defined as a function of lubricant viscosity, relative speed between the sliding surfaces and the load carried $\left(\frac{\mu N}{P}\right)$. In hydrodynamic lubrication the friction surfaces are completely separated by an oil film minimising friction and mechanical wear. As the oil film thickness is reduced hydrodynamic lubrication eventually gives way to mixed lubrication in which the oil film thickness is comparable to the surface asperities. The lubricant film no longer separates the rubbing surfaces completely and intermittent metal to metal contact occurs, raising the friction coefficient. In the mixed lubrication regime a sharp increase in friction coefficient occurs with a decrease in the duty parameter. As the duty parameter is further reduced (through a reduction of relative velocity or an increase in load), boundary friction results. In this case the friction coefficient is independent of the duty parameter and a function only of the ratio of the shear strength of the adsorbed oil layer and yield stress of the softer material in the friction pair. In this case oil viscosity is not as important as its chemical composition. Friction modifiers are used extensively to minimize friction in boundary lubricated components [38]. Molybdenum dithiocarbamate (MoDTC) is a commonly used organometallic friction modifier that works by bonding flakes of molybdenum disulfide (MoS_2) onto surface asperities. MoS_2 is a solid lubricant and its low friction properties are a result of its lamellar structure.

All three friction regimes are encountered in i.c. engines. Main bearings predominantly operate in the hydrodynamic regime (except on start up). Piston rings operate in all three friction regimes depending on piston position. At TDC/ BDC the piston is effectively stationary and in a boundary lubrication state. As the piston accelerates away from these positions the oil film thickness between the ring and liner increases and this moves the ring into the mixed and hydrodynamic regimes. The increased friction force at TDC/ BDC positions does not translate into a significant friction power loss due to the low piston velocity, but liner wear at these

positions is generally increased. Valve train components operate in all three friction regimes, but mixed and boundary lubrication generally predominates particularly at low speeds and viscosities [39].

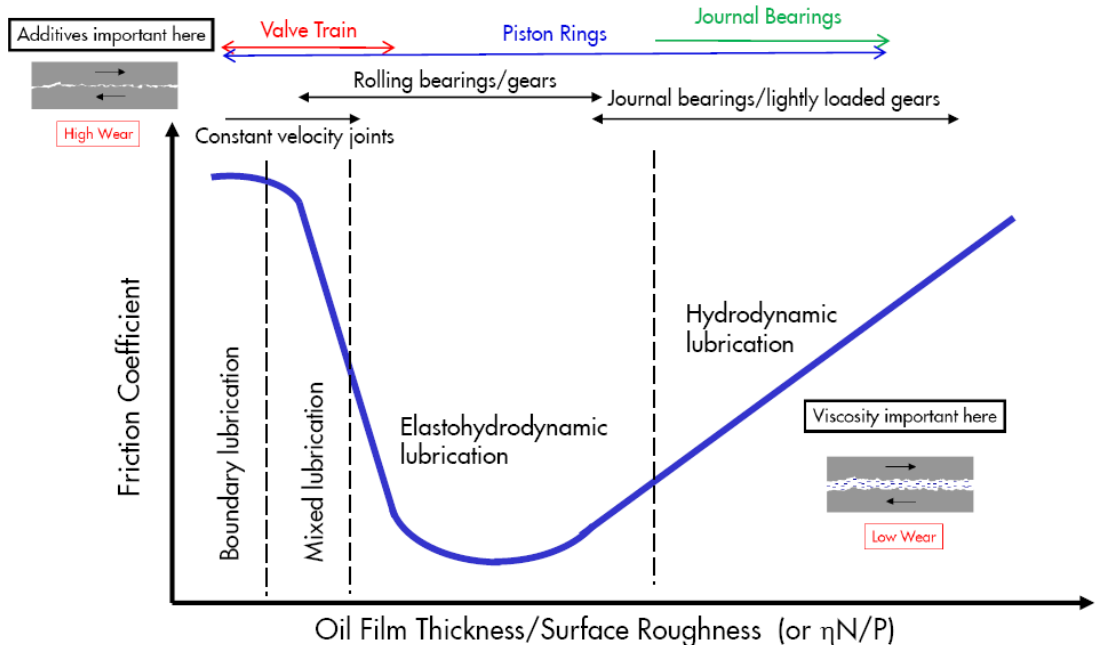

Figure 9: Stribeck diagram (log-log scale) [37]. η-dynamic viscosity, N-engine speed, P-load per unit area.

The four most common methods of measuring engine friction are [2]:

1. The indicator method: This involves measurement of the cylinder pressures over the engine cycle so as to determine the indicated power from which the engine brake power, generally measured using a dynamometer, is then subtracted giving friction power.

2. Motoring Tests: In this case the power required to 'motor' the engine using an external power source (such as a dynamometer) is measured. This method can also be used on a progressively disassembled engine to measure the frictional loss contribution from each major engine sub-assembly.

3. Willans Line: This involves plotting engine fuel consumption against brake power and extrapolating back to 'zero' fuel consumption.

4. Morse Test: This technique is used on multi-cylinder engines. Individual cylinders are cut out in turn, while the remaining cylinders are left to motor the cylinder cut out. The engine speed is maintained the same and the reduction in brake torque is recorded. A set of equations is generated which is used to determine engine friction.

From the above methods, only the first can give a true measurement of friction in a firing engine. However, a number of issues can limit the accuracy of this method; these include cylinder-to-cylinder variation in indicated power and the difficulty of acquiring accurate, repeatable and in-phase cylinder pressure data (due to inaccuracies in determining the TDC position). Due to the above, motoring tests are still used extensively. Moreover the indicator method provides a measure of total engine friction but cannot differentiate between rubbing and ancillary losses. Motoring losses are claimed to be different from firing losses due to a number of factors. In-cylinder gas loading is lower in a motored engine. Piston and bore temperatures are also lower increasing oil film viscosity, while piston-bore clearances tend to be greater. Despite this, very good agreement was observed between motored and fired engine friction measurements taken on a 4 cylinder 1.8l diesel engine at the University of Nottingham [40]. However, determining engine friction still remains a challenging task and according to Monaghan [41] even in nominally identical engines, differences in measured friction can be up to 10 %.

2.2.2. Modelling

Engine friction models described in the literature can be broadly classified into two categories: crank-angle resolved models and cycle-averaged correlations. The former allow instantaneous evaluation of friction losses at any point in the engine cycle. They can be further subdivided into models that are derived from first principles solving the Reynolds equation of lubrication [42], and more commonly models that use analytical and semi-empirical correlations. The first significant research into instantaneous friction models is that of Rezeka and Henein [43] who used measurements of cylinder pressure and engine speed to calculate the different friction components. Analytical equations were used in this case. Kouremenos et al. [44] developed a friction model which was heavily based on that of Rezeka and Henein to

investigate the effect of peak cylinder pressure on engine friction. A strong influence of speed and load on engine friction mean effective pressure (FMEP) was observed, while the effect of combustion pressure was relatively small. In [44], this was attributed to the fact that peak cylinder pressure mainly affects engine friction torque around TDC position only. Derived values of engine FMEP (averaged over an engine cycle) compared well with measured values. A semi-empirical correlation was also derived taking into account the effect of engine speed (V_p represents mean piston speed), load (IMEP) and peak cylinder pressure (P_{max}):

$$FMEP = c * 0.0104 * IMEP + 0.15 * Vp + 1.0955e^{-3} * Pmax \quad \text{Equation 1}$$

Thring [45] developed a model to investigate the effect of design changes on the friction of a generic two litre four cylinder gasoline engine. The model was derived from first principles and adjusted with empirical constants. For the piston assembly, Thring ignored boundary friction at the end of the stroke, due to the relatively low piston velocity and hence low power dissipation associated with these points in the engine cycle. Changes to bearing aspect ratio resulted in significant reductions in friction, particularly for the valve train. A maximum reduction in total engine friction of 2.5% was achieved from changes to the camshaft bearings, whereas a maximum reduction of 1% was achieved with changes to main bearing design. Unlike the findings reported by Kouremenos on the effects of maximum cylinder pressure, Thring predicted significant increases in friction from higher cylinder pressures, especially in the case of piston rings and main bearings. On the other hand, experimental measurements by Muira and Shiraishi [46] indicate that cycle-averaged main bearing friction is almost independent of load. Engine load has a substantial effect on bearing friction but over only a small fraction of the engine cycle. Load, however, does dictate bearing size which bears a strong impact on friction. Likewise investigations by Leong [39] showed that piston ring tension and gas pressure loading have a small to negligible influence on piston friction. Leong associated the latter to the small area behind the rings that is subjected to increased gas loading. Whilst it is clear that different authors have reported conflicting findings, overall, the majority suggest that the effect of engine load on FMEP is weak [47] [48].

Livanos et al. [49] also developed an instantaneous friction model, capable of predicting oil film thickness at the rubbing surfaces and the transition between different lubrication regimes. Livanos adopted this approach for the piston assembly but used analytical solutions developed by Hirani [50] for journal bearings. The valve train friction torque was calculated according to a formulation developed by Zweiri [51] who also developed a crank resolved friction model for diesel engines. The model consisted of analytically derived equations based on the Reynolds equation and dynamic analyses. The effect of changes in oil viscosity was also taken into account.

Crank-angle resolved friction models are widely used in conjunction with engine dynamic models to simulate engine transient behaviour [51] which in turn facilitates on board diagnostic and engine starter modelling [52] applications. However, crank-angle resolved models require the determination of numerous parameters and constants which can be challenging. Ciulli [53] comments on how comparisons of engine performance simulations with both types of friction models (crank resolved and cycle averaged models) showed only small differences in the predictions of temperature, pressure and other quantities. In this case the increased complexity of crank-angle models, when compared to mean-value formulae, does not seem to be justified. Cycle-averaged models calculate the averaged engine FMEP as a function of only basic engine parameters and dimensions such as cylinder bore, stroke and bearing dimensions. The simplest express total engine friction as a function of engine speed in the following form [36] [54]:

$$FMEP = C_1 + C_2N + C_3N^2 \qquad \text{Equation 2}$$

The above expression reflects how engine friction is a contribution of friction components independent of engine speed (boundary friction) others proportional to engine speed (hydrodynamic friction) and finally components proportional to the square of the speed (turbulent dissipation). More pertinent to this research are models that calculate the mean-value engine FMEP on a component basis. The models developed by Bishop [55] and Patton [56] are typical examples of this type of model. Ciulli [53] compared the friction predictions of ten different models applied to a four cylinder four-stroke direct injection diesel engine. The substantial spread in the

results points at the difficulty in obtaining consistent friction predictions. However, Ciulli [53] explains that most of the formulae cannot be compared directly as they were derived for different engines and operating conditions (diesel or gasoline, single or multi-cylinder configurations, motoring or firing conditions, including or excluding pumping losses etc.).

The friction model incorporated in PROMETS is a development of that of Patton et al. [56]. The original is a modular, fully warm friction model based on a combination of lubrication theory and empirical results. Predictions were calibrated against experimental data collected between 1980 and 1988. An improved version of this model was presented more recently by [57] to account for improvements in engine design. The findings of [57] suggest that total engine friction decreased by 15-20 % over a period of 15 years, particularly due to improvements in the areas of piston friction and pumping losses. Lubricant viscosity scaling with temperature was also added to predict friction losses at colder temperatures. A modified version of the Patton model was also developed by [58] and is used in this investigation. This was based on tear-down tests performed on four, in-line 4-cylinder diesel engines, one of which is of the same family as the engine used in this study. The revisions carried out by Leong to the friction formulations are described in greater detail in Chapter 3.

2.3. Engine Thermal Modelling

Generally engine modelling serves two main purposes: to reduce the dependency on engine testing and to infer parameters and quantities which are difficult to measure in tests. A variety of engine thermal models are reported in the literature. Jarrier et al. [59] investigated the warm-up behaviour of a diesel engine using both experimental and modelling techniques. Of particular relevance to the work presented in this thesis, was the variation in the distribution of heat released from combustion throughout the engine warm-up phase, Figure 10. On start up, heat directed towards warming up the engine metallic components can be up to 50 % of heat released from combustion and does not drop below 40 % for the first 5 minutes of engine operation. This heat could be preferentially directed to the coolant to improve cabin heater performance or to the oil to reduce engine friction. Oil temperature is shown to lag

behind that of coolant when the engine is driven over the NEDC. Simulated results from a nodal type engine thermal model also showed how the lower block exhibited the slowest rate of temperature rise. Jarrier attributed the relatively slow warming of the oil to a combination of two effects: a low heat input into the oil, but more importantly a redistribution of this heat to the lower engine structure.

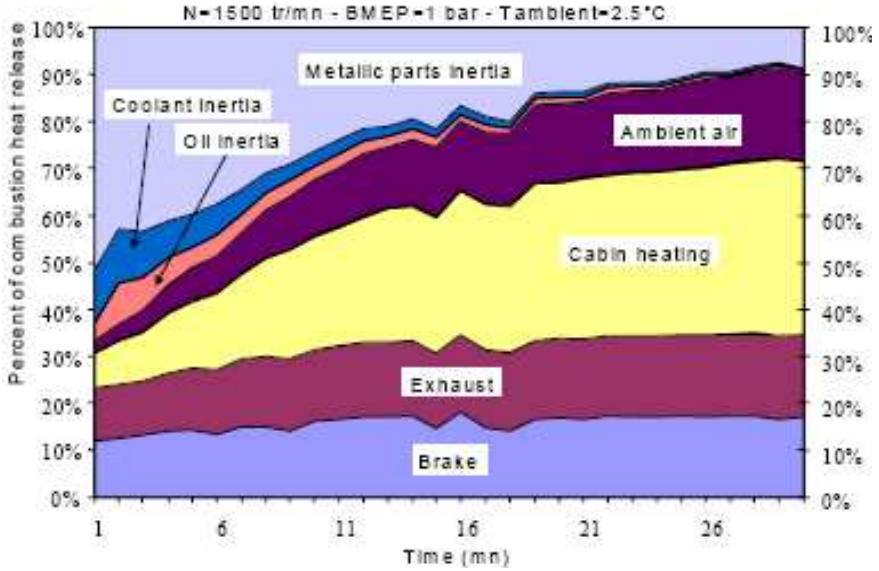

Figure 10 Redistribution of heat energy released from combustion during warm-up [59]

Farrant et al. [5] developed a lumped-capacity thermal model to investigate the influence of engine and transmission oil warm-up rates on fuel consumption. The unit investigated was a 3 L V6 spark ignition engine coupled to a six speed automatic transmission. Farrant simulated the effects of a fully warm engine and a fully warm transmission. The benefit in fuel consumption over the NEDC observed in the first case was 12%, versus an improvement of only 3 % in the second. This implies that there is greater potential to improve vehicle fuel economy from shortening the engine warm-up phase, rather than that of the transmission. Heat flux into the combustion chamber face was modelled as a function of fuel flow rate, whereas heat sources to the oil included heat exchange with the piston and friction heat dissipation. An empirical equation from Barnes-Moss [60] was adapted to evaluate friction losses throughout the warm-up but unlike other authors of similar modelling [34] [9], Farrant does not specify the proportion of friction heat retained in the oil. Having validated the baseline engine model for coolant, engine and transmission oil temperatures, Farrant went on to investigate the effect of exhaust-to-coolant and

exhaust-to-oil heat exchangers. The mechanical water pump was also replaced with an electric unit, and the standard wax-filled thermostat replaced by an electrically controlled diverter valve. The coolant warm-up rate was not significantly different from the baseline case but the coolant temperature was allowed to rise above the baseline fully-warm temperature. Faster engine and transmission oil warm-up rates resulted in a 5 % reduction in fuel consumption over the NEDC. The effect of cabin heating was not included in the simulations.

Finol et al. [61] measured in-cylinder heat flux of a turbo-charged diesel engine at different engine speed and load conditions. By arranging thermocouples at different radial positions, the thermal gradient through the cylinder wall was obtained which allowed calculation of the heat flux and extrapolation to obtain in-cylinder wall temperatures. This in turn allowed the convective heat transfer coefficients on the gas and coolant sides to be determined. A finite-difference conduction model was also developed to evaluate the effect of the thermocouples' intrusiveness on the thermal profile obtained, showing a worst case relative error of 2.5 % in the temperature distribution at the measurement points. Results showed two peaks in the measurement of heat flux down along the cylinder liner. The first peak, as expected, was at the top of the liner, resulting from the high gas temperatures at the beginning of the expansion stroke. The second peak was mid-way down the stroke, close to the position of maximum piston velocity indicating the importance of friction dissipation on cylinder heat flux. The estimated cylinder wall temperatures showed a similar trend, but with a less pronounced secondary peak.

Torregrosa et al. [62] also showed an interest in evaluating cylinder wall temperatures, but unlike Finol et al. [61] opted to develop a simulation tool rather than relying solely on experimental measurement. Torregrosa points out the difficulty of installing thermocouples in certain engine locations due to the presence of water jackets in the case of cylinder walls, or the need to resort to wireless transmission in the case of piston temperature measurements. Unlike computationally intensive co-simulation methods using finite element models, the aim of the model described by Torregrosa was to give a quick estimate of cylinder wall temperatures when the precision required is not so great. Experimental measurements were carried out to evaluate the effect of different engine operating parameters on wall temperatures.

These included speed, load, start of injection, intake manifold pressure, coolant and oil temperatures. The model developed by Torregrosa was a 3-node model, representing the piston, cylinder liner and cylinder head, with the oil, coolant and combustion gases acting as boundary conditions. The conductance between different elements was generally defined by a constant and a variable-dependent component. A speed dependency was only observed for heat transfer between the piston and oil. The remaining conductance values, including that between the coolant and cylinder liner, were defined as constant values. This contradicts the mass flow dependency proposed by the Dittus – Boelter [63] relation for the heat transfer coefficient on the coolant side. Separate tests also showed that reducing the coolant flow by as much as 70% had little effect on wall temperatures. Reducing the flow simply increased the coolant temperature rise across the engine. This suggests that the thermal resistance between the in-cylinder gases and coolant is dominated by that between the gases and flame deck.

Veshagh et al. [64] describe a lumped capacity model used to simulate the warm-up behaviour of a four-cylinder spark ignition engine. In addition to modelling the oil, coolant and internal gas flow circuits, the model also took into account heat transfer between the engine and under-bonnet airflow. Having validated the model, the authors went on to do a parametric study investigating the effect of engine running condition, combustion chamber wall thickness, together with coolant and lubricant volumes, on the engine's warm-up characteristic. Operating the engine at the same power, but at double the engine speed of the baseline condition resulted in quicker heating of the oil. The lighter load condition led to a lower mean gas temperature and hence decreased cylinder head and liner temperatures. This suggests that heat input to the oil from friction dissipation generally outweighs heat exchange from hot engine surfaces. However, it is important to point out that Veshagh's model was based on the assumption that 50 % of the friction power loss at the rubbing surfaces is dissipated into the oil whereas Baylis [33] used a lower value of 20 %. Baylis also investigated the effect of operating at higher engine speeds on cabin heater performance. Although higher engine speeds led to shorter warm-up times, it was at the detriment of fuel consumption. Veshagh also acknowledged that the use of higher engine speeds to shorten oil warm-up times might be of limited practicality due to a possible increase in engine wear.

Torregrosa et al. [65] describe the development of a thermo-hydraulic model used to evaluate the effect of different coolant system setups on engine warm-up, emissions and fuel consumption. The model was of the lumped capacity type with sub models to provide boundary conditions, such as the Woschni [66] correlation for in-cylinder heat transfer. The model was calibrated by running steady state engine tests, and then validated over the NEDC. As reported by Jarrier [59], results show that during warm-up, engine heat rejection is mainly absorbed by the structure's thermal inertia and the coolant. Torregrosa looked at the effect of placing a valve in the bypass branch to throttle the coolant flow rate and another valve in the water tank branch, to change the coolant 'participating' volume during warm-up. Completely shutting both valves produced the greatest benefit in terms of shortening coolant warm-up time. Torregrosa reports a reduction of just over 23 % in the time required to reach 80 °C when compared to the baseline case with both valves open, leading to a reduction in fuel consumption of 1.62 %.

Zoz et al. [67] describe a thermal model designed specifically to predict oil sump temperatures with the aim of understanding the influence of different engine design parameters on oil warm-up rate and fully-warm temperatures. The model, representative of a V8 gasoline engine with push-rod operated valves, was built in FLOWMASTER, a commercially available 1-D thermo-hydraulic software package. Three engine operating conditions were considered: 2000 rpm road load, 2000 rpm wide-open throttle (WOT) and 4000 rpm WOT. For the WOT cases, simulation results validated well with experimental data, but the model under-predicted oil sump temperature for the road load case. The authors attributed this to the fact that the empirical correlation for heat flux into the piston crown was derived for the full load condition. The major heat input to the oil was from the piston undercrown, accounting for 70-80 % of the energy transfer. The remaining heat input was from the bearings. This is in contrast with the findings of Trapy et al. [68] who reported that for an engine without PCJs friction heating in bearings accounted for up to 90% of the total heat input to the oil. With PCJs the split between friction heating in bearings and heat transfer from the piston was roughly 60:40. Like Kaplan et al. [69], Zoz assumed that friction heating at the piston – liner interface is entirely dissipated into the cylinder liner. This differs from the approach of Veshagh [64] and Morgan [34]. Zoz et al. observed a linear relationship between oil and coolant temperatures even

without an oil-to-coolant heat exchanger. The addition of PCJs was simulated by increasing the oil mass flow rate to the piston undercrown and heat transfer coefficient on the piston underside, resulting in a 14 °C increase in sump temperature. Reducing the water jacket depth also resulted in a 15 °C rise in sump temperature, mainly due to an increase in piston temperatures.

2.4. Advanced lubrication systems

The investigations of Shayler et al. [4] show that following a cold start, the drop in engine friction is governed by oil film temperatures at the rubbing surfaces. These in turn are governed by local metal temperatures due to the strong thermal coupling that exists between the two. By means of a 1-D finite difference thermal model, Shayler looked at the balance of energy transfers in main bearings after a cold start. On start up and for the first minutes of engine operation, the majority of friction heating is conducted into the engine block (via the bearing shells) and into the crankshaft journal. The proportion between heat conducted to the journal and to the bearing shells was not specified in this case. Shayler et al. then investigated the effect of reducing heat transfer from the bearing shells to the block. By decreasing the contact area between the back of the shells and engine block through a chemical etching process, the rate of oil film temperature rise was increased and a reduction in friction was observed in motoring tests. A good agreement was shown between model predictions and experimental measurements. The greatest gains in friction were observed for bearings running with minimum clearance, since in this case the reduced film thickness results in higher friction losses.

The impact of the engine structure's thermal inertia on warm-up was also exposed by Law [70]. His investigation focussed on design changes that could increase the oil temperature stratification in the sump and feed hotter oil to the pump inlet. Law observed that the temperature at the oil pump pick up position remained static for up to 100s after start up, and that a maximum temperature difference of 10 °C existed between the hottest and coldest regions of the sump. Law went on to test the performance of three sump designs, all aimed at limiting oil mixing in the sump. Tests were conducted from two soak temperatures, ambient (20 °C) and -10 °C. The best design showed a maximum difference of 25 °C between the pump pick up

position and the sump average temperature. However, the improvement in main gallery feed temperature was significantly lower than this. For an ambient start the maximum improvement in main gallery feed temperature was 5 °C, this proving to have negligible effect on engine friction. For the -10 °C start, the improvement in main gallery feed temperature was more substantial, at 12 °C. The sensitivity of oil viscosity to temperature changes is greater at low temperatures, and this resulted in friction reductions of 50 kPa, or 10 % for up to two minutes after engine start up. The observations of Law show that the potential to reduce friction by raising the oil feed temperature to the rubbing surfaces was substantially reduced by heat losses in the main gallery.

The application of high pressure direct injection fuel systems and turbo-charging in diesel engines has led to higher peak cylinder pressures and, as a result, a significant increase in the thermal and mechanical loading of the piston-cylinder assembly. Recent changes to the piston bowl design, aimed at improving the airflow characteristics in modern combustion chambers, have reduced the thermal capacity of critical areas such as the piston bowl edge, making thermal management of the piston assembly even more crucial [71]. To account for this, the majority of modern diesel engines are equipped with some form of additional piston cooling [72], further to that inherently provided by the rings and crankcase oil splash, as illustrated in Figure 11. With additional cooling from the oil jets, heat conduction through the rings and skirt no longer dominates heat outflow from the piston, and instead accounts for around 50% of the heat dissipation, with the remainder being rejected to the oil. In the case of high speed diesel engines, as considered in this study, the most common setup is the cooling gallery type. In such applications, oil jet nozzles situated in the engine block direct high pressure cooling oil from the main gallery into a ring shaped cavity in the piston crown as illustrated in Figure 12. While the prime purpose of PCJs is to avoid overheating of the pistons, the additional heat input to the oil circuit is significant [68], and therefore of significance to the investigations presented in this thesis. The following outlines the major heat transfer mechanisms taking place within such piston cooling applications.

Piston Cooling Structure		Spray Cooled Type	Oil Jet Type	Cooling Gallery Type
		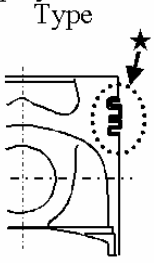	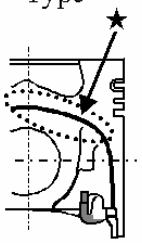	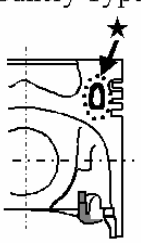
Heat Input	Combustion Bowl	100%	100%	100%
Heat Dissi-pation	Ring Belt	★ 60～70%	30～40%	10～20%
	Backside of Crown	20～30%	★ 40～50%	～10%
	Skirt	10～20%	～10%	～10%
	Cooling Gallery	—	—	★ 60～70%

Figure 11 Heat dissipation distribution for different piston cooling setups [71]

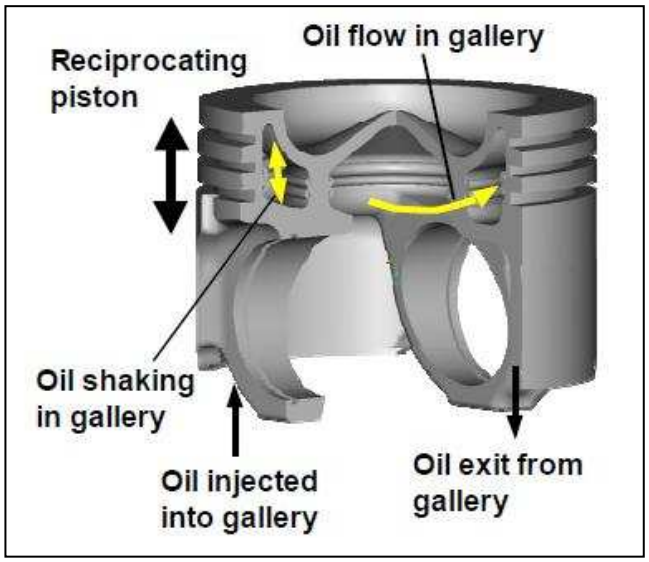

Figure 12 Cooling gallery type setup [73]

Different heat transfer mechanisms are in action with such piston cooling setups. A degree of jet impingement cooling is provided at the location where the oil jet hits the gallery surface on inlet. Although heat transfer coefficients are high in this location, the area affected is relatively small and the contribution to the overall heat transfer is therefore also small. Correlations for impingement cooling are provided by Metzger et al. [74] and Steven and Webb [75]. These correlations were adapted by Law [20] to experimental data from a Puma 2.4l engine (as used in the work reported in this

thesis), Figure 13. In this case the heat transfer coefficient is directly proportional to the oil jet flow rate which increases with engine speed up to 2000 rev/ min, but levels off at higher engine speeds due to the opening of the pressure relief valve.

The dominant heat transfer mechanism results from the agitation of oil in the gallery by the piston's high frequency reciprocating motion. This is referred to as the 'Cocktail – Shaker' effect. In this case, heat transfer depends on a number of parameters but is dominated by the piston shaking frequency (engine speed) and to a lesser extent by the amount of oil retained in the oil gallery. Engine speed and oil jet flow rate determine the oil fill ratio (the percentage of oil volume retained within the crown cavity in relation to the total cavity volume). While too low a volume of oil results in insufficient coverage of the gallery area, high oil fill ratios restrict the 'sloshing' movement of oil within the gallery and instead promote circumferential oil flow. In this case heat transfer occurs more by a 'pipe flow' mechanism, and heat transfer coefficients are generally lower than those generated through the 'Cocktail – Shaker' effect. In reality the overall heat transfer is mainly a contribution of these two effects. This characteristic is illustrated in Figure 14 [71] which shows measured variations in oil gallery heat transfer coefficient at different engine speeds and oil jet flow rates. For oil flow rates below 3 l/ min, the cocktail shaker effect dominates with the optimum flow rate appearing to be around 1.5 l/ min. Kajiwara et al. claim that the drop in heat transfer coefficient at the lowest flow rates is due to a substantial rise in oil temperature. CFD simulations by Pan et al. [73] also show that heat transfer coefficients within the cooling gallery are affected by oil fill ratio. In this case the optimum fill ratio appeared to be ~60 % but overall, the variation in gallery heat transfer coefficients, for oil fill ratios between 30-80 %, was small. Only at extremely low or high fill ratios was a clear drop in HTC observed. Law [20] predicted oil fill ratios for the piston cooling configuration used in this study by using the correlations reported by Kajiwara [71]. Law predicted that for the engine speed range considered in this study, the oil fill ratio dropped from a value of 60 % at 1500 rev/ min to 20 % at 3000 rev/ min. Law also derived the oil gallery heat transfer coefficient by adapting a Nusselt-Reynolds number type correlation for the cocktail shaking mechanism developed by Bush and London [76], Figure 13. However, comparison with empirically derived heat transfer coefficients required to match model predictions of piston temperatures with measured values proved unsuccessful.

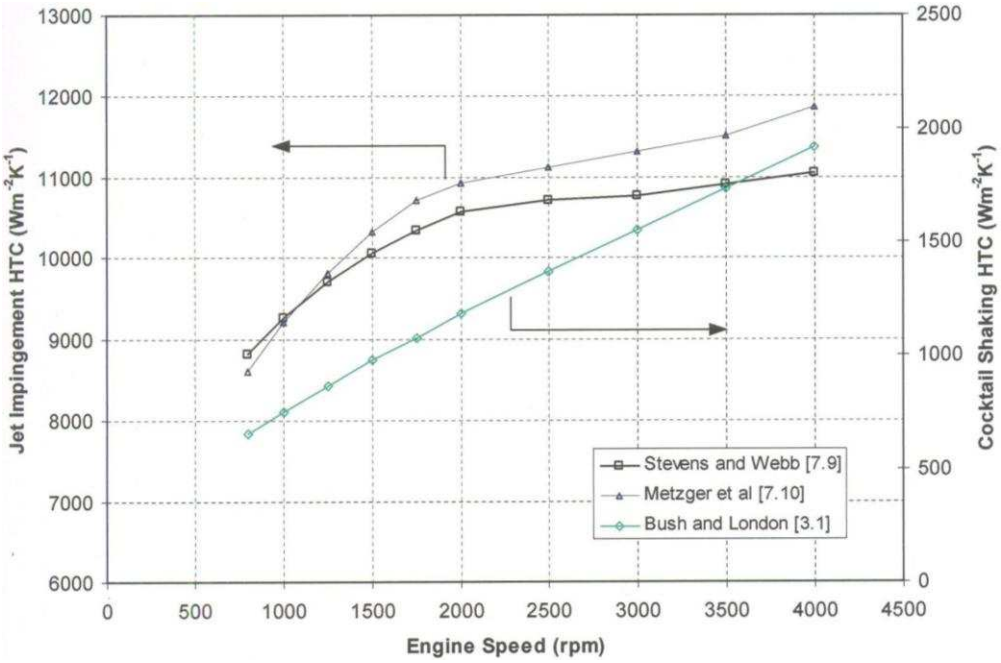

Figure 13 Jet impingement and cocktail shaking heat transfer coefficients for Puma 2.4 PCJs as derived by Law [20]

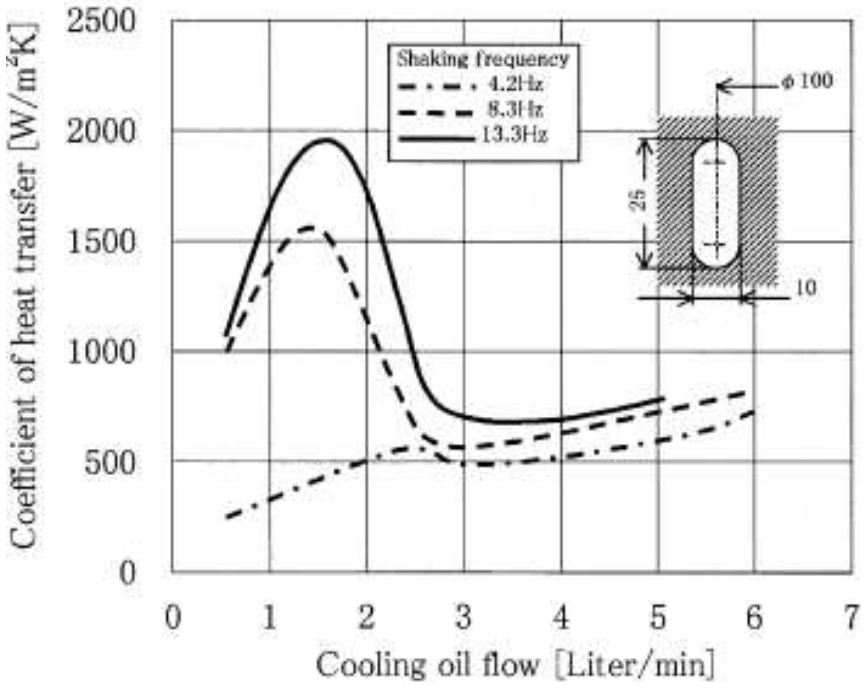

Figure 14 Measured oil gallery heat transfer coefficients [71]

2.5. Energy recovery and Storage

A generic vehicle heat balance by Kuze et al. [77] suggests that as much as two-fifths of fuel energy released from combustion is lost as heat transfer to ambient from the exhaust gases and coolant. The coolant represents a low temperature, high density

energy source which can either be stored directly or as the latent heat of another medium. Exhaust energy utilization on the other hand generally requires some form of conversion, incurring energy losses. Kuze et al. reported the development of a coolant storage system used to pre-heat the intake port walls of a gasoline engine. A hot coolant reservoir capable of maintaining coolant above 50 °C for 3 days, recovered hot engine coolant during or after engine operation. Before a cold start, the stored coolant was pumped into the cylinder head. With coolant at 75 °C, it took less than 7s for the intake port walls to reach the target temperature of 40 °C (see Figure 15). As a result, the fuel demand on engine start up was reduced considerably, by 41 %. Reduced wall wetting contributed to lower emissions of hydrocarbons while better combustion stability allowed an earlier retard in ignition timing. Increased exhaust gas temperatures led to shorter catalyst light off times which further reduced hydrocarbon emissions. Reductions in fuel consumption were achieved through a reduction in engine friction and a shorter fast-idle period.

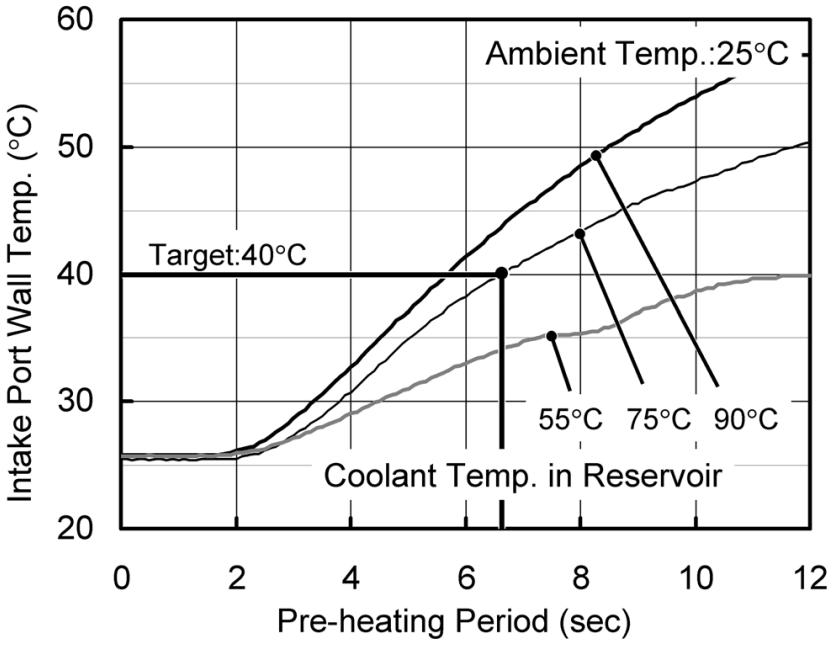

Figure 15 Intake port wall temperature response to pre-heating with coolant at different temperatures [77].

Schatz [78] also described a thermal storage device used for pre-heating the engine in cold starts. In this case energy was stored as the latent heat of a water/ salt mixture. A cylindrical unit with an outside diameter of 170 mm and 370 mm in length, provided 600 Wh when cooled from 80 to 50 °C. High rates of heat transfer (50-100 kW) were

achieved in the first 10 s of heat store operation. Tests on a 1.8 l gasoline engine started from -7 °C showed reductions in HC and CO emissions of 40 and 50 % respectively when the heat store was activated on start up. If 60s of pre-heating were applied, the reductions achieved were even greater at 70 and 80 %. Over the FTP [79] drive cycle improvements in the mpg figures of 2.4 % and 1.6 % were achieved with and without pre-heating. Schatz reported that improved engine driveability could allow modifications to the fuel management strategy to reduce fuel enrichment on start-up further reducing fuel consumption.

Diehl [80] claimed that at low ambient temperatures (-18 °C) and light engine loads, the requirements to provide cabin heat while keeping engine warm-up times short cannot be satisfied simultaneously. Diehl referred to this as a heat deficit. For a middle class vehicle with a DI diesel engine, this can be up to 6 kW during warm-up and 1-2 kW when fully-warm. Gasoline engines running stoichiometric mixtures can typically achieve 20 °C cabin temperatures after 15 mins at a 50 km/h cruise. Diesel engines can only achieve 0 °C cabin temperatures at the same operating condition. Fuel burning heaters are capable of providing up to 5 kW of supplementary heat input to the coolant at an approximate fuel consumption penalty of 0.6 l/h. Electrical heating options are also available but are limited according to the alternator power rating. The energy conversion chain generally also leads to lower efficiencies in this case and higher fuel consumption penalties when compared to fuel burning heaters. Heat recovery from the exhaust can, depending on ambient conditions, partially or totally nullify this heat deficit, with little or no fuel consumption penalty. Having validated a thermal model of the baseline engine, Diehl went on to investigate the improvement in cabin warm-up times from using an exhaust-to-coolant heat exchanger. Heat input to coolant can be further increased at the expense of an increase in fuel consumption by throttling the exhaust gas stream. Increased engine pumping work must be compensated for by increased fuelling, leading to greater heat transfer rates from the combustion chamber walls to the coolant. Higher exhaust gas temperatures also increase heat recovery in the heat exchanger. Simulations showed that to achieve similar levels of cabin heating as SI engines, exhaust throttling is in fact necessary in the case of diesel engines. The level of which and the associated fuel consumption penalty, however, was not specified. Diehl also reported the

simulation of a mid class vehicle with a diesel engine including a heat exchanger in un-throttled operation mode. The drive cycle used in this case was the ECE repeated twice from a soak temperature of -7 °C. Fuel consumption with the heat exchanger was marginally lower than for the baseline vehicle. Coolant temperatures were approximately 7 °C higher at the end of the drive cycle and cabin heating levels were raised by 0.5 kW.

It is estimated that for 90 % of the time an engine is utilized at 30 % of its rated power [81]. The cooling system, however, must be designed to cope with extreme driving conditions, such as vehicle accelerations and hill ascents. Vetrovec [81] proposed a passive heat accumulator in the form of a phase change material introduced in the radiator loop to average out these peak heat loads and allow downsizing of the cooling system. Vetrovec described phase change materials with a latent heat of fusion as high as 339 kJ/kg, allowing coolant mass to be reduced from 10 to 7 kg. A reduction in radiator size was also possible, resulting in packaging advantages with no weight penalty. The down sized cooling system showed, through a reduction in thermal inertia, a superior warm-up performance together with better performance in high load transient conditions.

An increase in ambient air temperature causes a drop in radiator performance and must be taken into account in the specification of the cooling system. Hughes et al. [82] suggested designing the cooling system for the mean operating condition and compensating for extreme cases by de-rating engine performance. An increase in ambient temperature could also be compensated for by allowing a higher coolant temperature, but this could have serious consequences on engine life due to increased thermal stresses in the engine structure. A forward-facing Simulink model was developed to assess the feasibility of a de-rating strategy for two benchmark tests. These simulated the vehicle being driven on level ground and on a 6 % incline. The model was representative of a minivan style vehicle with a V6 gasoline engine. For level ground driving and an ambient air temperature of 25 °C, a maximum speed of 108 mph was achieved, but coolant temperature reached 144 °C in this case. This is higher than the coolant's boiling point and hence unacceptable. However, de-rating engine power and dropping vehicle top speed to 104 mph was enough to control the coolant temperature to 125°C, deemed an acceptable upper limit. If an ambient

temperature of 45 °C is considered then engine power would have to be de-rated further dropping vehicle speed to 97 mph. Hughes claimed that without engine de-rating, the cooling capacity would have to be increased by 33 %.

BMW [83] developed a steam-powered auxiliary drive called the Turbosteamer which, when tested in conjunction with a 1.8l four cylinder gasoline engine, reduced fuel consumption by up to 15 % while generating an additional 14 hp, or 20 Nm of additional torque. Up to 80 % of exhaust heat is recovered by means of a heat exchanger. This generates steam which is then led to an expansion unit linked to the engine crankshaft. Honda [84] is also looking at exhaust heat recovery, through the integration of a Rankine cycle co-generation unit, with the aim of providing an alternative means of recharging the battery pack in hybrid vehicles. Honda opted specifically for the Rankine cycle because the exhaust gas temperature range in IC engines is particularly suited to this kind of thermodynamic cycle. Honda claimed that at 100 kph, engine thermal efficiency was improved by 3.8 %, and that on the US highway cycle, the Rankine cycle was capable of generating three times as much energy as the vehicle's regenerative braking system. The test vehicle used a 2.0 L gasoline direct injection engine with a modified cylinder head incorporating insulated exhaust ports. The evaporator unit was incorporated into the catalytic converter to use the reaction heat of the catalyst while the expander unit was an axial piston swash plate type. Steam was maintained in the range of 400-500°C at a pressure of 7-9 MPa, depending on engine load. Maximum power provided by the expander was 32 kW, while a maximum thermal efficiency of 13 % was achieved at 23 kW.

Crane et al. [85] looked at integrating a thermoelectric device into the radiator for waste heat recovery. Heat recovery from the exhaust could potentially offer greater benefit than heat recovery from the coolant, as the higher temperature promotes higher efficiencies. However, this requires an additional heat exchanger, usually integrated into the muffler, and is hence a more expensive solution than simply modifying the radiator. Increased exhaust back pressure is also undesirable. The scope of Crane's investigation was to determine whether a thermo electric heat recovery device could replace the alternator, thus reducing engine parasitic losses. Typical under hood temperatures for a warm engine are in the region of 37 °C. Given

that the maximum allowable coolant temperature is 120 °C, the maximum working temperature difference available to the thermoelectric device is about 80 °C. A numeric model was developed in Matlab to quantify the power output achievable by such thermoelectric devices together with the radiator performance loss. Results showed that, even with current thermoelectric technology, power outputs of 1-2 kW over a range of engine operating conditions are possible. The heat rejection penalty can be compensated for by an increased water pump flow rate, the additional work of which is also offset by the energy recovered.

2.6. Advanced cooling systems

The cooling system serves a number of purposes, from protecting thermally loaded components within the engine, to providing a means for cabin heating. Pang et al. [86] presented an overview of possible design changes and thermal management strategies that could be implemented into current cooling systems to improve engine overall efficiency. These include split cooling systems which have separate coolant circuits for the cylinder head and block. Allowing the head to run cooler improves volumetric efficiency and enables an increased compression ratio for greater thermal efficiency. The block, on the other hand, can be run up to 100 °C hotter than the head according to Finlay et al. [87] reducing friction. Kobayashi et al. [88] reported that the minimum practical coolant temperature in the cylinder head was 50 °C, allowing an increase in compression ratio from 9:1 to 12:1. This brought a benefit of 10 % in engine power and a 5 % improvement in part load fuel consumption. HC emissions were increased due to the combined effect of lower exhaust gas temperatures and increased quenching on the cooler combustion chamber surfaces. Robinson [89] pointed out that because the compression ratio was increased by ‘skimming’ the bottom deck of the cylinder head, this effectively brought the coolant in closer proximity to the edges of the wedge shaped combustion chamber, and hence closer to the end-gas region. The increased knock resistance was therefore believed to be partly due to a lower coolant temperature, but also due to a cooler end-gas region in the combustion chamber.

Precision cooling involves designing the cooling jacket to target thermally critical areas such as the exhaust valve bridge with higher coolant speeds, increasing heat removal rates. This allows a more uniform temperature distribution with a lower overall coolant flow rate. Clough [90] claimed a reduction in coolant pump power of 54 % through precision cooling. Brace et al. [91] also claimed that whereas conventional cooling systems with mechanically driven water pumps typically require between 2-2.6 l/min/kW, using an electric water pump and diverter valve, together with precision cooling and nucleate boiling sensing, may allow flows of under 1 l/min/kW. Brace et al. went on to describe simulations of a cooling system employing an electric coolant pump and water diverter valve. Pump speed in the case of the electrical system was reduced while better control offered by the diverter valve allowed lower system hydraulic losses when compared to a conventional system using a wax filled thermostat. Hydraulic power loss in the electrical system was reported to be two orders of magnitude lower than that in the mechanical system. Clough claimed that whereas coolant heat rejection was reduced with precision cooling, lower coolant flow rates and a smaller coolant volume resulted in shorter warm-up times. Working with a 4-valve per cylinder gasoline engine, Clough observed that a 64% reduction in total coolant volume was possible, reducing engine warm-up time by 18% when the engine was operated at 2000 rev/ min and 100 Nm brake load. The warm-up time in this case was defined as the time to achieve 80 °C coolant temperature from a 20 °C start. Clough also observed an increase in full load BMEP of 0.6-0.7 bar across the speed range. The increase in power was partly attributed to an increased knock resistance and volumetric efficiency, but also to a reduction in engine friction and water pump power demand. Precision cooling depends on good heat conduction characteristics and is hence generally limited to aluminium cylinder heads.

2.7. Summary and Discussion

The majority of researchers engaged in studies of engine thermal management use lumped-capacity models. These models are usually preferred as they are less computationally intensive than their finite element counterparts. While crank-angle resolved friction models are widely used to model transient engine response [51], their increased complexity when compared to mean value models is not justified in engine performance and thermal modelling applications. Mean-value friction models as developed by Patton [56] are still the most widely used. As they predict fully warm engine friction, a correction based on oil temperature is generally applied throughout the warm-up phase [4] [5].The effect of engine load on FMEP is weak [39] and for the modelling purposes presented in this thesis can be neglected. Some uncertainty remains in modelling the percentage of friction heat transferred to the rubbing surfaces and that retained in the oil film. Different approaches are presented: Veshagh [64] and Christian [9] apply a split to the total friction value, while Kaplan [69] and Zoz [67] differentiate between the different rubbing surfaces.

Generally measures to shorten engine warm-up times can be categorised as heat recovering, heat storing or heat preserving. The requirement to provide cabin heat conflicts with that of achieving short warm-up times. Heat recovery from the exhaust has been identified by Diehl [80] as one possible solution to satisfy both. Heat storage has been shown to have additional advantages to shortening warm-up time in the case of gasoline engines. Pre-heating the inlet ports with hot coolant also reduces HC emissions on engine start up [77]. Many of the above thermal management studies are centred on the coolant circuit. Nonetheless, the greatest benefits in fuel consumption following a cold start are achieved when the oil warm-up phase is shortened. The interaction of oil with the lower regions of the engine block was identified by different researchers as the main reason for the low rates of oil temperature rise. Jarrier [59] claimed that the interaction of the oil mist with the crankcase surfaces resulted in friction penalties of up to 5% over the NEDC. Law [70] investigated a novel sump design to increase the oil temperature stratification within the sump and feed hotter oil to the pump pick up. While an increase in oil temperature was realized at the pump pick up, heat losses from oil flowing in the main gallery damped the temperature rise in the main gallery reducing the friction

benefit achieved. Reducing heat losses from the oil to the engine structure may therefore offer an opportunity to promote faster oil warm-up rates which has not been well exploited as yet. The findings of Law also highlight some of the uncertainties introduced when friction is modelled using oil temperatures remote from the rubbing surfaces. Characterising friction using oil temperatures local to the rubbing surfaces is one area of model development which could improve the robustness of friction predictions, particularly when conditions in the oil circuit are perturbed from the norm.

Shayler et al. [4] investigated the thermal-friction interactions in main bearings using modelling and experimental measurement. Reductions in bearing friction were achieved by reducing heat transfer from the oil film to the bearing shells. However, no means to insulate the crankshaft journal was identified, and is one possible area where further reductions in friction could be made.

Thermal-friction interactions in the oil circuit are inherently complex to model and difficult to measure. This is confirmed by the contradictory predictions of heat flows in the oil circuit [68] [67] and the various modelling approaches adopted by different researchers [69] [34]. When used in conjunction with engine testing, PROMETS is particularly suited to help quantify the major thermal-friction interactions in the oil circuit thus identifying means to shorten oil warm-up times and reduce the friction penalty following a cold start.

Chapter 3 - PROMETS Theory

3.1. Introduction

This chapter explains the theory behind each major section within PROMETS, starting from the lumped mass engine representation to the various sub-models providing the required boundary conditions. Particular attention is given to the gas-side heat transfer calculation, friction and lubrication circuit models. In-cylinder heat release is calculated according to a time-averaged correlation initially developed by Taylor and Toong [92] and extended by Shayler et al. [29]. The friction models are heavily based on the correlations developed by Patton et al. [56], but modified to account for the findings of Leong [39]. Friction heat dissipation into the lubricant and engine structure is reviewed, as is modelling of heat transfer in the oil galleries and interaction of oil mist with the piston underside and engine crankcase. The following is mainly a summary of previous model developments originally presented in papers [9] [58] and PhD theses at the University of Nottingham [32] [30]. A number of features of the model are therefore only mentioned briefly with greater detail having been reported by previous researchers.

As will be explained in due course, a number of the model developments and computational investigations presented in the thesis have made use of test data from a Ford Puma 2.4l diesel engine, details of which can be found in Appendix A. These test facilities are described in considerable detail in [20]. Of the test data used, some were provided by previous researchers and these are referenced accordingly, while other data were gathered during engine testing carried out by the author. Additional test equipment was also set-up by the author to carry out the experimental investigations described in Chapter 6 regarding the effectiveness of pre-heating the oil feed to the main bearings.

3.2. Generic Engine Representation and Lumped Capacity Analysis

The version of PROMETS used in the work reported here makes use of a single representative cylinder of a 4 cylinder engine. All components with significant impact on the thermal behaviour of the engine are included in this representation. These include the cylinder head and engine block castings, piston and valve train

assemblies, oil and coolant masses, Figure 16. The coolant external circuit (radiator) is not modelled while components in the internal circuit which are modelled include the EGR cooler and filter cooler assembly. Although not forming part of the core engine structure, components in the coolant circuit like the water pump, hoses and thermostat housing, are also accounted for. The same applies for the oil pump. However, engine peripheral components like the alternator, starter motor and flywheel are considered to be sufficiently thermally detached to have insignificant influence on the engine's thermal behaviour. The intake and exhaust manifolds are also not modelled. However, heat transfer from the exhaust manifold to the cylinder head is accounted for in the gas-side heat transfer calculation, Section 3.5.1.

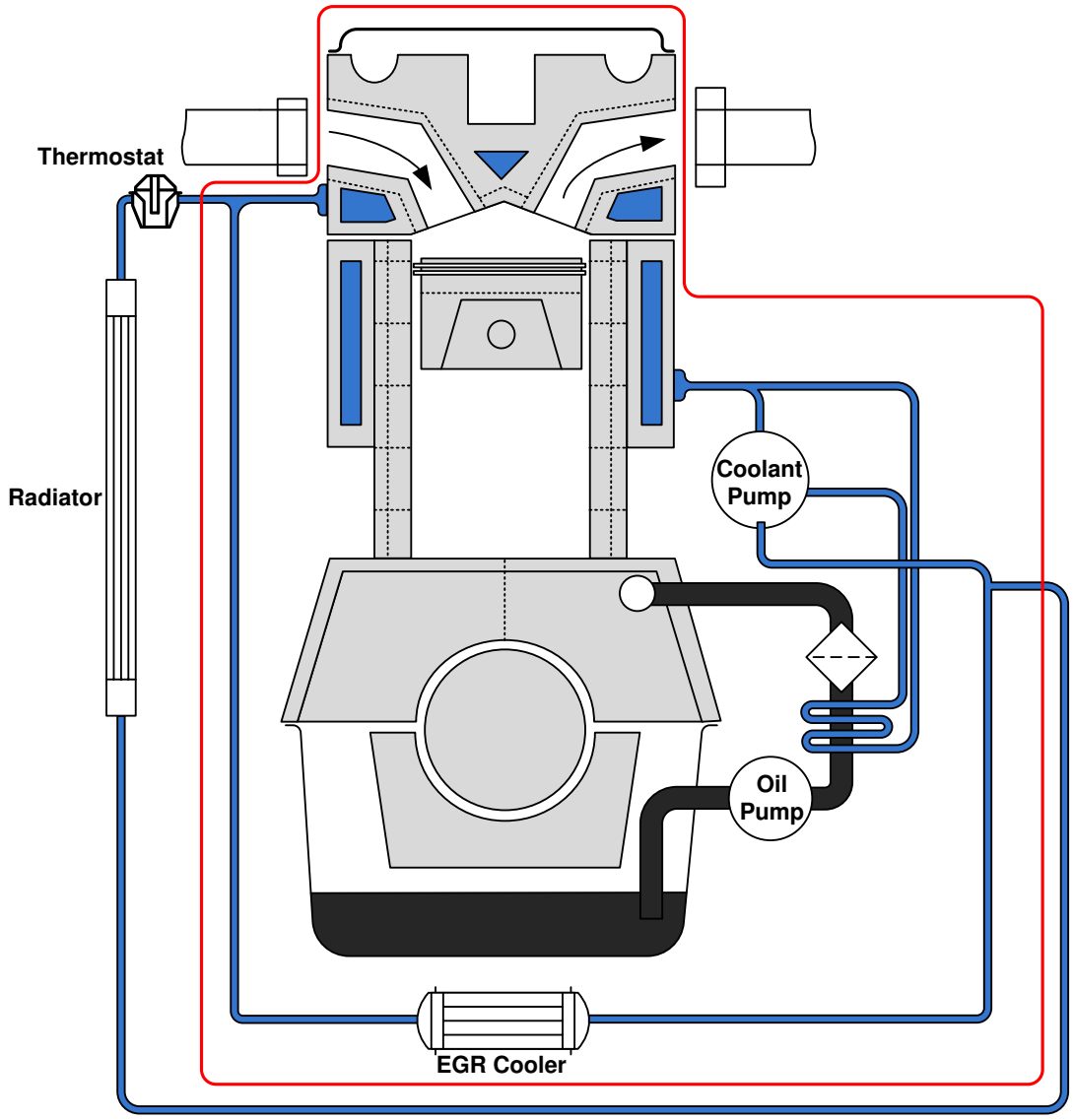

Figure 16 PROMETS system boundary. Engine components inside the red line are modelled.

An illustration of how the engine structure is divided into elements is given in Figure 17. Elements are also allocated to the valve stems but are not shown below. Historically, 41 elements have been used for engines with an in-line cylinder arrangement and this approach was initially also adopted here. However, as part of integrating the bearing model into PROMETS (see Chapter 5), additional elements were included in the engine crankcase to better represent the main bearing journal assembly. The cylinder head is assumed to be thermally isolated from the engine block due to the presence of the gasket [93]. This is generally true for engines with conventional cooling systems in which coolant temperatures in the block and head are very similar. This minimises the temperature difference and therefore heat exchange between the head and block. However, this assumption may not be valid for split cooling designs, in which the temperature difference between the head and block may be as high as 100ºC. In this case suitable thermal connections would need to be set-up between elements in the head and block to account for heat conduction between the two.

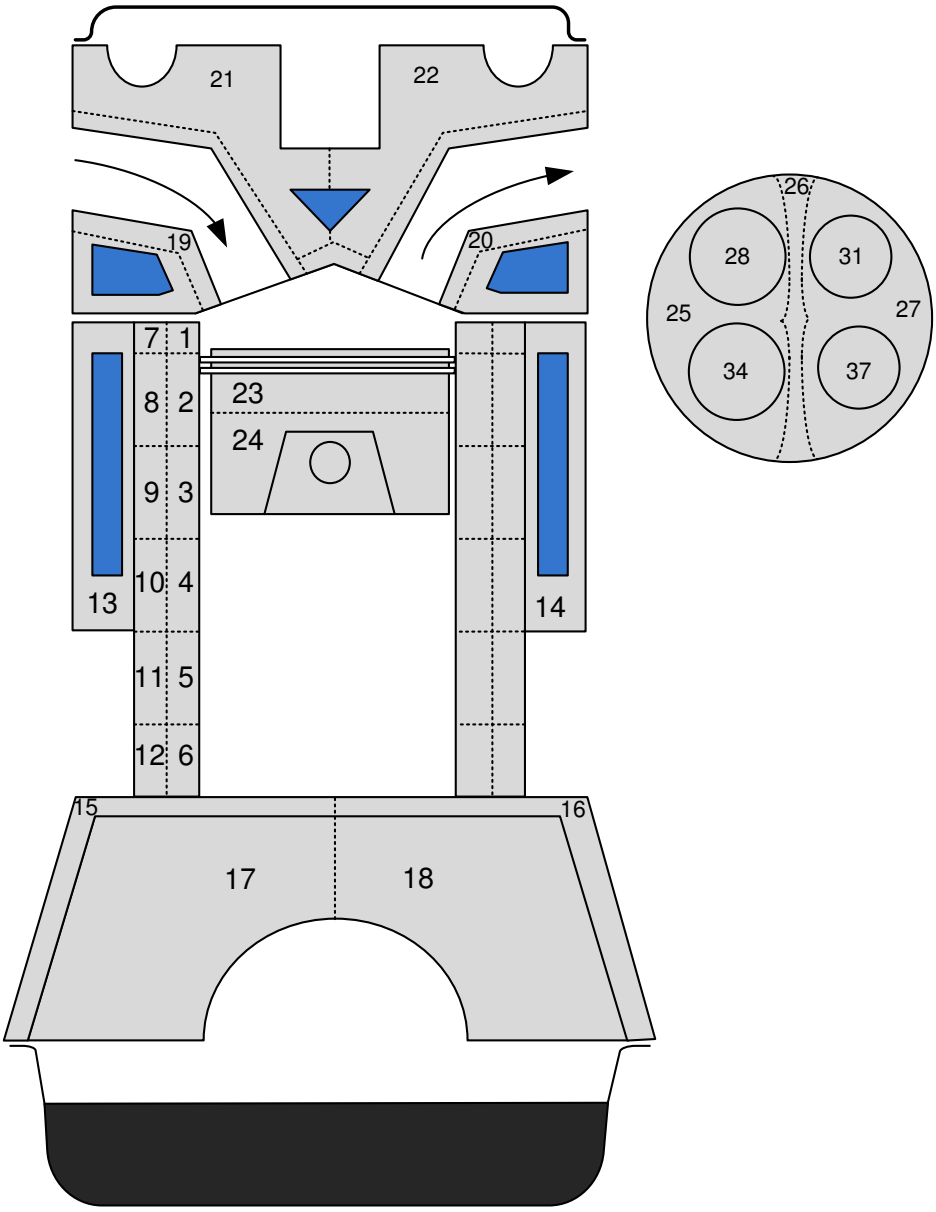

Figure 17 PROMETS generic engine representation

Each lumped mass element is assumed to have a uniform temperature. An energy balance for an element 'i' thermally coupled to an element 'j' can be written as [30]:

$$\dot{Q}_i + \sum_j \frac{T_j^p - T_i^p}{R_{ij}} = C_i \left(\frac{T_i^{p+1} - T_i^p}{\Delta t} \right) \qquad \text{Equation 3}$$

where Δt is the time-step length, $\dot{Q}_i$ is the element's internal heat generation and R_{ij} is the conductive resistance between the elements and

$$C_i = \rho_i c_i \Delta V_i \qquad \text{Equation 4}$$

where ρ_i is the element density, c_i is the element specific heat capacity and ΔV is the element volume. In PROMETS an explicit forward difference method is used; Equation 3 is re-arranged such that the temperature of each element at a time step **p+1** can be determined from temperatures of the element, and its adjacent elements at the previous time step **p**:

$$T_i^{p+1} = \frac{\Delta t}{C_i} \left[\dot{Q}_i + \sum_j \frac{T_j^p - T_i^p}{R_{ij}} \right] + T_i^p \qquad \text{Equation 5}$$

3.3. Accuracy & Stability Criteria

For the approximation of a uniform element temperature to be valid two different criteria must be met depending on whether the element is in thermal contact with another element or a fluid. For the first case the temperature difference between the two elements must be kept to a minimum and both elements should contribute equally to the thermal resistance across the interface. The thermal resistance between two elements 1 and 2 is defined according to,

$$R_{1\to 2} = \frac{1}{A_{12}} \left(\frac{\Delta X_{1\to 2}}{k_1} + \frac{\Delta X_{2\to 1}}{k_2} \right) \qquad \text{Equation 6}$$

where k is the material thermal conductivity.

The contact area A_{12} and the conduction path length ΔX are as defined in Figure 18. The number and size of the elements are chosen to avoid large thermal gradients in any of the elements and this was based on comparisons of predicted temperature fields and heat flows with those from FE simulations [30]. In areas where the thermal response is of particular interest, such as regions of high heat flux like in the cylinder liners and cylinder head, a larger number of smaller elements are used.

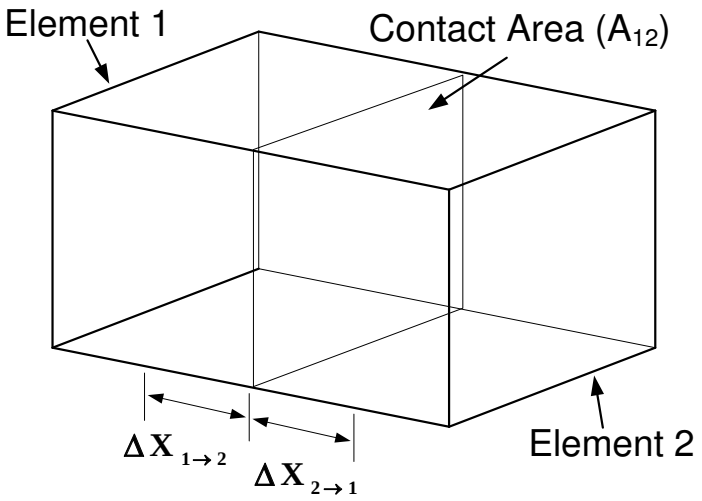

Figure 18 Definition of conductive resistance between elements. ΔX is the distance from each element's centroid to the contact area.

For elements in contact with a fluid, a parameter called the Biot number [63] can be defined as:

$$\mathbf{Bi} = \frac{\mathbf{hV}}{\mathbf{kA}} \qquad \text{Equation 7}$$

A Biot number well below unity implies that the resistance to heat conduction within the element is small when compared to the thermal resistance to convection at the element's surface. This ensures that a uniform element temperature is maintained during thermal transients. For $Bi \leq 0.1$ the error in the lumped capacity assumption is 5 % or less [63] and should be ensured for elements in which the temperature response is of particular interest. Finally, for Equation 5 to be numerically stable a limit must be placed on the time step size. This can be estimated by considering the case when the internal heat generation $\dot{\mathbf{Q}}_i$ =0. Then:

$$\left[1 - \frac{\Delta t}{C_i}\sum_j \frac{1}{R_{ij}}\right] \geq 0 \qquad \text{Equation 8}$$

The significance of the above criterion for the numerical stability of the model can be illustrated by considering the case of an element i adjacent to an element j at a lower temperature. If the above condition is not satisfied, element i will be at a lower temperature than element j on the following time step contradicting the direction of heat flow. The maximum allowable time step is calculated for all elements in the model with the smallest one being used for the simulation. Typically the maximum allowable time step for thermal models generated in PROMETS is around 0.3s [34], but a time step of 0.1s is generally used. Nonetheless, while the above applies to the majority of heat transfer processes within the engine structure, thermal-friction interactions at rubbing surfaces are particularly difficult to model using explicit time marching schemes. On start-up, rapidly changing temperatures coupled to the high sensitivity of oil viscosity to changes in temperature, mean the computation of friction and temperature at friction surfaces is prone to become unstable. Normally empirical corrections are used in PROMETS to model friction in these early seconds of engine operation which do not require the calculation of film temperatures, as described in Section 3.6. In Chapter 5 details of a model extension to calculate temperature and friction dissipation in main bearing films are described as an example of one way of characterising friction using temperatures local to the rubbing surfaces and the improvement in the predictive power of the model from using this approach.

3.4. Model Inputs

In addition to the engine geometry data required by PROGEN to generate the lumped mass engine representation, the user must define the initial state of the engine, i.e. oil, coolant and metal starting temperatures. Operating conditions are also required to define the case to be simulated, whether it is a drive-cycle, steady state or warm – up simulation. For the diesel version, the operating conditions input file consists of 11 variables specified in time. Engine speed, brake load, heater matrix airflow, EGR ratio, road speed and supplementary heat input to the coolant must be defined by the

user while AFR, fuel flow rate, coolant flow rate, heater matrix coolant flow rate and exhaust gas temperature are optional as they can be predicted in PROMETS. In the following work, initial simulations (presented in Chapters 4, 5 & 6) were carried out using pre-defined fuel flow rates representative of the fuelling levels used on the test bed. In these cases assessment of the thermal behaviour of the model was the prime objective of the work, specifically through a comparison of predicted and measured oil and coolant temperatures. In Chapter 7 the aim was to assess potential fuel savings from an improved engine warm-up characteristic. In this case the fuel prediction calculation in PROMETS was enabled and is explained in Section 3.10.

3.5. Gas-side heat transfer

In-cylinder heat flux is highly unsteady and non-uniform in nature. It is highest during the early phases of the power stroke, reaching as high as 10MW/m^2 [2] but effectively drops to zero during the remainder of the engine cycle. Different types of correlations have been developed to describe in-cylinder heat transfer. They can be broadly classified as of three types. **Time averaged correlations**, as used in PROMETS estimate the mean heat flux over the engine cycle and are useful in heat balance calculations where an estimate of the bulk heat transfer to the engine structure is sufficient. Correlations to obtain the **instantaneous spatial-averaged** heat flux, as derived by Annand [94], are useful in engine performance, efficiency and emissions predictions. In this case the spatial variation in heat flux is not of interest, but knowledge of the time-dependent heat losses is necessary for net heat release calculations. Finally correlations to estimate **local instantaneous** heat transfer [95] are particularly useful in thermal stress analyses.

Taylor and Toong [92] developed a cycle-averaged correlation for gas side heat transfer in the form of a Nusselt-Reynolds number relationship by measuring the heat rejected to coolant from the cylinder head of four engines. The gas-side heat transfer was calculated from a heat balance between the heat rejection to coolant, estimated engine friction losses and heat transfer across the oil cooler. However, Shayler et al. [29] showed that this was an incomplete heat balance and carried out revisions to the correlation. The following section briefly presents the revised heat transfer correlation which is currently implemented in PROMETS.

3.5.1. In-cylinder and Exhaust Port Gas-side Heat Transfer (QC_1C_2)

Under steady state conditions the change in internal energy of the engine structure control volume is zero, such that an energy balance can be written between energy flows into the structure and energy flows out:

$$\dot{Q}_{cyl} + \dot{Q}_{pt} + \dot{Q}_{ex.man} + \dot{Q}_{fric} = \dot{Q}_c + \dot{Q}_b + \dot{Q}_{oc} \qquad \text{Equation 9}$$

From the above terms, only $\dot{Q}_{cyl}$ and $\dot{Q}_{pt}$ represent gas-side heat transfer contributions. $\dot{Q}_c$ and $\dot{Q}_b$ represent heat rejection to the coolant and ambient respectively, and $\dot{Q}_{oc}$ is heat transfer across the oil cooler. Given that the rate of heat conduction from the exhaust manifold to the cylinder head ($\dot{Q}_{ex,man}$) can be related to the exhaust port heat flux ($\dot{Q}_{pt}$), these two terms are combined together [96]. The gas side heat transfer can then be expressed as:

$$\begin{aligned}\dot{Q}_{c1c2} &= \dot{Q}_{cyl} + \dot{Q}_{pt} \\ &= C_1(A_{cyl,eff} + C_2 A_{ex,pt})\frac{k_g}{B}(T_{g,a} - T_{cool})Re_g^{0.7}\end{aligned} \qquad \text{Equation 10}$$

$A_{ex,pt}$ is the exhaust port area and $A_{cyl,eff}$ is the cylinder effective area. The gas-side Reynolds number is defined as a function of the fuel mass flow ($\dot{m}_f$):

$$Re = \frac{4\dot{m}_f(1 + AFR/(1 - EGR))}{\pi B \mu_g} \qquad \text{Equation 11}$$

In the case of diesel engines, the mean effective in-cylinder gas temperature, $T_{g,a}$, is defined as a function of exhaust gas back pressure, P_{ex} and equivalence ratio ϕ [33]:

$$T^*_{g,a} = 340 + 0.12*10^{-3}P_{ex} + (310 + 0.47*10^{-3}P_{ex})\phi \qquad \text{Equation 12}$$

Exhaust manifold pressure is in turn defined as a function of exhaust mass flow rate and engine swept volume [33].

To account for turbo-charging and the influence of higher intake temperatures, a correction is applied to the effective gas temperature, as follows:

$$T_{g,a} = T^{*}_{g,a} + 0.35 * (T_i - 298) \quad \text{Equation 13}$$

The cylinder effective area is calculated from an algorithm developed by Christian [30], which accounts for the variation in heat flux along the cylinder liner. An approximation to this algorithm is the following:

$$A_{cyl,eff} \approx [0.38\pi B(B+S)] \quad \text{Equation 14}$$

Heat transfer to the liner, piston crown and cylinder head are calculated assuming a uniform in-cylinder flux density defined as:

$$\dot{q}'' = \frac{\dot{Q}_{cyl}}{A_{cyl,eff}} \quad \text{Equation 15}$$

Heat transfer rates to the cylinder head and piston crown are determined by multiplying $\dot{q}''$ by their respective areas. For the liner, a function as defined by [30], relates heat flux at different points down the liner to the value at the top which is always exposed to the combustion gases.

C_1 and C_2 are empirically determined constants taken from [33]. For DI diesel engines, as considered in this investigation, C_1=2.3 and C_2=1.5. The C_1 value assigned for diesel engines is typically higher than in gasoline variants due to radiative heat transfer in the former. In diesel combustion the flame is highly luminous and soot particles form at an intermediate phase in the combustion process [2]. While radiative heat transfer in spark-ignition engines is small when compared to the convective component, it contributes 20 -30% of the total in-cylinder heat transfer in the case of diesel engines. The mean effective gas temperatures in diesel engines is however, lower than in spark-ignition engines, due to the typically low equivalence ratios with which they operate. This partly offsets the higher C_1 value such that overall gas-side heat transfer rates in diesel and gasoline engines are comparable.

3.6. Friction Model

The friction formulations implemented in PROMETS are a development of the PNH model [56]. This is a mean value type model which uses lubrication theory together with experimental measurement to derive the fully warm FMEP values of the four main friction sub-assemblies: the piston group, crankshaft assembly, valve-train and auxiliary components. Comparison of model predictions with experimental measurements by Leong [39] reveals good agreement under fully warm conditions. The calculated fully-warm friction components and their variation with engine speed for a 2.4l Puma diesel engine (see Appendix A) are illustrated in Figure 19. The variation with engine speed of each friction contribution reflects the friction regime in which that particular friction group operates. Journal bearings and piston ring-liner contacts are predominantly hydrodynamic and as a result their FMEP contribution increases with engine speed. The valve train predominantly operates in boundary and mixed lubrication such that its FMEP remains relatively constant as engine speed increases. As the piston and bearing friction contributions are dominant, total engine FMEP increases with engine speed.

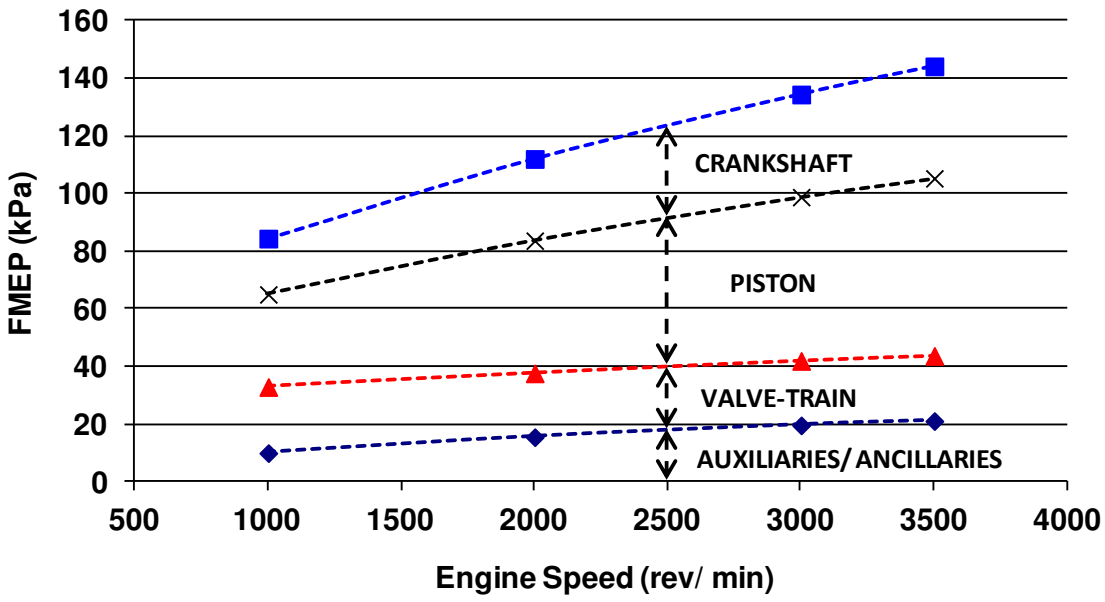

Figure 19 Predicted fully-warm (90°C) FMEP breakdown

During warm-up the fully warm FMEP values must be corrected to account for a higher oil viscosity at low temperatures. As the major sources of engine friction

operate in the hydrodynamic lubrication regime, during warm-up, engine friction can be shown to follow a power-law dependence on oil viscosity [30] according to the following equation:

$$\mathbf{FMEP_{wu}} = \left(\frac{\mu_{\mathbf{oil}}}{\mu_{\mathbf{oil,\,fw}}} \right)^{\mathbf{n}} \mathbf{FMEP_{fw}} \qquad \text{Equation 16}$$

where the fully warm temperature is taken to be 90°C. In reality fully-warm oil temperature can be several tens of degrees hotter than this. A temperature of 90ºC is used as reference given that viscosity changes slowly once oil temperature rises above 90ºC. Based on the observations of [33] the exponential n was set at 0.24 for diesel engines. As the engine structure warms up, changes in the operating clearances of various components also lead to changes in friction further to those resulting from a reduction in oil viscosity. The viscosity based correction in Equation 16 encompasses the overall effect of temperature on a number of parameters and their influence on engine friction. However, these are assumed to be of secondary importance when compared to the effect of reducing viscosity.

The oil dynamic viscosity (Pa.s) is in turn calculated according to the Vogel equation [97] [98]:

$$\mu = \mathbf{k_v}\, \mathbf{exp}\left(\frac{\theta_1}{\mathbf{T} + \theta_2} \right) \qquad \text{Equation 17}$$

where k_v, θ_1 and θ_2 are constants determined for a specific oil and T is temperature (°C). For an SAE 10W-30 oil grade, as used in this study, these constants are summarized in Table 2 and the variation of oil viscosity with temperature is illustrated in Figure 20.

Oil Type	k_v (Pa.s)	θ_1 (°C)	θ_2 (°C)
SAE 10W-30	5.68×10^{-5}	1171.2	126.9

Table 2 Vogel parameters for SAE 10W-30 oil [20]

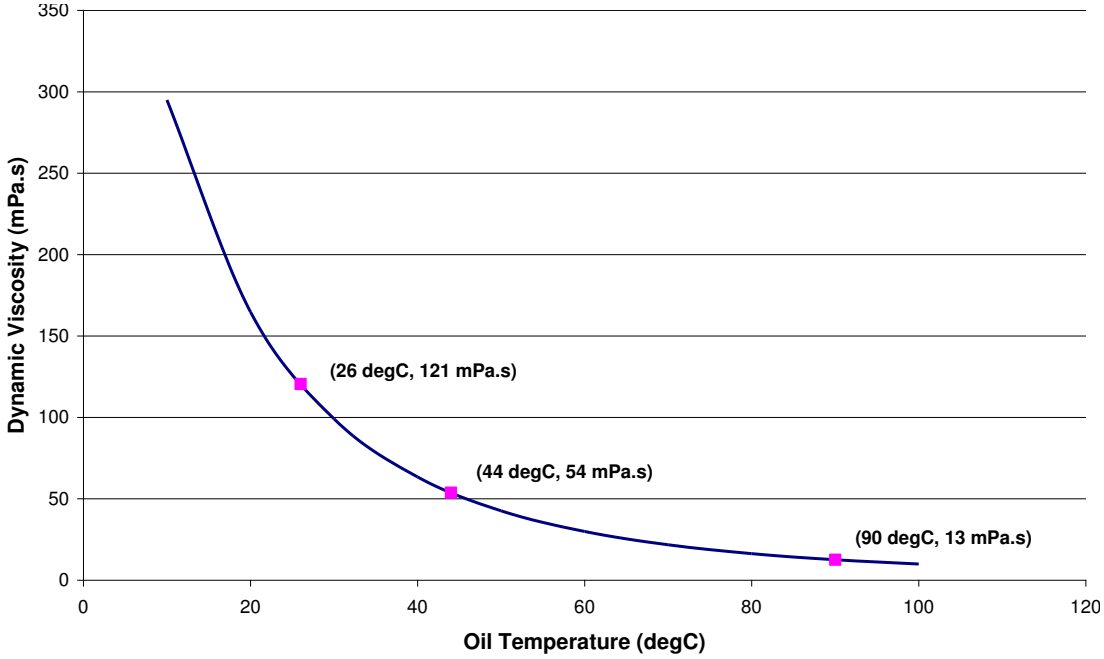

Figure 20 Viscosity-temperature relationship as predicted by the Vogel equation for SAE 10W-30 oil

During the first minute or so of engine operation friction levels are higher but drop more rapidly than predicted by Equation 16. Friction dissipation at the rubbing surfaces is determined by local oil film temperature and viscosity. Local heating at the friction surfaces raises local oil film temperatures rapidly such that a sharp drop in friction results. This rapid rise in oil temperature, however, is not measured in the bulk oil due to a strong thermal coupling with the lower engine block and the temperature stratification occurring within the sump [70]. This causes a divergence from the power law dependence between engine friction and oil viscosity when evaluated using bulk oil temperature, as illustrated in Figure 21.

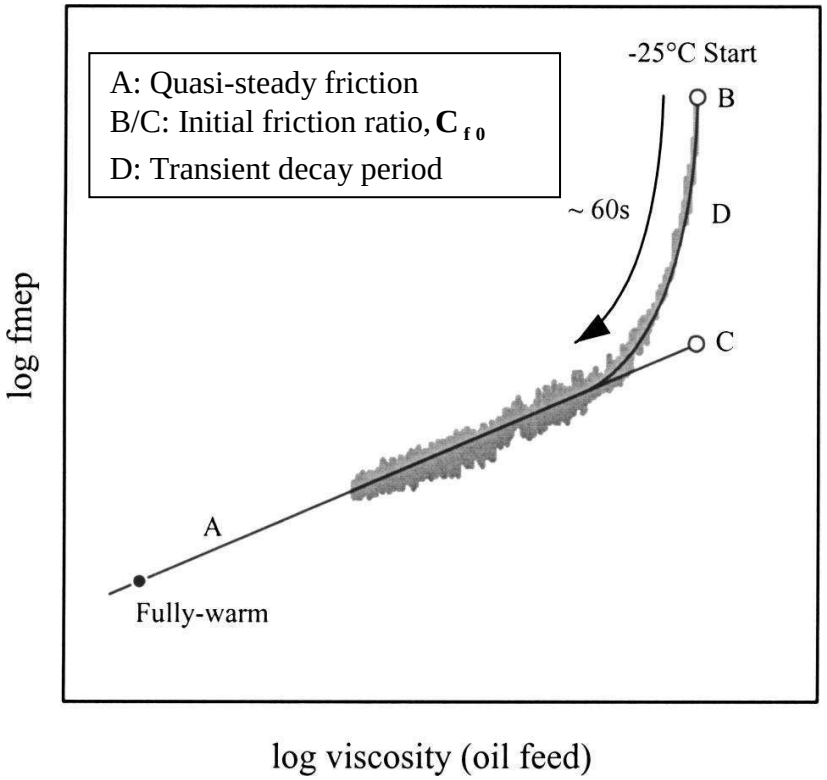

Figure 21 FMEP – oil viscosity characteristic during engine warm-up [4]. The trend illustrated is for a case when oil viscosity is determined using temperatures in the oil sump or main gallery.

Bulk oil temperature is generally easier to measure and predict than oil film temperatures, meaning that bulk oil viscosity provides a convenient way of characterising engine friction. To account for the variation between local and global oil temperatures in the early phases after start up, a correction is applied up to the point where quasi-steady state thermal conditions are reached. At this point local thermal conditions at the friction surfaces stabilise such that the bulk oil and oil films at the rubbing surfaces warm up at similar rates. Experimental measurements by Burrows [40] on different engine types reveal that the initial friction ratio (B/C in Figure 21) is a function of the starting oil temperature, $T_{oilfeed}$:

$$C_{f0} = 1 + 0.55e^{-T_{oilfeed}/35} \qquad \text{Equation 18}$$

Throughout the transient decay period, the quasi-steady value of friction calculated from Equation 16 is adjusted by multiplication with the factor C_f, where:

$$C_f = (C_{f0} - 1)e^{(-t/\tau)} + 1$$ Equation 19

The rate of decay of the initial friction spike is determined by the time constant τ. According to Baylis [33] a value of 50 s provides a good approximation for modelling engine behaviour and has been adopted in this work.

Historically, a universal friction index n was used to apply the oil viscosity correction to the fully-warm total engine friction value. In reality, because different engine components operate under different lubrication regimes, their friction contributions show a different dependency on oil viscosity. Leong [39] performed tear-down and motoring tests to derive separate friction decay indices for the individual friction groups. The revised formulations, as used in this investigation, are explained briefly and the various indices and constants are summarised in Appendix A.

3.6.1. Crankshaft group

The crankshaft friction contribution is composed of two components. The greatest contribution comes from hydrodynamic friction dissipation in the main bearings. This term is corrected throughout warm-up according to oil viscosity,

$$\mathbf{fmep_{crank}} = \mathbf{C_{cb}}\left(\frac{\mathbf{N^{0.6} D_b^3 L_b n_b}}{\mathbf{B^2 S n_c}}\right)\left(\frac{\mu}{\mu_{ref}}\right)^{\mathbf{n}} + \mathbf{C_{cs}}\left(\frac{\mathbf{D_b}}{\mathbf{B^2 S n_c}}\right)$$ **Equation 20**

The other is due to the front and rear crankshaft seals. The seals are assumed to operate in the boundary lubrication regime. While seal friction may change throughout warm up, this is attributed to changes in its material properties and not oil temperature. According to the findings of Leong [39] this effect is small enough to be neglected. The original PNH model also included a turbulent dissipation term which accounted for the work done in pumping oil through the bearings. This has been accounted for in the oil pump parasitic loss term.

3.6.2. Piston Group

The piston group, also referred to as the reciprocating assembly, includes friction contributions from the big-end bearings, the piston ring-pack and piston skirt. All of these contributions are assumed to be hydrodynamic and a viscosity-based correction is applied to all terms, Equation 21.

$$\mathbf{fmep_{piston}} = \left(\mathbf{C_{pb}} \left(\frac{\mathbf{N^{0.6} D_b^3 L_b n_b}}{\mathbf{B^2 S n_c}} \right) + \mathbf{C_{ps}} \left(\frac{\mathbf{V_p^{0.5}}}{\mathbf{B}} \right) + \mathbf{C_{pr}} \left(\frac{\mathbf{V_p^{0.5}}}{\mathbf{B^2}} \right) \right) \left(\frac{\mu}{\mu_{\mathbf{ref}}} \right)^{\mathbf{n}} \quad \text{Equation 21}$$

The gas loading term in the original version of the PNH model has been omitted. Comparison of engine motoring torque in a compressed and decompressed state by Leong [39] indicates that the gas loading effect is small. The oil film thickness between the ring-pack and cylinder liner varies throughout the engine cycle [99] such that the piston-cylinder pair may operate in all three friction regimes. Zero piston velocity and high in-cylinder pressure at TDC results in boundary lubrication and hence high friction forces. However, given the relatively low piston velocity at this point in the engine cycle, the associated power loss is also low. The friction contributions from the rings and skirt are instead weighted by 'mid-stroke' conditions and made proportional to the square root of the mean piston velocity [100]. In the original PNH model the piston ring contribution was made proportional to the term $\left(\mathbf{1} + \frac{\mathbf{1000}}{\mathbf{N}} \right)$, to reflect the friction turn-up at low engine speeds, a characteristic of mixed lubrication. Leong reports that no turn-up was observed in his motoring tests, and therefore does not include this correction in the revised formulations. Separating the friction contribution from the skirt and rings is based on typical ratios reported in literature. The split is assumed as 70 % for the piston rings and 30 % from the skirt.

3.6.3. Valve- train Assembly

Valve train friction is expressed as the total of five contributions:

$$\mathbf{fmep_{valvetrain}} = \left(\mathbf{C_{vb}} \left(\frac{\mathbf{N^{0.6} n_b}}{\mathbf{B^2 S n_c}} \right) + \mathbf{C_{v,oh}} \left(\frac{\mathbf{L_v^{1.5} N^{0.5} n_v}}{\mathbf{B S n_c}} \right) \right) \left(\frac{\mu}{\mu_{\mathbf{ref}}} \right)^{\mathbf{n}} + \mathbf{C_{v,om}} \left(\mathbf{2} + \frac{\mathbf{10}}{\mathbf{5} + \mu \mathbf{N}} \right) \frac{\mathbf{L_v n_v}}{\mathbf{S n_c}} + \mathbf{C_{vs}} + \mathbf{fmep_{follower}}$$

The first term represents the camshaft bearings contribution and is of similar form to the main bearings hydrodynamic friction term. The second is the oscillating hydrodynamic friction term and accounts for the remaining valve-train components operating in the hydrodynamic regime, such as valve lifters and valve guides. The third term accounts for mixed lubrication losses, which represent the greatest friction contribution. As for the piston rings, this term was made proportional to $\left(\mathbf{1} + \frac{\mathbf{1000}}{\mathbf{N}} \right)$ in the original PNH model. Leong claims that this over-predicted friction at low engine speeds and replaced this term with $\left(\mathbf{2} + \frac{\mathbf{10}}{\mathbf{5} + \mu \mathbf{N}} \right)$. The fourth term is a constant and accounts for camshaft seals. The engine used in this investigation makes use of roller followers, for which the following formulation is used:

$$\mathbf{fmep_{rollerfolbower}} = \mathbf{C_{v,rf}} \left(\frac{\mathbf{N n_v}}{\mathbf{S n_c}} \right) \qquad \text{Equation 22}$$

3.6.4. Auxiliaries

As in the original PNH model, a second-order polynomial function of engine speed is used to describe auxiliary friction losses, in which only the speed dependent terms are corrected for viscosity throughout warm-up:

$$\mathbf{fmep_{auxiliary}} = \alpha + \left(\beta \mathbf{N} + \gamma \mathbf{N}^2 \right) \left(\frac{\mu}{\mu_{\mathbf{ref}}} \right)^{\mathbf{n}} \qquad \text{Equation 23}$$

Components accounted for include the water, oil and fuel injection pumps. Coolant viscosity is used to correct the water pump friction contribution, while oil pump coefficients were derived for a fixed displacement pump in which the oil supply pressure was controlled according to the standard pressure relief valve [39].

3.7. Oil Circuit

The oil circuit as modelled in PROMETS is illustrated in Figure 22. Oil is pumped from the sump and fed through a section of gallery 11mm in diameter, 300 mm long, to the Filter Cooler Assembly (FCA). This is an oil filter unit integral with an oil-to-coolant heat exchanger. On exiting the FCA, ~20 % of the total pump flow is directed to the cylinder head [101] through 300 mm of gallery. The remainder of the oil flow is fed to the crankshaft main bearings through 400 mm of gallery also 11 mm in diameter. Heat transfer from oil flowing in the galleries is modelled using a laminar pipe flow correlation [63]:

$$\mathbf{Nu_D = 3.66 + \left(\frac{\frac{0.0668\,Re\,Pr}{(L/D)}}{1 + 0.04\left(\frac{Re\,Pr}{L/D}\right)^{0.66}} \right)} \qquad \text{Equation 24}$$

Transition from laminar to turbulent flow occurs at a Reynolds number ranging from 2000 to 4000. Given the gallery dimensions and oil flow rates considered in this investigation, the laminar pipe-flow correlation was considered suitable and was unmodified. Oil flow rate is calculated from a lookup table as a function of engine speed and oil temperature, Figure 23. This method has been used previously by Law [20] with data being provided by Ford Motor Co. [101]. The test engine in this study was fitted with a positive displacement, gear type pump of fixed capacity, equipped with a pressure relief valve. This opens whenever the pump delivery exceeds the engine demand, re-circulating a portion of the pump outflow back to the sump. The engine speed at which this opens depends on the oil viscosity, and therefore temperature.

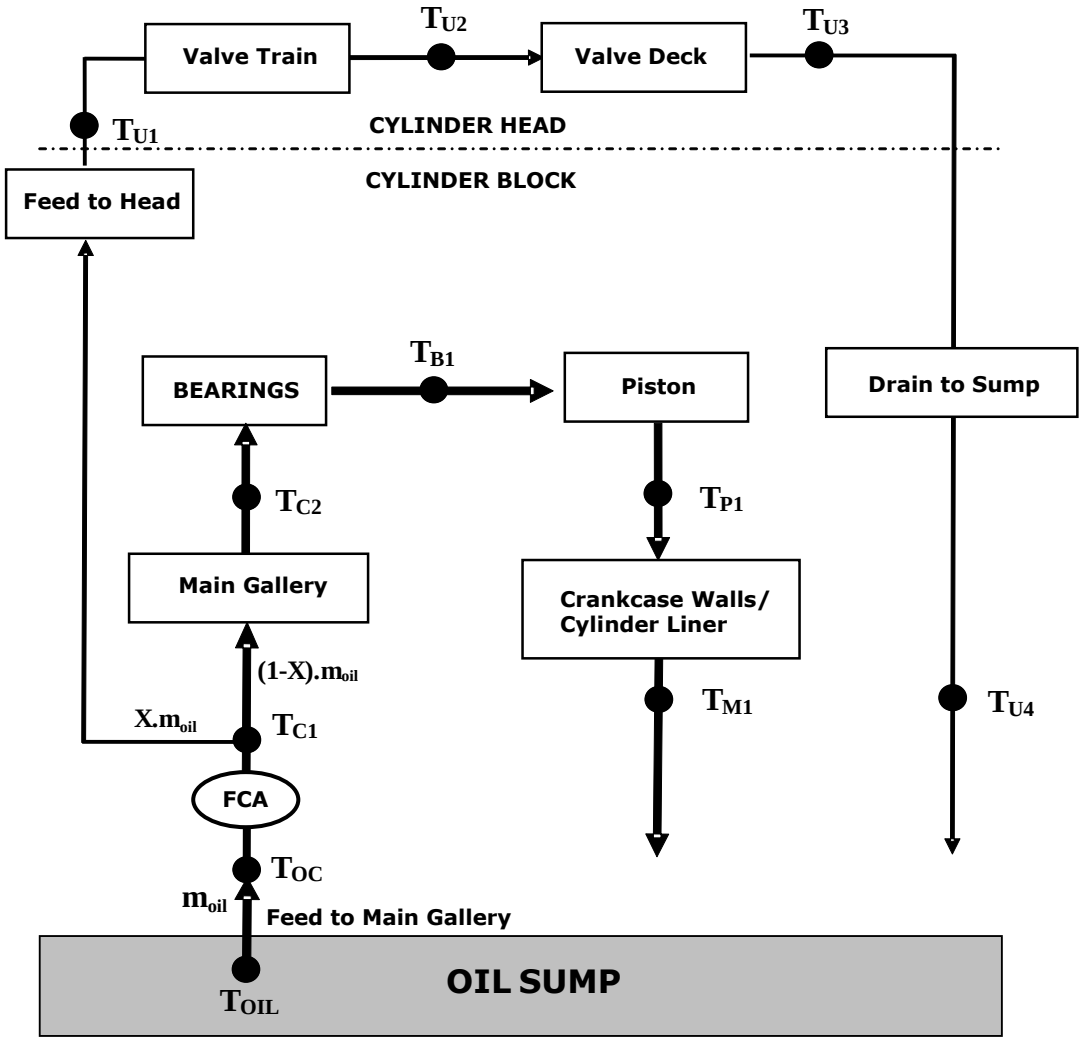

Figure 22 Lubrication Circuit as modelled in PROMETS

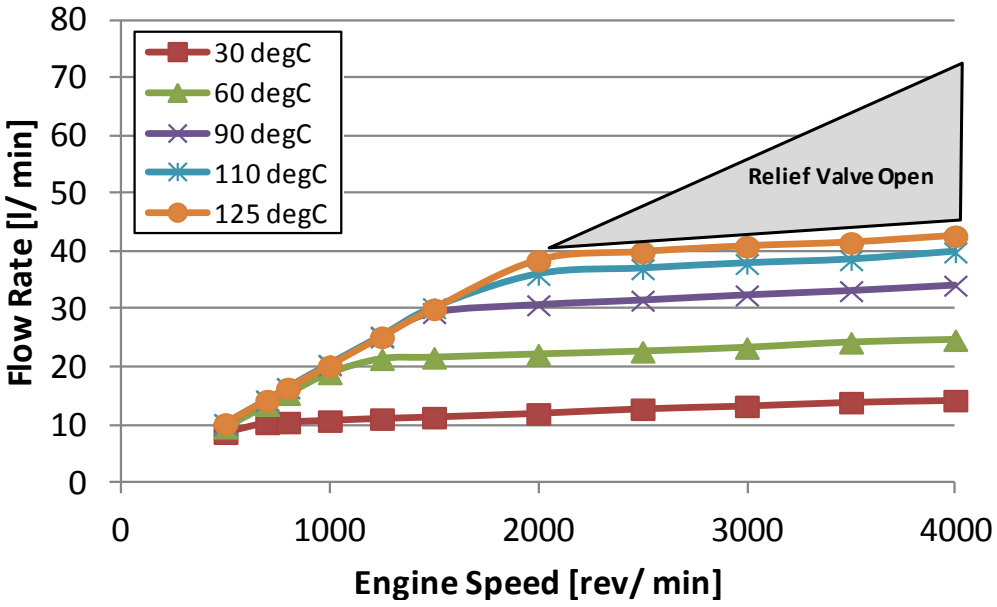

Figure 23 Oil flow rate as a function of engine speed and oil temperature. When fully-warm the pressure relief valve opens around 2000 rev/ min (dashed area).

Friction dissipation heats the oil flow through the bearings. Heat transfer to the bearing shells and crankshaft journal is accounted for and is discussed in Section 5.5.1. Oil side leakage flow from the bearings onto the crankshaft webs is assumed to be flung out onto the piston underside, lower parts of the cylinder liner and crankcase walls. Heat transfer between these components and the oil mist is modelled using an empirically determined heat transfer coefficient (HTC) of 50 W/ m^2K [30]. Heat transfer from oil flowing onto the valve deck is also modelled using this same HTC. The sensitivity of model assumptions to the chosen value of oil mist HTC will be discussed further in Section 4.5. The percentage of friction dissipation retained in the oil for diesel engines was previously set at 20 % [33]. Revisions to this assumption have been carried out and are discussed in greater detail in Section 5.2.3.

Based on the net heat flow to the lubricant, a bulk oil temperature is calculated which is representative of the sump temperature on the test engine. From estimates of the oil flow rate, temperatures at a number of key locations around the oil circuit are also determined (Figure 22). During the early phases of warm-up significant temperature stratification exists within the sump [70]. This is not accounted for in the model and oil temperature is assumed to be spatially uniform at all times. Heat transfer from the sump is modelled under the assumption that the thermal resistance to heat transfer on the oil side and through the sump wall thickness is negligible when compared to the convective thermal resistance to ambient. The external (air side) sump surface temperature is therefore assumed to be identical to that of the oil. The validity of this assumption can be demonstrated as follows. Assuming the oil sump is constructed from 1mm thick steel, its conductive thermal resistance can be worked out a 1.66×10^{-4} K/ W. Taking a typical convective heat transfer coefficient of 20 W/ m^2K the equivalent convective thermal resistance to ambient is 0.357 K/ W, which is three orders of magnitude greater than the steel wall thermal resistance.

3.8. Ambient Heat Losses

Ambient heat transfer coefficients will vary depending on whether the engine is installed on a laboratory test bed or in a moving vehicle. In the latter case, vehicle speed together with under-hood packaging and the extent of ventilation provided to the engine bay are what determine the degree of cooling provided. CFD modeling by

[102] [103] shows how the air velocity distribution in typical engine bays is highly non-uniform. High air velocities are generally observed underneath the vehicle (in the region of the sump), with low speed re-circulating flows in the core of the engine bay. Convective heat transfer from the sump surface can be estimated using an isothermal flat plate analysis. For Reynolds numbers in the range, $Re < 5 \times 10^5$, a laminar Nusselt-Reynolds number correlation can be used [63]:

$$\mathbf{Nu = 0.664\,Re^{1/2}\,Pr^{1/3}} \qquad \text{Equation 25}$$

For turbulent flows ($Re > 5 \times 10^5$) the following correlation can be applied [63]:

$$\mathbf{Nu = Pr^{1/3}(0.037\,Re^{0.8} - 871)} \qquad \text{Equation 26}$$

In the model, the sump is represented by a rectangular area, 0.5m long by 0.28m wide. The variation in heat transfer coefficient with vehicle speed calculated from the above correlations is shown in Figure 24. Air properties (Table 3) were evaluated at a mean film temperature of 63 ºC, while the length of the sump was used as the characteristic length to evaluate the Reynolds number given that the engine is installed in a longitudinal fashion in the vehicle. In this case transition to turbulent flow occurs at a vehicle speed between 40-50 mph. The transition from laminar to turbulent flow is in reality dependent on the surface-roughness conditions and the degree of free stream turbulence. For airflows with a high degree of turbulence (as can be expected in the case of an in-vehicle installation) transition may start earlier at Reynolds numbers as low as 10^5 [63] while for low turbulence flows transition may occur later at Reynolds numbers as high as $2x10^6$. The above consideration may cause the actual values of heat transfer coefficient to stray from the variation illustrated in Figure 24. In the following work, experimental data was collected from two engine test beds, one at the University of Nottingham, the other at the University of Bath [104]. The latter was equipped with cooling blowers that replicated the free-stream vehicle speed over the drive cycle, while in the former no forced air cooling was provided. It has been assumed that the ambient heat transfer coefficient is uniform across all engine exposed surfaces and under natural convection conditions it is adjusted so that the heat losses to ambient, when fully-warm, account for 5-10 % of the total energy released from fuel combustion [32]. For drive cycle simulations a

constant convective heat transfer coefficient of 60 W/ m^2K was found to give good correlation between model predictions and test bed measurements of coolant and oil warm-up trends. This aligns with a vehicle speed of 70 mph, representative of speeds in the EUDC, but substantially greater than the average speed in the urban sector of the drive cycle. Heat losses to ambient only become significant late in the drive cycle, while they are relatively small in the urban section when the engine structure and fluids are still cold. As a result assuming a constant ambient heat transfer coefficient was sufficient for the modelling purposes presented here.

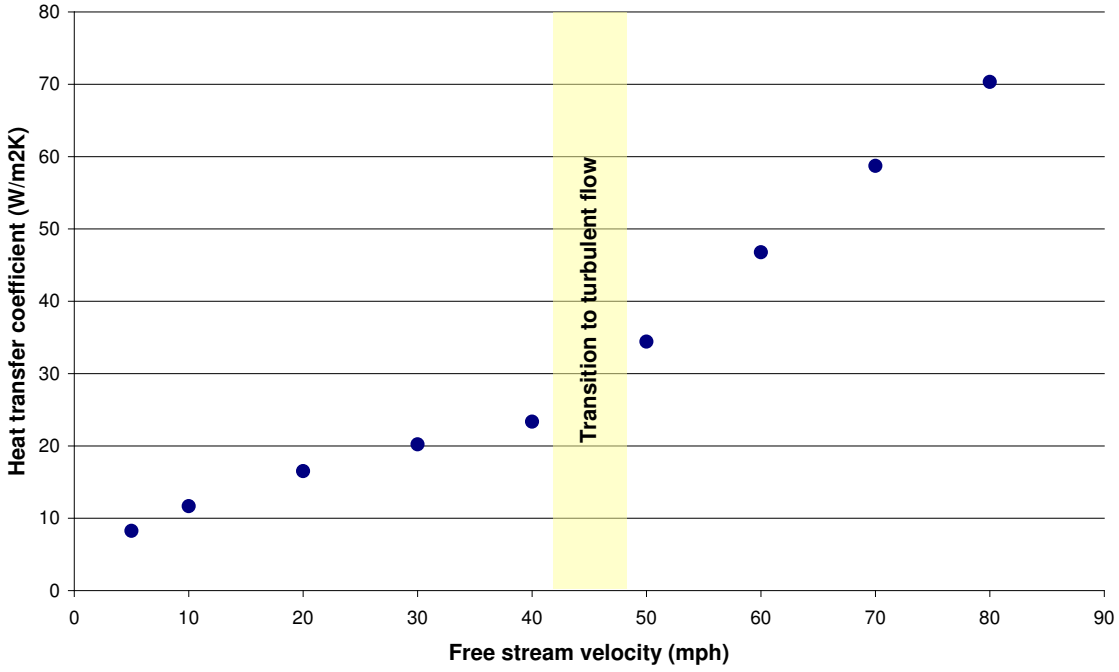

Figure 24 Heat transfer coefficient at different air speeds evaluated from a flat plate correlation

T_{amb}	T_{sump}	ν	Pr	k
℃	℃	m^2/s	-	W/ mK
26	100	$18.8x10^{-6}$	0.709	0.0285

Table 3 Air properties evaluated at the mean film temperature [105].

3.9. Coolant Passage and Internal Circuit Heat Transfer

The external coolant circuit of the University of Nottingham engine build is illustrated in Figure 25. With the thermostat closed, the main heat input sources to the coolant are from heat transfer in the engine coolant jacket and from EGR gases. The

coolant volume retained in the block, in the external pipe-work and de-gas bottle, assumed to be 'active' prior to opening of the main thermostat, is taken to be just under 5l. The thermal capacity of miscellaneous components in contact with the coolant flow such as the thermostat, coolant pump, hoses and fittings, is represented by an additional element in PROMETS, estimated to be around 4 kg. Coolant temperatures in the engine block and head are assumed to be the same given that the variation on an actual engine is generally small anyhow, of the order of 5 ºC. The radiator, which on the test bed is replaced by a bowman shell and tube heat exchanger, is not modelled as it has no effect on warm-up. Once thermostat opening temperature (~90 °C) is reached, the simulated coolant temperature is fixed to this value.

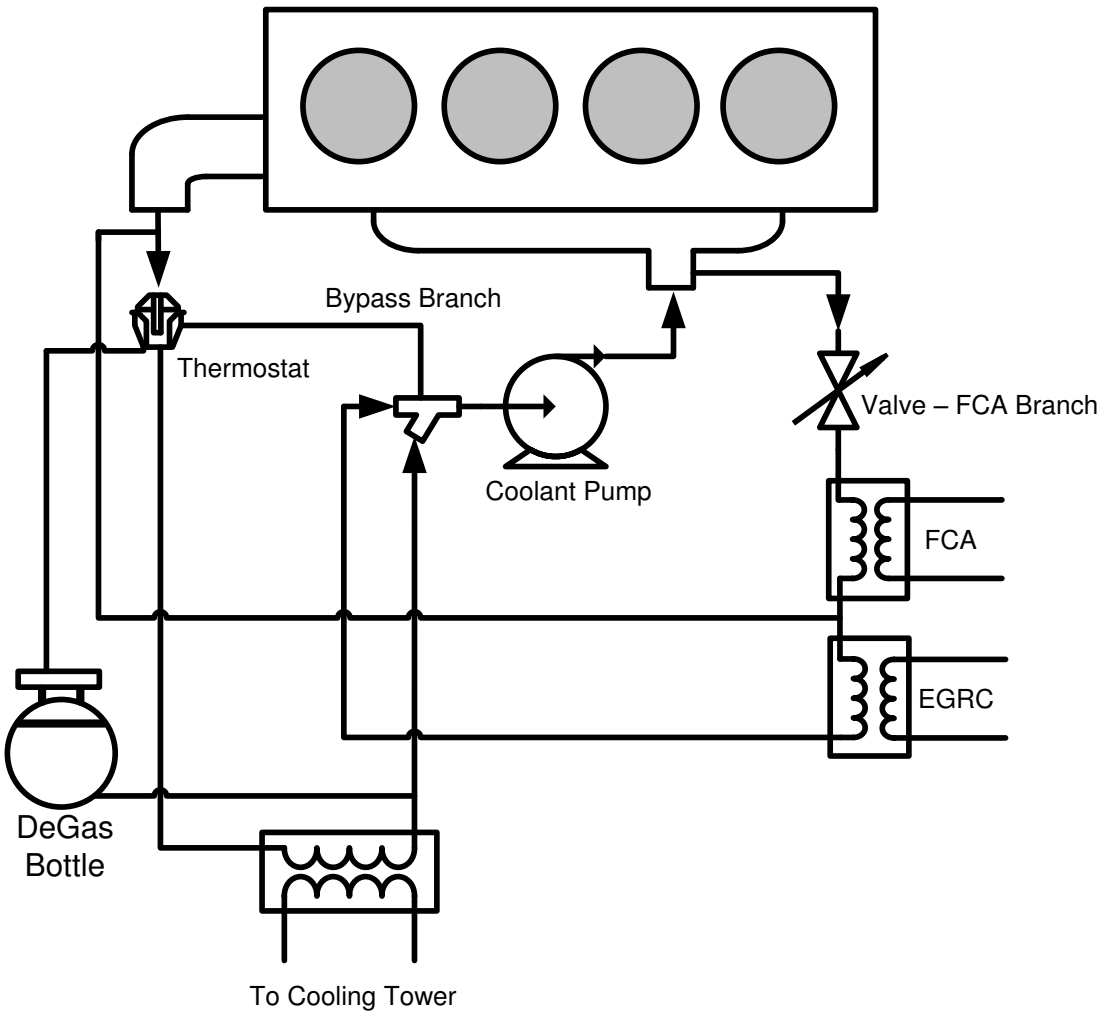

Figure 25 Engine coolant circuit as installed on test bed at the University of Nottingham

Heat transfer in the coolant passages occurs predominantly by forced convection, with nucleate boiling in regions of very high heat flux. The effective heat transfer coefficient can then be expressed as [106]:

$$\mathbf{h = h_{conv} + h_{nucl,boiling}\left[\frac{\left(T_s - T_{sat}\right)}{\left(T_s - T_{cool}\right)}\right]} \qquad \text{Equation 27}$$

Nucleate boiling allows significantly higher rates of heat transfer than those achieved with forced convection alone, but once a critical heat flux is exceeded film boiling occurs [63]. In this case, the heat transfer coefficient is significantly lower than that for forced convection and metal temperatures may increase rapidly leading to damage in thermally critical areas. The convective heat transfer coefficient is evaluated from a modified Dittus – Boelter equation [63]:

$$\mathbf{h_{conv} = 0.023\,Re^{0.8}\,Pr^{0.4}\,\frac{k}{D}} \qquad \text{Equation 28}$$

while the nucleate boiling term is calculated according to the following relation [107]:

$$\mathbf{h_{nucl,boiling} = 0.00122\Delta T_{sat}^{0.24}\Delta p_{sat}^{0.75}S\left[\frac{k_l^{0.79}c_{p,l}^{0.49}\rho_l^{0.49}}{\sigma_l^{0.5}\mu_l^{0.29}\left(\Delta h_{lg}\rho_g\right)^{0.24}}\right]} \qquad \text{Equation 29}$$

Further detail on modelling heat transfer in the engine coolant jacket is provided in [34]. In PROMETS, the internal coolant circuit includes an oil-to-coolant heat exchanger, also referred to as the filter cooler assembly (FCA), an EGR cooler, a cabin heater and a supplementary coolant heater. The last two elements are not considered in the following analysis while particular importance is given to the effect of the oil and EGR coolers. Coolant streaming to the FCA is controlled by an additional wax-element thermostat which generally opens when the coolant temperature in the block reaches around 70 ºC. Initial testing was done with the thermostat in place but this was subsequently replaced with a manually operated

gate-valve, Figure 25. This was done to control coolant flow through the FCA independent of the coolant temperature in the block. In PROMETS, heat exchange in the FCA is modelled under the assumption of no heat losses to ambient. Assuming a quasi-steady state, a heat balance can be set up between the oil and coolant streams where the heat lost from the hot fluid is equal to that gained by the cold fluid. The heat transfer effectiveness is defined as the ratio of actual heat transfer to the maximum possible heat transfer:

$$\varepsilon = \frac{\dot{q}_{actual}}{\dot{q}_{max}} \qquad \text{Equation 30}$$

Assuming no heat losses, then the heat lost from the oil is transferred to the coolant such that:

$$\dot{q}_{actual} = C_{cool}\left(T_{cool,out} - T_{cool,in}\right) = C_{oil}\left(T_{oil,in} - T_{oil,out}\right) \qquad \text{Equation 31}$$

where $C_{cool} = \left(\dot{m}C_p\right)_{cool}$ and $C_{oil} = \left(\dot{m}C_p\right)_{oil}$ Equation 32

The maximum possible heat transfer is achieved when the fluid with the minimum heat capacity rate is taken through the maximum temperature difference available, such that:

$$\dot{q}_{max} = C_{min}\left(T_{oil,in} - T_{cool,in}\right) \qquad \text{Equation 33}$$

The actual heat transfer can then be defined as:

$$\dot{q}_{actual} = \varepsilon C_{min}\left(T_{oil,in} - T_{cool,in}\right) \qquad \text{Equation 34}$$

The heat exchanger effectiveness can in turn be expressed as a function of the flow arrangement and two non-dimensional parameters; the number of transfer units (NTU) and the ratio of the minimum to the maximum thermal capacity rates [63]. For the FCA used in this study effectiveness values were expressed as a function of the oil and coolant flow rates [34] and these are summarized in Table 4.

		Oil Flow Rate (l/ min)						
		0	8	13	15	17	20	22
Coolant Flow Rate (l/ min)	3	0.400	0.311	0.249	0.226	0.206	0.189	0.175
	7	0.400	0.354	0.305	0.285	0.266	0.250	0.235
	11	0.400	0.359	0.330	0.312	0.295	0.279	0.265
	14	0.400	0.376	0.343	0.326	0.311	0.296	0.284
	18	0.400	0.380	0.351	0.336	0.322	0.308	0.296
	21	0.400	0.383	0.355	0.342	0.329	0.315	0.304
	25	0.400	0.385	0.360	0.347	0.335	0.323	0.311
	29	0.400	0.386	0.363	0.351	0.339	0.327	0.315

Table 4 Oil cooler effectiveness for Puma 2.4l engine [34]

External exhaust gas recirculation (EGR) is commonplace on modern diesel engines [108] [109]; a portion of the exhaust gases is re-circulated to dilute the intake charge with the aim of reducing NO_x emissions through a reduction in oxygen availability [110]. The introduction of EGR has a direct effect on heat rejection to coolant in two ways. Firstly, it changes in-cylinder heat transfer characteristics and this effect is different in gasoline and diesel engines. In a diesel engine re-circulated exhaust gas generally displaces fresh air leaving the total trapped in-cylinder charge approximately the same. The change in charge thermal capacity is also negligible. The change in the effective gas temperature due to a higher intake temperature is accounted for using Equation 13, while a correction is applied to the in-cylinder Reynolds number according to Equation 11. Lowering the intake temperature is desirable as it contributes further to reducing NO_x emissions. Higher rates of EGR are also possible without increasing hydrocarbon and particulate emissions [33]. EGR coolers are therefore used, and these are generally shell in tube heat exchangers streamed with engine coolant. As for the FCA, heat transfer is modelled using the effectiveness – NTU method:

$$\mathbf{Q_{EGRC} = \varepsilon * \dot{m}_{egr} * Cp_{egr} * (T_{exh} - T_{cool,in})} \qquad \text{Equation 35}$$

The effectiveness value was set by comparing simulated and measured heat transfer rates from the EGR gases to the coolant (Chapter 7, Section 7.1). EGR rates in this thesis are defined by the following equation:

$$\mathbf{k_{EGR} = \frac{\dot{m}_{egr}}{\dot{m}_{egr} + \dot{m}_{air}}} \qquad \text{Equation 36}$$

The above equation is used to calculate EGR mass flow rates from measurements of the EGR rate and the calculated mass air flow (MAF). The MAF is in turn calculated from the fuel flow rate (calculated) and AFR (measured). Coolant flow rates can either be specified by the user in the operating conditions file, or predicted as a function of engine speed (N) with an expression of the following form:

$$\mathbf{\dot{V}_{cool} = aN + b} \qquad \text{Equation 37}$$

where a and b are coefficients specific to the engine and N engine speed in rev/ min.

Fixed speed engine simulations were carried out with the coolant flow rate prediction enabled, while flow rate measurements were provided [104] and used for drive cycle simulations presented in Chapter 7.

3.10. Indicated Specific Fuel Consumption Calculation

Fuel flow rate strongly influences in-cylinder heat transfer, and as a result the engine's warm-up rate. To assess the potential fuel savings from reduced friction losses following a cold engine start, modelling the interaction between fuel consumption, gas-side heat transfer and engine friction losses is essential. In-cylinder heat release and friction models have been reviewed earlier in this chapter (Sections 3.5.1 and 3.6). This section describes the fuel consumption prediction implemented in the model.

Generally an engine's fuel consumption is characterised by plotting its brake specific fuel consumption (BSFC) against engine speed and brake mean effective pressure (BMEP) [2]. For contemporary DI diesel engines, minimum brake specific fuel

consumption is typically between 200 to 240 g/ kW hr at mid-operating conditions [33]. However, BSFC maps are engine specific, since fuel consumption depends on engine friction, combustion system type, calibration and other parameters. Such a map was not available for this study. Instead fuel flow rates were estimated by calculating the indicated specific fuel consumption.

The gross indicated specific fuel consumption is the rate of fuel consumption needed to produce a gross indicated power output and can be expressed as:

$$\mathbf{isfc_{gr}} = \frac{\dot{\mathbf{m}}_{\mathbf{f}}}{\dot{\mathbf{W}}_{\mathbf{g,i}}} \qquad \text{Equation 38}$$

where the gross indicated power can in turn be defined as:

$$\dot{\mathbf{W}}_{\mathbf{g,i}} = \frac{\mathbf{IMEP_g V_s N}}{\mathbf{120}} \qquad \text{Equation 39}$$

$\mathbf{V_s}$ is the engine swept volume and **N** is the engine speed in rev/ min. The gross indicated mean effective pressure is defined as in [2]:

$$\mathbf{IMEP_g = BMEP + FMEP + AMEP + PMEP} \qquad \text{Equation 40}$$

The brake mean effective pressure is determined from measurements of engine speed and torque on the dynamometer. The mean effective pressure losses due to rubbing friction (**FMEP**) and those from auxiliary loads associated with the oil, fuel and water pumps (**AMEP**) are grouped together into a total engine friction term and are predicted from the friction models described in Section 3.6.

The pumping mean effective pressure (PMEP) depends on the intake and exhaust manifold pressures, and the losses across the inlet and exhaust valves:

$$\mathbf{PMEP} = \left(\mathbf{P_{ex,man} - P_{in,man}}\right) + \mathbf{PMEP_{valve}} \qquad \text{Equation 41}$$

According to [32] the contribution from the valves only becomes significant at high engine speeds and has been neglected in this analysis. In turbo charged engines the inlet and exhaust manifold pressures are mainly determined by the turbocharger calibration and type (whether it is waste-gated, variable geometry etc). Inlet and exhaust manifold pressures were measured over the drive cycle and were used to estimate the PMEP. In due course it is shown that the pumping loss contribution to fuel consumption is less than 3 % over the NEDC. The small difference in pumping losses induced by changes to the engine warm-up rate, have therefore been neglected in this analysis.

The gross indicated specific fuel consumption can also be expressed in terms of the gross indicated thermal efficiency $\eta_{g,i}$ and the combustion efficiency η_{comb} as follows:

$$\mathbf{isfc_g} = \frac{\mathbf{1}}{\mathbf{Q_{LHV}}\,\eta_{comb}\eta_{g,i}} \qquad \text{Equation 42}$$

$\mathbf{Q_{LHV}}$ is the lower heating value of the fuel and is taken here as 42.5 MJ/kg [2]. In the case of diesel engines, which generally operate at lean equivalence ratios, combustion is essentially complete. In PROMETS the combustion efficiency is taken according to:

$$\eta_{comb} = \mathbf{min}\left[0.98, 0.94 - 0.941\ln(\phi)\right] \qquad \text{Equation 43}$$

The gross indicated thermal efficiency is defined as:

$$\eta_{g,i} = \frac{\dot{\mathbf{W}}_{g,i}}{\dot{\mathbf{Q}}_f} \qquad \text{Equation 44}$$

where $\dot{\mathbf{Q}}_f$ is the rate of fuel energy released:

$$\dot{\mathbf{Q}}_f = \dot{\mathbf{m}}_f \mathbf{Q_{LHV}}\,\eta_{comb} \qquad \text{Equation 45}$$

The gross indicated thermal efficiency depends on a number of parameters such as equivalence ratio [33], engine speed [111], compression ratio and injection timing. On the test engine, injection timing is adjusted throughout warm-up according to coolant temperature. Faster coolant warm-up rates lead to an earlier retarding of injection timing to control engine NO_x emissions which partly offsets the fuel consumption benefit from a faster drop in engine friction [112] [10]. The effect of injection timing and other parameters on thermal efficiency is not accounted for in the model. The predicted changes in fuel consumption presented in this study are solely from changes to engine friction losses. Measurements of gross indicated thermal efficiency were unavailable. Instead the thermal efficiency has been assumed to be constant at 41 % in all calculations, as this gave good correlation between predicted and measured fuel flow rates (Section 7.1).

The above set of equations can be used to predict a fully warm fuelling level based on calculated values of fully warm FMEP. This can then be corrected during warm-up to account for higher frictional losses according to [30]:

$$\dot{\mathbf{m}}_{\mathbf{f}} = \dot{\mathbf{m}}_{\mathbf{f,fw}} \left[\frac{\mathbf{BMEP} + \mathbf{FMEP}}{\mathbf{BMEP} + \mathbf{FMEP}_{\mathbf{fw}}} \right] \qquad \text{Equation 46}$$

3.11. Concluding Remarks

The sub-models implemented in PROMETS have been developed from both physical and empirical correlations. Several sub-models utilise heat transfer coefficients and constants based on empirical data taken from specific engines [30] [33]. While the model is largely comprehensive, some of the assumptions need addressing. The performance of the sub-model developments and of PROMETS as a whole is mainly evaluated by comparison of model predictions with experimental measurements. Where appropriate, the sensitivity of predictions to model assumptions is also explored, both as a way of inferring the value of constants that are difficult to determine from theory but also as a means of quantifying the level of uncertainty that is introduced by different assumptions.

Thermal-friction conditions in the oil circuit in particular are difficult to model due to uncertainties and measurement difficulties. One specific area is the interaction of crankcase oil mist with the piston underside and crankcase walls. Heat transfer from the piston to the oil is further compounded by the addition of cooling jets, which result in substantially higher heat transfer rates than those in oil-splash systems. Revisions to the piston heat transfer model to account for PCJ applications have been made and described in Chapter 4. The sensitivity of model predictions to the oil mist heat transfer coefficient is also explored.

The oil temperature in the sump is a reflection of the general thermal state of the lubrication circuit and is a convenient way of correcting the predicted values of fully-warm friction throughout the warm-up phase. However, if oil temperatures at the rubbing surfaces are perturbed through heat application or thermal isolation, large uncertainties are introduced if the friction calculation is based on sump temperature. A more robust method is to predict friction using temperatures at the rubbing surfaces. This method was applied to the crankshaft main bearings and the modifications carried out to the model are the topic of Chapter 5. While the original crankcase elemental representation in PROMETS is sufficient to model bulk heat exchange between the oil and lower engine block, (heat transfer in the oil main gallery and from the crankcase oil mist), a higher resolution of the temperature field around the main bearing oil film was required to model the film temperature rise. Ideally a similar approach is to be adopted for the piston-liner friction pair. However, modelling thermal-friction conditions in the piston assembly is further complicated by a number of uncertainties discussed further in Chapter 8.

The proportion of friction heat retained in the oil represents another model uncertainty. Current values in PROMETS were derived by empirical correlation [33] [30], with a fixed proportion assumed for all rubbing surfaces. An extensive analysis was carried out by Morgan [34] to show the sensitivity of model predictions to this uncertainty. Revisions to the bearing sub-model described in this thesis mean that heat flows in the bearing oil film are inherently calculated in the film temperature prediction. There still remains uncertainty as to which approach would be most suited to the piston assembly; this is also discussed in Chapter 5.

Chapter 4 - Piston Heat Transfer and the Influence of Piston Cooling Jets on Energy Flows

4.1. Introduction

Heat exchange between the piston and its surroundings is dominated by transfer in from the combustion gases, transfer out through the piston rings, and heat exchange with the piston cooling jets and oil mist in the crankcase. The increased heat flow from the piston to the oil due to the inclusion of PCJs is substantial. Quantifying this allows for a better representation in the model of the major heat inputs to the oil circuit.

A review and extension of the piston heat transfer model used in PROMETS is presented in this chapter. The chapter is divided into three main parts. In the first section, the method used to set the ring pack thermal resistance and underside heat transfer coefficient, is described. This was done with the jets off and the calibration of the sub models was based on their simulated influence on bulk oil and piston temperatures and agreement with experimental values over a range of transient and steady operating conditions. The computational study has made use of test data from a Puma 2.4L engine modified in previous work to allow its PCJs to be switched on or off on demand [113], and the effect on piston temperature to be recorded. The change in steady state piston temperatures between jets on and jets off cases allowed the effect of the oil jets to be isolated, and this is outlined in the second part. The third and final section is concerned with the exploitation of the model, in particular the effect of the PCJs on the heat rejection to the oil and coolant circuits.

4.2. Piston Temperature Measurements

In previous work, the piston of a 2.4l Puma engine was instrumented with thermistors and a wireless pick-up system to record their temperature, as described by Luff et al. [113]. While a total of six thermistors were installed, only four measurements were available as two of the thermistors failed during commissioning. These locations are shown in Figure 26. Temperatures were recorded behind the top ring groove (1), at the bowl edge (2), beneath the bowl (4), and on the crown underside (4). Each thermistor was allocated its own inductive pickup circuit; a female wire coil (fixed

into drilled cavities in the piston with high temperature epoxy) mated with a male coil (fixed at the bottom of the liner), when the piston reached BDC updating the temperature measurement every crankshaft revolution. The measurable temperature range lower limit was 100 °C and was imposed by the minimum temperature requirement for accurate operation of the thermistors. An upper limit of 350°C was needed to avoid overheating of the pistons with the jets off. Further detail on the instrumentation of the pistons and the modifications carried out to the oil system to allow PCJs control is given in [20].

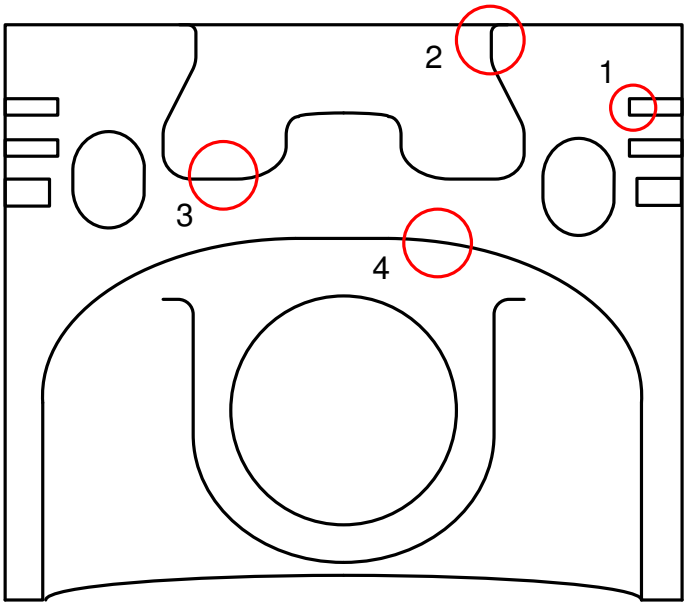

Figure 26 Piston Thermistor Positions. 1: Top Ring Groove. 2: Bowl Edge. 3: Bowl Bottom. 4: Undercrown

4.3. Ring Pack Thermal Resistance and Underside Heat Transfer Coefficient

This section describes how the ring pack thermal resistance and piston underside heat transfer coefficient were derived by comparing model predictions of piston and oil temperatures with experimental measurements taken with the PCJs switched off. It will be shown that there is some uncertainty in determining the split between heat conducted through the rings and heat transfer to the crankcase oil mist. Steady state piston temperature measurements alone are insufficient to determine this but oil warm-up rates and the sensitivity of piston temperature predictions to underside heat transfer can provide additional insight. While a complex temperature field exists in a real diesel piston[114], the aim of the model presented here is to quantify the bulk

heat flows occurring to and from the piston; the proportion of combustion heat dissipated into the coolant via the liner and that transferred to the engine lubricant. The simplified two element lumped mass model historically used in PROMETS was retained in this analysis to represent the piston assembly. Element 23 represents the piston crown and ring pack, while Element 24 accounts for the piston skirt and connecting rod, as shown in Figure 27.

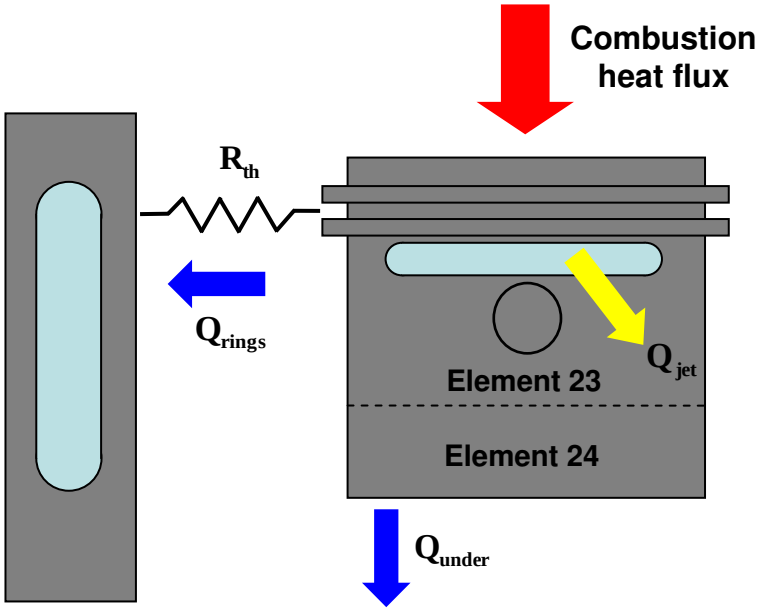

Figure 27 Schematic showing the assumed heat outflows from the piston: Q_{rings} represents conduction through the rings into the cylinder liner, Q_{under} is heat transfer from the piston skirt to the crankcase oil mist and Q_{jet} is heat transfer from the crown gallery to the oil jets whenever these are enabled.

Heat input into the piston crown is according to the in-cylinder heat release correlation reviewed in Section 3.5.1. With no PCJs, the majority (over 70%) of combustion heat transfer from the piston crown is conducted through the rings into the cylinder liner [2]. Heat conducted to the piston skirt can be transferred by conduction to the cylinder liner or to the lubricant by interaction with the crankcase oil mist. Furuhama et al. [115] claims that conduction through the piston skirt accounts for only 6-7 % of the total heat outflow from the piston. Li [116] also reports that heat conducted through the skirt was substantially lower than that through the rings. At this stage of model complexity there is no real benefit in distinguishing between heat conducted to the liner from the ring pack and heat conducted from the skirt, especially since the latter is an order of magnitude lower than the former. Therefore, heat conduction through the skirt has been grouped with

that through the ring pack. In previous versions of PROMETS, heat flow through the rings to the cylinder liner neglected any resistance contribution between the piston and the ring and between the ring and liner. In this case the thermal resistance between the piston and cylinder liner is simply due to the thermal conductivity of the ring material and the dimensions of the rings:

$$R_{th} = \frac{1}{Z.\frac{\pi B k_{rings} w}{\delta_c}} \qquad \text{Equation 47}$$

where Z is the number of piston rings, k is the ring thermal conductivity, B is the cylinder bore diameter, w and δ_c are the ring thickness and width respectively. Ring pack details for the engine used in this investigation are given in Table 5. According to Equation 47 the ring pack thermal resistance is 0.052 K/W.

Parameter	Value
k_{rings}	54 W/ mK
w	$2.2x10^{-3}$ m
δ_c	$5.2x10^{-3}$ m

Table 5 Ring pack details [34]

For a more complete analysis, conduction through different paths including oil flooding the ring grooves and the oil film present on the cylinder liner must be considered. This is generally represented in the form of a thermal resistance network as proposed by Sitkei [117] and Li [116] and reported by Law [20] and Heywood [69].

Figure 28 illustrates the major thermal resistances associated with each heat flow path:

- Conduction through the oil gaps into the top and bottom oil ring flanks (R_1 and R_2)
- Conduction through the ring (R_3)
- Conduction through the oil film present on the liner (R_4)

To estimate the thermal resistances R_1 and R_2 knowledge of the ring-groove side clearance ($t_1$and t_2, see Figure 28) is required. A typical value is reported by Li [116] as being 0.05 mm. In a firing engine the ring is not stationary in its groove. Li assumed that the ring rests on its lower flank throughout most of the engine cycle, and only moves to the upper surface during the induction stroke. Li also assumed a 0.01 mm gap on the contact side to take into account a non-perfect seating due to ring groove distortion caused by machining and thermal deformation. Taking into account the above results in average clearances of t_1=0.0325 mm and t_2=0.0175 mm respectively. However, measurements on diesel piston rings by Furuhama [115] suggest that the mean heat flux through the upper and lower ring flanks are in fact very similar. While Furuhama acknowledges that the ring is in contact with the lower surface of the ring groove for the majority of the engine cycle, the temperature difference between the ring's upper flank and upper ring groove surface is ~ 4-5 times greater than on the lower ring flank. Given that in this analysis a single temperature is representative of the piston crown, the upper and lower ring flank gaps have been assumed equal at $t_1 = t_2 = 0.025$ mm. In his derivation Li assumed the ring groove clearance spaces to be air gaps, while Law assumed them to be fully-flooded with oil at all times. The latter assumption results in a lower thermal resistance value given that the thermal conductivity of oil, assumed here to be 0.1316 W/ mK at a temperature of 160 °C, is significantly higher than that of air, 0.0386 W/ mK **[63]**. The difference in the calculated value of ring pack thermal resistance as a result of assuming air or oil filled gaps is shown in Table 6. The oil film thickness between the rings and cylinder liner varies throughout the engine cycle and is also dependent on engine speed and load. Values reported in the literature vary from ~1-10 μm [39]. A mean value of 2.5μm was assumed by Li. Two oil film thicknesses were considered here, 2.5μm and 5μm to quantify the sensitivity of the overall ring pack thermal resistance to the oil film thickness. It is assumed that heat transfer through the oil film takes place entirely by conduction [118]. According to [115] heat transfer from the ring lands accounts for no more than 3-4 % of the total heat outflow from the piston and has been neglected in this analysis. While the ring land area available for heat transfer is greater than that of the rings, the large clearance to the liner makes it a poor heat conduction path.

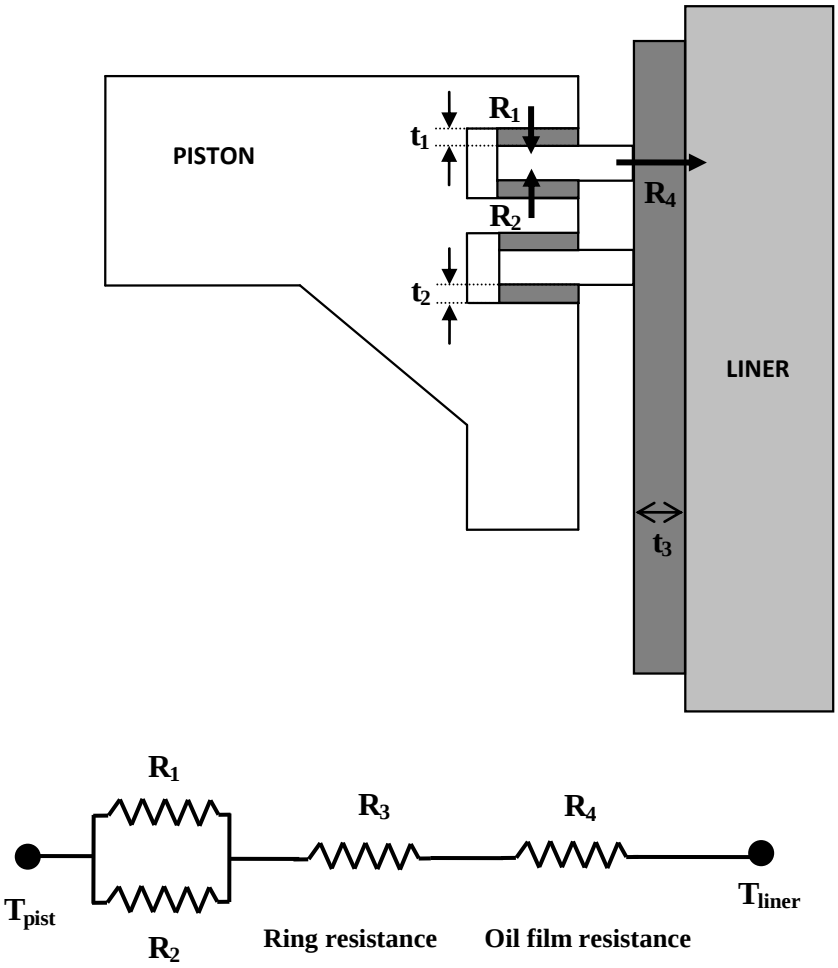

Figure 28 Ring Pack Thermal Resistance Schematic

	Equation	Air filled ring gaps		Oil filled ring gaps	
Thermal Resistance	-	**(K/ W)**		**(K/ W)**	
R_1	$\frac{t_1}{k_{oil}A}$	0.147		0.043	
R_2	$\frac{t_2}{k_{oil}A}$	0.147		0.043	
R_3	***Equation 47***	0.052		0.052	
Cylinder Liner OFT	-	**2.5µm**	**5µm**	**2.5µm**	**5µm**
R_4	$\frac{t_3}{k_{oil}A}$	0.0102	0.0205	0.0102	0.0205
$R_{overall}$	$\frac{R_1}{2} + R_3 + R_4$	0.1354	**0.1456**	**0.0836**	0.0938

Table 6 Ring-pack thermal resistance network summary, evaluated at T_{oil}=160 °C and at two oil film thicknesses (OFT).

Table 6 illustrates a breakdown of the total thermal resistance from the piston crown to the cylinder liner as derived from the above formulations and evaluated at an oil temperature of 160 °C. With oil filled ring gaps, the radial ring thermal resistance (R_3) as calculated from Equation 47 dominates, accounting for ~60 % of the total value. Assuming air filled rings gaps results in a substantial 50 % increase in the total ring pack thermal resistance. A change in oil temperature from 120 °C to 320 °C resulted in only a 5 % change in thermal resistance. The sensitivity of the thermal resistance to the oil film thickness is greater but still small. Doubling the oil film thickness from 2.5 to 5 μm increased the total ring pack thermal resistance by 12 %.

Heat transfer from the piston underside to the oil mist is modelled using a heat transfer coefficient (HTC) of 50W/ m^2K [30]. This was determined through comparison of predicted and measured results for oil warm-up and is subject to large uncertainty. In the literature it is reported that with the no piston cooling jets, underside heat transfer accounts for between 6.4 % [114] to 27 % [119] of the total piston heat outflow, with 20 % being typical. An underside HTC of 50W/ m^2K gave piston heat outflow splits consistent with values reported in the literature, as will be shown later in this chapter. Moreover, measurements by Mangianello [120] on an engine without piston cooling jets show that shielding of the piston under crown from the crankcase oil mist produced piston temperature rises of around 8 °C. The suppression of piston underside heat transfer in PROMETS resulted in piston temperature rises of the same order of magnitude as reported by Mangianello (Table 7, Section 4.3.1), further suggesting that a value of 50 W/m^2K provides a good representation of heat transfer rates from the piston underside. Dembroski [121] also looked at the effect of shielding the piston underside. At an engine speed of 3060 rev/ min, Dembroski noticed only small changes in piston ring heat flux indicating that heat transfer from the underside constitutes a small proportion of the total heat outflow from the piston.

4.3.1. Comparison with Experimental Data

Using the analytically derived value for the ring pack thermal resistance and an underside convective HTC of 50 W/ m^2K, resulted in poor correlation between predicted and measured piston temperatures, in particular an under-prediction of

piston temperatures at the lower engine speeds. The variation in overall ring pack thermal resistance derived empirically by matching piston temperature predictions with test bed measurements is shown in Figure 29 (pink line). This variation with engine speed has not been explained in terms of any known physical characteristic of the ring-to-liner contact that would lower the thermal resistance to heat transfer as piston speed increased. The shaded area in Figure 29 shows the range of uncertainty in the calculated value of ring pack thermal resistance introduced by the assumptions for oil film thickness (OFT) and whether the ring-groove side clearances are air or oil filled. The upper value is for air filled gaps and an OFT of 5µm, while the lower value is for oil filled gaps and a smaller OFT of 2.5µm. Alone it cannot account for the empirical variation observed. Oil film thickness is reported to change with piston speed but its contribution to the overall ring pack thermal resistance is relatively small and cannot account for the variation shown here. Moreover, modelling and experimental measurements by [99] show that the change in oil film thickness with engine speed is small; higher shear rates lead to a decrease in oil viscosity which counteracts the increase in oil film thickness generally seen with hydrodynamic lubrication.

The level of agreement between prediction and experimental results for piston temperature is shown in Figure 30, for two brake loads and a range of engine speeds. Simulated temperatures are of the piston crown (element 23), and experimental values are the average of the four measurements taken in the crown [20]. Also shown, for the 8 bar BMEP, 2000 rev/min operating condition, is the change in piston temperature produced by changing the assumed thermal resistance of the ring pack by +/- 20 %. The predicted large response of temperature indicates the value of thermal resistance is defined within a relatively narrow range. Validation with engine data was not possible at the lower engine speeds and light load conditions. At these conditions piston temperatures fell below the reliable measurement range of the thermistors installed on the test engine. The maximum engine speed considered was limited to 3000 rev/ min as this covers the engine speed range of the NEDC.

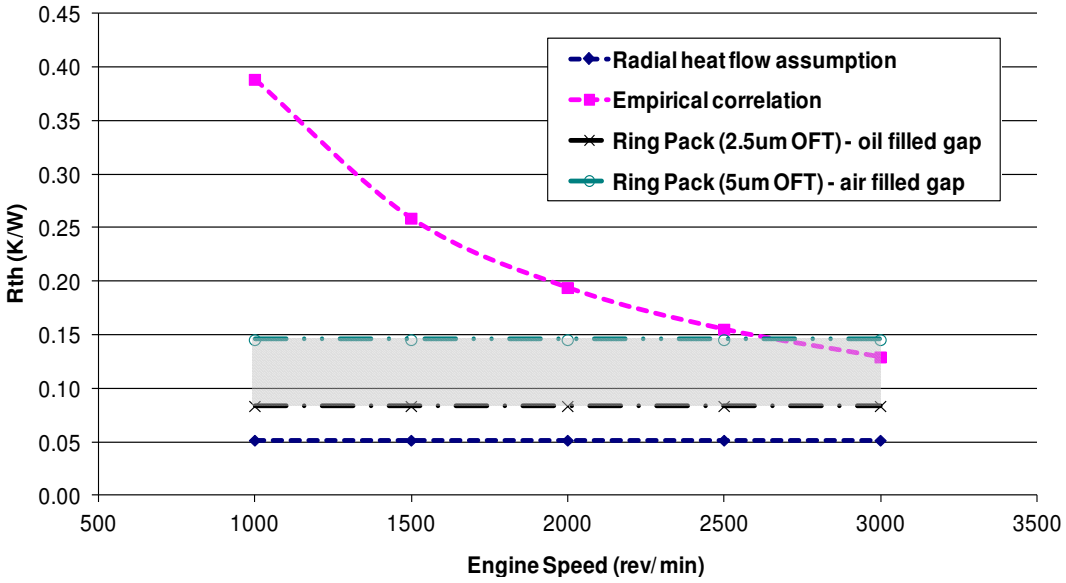

Figure 29 Ring-pack thermal resistance: empirically and analytically derived values. Also shown is the previously assumed value in PROMETS (radial heat flow assumption)

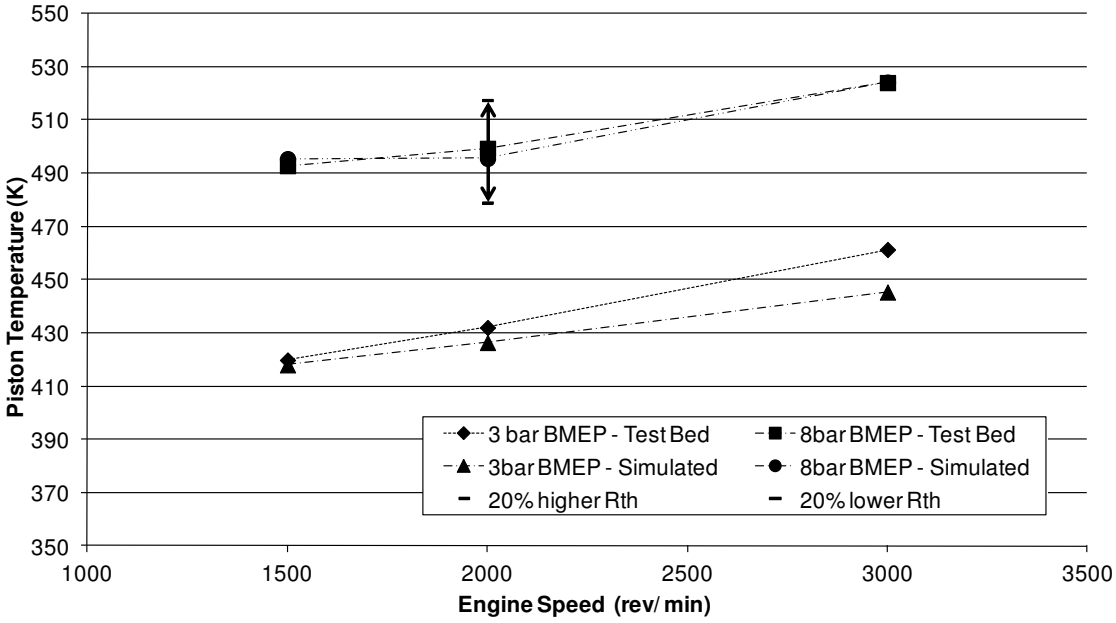

Figure 30 Piston temperature prediction correlation - PCJs Off
Range bars indicate effect of ±20% change in R_{th}

Piston Temperature (K) – PCJs OFF				
		Engine Speed(rev/ min)		
BMEP (bar)	Underside HTC (U_{HTC})	1500	2000	3000
3	U_{HTC}=50W/m^2K	418	426	445
	U_{HTC}=0W/m^2K	428	434	451
8	U_{HTC}=50W/m^2K	495	496	524
	U_{HTC}=0W/m^2K	518	512	537

Table 7 Predicted piston temperatures with a piston underside HTC of 50 and 0 W/ m^2K - illustrates temperature rise from suppressing underside heat transfer to crankcase oil mist

4.3.2. Sensitivity of model predictions to piston underside HTC

The predicted ratio of heat outflows through the piston rings and underside for different engine speeds is illustrated in Figure 31. At 1500 rev/ min it is typical of values reported in the literature [119] [114]. However, at 3000 rev/ min, heat transfer from the underside drops below 10 %, suggesting that convection to the crankcase oil mist may be under predicted at the higher engine speeds. Experimental measurements by Furuhama on a diesel piston [115] show that the split between heat conducted through the rings and the piston underside remained roughly constant with engine speed, as illustrated in Figure 32. The sensitivity of model predictions to the assumed value of piston underside HTC was therefore investigated further. Simulations were performed in which the ring pack thermal resistance was assumed constant while the oil mist HTC was increased at the higher engine speeds to match predicted and measured piston temperatures. The ring pack thermal resistance was adjusted to a constant value of 0.25 K/ W as this gave good correlation between predicted and measured piston temperatures at an engine speed of 1500 rev/ min. For the underside HTC, a value of 50 W/m^2K was retained at 1500 rev/ min but was increased at the higher engine speeds, as shown in Figure 33. In this case, only the 3 bar BMEP load case was simulated.

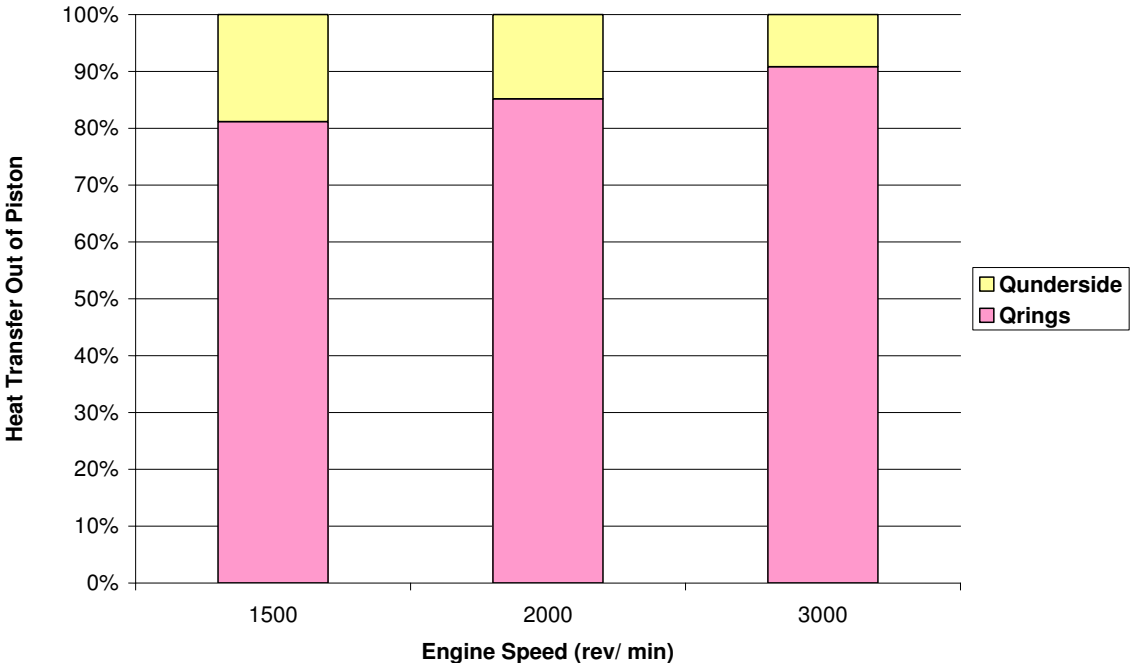

Figure 31 Proportion of heat outflows from piston with PCJs off. Piston underside HTC = 50W/ m^2K.

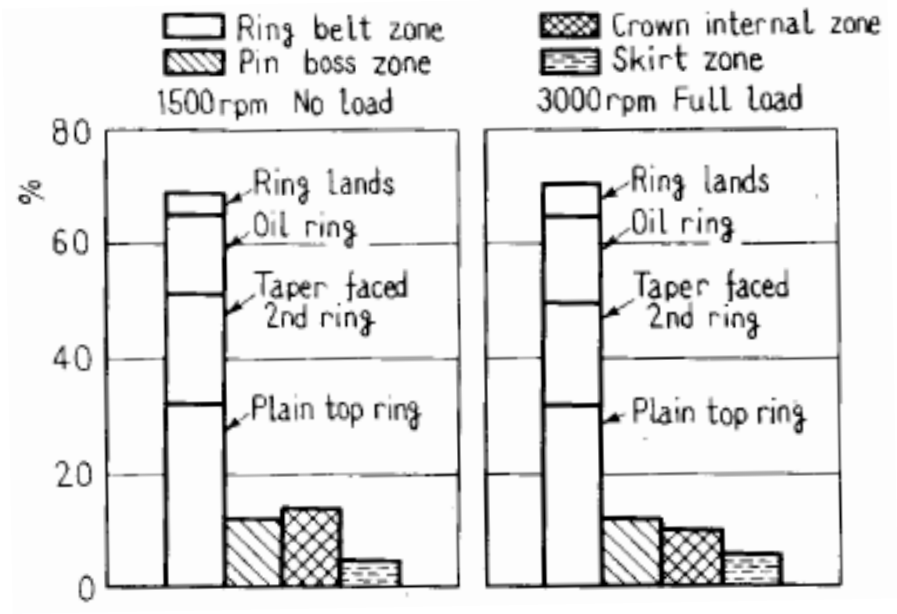

Figure 32 Measured heat outflows from different piston regions [115]

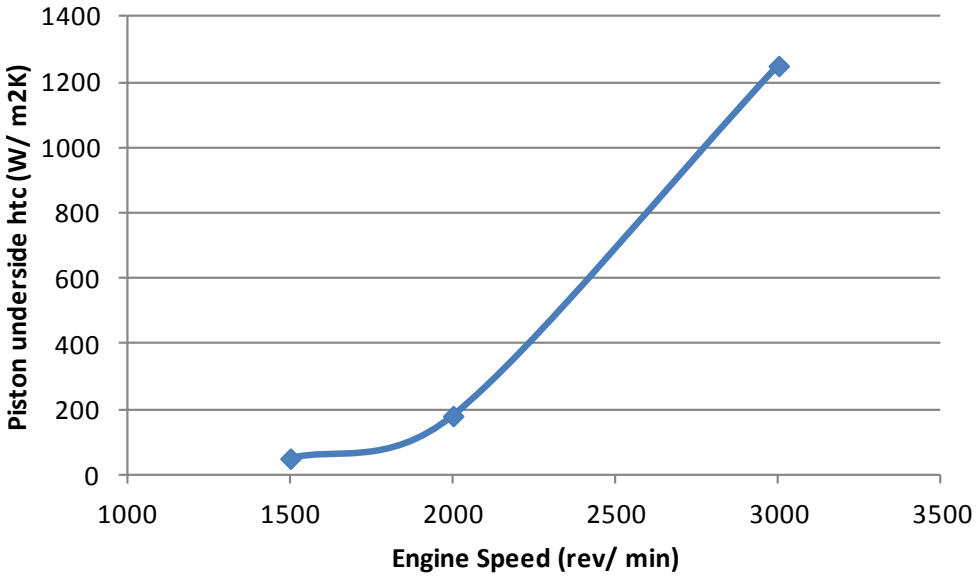

Figure 33 Piston underside HTC variation with constant ring pack thermal resistance (0.25K/ W). A value of 50W/ m^{2}K was retained at 1500 rev/ min.

With the piston underside HTC variation shown in Figure 33, heat flow from the underside to the crankcase oil mist increases considerably; at 2000 rev/ min it accounts for ~35 % of the total heat outflow from the piston and at 3000 rev/ min it increases to 50 %, more typical of setups employing additional piston underside cooling from oil jets [71] rather than the splash cooling mechanism considered here. The increased sensitivity of the piston temperature prediction to underside heat transfer also means that inhibiting it results in greater piston temperature rises, 17°C at 2000 rev/ min and 65 °C at 3000 rev/ min. The increased heat flow to the oil circuit also results in fully-warm oil temperatures being over predicted by 6-8 °C, as illustrated in Figure 34. Based on the observed changes to the oil temperature prediction and the sensitivity of the piston temperatures, a value of 50 W/ m^{2}K was retained for the underside HTC together with the empirically derived variation of ring-pack thermal resistance (Figure 29).

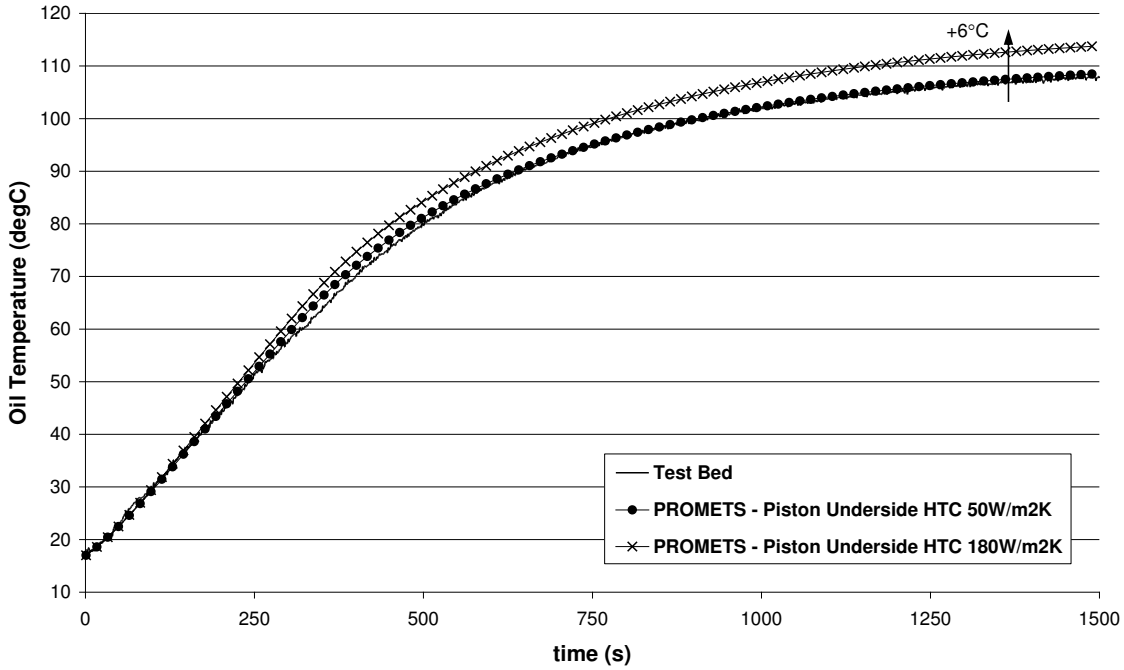

Figure 34 Predicted increase in fully-warm oil temperature at 2000 rev/ min, 3 bar BMEP as a result of increasing the piston underside HTC from 50 to 180 W/ m^{2}K

4.4. Heat Transfer in the Piston Cooling Gallery

Details of the heat transfer processes within the oil cooling gallery, discussed in Section 2.4, are not modelled in PROMETS but an effective oil gallery heat transfer coefficient was defined by matching simulated and measured fully-warm piston temperatures with the PCJs in operation, assuming that conduction through the rings and underside heat transfer to the crankcase oil mist remained unchanged when the PCJs were switched on. The drop in piston temperature observed experimentally when the PCJs were switched on was assumed to be solely due to additional cooling provided by the oil jets. In reality PCJs operation can be expected to increase the presence of oil mist within the engine crankcase [122]. The effect of this on the ring-to-liner heat transfer is difficult to quantify, although the ring pack thermal resistance showed little sensitivity to the assumed oil film thickness. It is reasonable to assume that an increase in the oil mass retained in the crankcase air will increase underside heat transfer from the piston skirt. However, at this stage of model complexity, there is no real benefit in quantifying changes to the piston underside heat transfer coefficient. The total increase in heat transfer from the piston to the oil due to the inclusion of the PCJs is of interest, but quantifying how much of this is due to an

increase in underside heat transfer is challenging and remains one of the model uncertainties.

Since in-cylinder heat transfer is referenced to the difference between a representative mean effective gas temperature and the coolant (Section 3.5.1), in the model, heat transfer into the piston crown is the same whether the PCJs are switched in or not. In reality heat transfer into the piston is governed by the temperature difference between the combustion gases and piston crown, the temperature of which drops by as much as 60 °C when the PCJs are enabled. As the piston crown is several tens of degrees hotter than the coolant under the majority of engine operating conditions, referencing heat transfer to the piston temperature would under-predict heat input into the piston crown. The heat transfer coefficient would have to be increased to compensate for the smaller temperature difference between the gas and piston crown. However, in doing so, the calculated heat transfer rates become increasingly sensitive to the piston temperature, and therefore on whether the PCJs are enabled or not. This would have introduced an additional model uncertainty and in this case it has been assumed that heat flux into the piston is identical whether the jets are on or off.

CFD simulations by Pan [73] provide insight into the typical heat transfer coefficients (HTCs) within piston cooling galleries. Figure 35 illustrates a considerable variation in the HTCs across different regions of the gallery, and a strong variation throughout the engine cycle caused by agitation of oil within the gallery. In PROMETS a mean conductance value between the piston crown and bulk oil was derived. The cooling gallery surface area was estimated at 0.003 m^2 and the empirically derived values of HTC are shown in Figure 36. They are comparable to the values reported by Pan, although in this case the engine speed and gallery dimensions were not reported. Over an engine speed range of 1500-3000 rev/ min the heat transfer coefficient increases by ~18%. Heat transfer in the cooling gallery is a combined effect of a number of processes which are difficult to determine in isolation. The speed dependency is believed to reflect the cocktail shaking mechanism becoming more effective as the shaking frequency is increased, although at higher speeds this may be partly counteracted by a drop in oil fill ratio, as explained previously in Section 2.4. The values derived for the oil gallery heat

transfer coefficient are also comparable to those derived by Law [20] from the correlations of Bush and London [76] although the speed dependency in this case was considerably greater. This discrepancy may be due to a number of factors which mean that the correlations of [76] may not be directly applicable to the gallery setup of the Puma engine used in this study. Firstly they were derived from very low speed data, ranging between 300-720 rev/min. Secondly the gallery used by Bush and London was cylindrical unlike the Puma gallery which is toroidal. Therefore, the heat transfer coefficients derived by Law should only be taken as an indication of trends.

Piston temperature predictions with the PCJs in operation, illustrated in Figure 37, are in good agreement with test bed data for different engine speeds and load cases. For the 8 bar BMEP, 2000 rev/ min operating condition, the change in piston temperature produced by changing the assumed cooling gallery HTC by +/- 20 % is also shown. The sensitivity shown in this case is not as large as that observed for a +/- 20 % variation in ring pack thermal resistance with the PCJs off. With the PCJs on, changes to either the ring-pack thermal resistance or the oil gallery heat transfer coefficient affect a smaller portion of the total heat outflow from the piston, and thereby bear a smaller influence on piston temperature than the assumed value of ring-pack thermal resistance has when the PCJs are off. Predicted heat flows through the rings, to the oil jets and from the piston underside, with and without PCJs, are shown in Table 8 and Table 9 for an engine speed of 2000 rev/ min and brake loads of 6 and 8 bar respectively. The splits are similar for both load conditions. With PCJs on, the predicted ratio of heat outflows through the piston rings, to the oil jets and from the piston underside at different engine speeds is illustrated in Figure 38. Heat flow to the oil jets accounts for between 40-60 % of the total heat outflow from the piston with the remainder being largely conducted through the rings. This is typical of heat flow splits reported in the literature [73] [71].

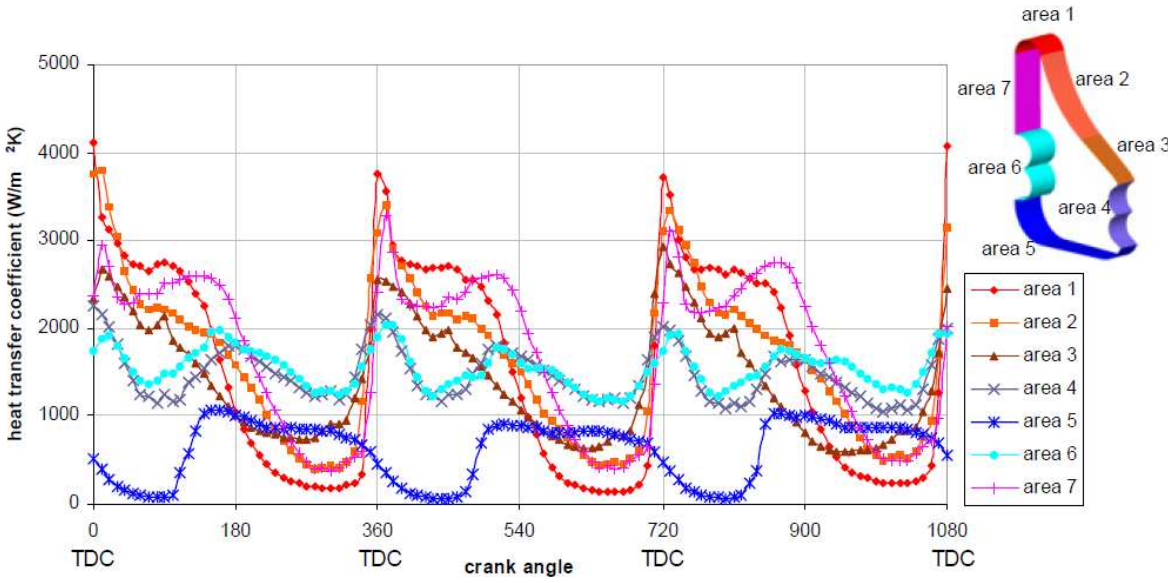

Figure 35 CFD prediction of gallery HTC variation over engine cycle [73].
The variation in HTC is shown for 7 separate areas on the inner surface of the oil gallery

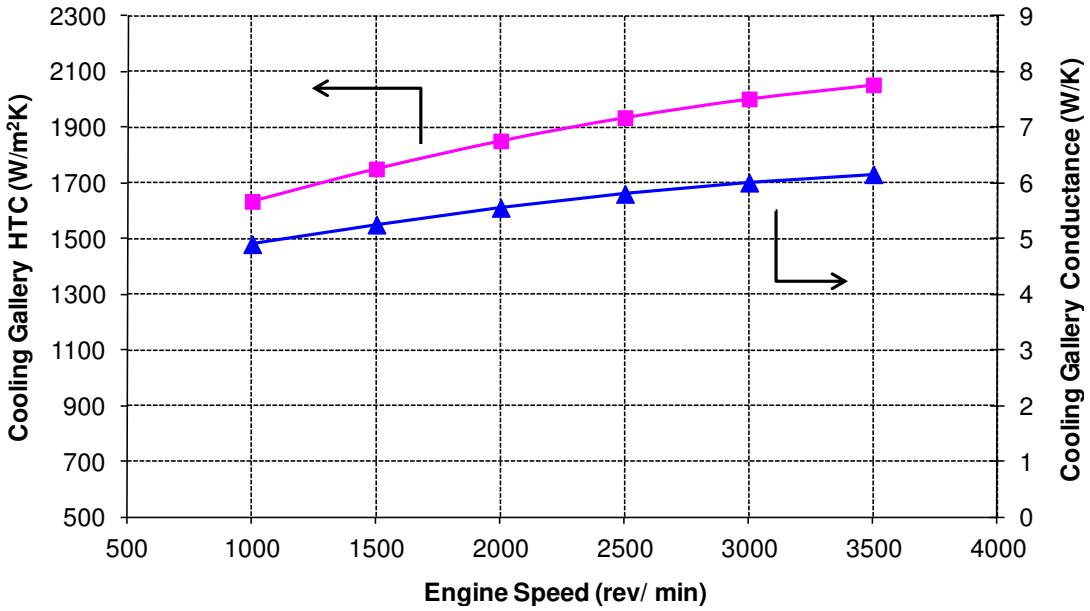

Figure 36 Empirically derived oil gallery HTCs at different engine speeds. Also shown is the thermal conductance value based on an assumed gallery surface area of 0.003m^2

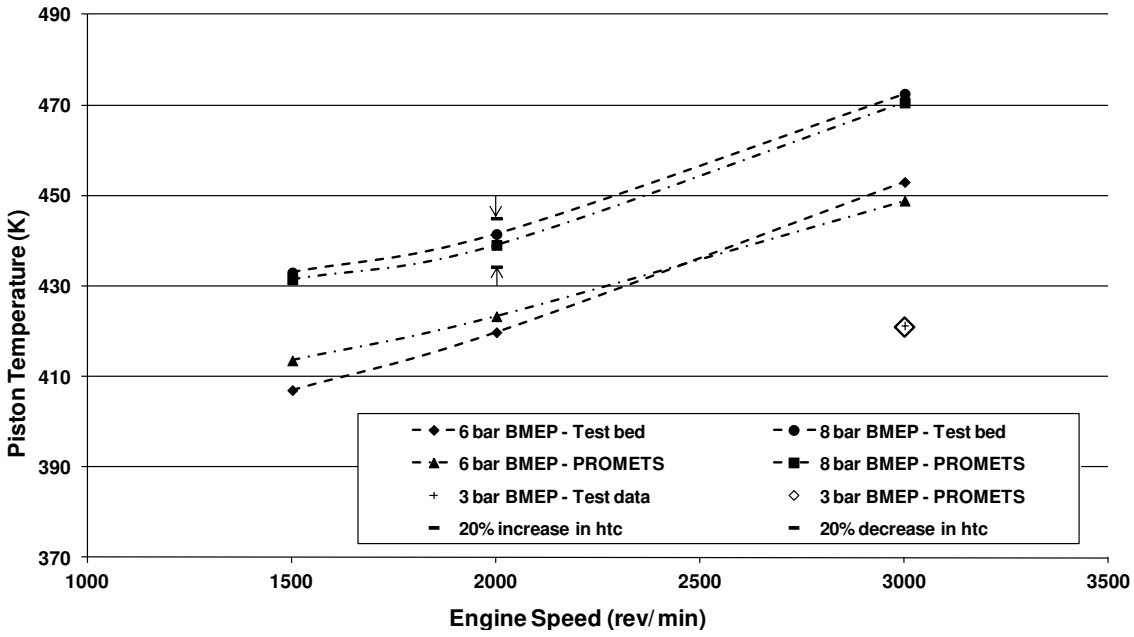

Figure 37 Piston temperature prediction correlation - PCJs On
Range bars indicate effect of ±20% change in gallery HTC

2000rpm/ 6bar BMEP	$Q_{under-side}$ (W)	Q_{PCJs} (W)	Q_{rings} (W)	$Q_{crown\ (input)}$ (W)
PCJs ON	35	291	252	578
PCJs OFF	80	0	498	578

Table 8 Comparison of predicted piston heat outflows with PCJs on and off – 2000rev/ min, 6bar BMEP

2000rpm/ 8bar BMEP	$Q_{under-side}$ (W)	Q_{PCJs} (W)	Q_{rings} (W)	$Q_{crown\ (input)}$ (W)
PCJs ON	38	320	282	640
PCJs OFF	83	0	557	640

Table 9 Comparison of predicted piston heat outflows with PCJs on and off – 2000rev/ min, 8bar BMEP

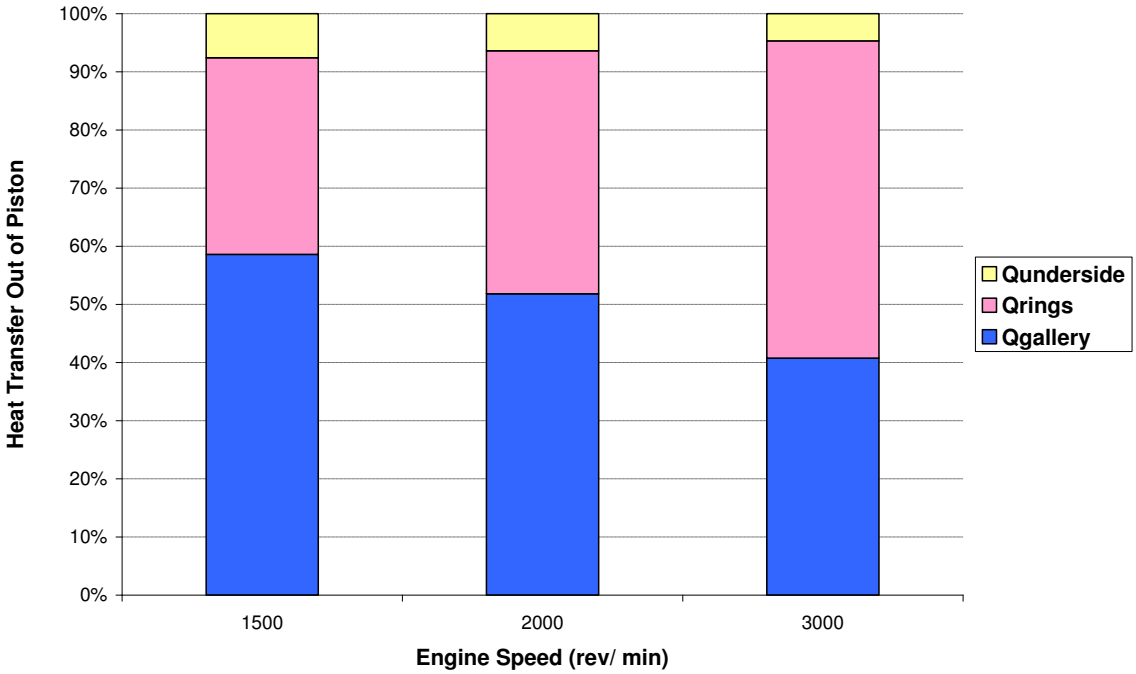

Figure 38 Proportion of heat outflows from piston with PCJs on.

4.5. Results and Model Exploitation

4.5.1. Effect of PCJs on Heat Rejection to Oil and Engine Friction

While the drop in piston temperature when the PCJs were switched on was the primary way of characterising the oil jets' effectiveness, the increase in heat rejection to the oil circuit offers a further way of validating the model. Additional heat input from the jets increases both the oil warm-up rate and fully warm temperatures. Figure 39 compares oil warm-up trends for a 2000 rev/ min, 6 bar BMEP load case with and without the PCJs in operation. The model prediction is good in both cases. In both cases no coolant is streamed through the FCA during the initial stages of warm-up. For the PCJs on case, the FCA is streamed with coolant at approximately 1200 s into the warm-up, which results in a drop in fully warm oil temperature of ~5 °C. With the PCJs switched on, better correlation between the predicted and measured oil temperatures was observed by increasing the oil mist to crankcase HTC from the baseline value of 50 W/m^2K (as applied for all PCJs off cases) to a value of 70 W/m^2K. The oil warm-up trend for the baseline heat transfer coefficient is shown by the black dotted line in Figure 39. In this case the oil temperature is over-predicted by ~5 °C from 300-800 s during the warm-up. Increasing the heat transfer coefficient between the oil mist and crank case walls is considered to be a reasonable

'adjustment' to the model given that enabling the PCJs is expected to increase the entrained volume of oil in the crankcase air [123]. The significance of this assumption is that a larger proportion of the heat transfer from the piston crown to the oil jet flow is redistributed to the engine structure during the warm-up. Further comparison of predicted and measured oil warm-up trends at different engine speed and load conditions is shown in Figure 40 and Figure 41.

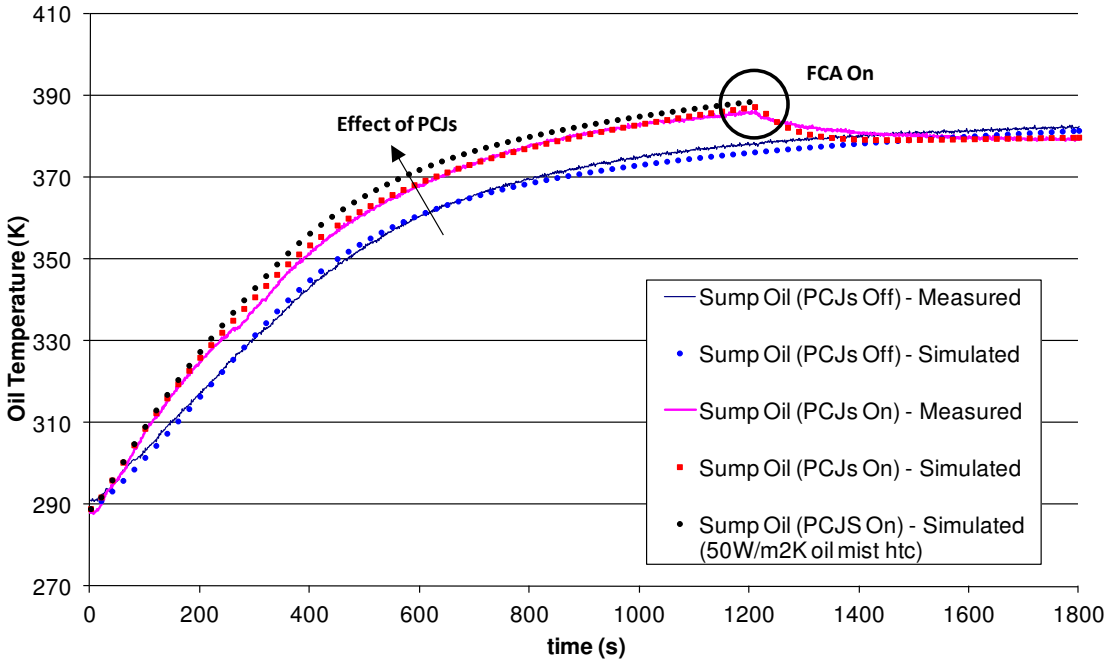

Figure 39 Effect of PCJs and FCA on oil temperature – 2000 rev/ min 6bar BMEP

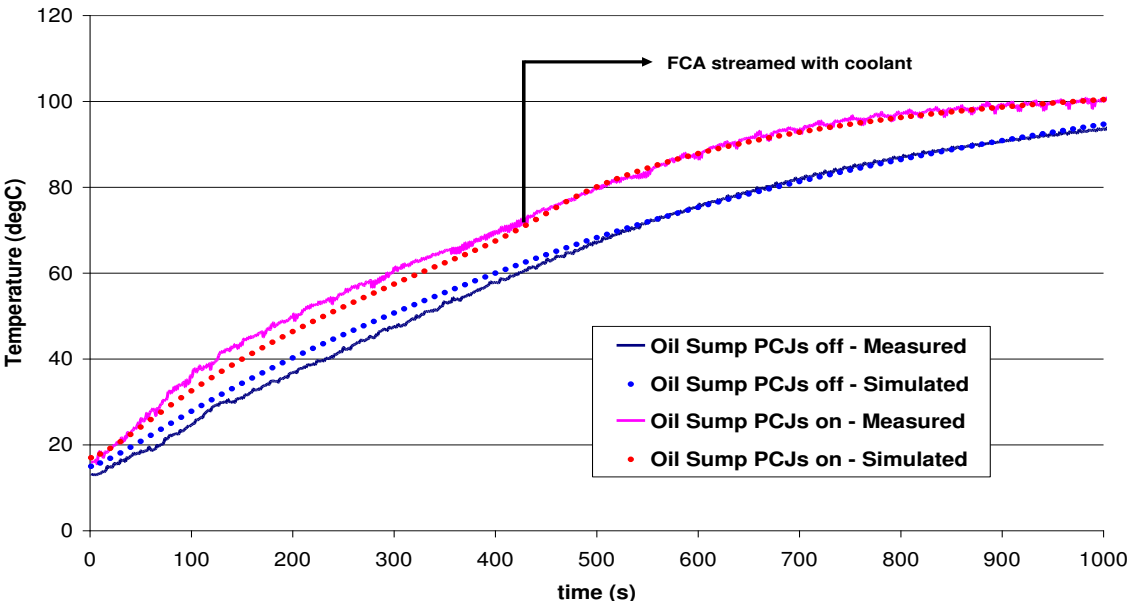

Figure 40 Effect of PCJs and FCA on oil temperature – 2000 rev/ min 3bar BMEP

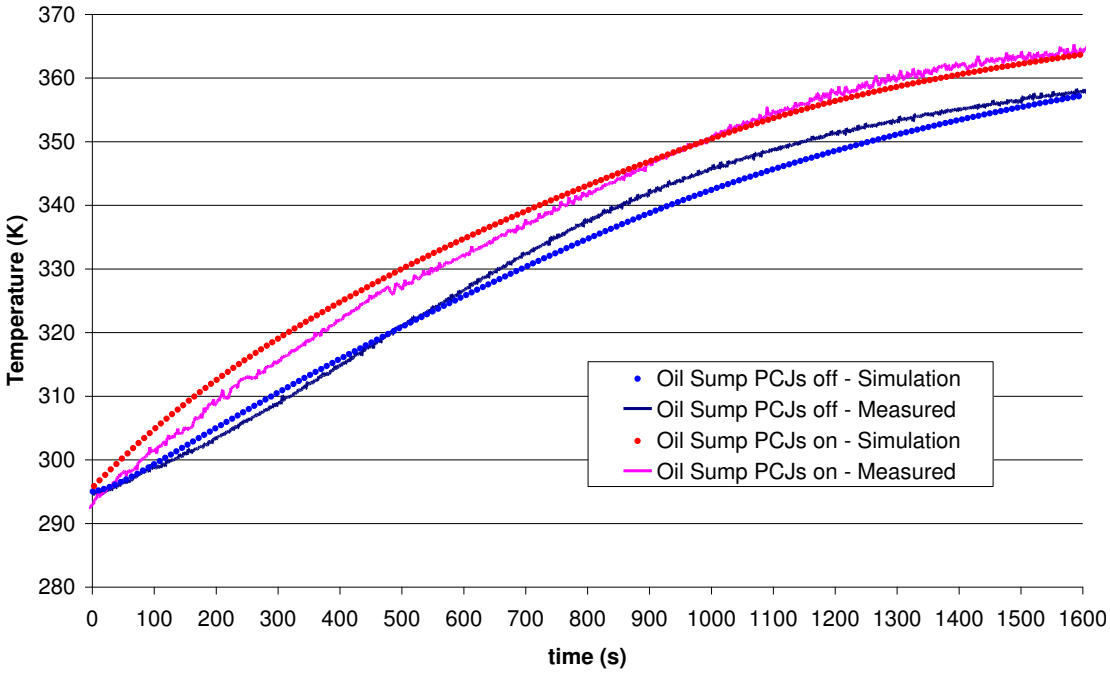

Figure 41 Effect of PCJs on oil temperature – 1000 rev/ min 6bar BMEP

The change in the net heat input to the oil as a proportion of the heat transfer from the PCJs is shown in Figure 42, for the 2000 rev/ min 6 bar BMEP load case. Initially all of the heat input from the jets is retained within the oil, but as the oil warms up, a higher oil temperature leads to increased heat losses to the engine structure. As a result, after about a minute into the warm-up, the additional heat input to the oil is ~40-50 % of the heat transfer from the PCJs, and this continues to drop steadily as the fully-warm state is approached. Changes in the heat flow paths into and out of the oil circuit in response to switching the PCJs on are illustrated in Figure 43. This shows that the greatest contributors to this redistribution of heat are heat transfer from the oil mist to the crankcase walls and heat losses from oil flowing in the main gallery. Higher oil temperatures also result in marginally lower friction dissipation in the main bearing oil films. The complexity of the thermal interactions in the lubrication circuit means that the net change in oil heat input cannot be used as a direct measure of the heat transfer from the PCJs.

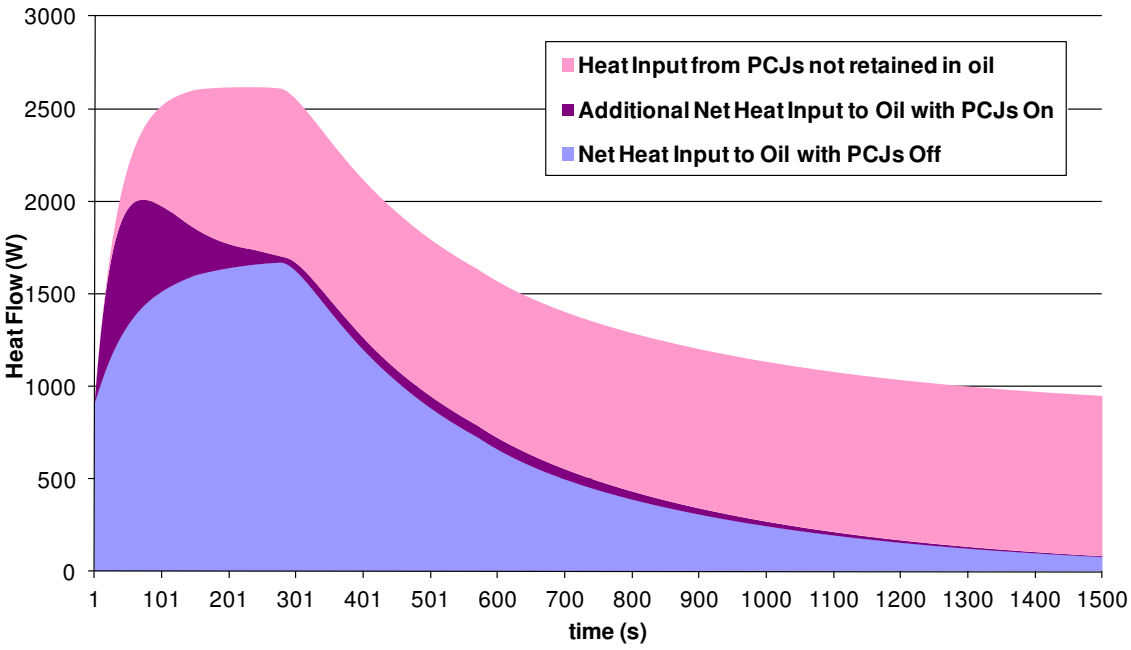

Figure 42 Change in net heat input to oil from switching the PCJs on during a 2000 rev/ min, 6bar BMEP warm-up. Also shown is the predicted heat input from jets.

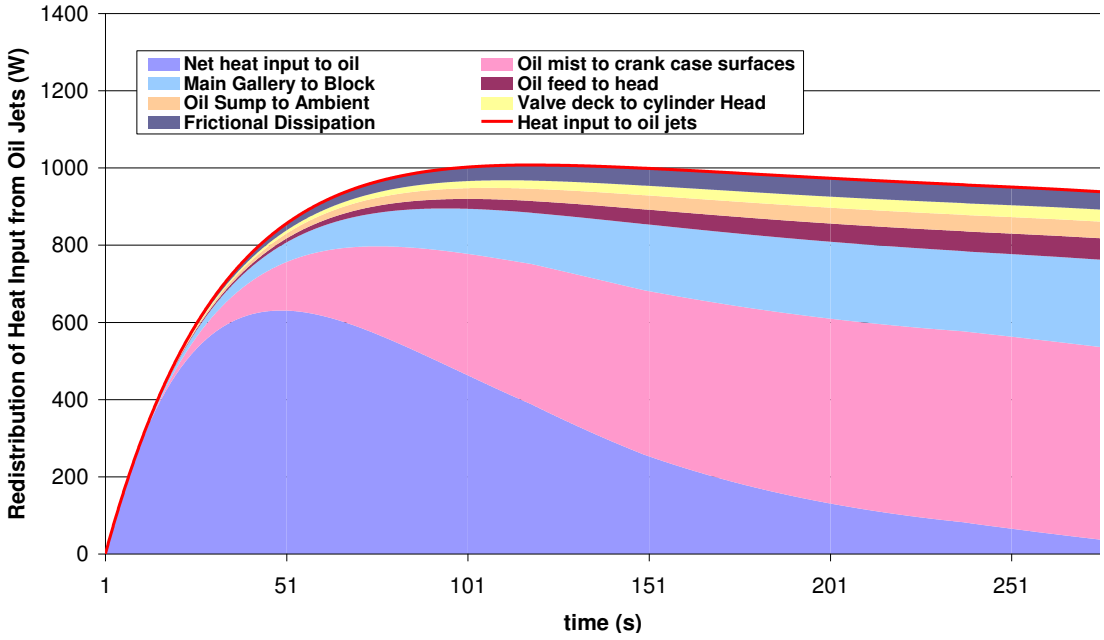

Figure 43 Heat input from PCJs retained in oil and re-distributed in the oil circuit.

The rise in oil temperature from enabling the PCJs results in lower predicted engine friction losses. With the PCJs on, total engine friction evaluated from a bulk oil viscosity correction at 2000 rev /min is on average 5 % lower throughout the warm-up and in steady state, Figure 44. This calculated benefit in friction only takes into account the effect of oil temperature on rubbing friction but in reality may extend further. Measurements by Law [20] show that switching on the PCJs causes a drop in main gallery oil pressure with an associated reduction in oil pump torque. For fully warm operation, the drop in oil pressure is ~100 kPa below 2000 rev/ min, but only 40 kPa above 2000 rev/ min. At engine speeds above 2000 rev/ min the oil pressure relief valve is open and helps to regulate the main gallery pressure in response to switching the PCJs on. Overall, this translates to a drop in engine FMEP of ~2 kPa at the lower engine speeds (when the pump relief valve is shut) and ~1 kPa from around 2000 rev/ min and above. This saving (~1 % at 2000 rev/ min) is small when compared to the predicted saving in rubbing friction. Moreover, following a cold start, higher oil viscosity causes the pressure relief valve to open even at the lowest engine speeds meaning the savings in pump torque from switching the PCJs on may be lower during warm-up than for fully-warm operation. A further effect not accounted for in the model, is an increased oil wetting of the liner when the PCJs are switched on. This could potentially have an additional influence on piston friction, but has not been quantified here.

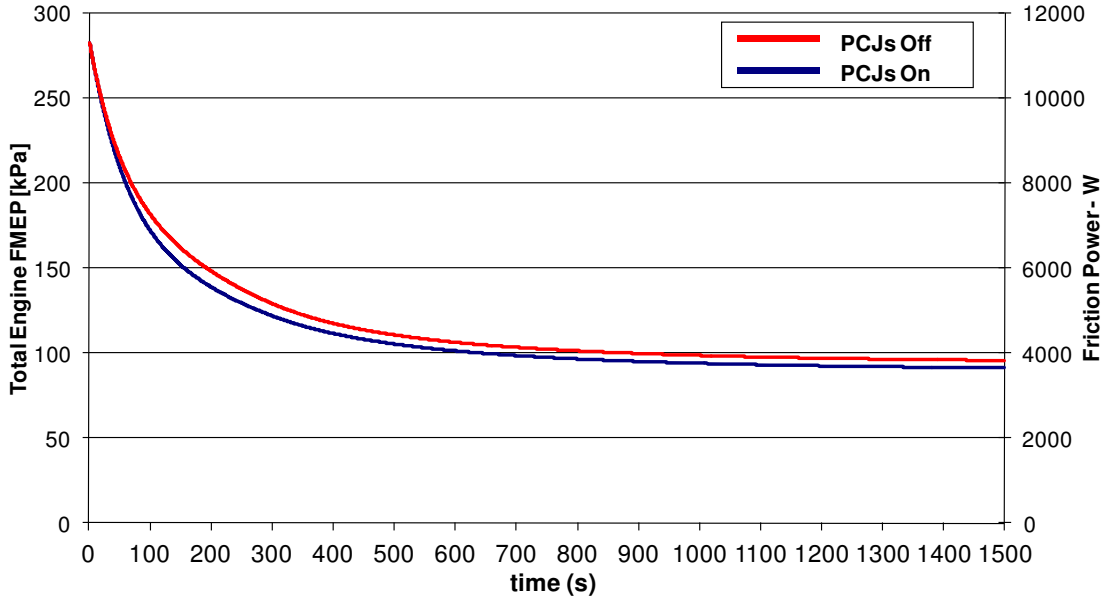

Figure 44 Predicted total engine friction during a warm-up at 2000 rev/ min, 6 bar BMEP with the PCJs switched on and off.

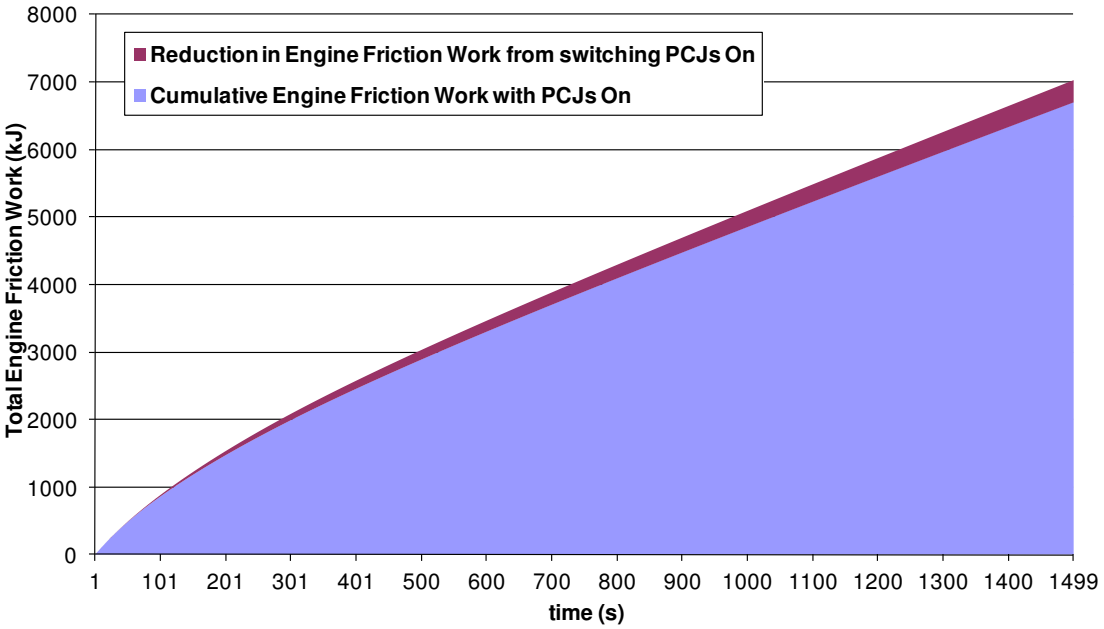

Figure 45 Model Predictions for Total Engine Friction Energy Dissipation with PCJs on and off.

4.5.2. Effect of PCJs on Heat Rejection to Coolant during Warm-Up

While heat rejection to the oil circuit is increased when the PCJs are switched on, simulated and measured coolant temperature trends both indicate that heat rejection to the coolant is reduced during warm-up, as illustrated in Figure 46. Predictions of the balance of energy transfers out of the piston show that, this is partly due to the cooler piston conducting less heat through the rings into the cylinder liner. The drop in heat rejection to the coolant during warm-up was estimated from measurements of coolant temperature according to the following equation:

$$\dot{Q}_c = Mc_v \frac{\delta T_c}{\delta t} \qquad \text{Equation 48}$$

where M is the mass of coolant in the inner circuit (active during the warm-up), and T_c is the coolant temperature. Figure 47 illustrates that enabling the PCJs reduced the measured heat rejection to coolant by ~1 kW between 50 – 150 s into a warm-up at an engine speed and brake load of 2000 rev/ min and 6 bar respectively. This is comparable to the simulated heat transfer rate to the oil jets at the same engine operating condition. However, the simulated drop in heat rejection to coolant is approximately half that calculated on the test engine, ~0.5kW.

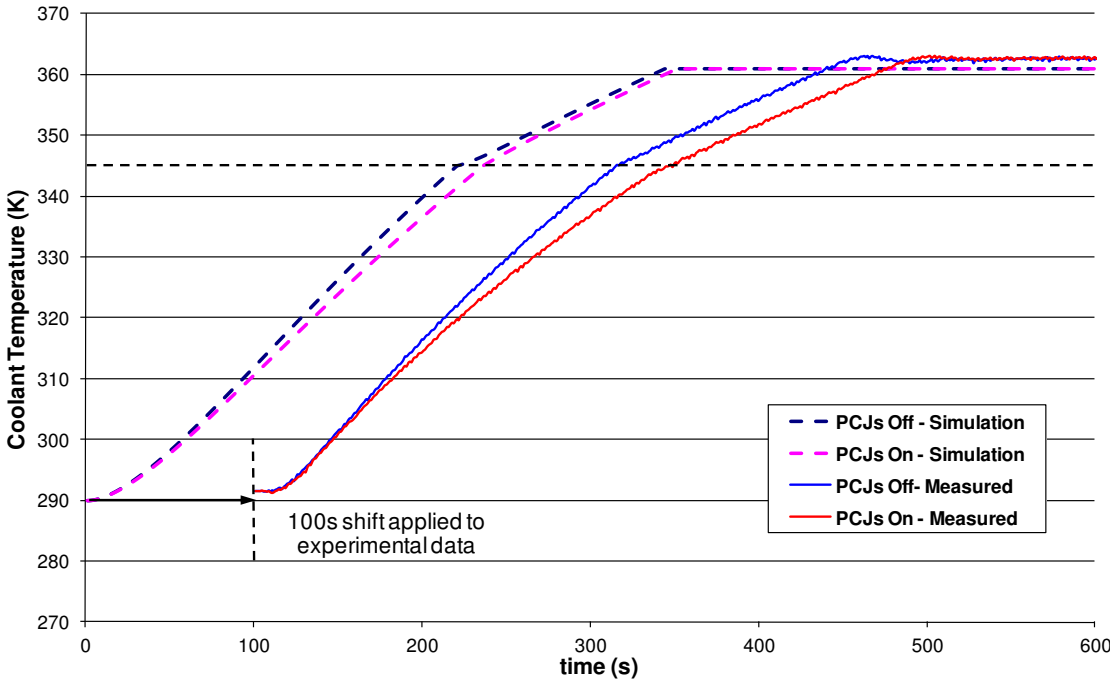

Figure 46 Comparison of model predictions for coolant temperatures made using PROMETS with experimental measurements. Engine coolant is streamed through the FCA from 280s. Engine operating condition is 2000 rev/min, 6bar BMEP.

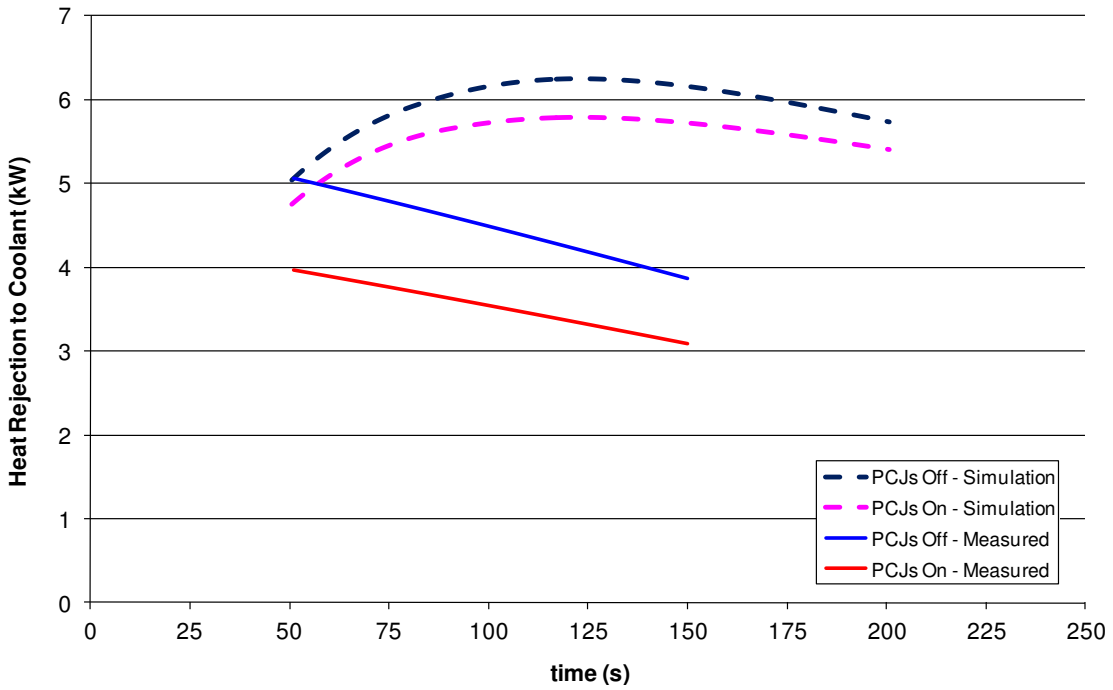

Figure 47 Measured and predicted heat rejection rates to coolant Engine operating condition is 2000 rev/min, 6bar BMEP.

Consequently, enabling the PCJs on the test engine resulted in the coolant temperature reaching 72 °C (the temperature at which the FCA thermostat opens) approximately half a minute later than with the PCJs switched off, as shown in Table 10. The simulated delay in the time to reach FCA thermostat opening was smaller, ~16 s.

2000 rev/min, 6bar BMEP	**FCA thermostat opening time (s)** (Coolant Temperature 72°C)	
	Simulation	**Measured**
PCJs Off	221	216
PCJs On	237	249

Table 10 Measured and predicted time to reach FCA thermostat opening temperature with PCJs on and off

Once the FCA thermostat opens, coolant warm-up rates are identical with and without the PCJs switched on. This is due to the redistribution of heat between the oil and coolant circuits via the FCA; with the PCJs on, higher oil temperatures result in lower heat transfer rates from the coolant to the oil across the FCA, compensating for a lower heat rejection from the engine block to the coolant. Overall the simulated trends agree well with the experimental observations but the simulated drop in heat rejection to the coolant in the early phases of warm-up is under-predicted in the model. One reason for this may be the model assumption that the in-cylinder heat flux distribution is identical with the PCJs enabled or not. In reality the drop in piston temperature caused by the jets being switched on may lead to higher heat transfer rates into the piston crown and an associated reduction in heat transfer to the cylinder head and liner which may contribute further to the reduction in coolant heat rejection.

4.5.3. Global Engine Heat Flows – Fully-warm operation

It has been shown in previous sections that the change in piston heat outflows as a result of enabling the PCJs affects the global heat flow paths through the engine structure, coolant and oil circuits. This is further illustrated in Figure 48 and 49 which show simulated results under fully-warm conditions for cases when the FCA is streamed with coolant. Heat input to the structure from gas-side heat transfer in the

combustion chamber and exhaust ports is shown by the orange flow lines. Heat input from friction dissipation at the rubbing surfaces is shown by the red flow lines. Overall, for the engine running condition considered here of 3000 rev/ min, 6bar BMEP, the PCJs affect a small proportion of the total heat flow through the engine structure as heat input to the piston crown accounts for only 1 3% of the total heat transfer. With the PCJs on, heat transfer to the oil is increased from 329 W (9 % of the piston crown heat input) to 1734 W (49 % of the piston crown heat input) resulting in an oil temperature rise of ~6 °C. On the other hand, heat transfer from the engine block to the coolant is reduced by 1168 W as a result of less heat being conducted through the rings into the cylinder liner. The increase in oil temperature promotes a higher heat transfer rate from the oil to the coolant circuit across the FCA, redirecting ~65 % of the additional heat input to the oil back into the coolant system. Higher heat transfer rates from the oil to the engine structure (from the crankcase oil mist, oil flowing in the main gallery and valve deck) account for the majority of the remainder. Heat losses from the oil sump to ambient under natural convection conditions increase but only marginally. Therefore, while heat transfer to the coolant across the engine block is reduced when the PCJs are enabled, the overall heat rejection to the coolant system is unchanged, as illustrated in Figure 50. This also reflects the observation made in the previous section that coolant warm-up rates with the PCJs switched on or off are similar once coolant is streamed through the FCA. On the test bed, measured changes in the coolant temperature rise across the engine and FCA also reflect the above observations [113]. With the PCJs on, the temperature rise across the engine is generally reduced by ~0.5-1 ºC. The small temperature change reflects the relatively high coolant flow rates through the engine.

With no coolant streamed through the FCA, the increase in oil temperature from switching the PCJs on is larger at ~14 ºC. This is due to a weaker thermal coupling between the oil and coolant circuits. As for cases where coolant is streamed through the FCA, enabling the PCJs does not alter the total coolant heat load. Additional heat flux to the oil circuit from the PCJs is re-introduced into the coolant system, in this case not via the FCA but through the engine structure. This in contrast to the behaviour observed during warm-up when the engine structure is cold. In this case heat transfer from the oil is absorbed by the structure’s thermal capacity and switching the jets on from a cold start, does lead to a temporary reduction in the heat rejected to the coolant circuit, with an associated delay in its temperature rise.

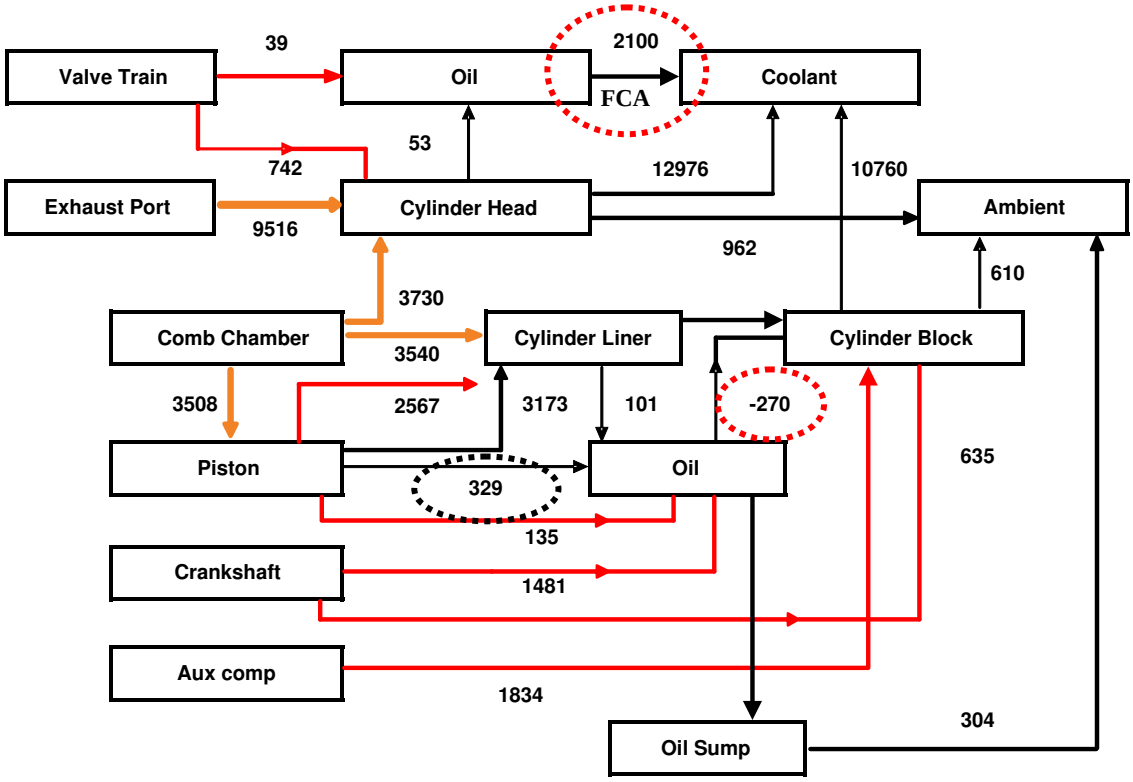

Figure 48 Engine heat flow at 25mins into warm-up (fully-warm) with PCJs off and FCA streamed with coolant

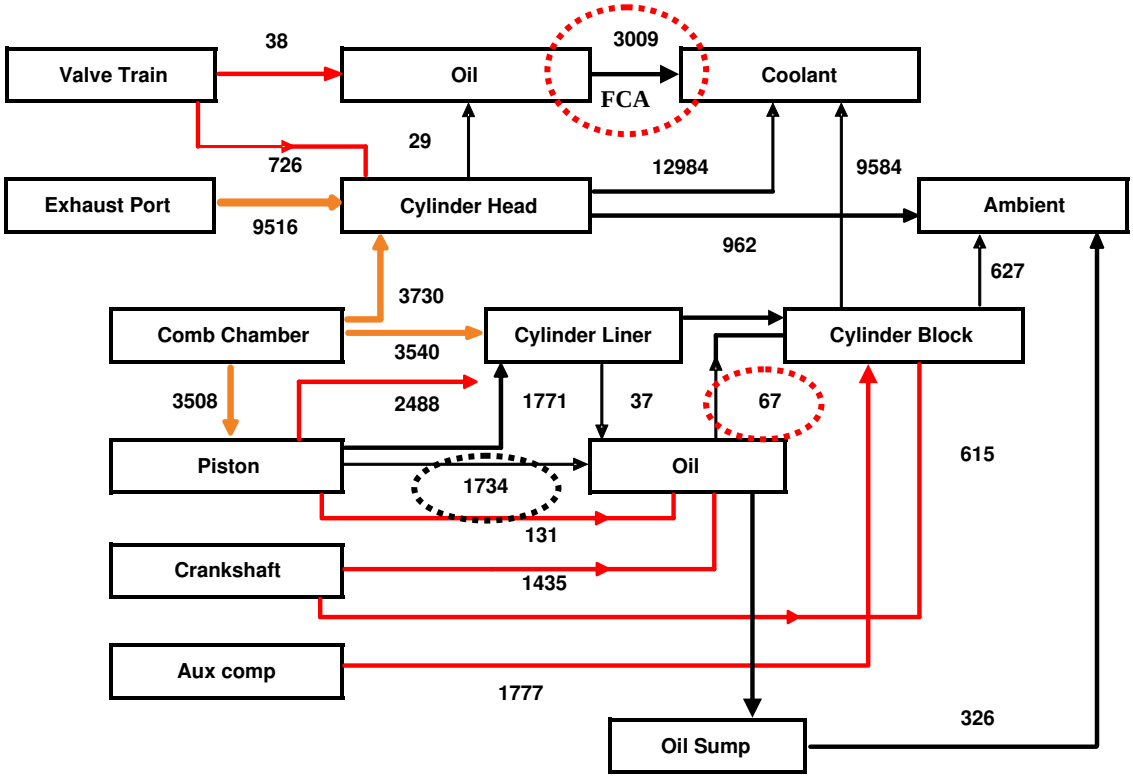

Figure 49 Engine Heat Flow at 25mins into warm-up (fully-warm) with PCJs on and FCA streamed with coolant

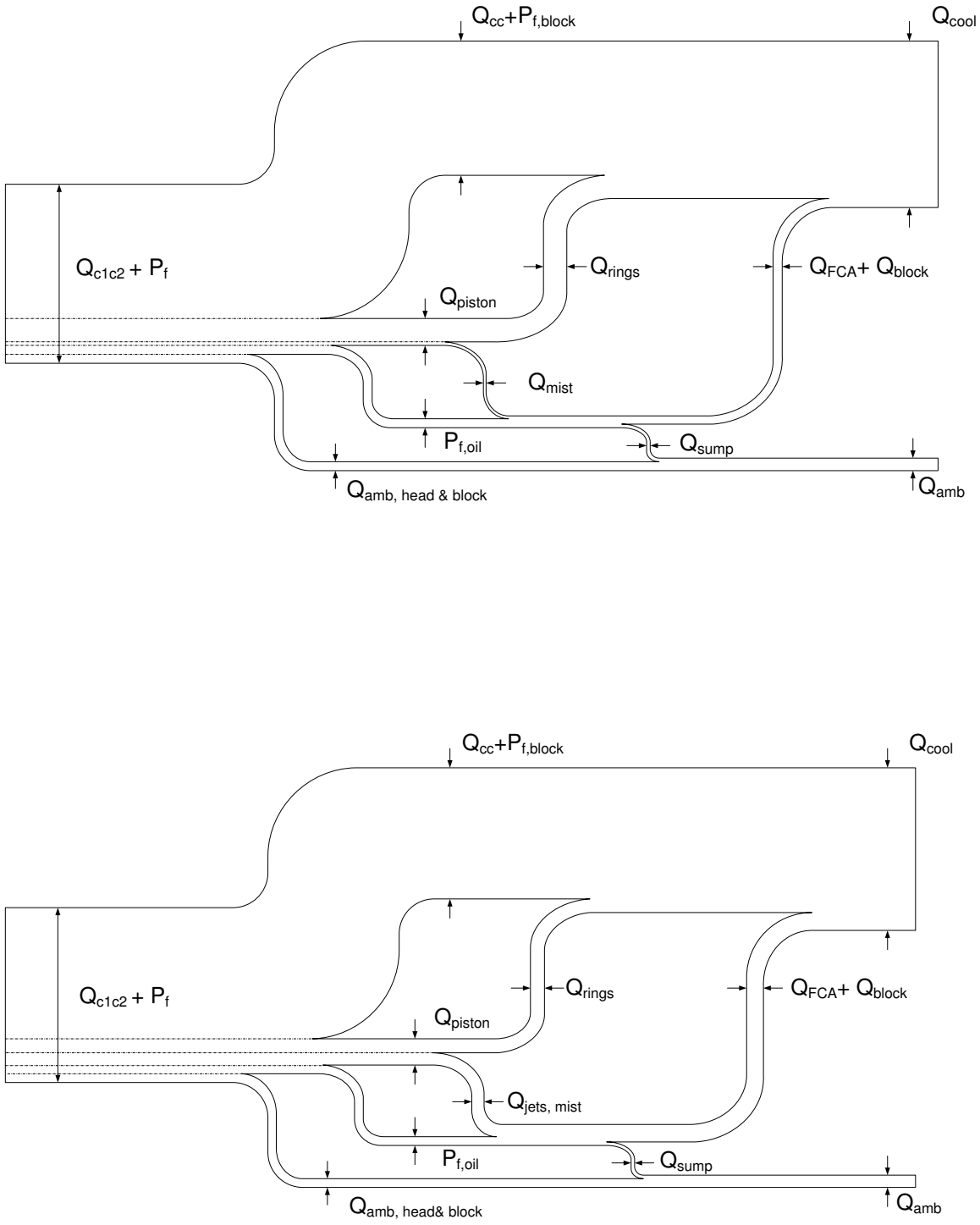

Q_{c1c2} – Gas side heat transfer, **P_f** – Frictional power loss, **$P_{f,\ block}$** – Frictional heating in engine block, **$P_{f,\ oil}$** – Frictional heating in oil, **Q_{cc}** – Heat Transfer to combustion chamber walls and exhaust port (excludes piston crown), **Q_{piston}** – Heat transfer to piston crown, **Q_{rings}** – Heat conduction through piston rings, **$Q_{jets,\ mist}$** – Piston heat transfer to oil jets and mist, **$Q_{amb,\ head\ \&\ block}$** – Heat transfer to ambient from cylinder head & block, **Q_{sump}** – Heat transfer to ambient from oil sump, **Q_{amb}** – Total heat transfer to ambient, **Q_{FCA}** – Heat transfer from oil to coolant across FCA, **Q_{block}** – Heat transfer from oil to engine block, **Q_{cool}** – Total heat transfer to coolant

Figure 50 Comparison of oil and coolant heat flows with PCJs on (top) and off (bottom). Heat input to the coolant from the piston crown via the rings and cylinder liners is reduced with the PCJs on but heat input to the coolant via the FCA is increased.

4.6. Summary and Discussion

Revisions to the piston heat transfer model to account for the effect of PCJs have been described. PCJs introduce an additional heat outflow path from the piston, redirecting a greater percentage of the combustion heat load from the piston crown to the oil circuit. Gas side heat transfer to the piston crown represents only a small proportion of the total heat flow through the engine. Nonetheless, switching the PCJs on or off has a clearly distinguishable effect on the heat rejection to the oil and coolant circuits and hence their respective warm-up rates and in the case of the oil circuit, steady state temperature too. Switching on the PCJs dropped piston temperatures under fully-warm conditions by ~40-60 °C depending on operating condition. As a result, heat conduction through the piston rings into the cylinder liner is reduced. Increased heat transfer to the oil circuit, means that throughout the warm-up, oil temperature is typically ~8-10 ºC hotter when the PCJs are enabled, with predicted benefits in friction of ~5 % for the range of engine operating conditions considered here. Model predictions of changes to the heat flows within the oil circuit in response to enabling the PCJs, show that the majority of the heat input from the oil jets is re-distributed to the engine structure, particularly from the crankcase oil mist. In the fully-warm state, the increase in oil temperature is dependent on whether the FCA is streamed with coolant or not. Heat balance analyses across the engine structure, coolant and oil circuits, show that higher oil temperatures promote increased heat transfer rates from the oil to the coolant across the FCA and engine structure. As a result while heat rejection from the engine block to the coolant was lower with the PCJs enabled, the total coolant heat load was unchanged.

It proved difficult to derive a value for the ring-pack thermal resistance that would give piston temperature predictions consistent with measured values with the PCJs off. In particular, the model under predicted values at the lower engine speeds. A thermal resistance network model of the piston-to-liner heat conduction path showed that neither changes in oil conductivity with temperature nor changes to the liner oil film thickness could explain the engine speed dependency of the empirically derived thermal resistance variation. Similarly, determining the split between heat outflow through the rings and from the piston underside to the crankcase oil mist is a challenging task. Heat transfer to the oil circuit with the PCJs disabled was based

upon the correlation of steady state oil temperature predictions with test bed measurements and the predicted rise in fully-warm piston temperature when heat transfer from the underside was inhibited. With the PCJs off conduction through the rings dominates accounting for over 80 % of the total heat outflow from the piston. The empirically derived variation of ring-to-liner thermal resistance with engine speed was determined solely to achieve good correlation between measured and predicted piston temperatures over the range of conditions investigated. The physical significance of this variation is uncertain and could rather point at other model deficiencies, particularly in accurately determining the piston crown heat input. While the in-cylinder heat release correlation adopted in PROMETS provides a convenient way of modelling bulk heat transfer rates to the coolant, there are still deficiencies when determining the in-cylinder heat flux distribution. As this is based solely on an area weighting method it cannot account for changes in piston temperature with engine speed and load and the effect that this might have on the in-cylinder heat flux distribution. Determining this would require a specific investigation perhaps using CFD analysis or experimental measurement [124]. However, this falls outside the wider scope of the model development described here which was mainly to account for the effect of PCJs on the heat rejection characteristic of the engine, in particular the increased heat flow to the oil circuit.

The heat transfer effectiveness of the oil jets was primarily determined from the drop in piston temperatures observed when the PCJs were switched on, assuming the thermal conductance of the other heat exchange paths were unchanged. Values derived for the crown gallery heat transfer coefficient were typical of those reported in the literature, as was the predicted heat outflow distribution from the piston. Changes in the oil warm-up trends between PCJs on and off cases were used as further validation of the model; these correlated well with test bed measurements. However, the predicted drop in heat rejection to the coolant in the early phases of warm-up was not as severe as that observed on the test bed. There still remains some uncertainty as to whether switching the PCJs on alters the in-cylinder heat distribution as a result of the colder piston bowl. This may lead to increased heat flow into the piston bowl and oil jets and an associated reduction in heat transfer from the cylinder head and liners into the coolant.

Chapter 5 – Modelling Thermal- Friction Conditions in Crankshaft Main Bearings

5.1. Introduction

In the following, the development of a thermal-friction model for a journal bearing and its integration into PROMETS is described. The principal requirement for this was to predict bearing oil film temperatures and friction losses from engine start-up through to fully warm operation. In doing so the viscosity based correction applied at cold temperatures to the crankshaft friction group can then be based on film viscosity, rather than that of the bulk oil. Changes to the engine aimed at promoting lower friction levels during cold operation must be assessed on their ability to raise local oil temperatures. The revised model offers a better tool to do so. Main bearing design changes that could potentially promote a faster oil film temperature rise and minimise the cold start friction penalty can also be explored. This is the topic of Chapter 6.

The ability to calculate local heat flows and friction dissipation controlling the bearing oil film represents a significant addition to the predictive power of the model. In the version of PROMETS used in [34] the proportion of friction work retained within the oil film was taken to be constant. However, investigations by Baylis [33] and Jarrier [125] suggest that the heat flow distribution within the bearings varies considerably from a cold start to fully warm operation.

Lubrication conditions in journal bearings are complex such that modelling heat transfer from first principles generally requires thermo-hydrodynamic (THD) models solving the Reynolds and Energy equations [126] [127], an approach that is beyond the scope of this investigation. Given that a requirement of the model was that it could be integrated into PROMETS, retaining the lumped capacity approach was essential. A finite difference, transient heat conduction model was developed by previous researchers at the University of Nottingham [33]. Agreement of model predictions with experimental data was excellent and proved that such models could provide insight into the rapidly changing thermal-friction interactions occurring between the bearing oil film and surrounding friction surfaces. The model described here uses only three additional elements to characterise temperature fields

surrounding the oil film while the oil film temperature is assumed to be isothermal. A small number of model parameters means that the model is relatively simple to setup and calibrate against experimental data.

This chapter is divided into three main parts. The first looks at the theory behind the model, in particular the thermal-friction governing equations. The second section describes how the model was integrated into PROMETS, including the revision of the generic crankcase elemental representation. The third section is concerned with validation of the model and the sensitivity of predictions to model uncertainties and assumptions.

5.2. Model Theory – Introduction

The oil film temperature in a journal bearing varies around the bearing circumference, from the feed temperature at the inlet to the highest temperatures in the thinner film regions [128]. In the fully warm state, the mean oil temperature rise across the bearing can be estimated by assuming that around 90 % of the friction power is retained in the oil film [129]. If adiabatic thermal conditions are assumed, the temperature variation may be up to 1.5-2 times as much as the mean oil film temperature rise. However, in reality the strong thermal coupling to the crankshaft limits this temperature fluctuation substantially. Measurements on connecting rod bearings of a 1.3 litre gasoline engine running at speeds of up to 6000 rev/ min showed that the temperature variation around the bearing circumference did not exceed 4°C [129]. The bearing and crankshaft were also at approximately the same temperature. Measurements of the oil film temperature distribution around the main bearing circumference by Shayler et al. [4] also showed a peak around the point of minimum oil film thickness. However, the variation in temperature persisted for only a few seconds after commencing engine motoring and was small enough to be neglected. Based on the observations of Jones [129] and Shayler [4] and with the simplicity of the model in mind, a uniform film temperature has been assumed in this analysis.

Even with an isothermal bearing assumption, there still remains the decision as to which value best represents the effective oil film temperature. Different definitions for the effective film temperature have been reported in the literature, generally as a

function of the bearing inlet and outlet oil temperatures [98] [130]. Dowson [128] observed that the oil outlet temperature provided a good estimate of the average bush temperature. Han et al. [131] compared bearing model predictions using an iso-viscous assumption with those obtained from a THD analysis. When oil viscosity was evaluated using the feed temperature to the bearing, predictions for load capacity and power loss were significantly different. However, when the average outlet temperature was used, results from the iso-viscous assumption correlated well with those from the THD analysis. For this investigation, no oil temperature measurements were available at the bearing outlet, just at the inlet and in the film. Given the limited data availability and based on the observations of Dowson and Han, the bearing outlet temperature has been assumed to be the same as the film temperature in the following analyses. This also follows the approach of Jarrier et al. [125] and Pinkus et al. [132].

5.2.1. Oil Film Energy Balance and Oil Flow Calculation

Given the small volume of oil retained in the bearing film, its thermal capacity (MC_v) is small and neglecting this, an energy balance for a control volume enclosing the film gives:

$$\dot{\mathbf{P}}_{\mathbf{fric}} - \dot{\mathbf{m}}\mathbf{C}_{\mathbf{p}}\mathbf{dT}_{\mathbf{oil}} - \dot{\mathbf{Q}}_{\mathbf{shell,cap}} - \dot{\mathbf{Q}}_{\mathbf{shell,block}} - \dot{\mathbf{Q}}_{\mathbf{journal}} = \mathbf{0} \qquad \text{Equation 49}$$

$\dot{\mathbf{P}}_{\mathbf{fric}}$ is the frictional power loss in the bearing and is calculated according to Equation 20. The second term in Equation 49 represents the net enthalpy out flow from the oil film due to the oil temperature rise across the bearing. The last three terms represent, in order, heat transfer from the oil film to the lower and upper shells, respectively and to the crankshaft journal.

Oil flow rate was calculated using the formulations developed by Cameron [98] and Martin [133] as the sum of two components: hydrodynamic and pressure fed flows. The hydrodynamic component is due to the ‘pumping action’ of the journal bearing itself. The rotation and eccentricity of the journal both contribute to the generation of an axial pressure gradient in the oil film which forces oil to flow out of the bearing sides. This flow component can be expressed as:

$$\dot{V}_h = Q^* \frac{UC_r L}{2}$$ Equation 50

where $Q^* = \varepsilon\left(2 - \frac{L}{D}\right)$ Equation 51

ε is the eccentricity ratio, C_r the radial clearance [98], **U** is the relative bearing surface speed and **L** the bearing length. The main bearing dimensions of interest are summarised in Table 11.

For bearings with a central oil feed groove extending 180° of the bearing circumference, the pressure flow can be calculated according to the equation derived by Martin [133]:

$$\dot{V}_p = \frac{C_r^3 P_{feed}}{\mu}\left[\frac{1.25 - 0.25\left(\frac{a}{L}\right)}{6\left(\frac{L}{a} - 1\right)^{0.333}} . f_1 + \frac{\frac{D}{L}}{6\left(1 - \frac{a}{L}\right)} . f_2\right]$$ Equation 52

The feed pressure (P_{feed}) is the main gallery gauge oil pressure measured on the test bed and is provided as a model input (see Figure 60 for experimental data), **a**, is the axial length of the groove and the functions f_1 and f_2 account for the effect of journal eccentricity. Under the narrow-bearing approximation (L/D < 1/3) the attitude angle is directly related to the eccentricity ratio according to:

$$\tan\beta = \frac{\pi}{4}\frac{\left(1 - \varepsilon^2\right)^{1/2}}{\varepsilon}$$ Equation 53

Based on the attitude angle, values for f_1 and f_2 can be derived from the formulations in [133] and these are summarised below in Table 12. The non-dimensional feed pressure flow for different eccentricity ratios is also shown.

		mm
D	Diameter	65
L	Length	22
a	Supply Groove axial length	4
C_r	Radial Clearance	0.035

Table 11 Main bearing dimensions

Eccentricity ratio	Attitude Angle β (°)	$\mathbf{f_1}$	$\mathbf{f_2}$	Non-dimensional feed pressure flow $\left(\dot{V}_p \mu\right)/\left(C_r^3 P_{feed}\right)$
0.2	75	2.22	3.64	2.46
0.4	61	2.73	5.12	3.41
0.6	46	3.13	7.58	4.94
0.7	39	3.15	9.15	5.89
0.8	31	2.99	10.96	6.96
0.9	21	2.61	12.97	8.13

Table 12 Non-dimensional feed pressure flow at different bearing eccentricity ratios

The total volumetric oil flow through the bearing is then given by:

$$\dot{V}_{oil} = \dot{V}_h + \dot{V}_p \qquad \text{Equation 54}$$

The oil flow rate prediction depends on the chosen values of radial clearance and eccentricity. The coefficient of thermal expansion of the crankshaft journal (chromium steel) is around 10 % higher than that of the main bearing housing (cast iron). Measurements by Baylis [33] show that the rate of change of journal diameter is typically 30 % higher than that of the bearing shells located in the cast iron block. For a typical temperature increase of 70 °C, the reduction in clearance can be estimated to be around 7μm. Based on the measurements of Baylis the radial clearance was set to a constant mean value of 35μm for all oil flow rate calculations presented in this analysis. While oil flow rate shows a strong dependence on clearance (Equation 52), the film temperature prediction is sensitive to the clearance value mainly in the later stages of warm-up and under fully-warm conditions (when

oil flow accounts for the major heat transfer route out of the film control volume). Good agreement between measured and simulated film temperatures throughout the warm-up phase show that the choosing a constant value for radial clearance was suitable for the modelling purposes presented here.

Journal bearing friction is directly proportional to the inverse of the radial clearance, as described by Petroff's equation [97]. Generally, an increase in radial clearance increases the oil film thickness resulting in lower shear rates and as a result lower friction dissipation [39]. Motoring tests by Baylis on main bearings with three different clearances reflect this behaviour. In the main bearing friction formulations used here, clearance is assumed constant and is taken into account by the constant $\mathbf{C_{cb}}$ (Equation 20).

Bearing eccentricity increases with load, particularly at low eccentricity values. The typical operating (design) value is between 0.6 and 0.7 [98] but according to Leong [39] may be as high as 0.9. Lower values than 0.6 may result in shaft vibration while high values are prone to shaft misalignment difficulties [97].The total oil flow rate through the crankshaft main bearings as predicted by the above formulations, for eccentricity ratios in the range 0.2 to 0.9, is illustrated in Figure 51. For the range of eccentricities in which the main bearings are expected to operate (0.7-0.9), the effect of flow rate on model predictions of sump oil and bearing film temperatures is negligible. The effect of changes to the oil flow rate through the bearings is discussed in more detail in Chapter 6, Section 6.2. From Petroff's equation it can be seen that friction force is relatively unaffected by changes in eccentricity ratio until a value of around 0.8 is reached [97]. As for clearance, bearing eccentricity is assumed constant in the friction formulations adopted here.

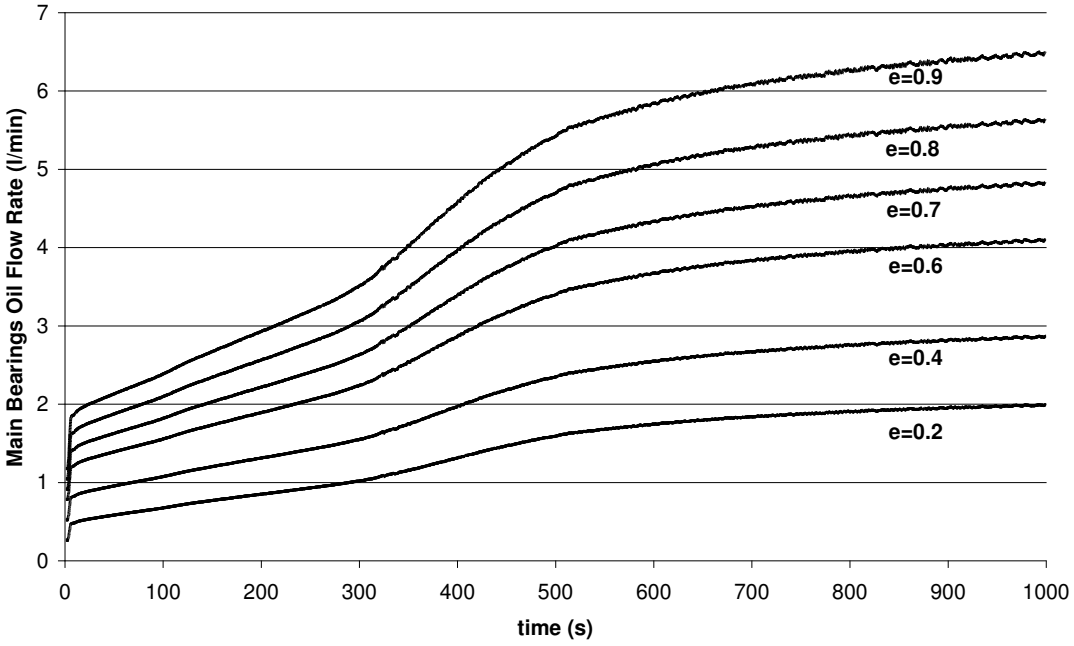

Figure 51 Total main bearings oil flow rate prediction for different eccentricity ratios at 2000rev/min

5.2.2. Model Implementation into PROMETS – Engine Crankcase representation

Integrating the bearing model into PROMETS required a revised elemental representation of the engine crankcase. Elements 17 and 18, in Figure 52, represent the bearing support walls. Historically, additional mass was associated with these elements to take into account the crankshaft thermal capacity. This simplified representation is suitable to model bulk heat exchange between the oil mass and the crankcase; predominantly heat transfer from the oil main gallery and crankcase oil mist. Under steady state thermal conditions in fact (refer to Section 5.5.2.) the temperature of the crankshaft, bearing support walls and sump oil equilibrate to within 4-8 ºC of each other. However, early in the warm-up, metal temperatures at the oil film interface change rapidly while those remote from the oil film change more slowly. Given that it is the former elements that govern the film temperature rise, an increased resolution of temperatures in the crankcase was required to model heat conduction from the oil film. This involved the addition of three elements illustrated in Figure 52, representing the crankshaft journal (element 42), the bearing cap (element 43) and part of the bearing support walls (element 44). The mass of elements 42-44 was removed from elements 17 and 18 to retain the same total mass in the crankcase as used in the previous simplified elemental representation.

All three elements are thermally linked to the crankcase oil mist. An empirically derived heat transfer coefficient of 50 W/m^2K [30] is used to calculate heat transfer between the oil mist and crankcase surfaces. A higher value of 350 W/m^2K is assigned to the crankshaft journal element. This value was chosen to give best agreement between measured and simulated oil film temperatures during warm-up, see Section 5.3. The value of heat transfer coefficient is higher than for heat exchange with other surfaces in the crankcase. This is to be expected because of the crankshaft's rotation. In reality the crankshaft journal is not directly exposed to the crankcase oil mist but conducts heat to the crankshaft webs and counterweights which are in turn exposed to the oil mist, Figure 53. Heat transfer to and from the crankcase oil mist will be governed by the temperature of the crankshaft webs which may be several degrees colder than the main journal during warm-up. This leads to some uncertainty when modelling the redistribution of heat from the crankshaft to the crankcase oil mist. The influence of this simplification on the main bearing film temperature rise is small but could have greater implication on predictions of bulk oil warm-up rates. Nonetheless good agreement between measured and simulated sump oil temperatures show that bulk heat exchange between the oil and engine structure is captured well in the model both during warm-up and in steady state.

The crank pins are not explicitly modelled in PROMETS. The proportion between friction heat conducted to the connecting-rod big-end and crankshaft pin, and that carried away by the oil flow is assumed to be the same as in the main journals. Given the absence of a connecting rod and crankpin element, the heat conduction component in this case is transferred to the bearing support wall elements (element 17 and 18), which are assigned additional mass to account for the crank-pins' thermal capacity. The modelling investigations of [125] [129] suggest that heat flow to the connecting rod is low anyhow, accounting for no more than 4-5 % of the big-end bearing friction dissipation; this justifies the simplified approach adopted in PROMETS of neglecting heat transfer from the big-end bearing films to the con-rods. The main implication of transferring friction heat from the big-end bearings to the bearing support walls rather than to a dedicated crankpin element, again, is the uncertainty in the redistribution of heat between the oil mist and crankcase surfaces and the influence of this on bulk oil warm-up rate.

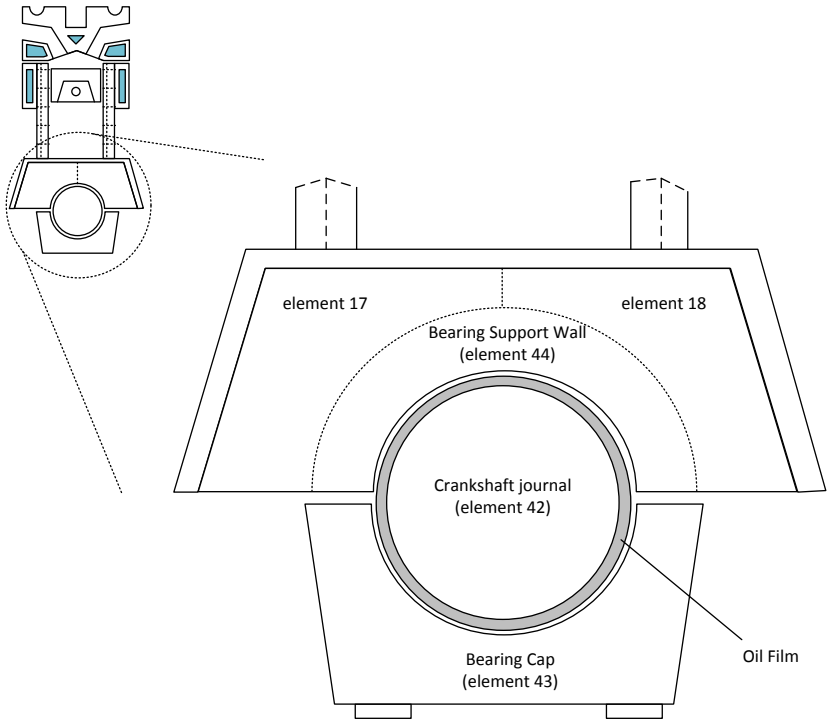

Figure 52 Revised engine crankcase representation in PROMETS required to implement the bearing film prediction - includes the additional elements 42 -44

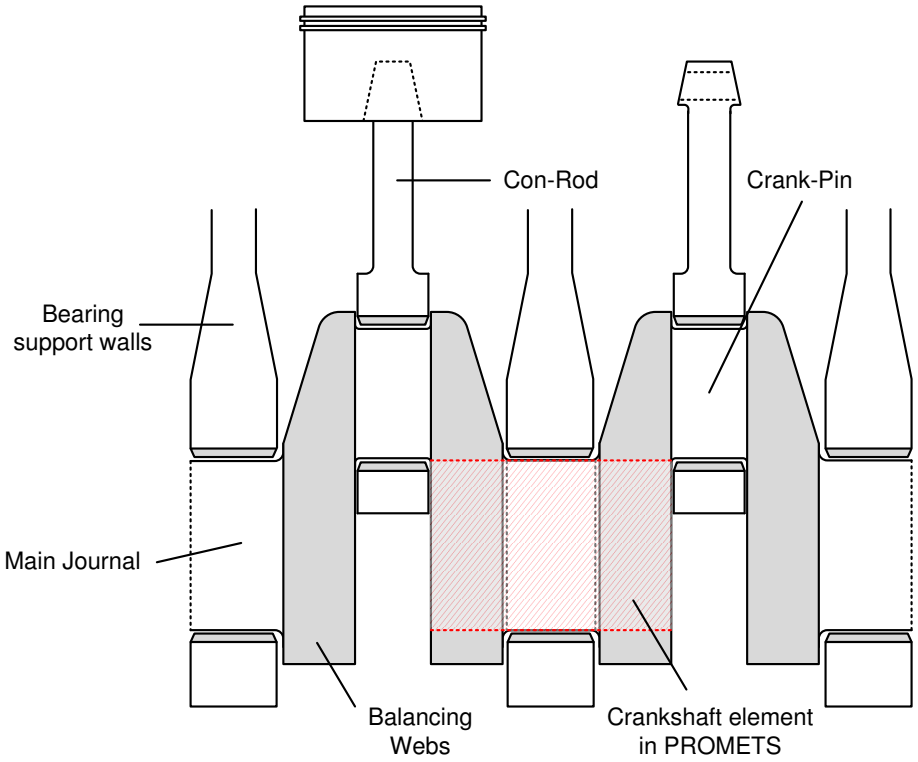

Figure 53 Engine Crankshaft Schematic. The section modelled in PROMETS is indicated by the red dashed area which includes an extended section of the main journal.

Element number	Element volume	Element mass
	m^3	kg
17	2.75e-4	2.082
42	2.75e-4	2.082
43	1e-4	0.757
44	1e-4	0.757

Table 13 Main bearing element masses

Having defined the elements at the oil film interface, the energy conservation equation, Equation 49, can be re-written as:

$$\dot{P}_{fric} - \dot{m}C_p\left(T_{film} - T_{in}\right) - \frac{\left(T_{film} - T_{ele,42}\right)}{R_{th}} - \frac{\left(T_{film} - T_{ele,43}\right)}{R_{th,1}} - \frac{\left(T_{film} - T_{ele,44}\right)}{R_{th,2}} = 0$$

The above can in turn be re-arranged to express the oil film temperature as:

$$T_{film} = \frac{\left(\dot{P}_{fric} + \frac{T_{42}}{R_{th}} + \frac{T_{43}}{R_{th,1}} + \frac{T_{44}}{R_{th,2}} + \dot{m}C_pT_{in}\right)}{\left(\dot{m}C_p + \frac{1}{R_{th}} + \frac{1}{R_{th,1}} + \frac{1}{R_{th,2}}\right)} \quad \text{Equation 55}$$

The numerical computation of temperature and frictional dissipation in the film is prone to become unstable in explicit time-marching schemes because of the strong coupling between the oil film temperature, friction dissipation and viscosity. An iterative solution outlined in Figure 54, which simultaneously satisfied film energy balance and consistency of temperature and frictional dissipation, proved to be stable and computationally efficient. The iteration is initiated using the oil film temperature from the preceding time-step to provide a first estimate of oil viscosity and friction. The film temperature is then re-evaluated using Equation 55 and the process is repeated until convergence criteria are met, i.e. when the absolute error between the oil film temperatures calculated from subsequent iterations is less that 0.05 ºC. Model predictions with a 'looser' convergence tolerance of 0.1 ºC were identical, showing that the chosen convergence criterion of 0.05 ºC was suitable. Different temperatures

(metal and oil sump temperatures) were used to initiate the iteration process and the calculated oil film temperature was shown to be independent of the temperature used.

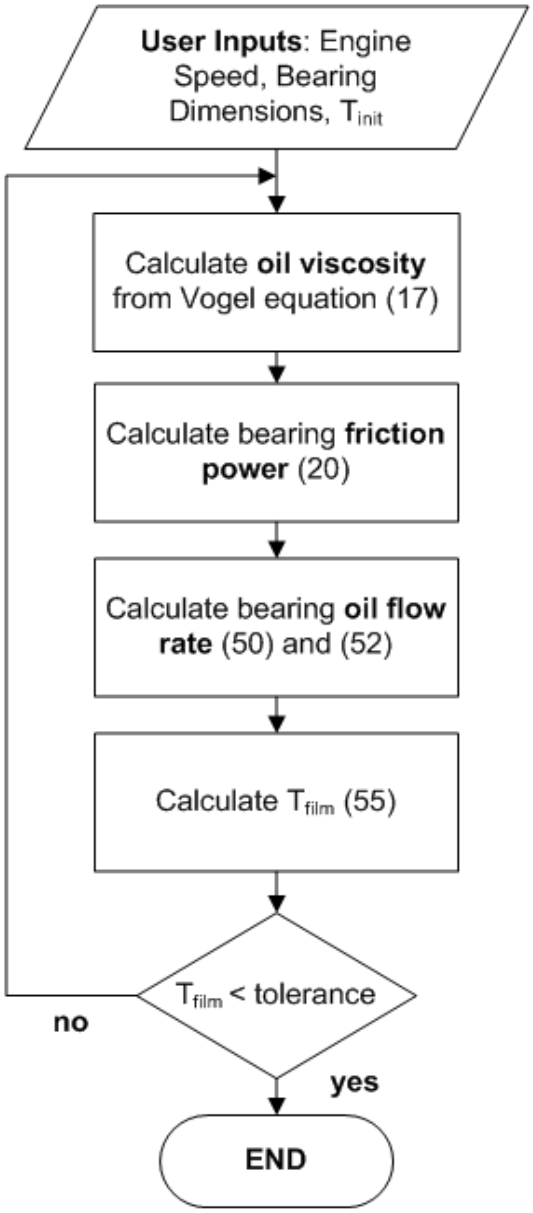

Figure 54 Flow diagram illustrating the bearing film temperature prediction

5.2.3. Friction Heat Retained in Oil - Oil Circuit Heat Flows

Friction dissipation in the bearings raises local oil film temperatures but also constitutes an important heat input to the bulk oil. In previous versions of PROMETS, the net proportion of frictional losses dissipated and retained as an increase in the internal energy of the oil was taken to be 20 % in the case of diesel

engines [33]. This was derived by comparison of predicted bulk oil warm-up rates with experimental measurements and is subject to some uncertainty. This proportion was assumed to be the same at all rubbing surfaces and to remain constant from a cold start through to fully-warm conditions. Under this assumption, net heat flows into the oil from friction dissipation at the rubbing surfaces are illustrated in Figure 55. Given that friction dissipation is highest on start up, so is heat input to the oil; at an engine speed of 2000 rev/ min total heat input to oil from friction starts at 1600 W and drops to a fully warm value of 600 W. Heat transfer from the cylinder liners to the crankcase oil mist and from the valve-deck to the oil is accounted for separately, and is not shown below.

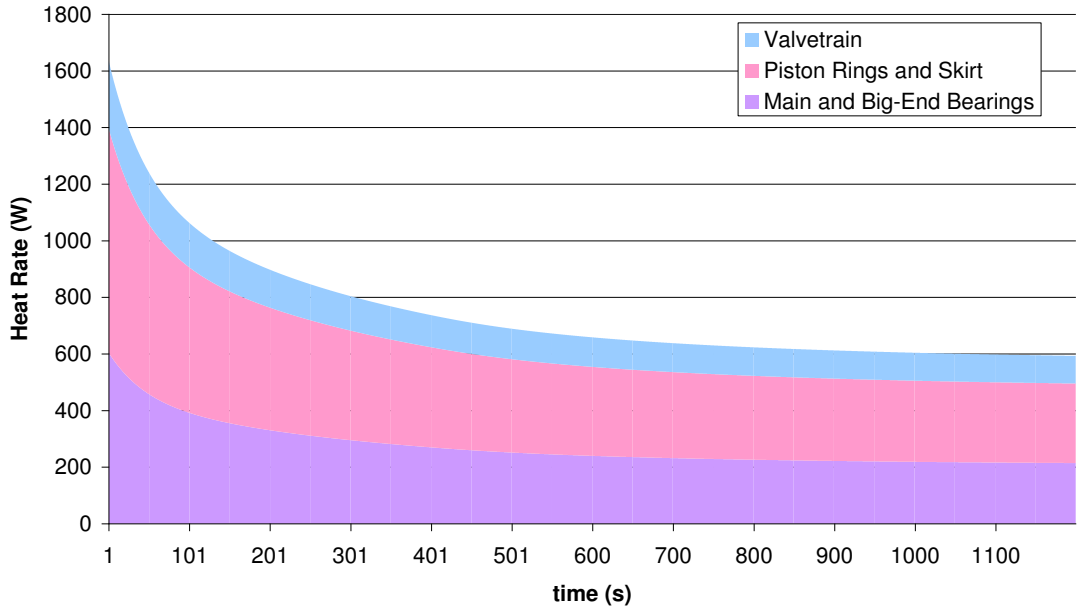

Figure 55 Heat input to oil from friction for a 20°C start at 2000 rev/ min, 3 bar BMEP using the 20% Friction-To-Oil (FTO) assumption

The investigations of Shimada [134] suggest that viscous dissipation retained in the oil film at ring-to-liner contacts is small, while modelling results in this chapter show that in steady state the enthalpy gain of the oil flow through the bearings may be as high as 80 % of the friction power (see Section 5.5.1). As part of integrating the revised bearing model in PROMETS, the proportion of friction heat retained in the oil films at the different rubbing surfaces was revised as follows:

- Friction dissipation in the piston rings and skirt was assumed to be entirely conducted into the cylinder liner following the approach of [69] [67].

- The heat flows within the main bearing oil film are inherently predicted in the film temperature calculation and need not be defined by the user as a proportion of the bearing friction power.

- It is as yet unclear what proportion of valve-train friction is retained in the oil and how this changes throughout warm-up, although camshaft bearings could potentially be assumed to behave similarly to crankshaft main bearings. The contribution of the valve-train to the total friction heat input to oil is small anyhow. Its effect on the oil temperature prediction is consequently also small and was hence unchanged.

The variation in heat input to the oil with this revised approach is shown in Figure 56, for an engine speed of 2000 rev/ min, 3 bar BMEP load. Also shown for direct comparison, is the heat input according to the approach previously adopted in PROMETS (red trace). The only significant difference between the two trends is at key on when the revised model accounts for increased heat losses from the oil to the cold engine structure; in the revised model heat input increases steadily from start-up from a value of 800 W to a maximum value of 1200 W at ~100 s into the warm-up. After about a minute of engine operation both trends are practically identical. As a result, the differences in simulated oil warm-up rates from using one approach over the other are small, such that there is no clear distinction as to which approach best represents thermal-friction conditions in the actual engine. However, if the piston friction heat contribution is included on top of that from the bearings in the revised approach, then temperature predictions for oil in the sump, and bearings films are over-predicted by 3-4 °C. Therefore, what is clear is that the contribution from the bearings was under-predicted, while that from the piston-liner pair could potentially have been over-predicted in the previous assumption. These trends are similar across the engine speed range.

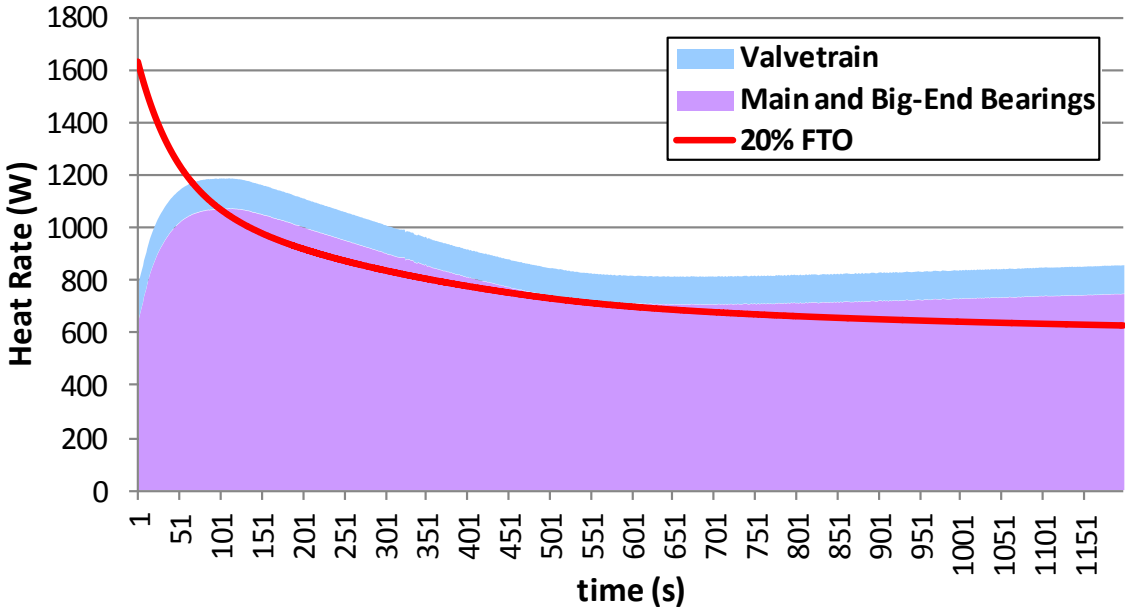

Figure 56 Revised heat input to oil from friction for a 20°C start at 2000 rev/ min, 3 bar BMEP. Red trace shows heat input to oil from using a constant 20% FTO (Friction-to-Oil).

5.3. Comparison of Model Predictions with Experimental Data

The thermal resistance values between the film and rubbing surfaces were assigned by comparison of model predictions of oil film temperature with experimental measurements. Data were taken from a 2.4 l Puma engine with instrumented bearing caps. Two 0.5 mm K-type thermocouples were installed in each of the five main bearings, one on the back of the lower shell (on the bearing cap side) and the other measuring oil film temperature. Details of the thermocouple installation are reported by Shayler et al. [4]. Initial comparisons were done for fixed speed and load conditions at different cold start temperatures. In all three cases shown, Figure 57 - Figure 59, correlation between measured and simulated trends is generally good, for both the bulk oil and bearing film temperature. For the 1000 rev/ min case, the film temperature rise relative to the oil temperature in the sump is lower than for both the 2000 rev/ min cases reflecting a lower frictional dissipation in the bearings. While the majority of the work in this research is conducted from ambient start temperatures of ~20 °C, a colder start temperature (-10 °C) is a further indicator of model performance, given that thermal-friction interactions are more severe at the colder temperature. By considering the surface area available for heat transfer (π**DL** for the journal) the thermal resistances can be converted into an effective heat transfer coefficient of 6300 W/m^{2}K (assumed the same on both the journal and shell sides).

This compares well with values of 8000 and 10000 W/m^{2}K reported by Baylis [33] and Law [20] respectively.

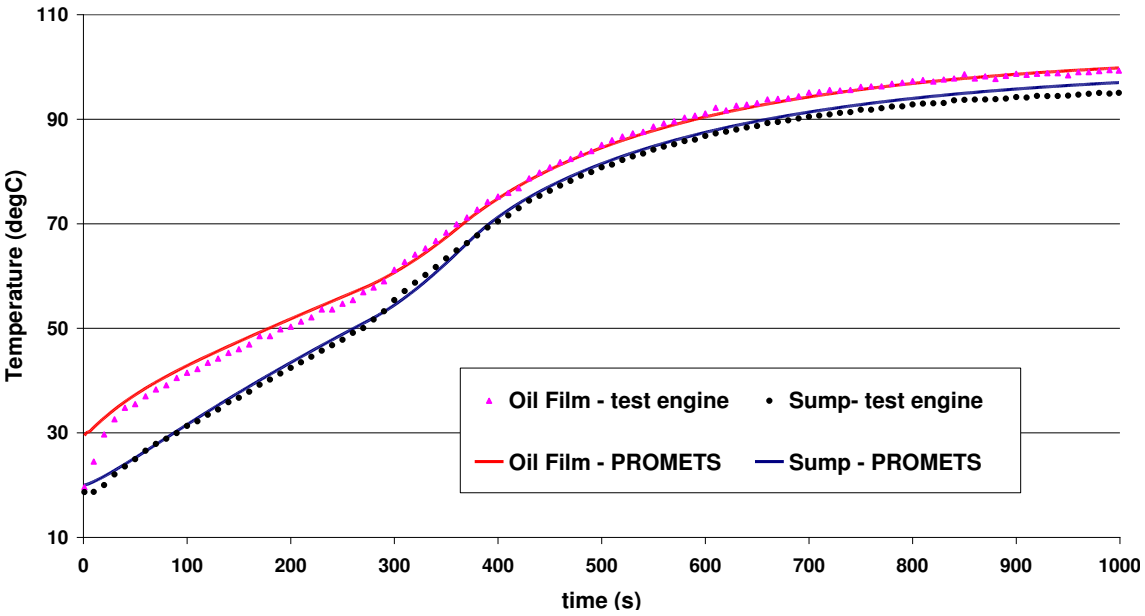

Figure 57 Comparison of model predictions for main bearing film and sump oil temperatures made using PROMETS with experimental measurements. Engine coolant is streamed through the FCA from 280s. Engine operating condition is 2000 rev/min, 3bar BMEP (20°C start)

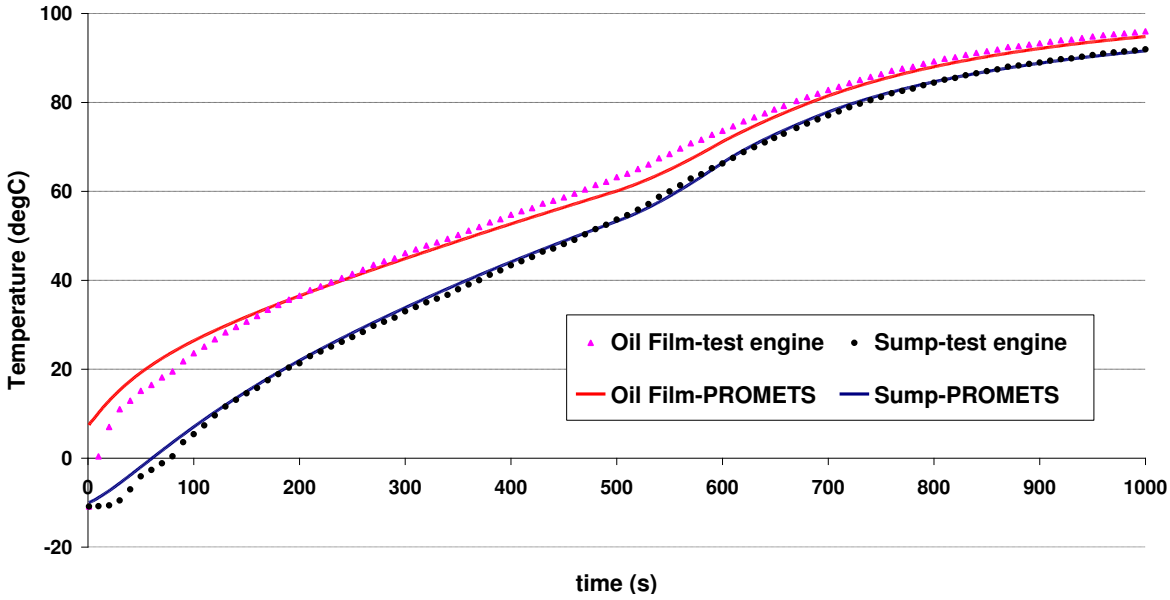

Figure 58 Main bearing film and sump oil temperature warm-up rates at 2000 rev/min, 3bar BMEP (-10°C start). Engine coolant is streamed through the FCA from 600s.

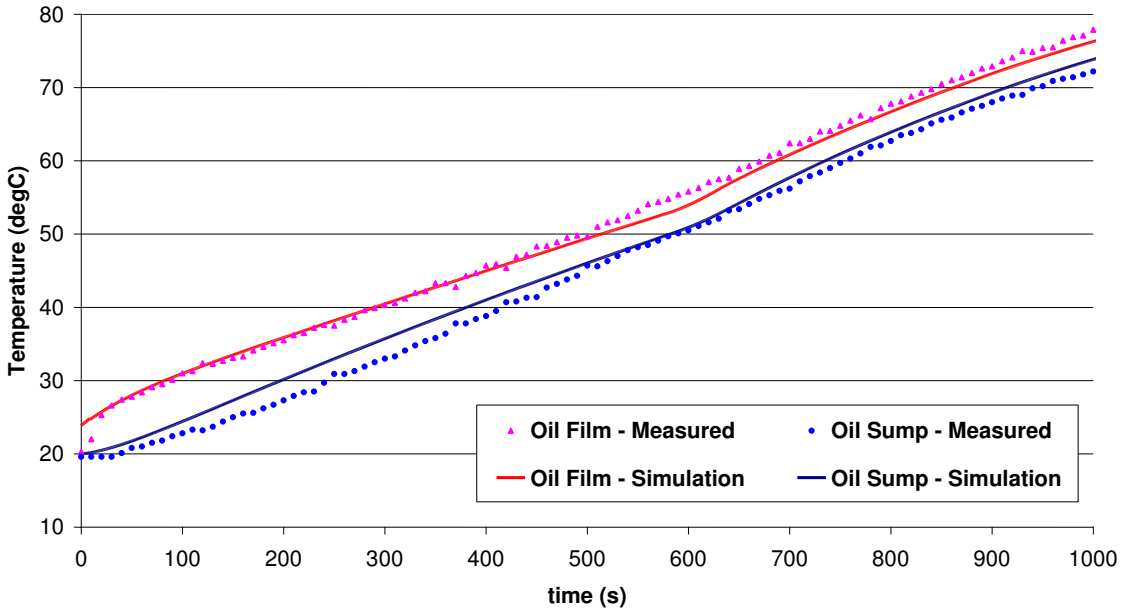

Figure 59 Main bearing film and sump oil temperature warm-up rates at 1000 rev/min, 3bar BMEP (20°C start). Engine coolant is streamed through the FCA from 600s.

The variation in measured main gallery oil pressure and predicted oil flow rate through the bearings is illustrated in Figure 60 for the 2000 rev/ min, 3 bar BMEP load case. The main bearings total flow rate is approximately 17 % of the total pump outflow which is in good agreement with the calculations provided by [101]. The reduction in pressure and increase in oil flow rate with time is a result of the drop in oil viscosity which reduces the head loss in the oil circuit.

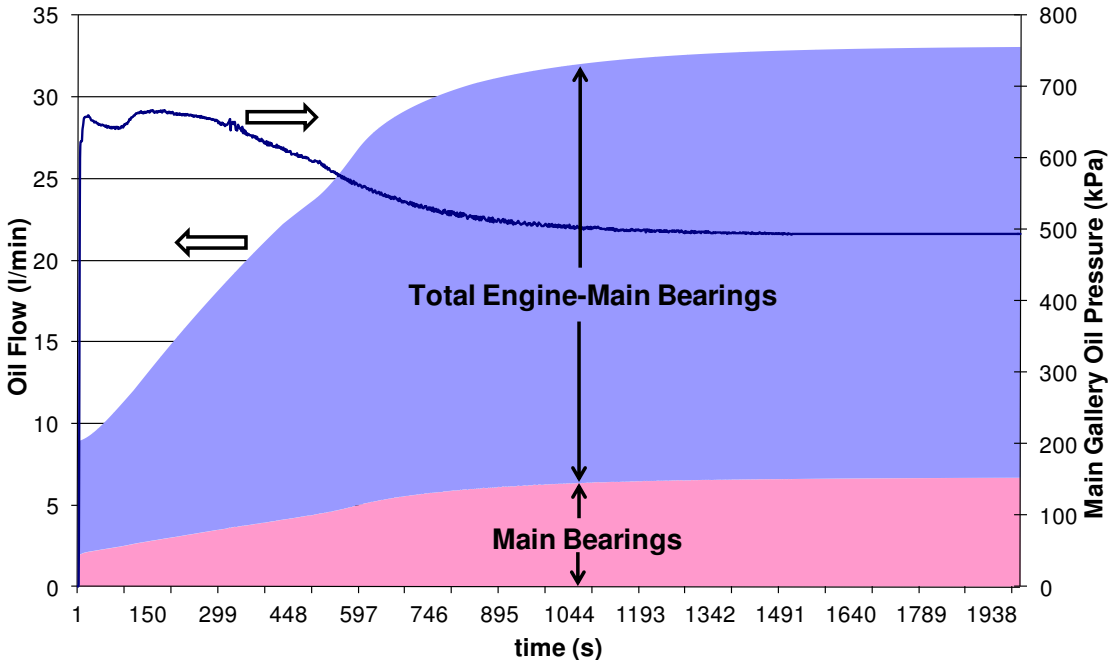

Figure 60 Measured variation in main gallery oil pressure (gauge) for a warm-up at 2000 rev/ min, 3 bar BMEP. Also shown is the predicted engine total and main bearings oil flow rate.

5.4. Sensitivity of Predictions to Model Assumptions

5.4.1. Oil Film to metal heat transfer coefficient

The main uncertainty of the model lies in the derivation of the thermal resistance to heat transfer between the oil film and bearing surfaces (bearing shells and crankshaft journal). A baseline value of 0.07 K/W was obtained by matching model predictions of film temperature to experimental data, as explained in the previous section. The assumed thermal resistance was increased and decreased by 50 % with respect to the baseline value to determine the model sensitivity to this parameter. For a fixed engine speed and load operating condition, the oil film temperature prediction is only sensitive to the thermal resistance in the early seconds after engine start-up (Figure 61). Beyond 100 s into the test, the variation between film temperature predictions with different thermal resistance values is barely distinguishable. On start up, a relatively large temperature difference of around 10-15 ºC is established between the film and bearing elements. The thermal resistance between the two has a strong influence on this initial temperature rise. However, after a few seconds of operation, quasi-steady state thermal conditions are established, from which point the film and bearing elements warm up at very similar rates. Heat conducted into the bearing elements and their thermal capacity dictates their rate of temperature rise, which in

turn dictates the oil film temperature. Changing the thermal coupling between the two merely offsets the film temperature closer or further away relative to the metal temperatures, but the rate of warm up is similar for all three thermal resistances considered. The effect on the bulk oil warm-up is even smaller and is hence not shown here. The change in the predicted friction is illustrated in Figure 62. The biggest difference (up to 20 %) is on start-up, given that the friction sensitivity to oil film temperature is greatest at cold temperatures. This behaviour is similar to the experimental observations of Baylis [33] who looked at increasing the thermal contact resistance between the back of the bearing shells and engine block. In all cases the reduction in friction is hardly discernable after 50s into the test, and completely nullified by 100 s into the test. Based on the observed sensitivity of the film temperature predictions alone, it is difficult to confidently infer the value of the thermal resistance to heat transfer between the oil film and rubbing surfaces. The baseline value of 0.07 K/W gives good correlation between measured and simulated temperature trends, with a lower value of 0.035 K/W providing better correlation in the first minute of operation.

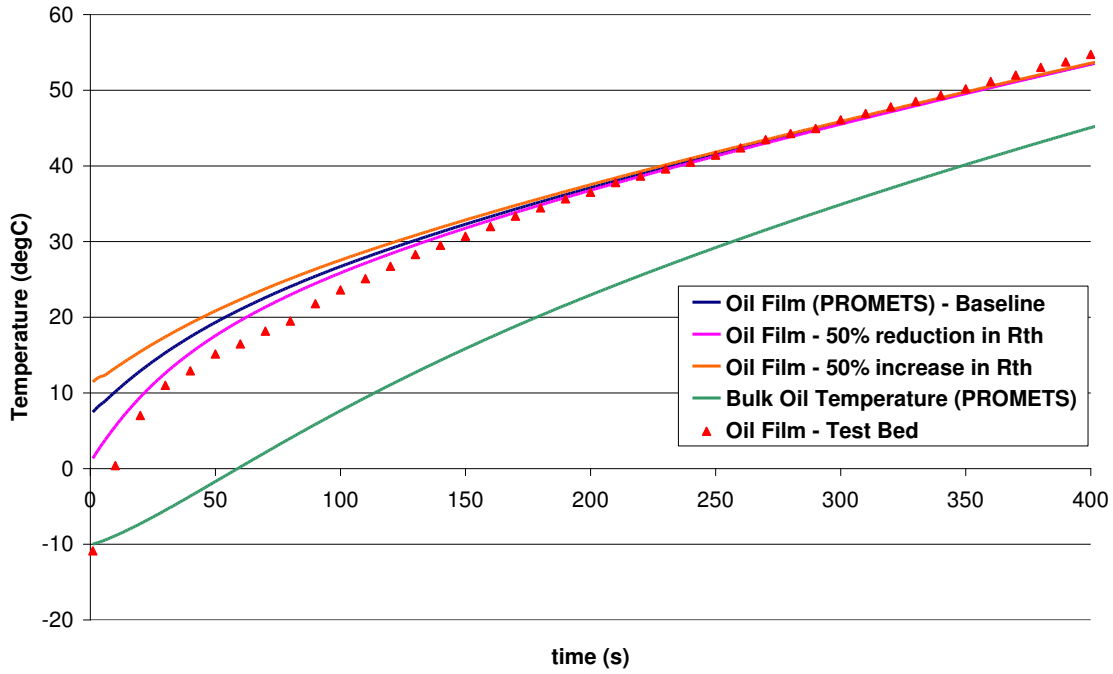

Figure 61 Sensitivity of oil film temperature prediction to +/- 50% change in the thermal resistance between the oil film and bearing surfaces (R_{th})

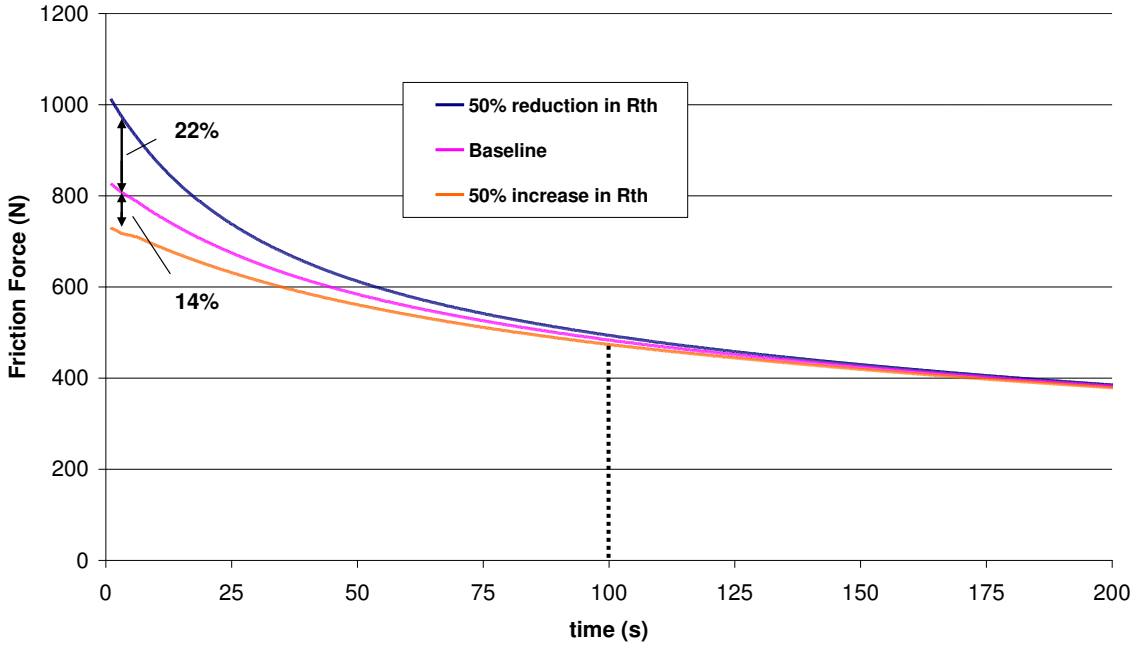

Figure 62 Sensitivity of main bearing friction force prediction to +/- 50% change in the thermal resistance between the oil film and bearing surfaces

Further comparisons of model predictions were carried out against experimental data obtained over transient (drive cycle) engine speed and load conditions. These data were provided by the University of Bath [10] from an engine of the same family as that used for this study. In this case each main bearing was instrumented with three thermocouples, measuring oil film temperature and metal temperatures at 1 and 15mm from the bearing cap's inner radius, as illustrated in Figure 63. The chosen value of thermal resistance depends on which metal temperature heat transfer from the oil film is referenced to. In the engine, heat transfer is governed by the temperatures at the inner radius of the bearing shells and outer radius of the crankshaft journal. However, simulated element temperatures in PROMETS are representative of metal temperatures more remote from the oil film. With reference to Figure 63, the thermocouple measurement at 15mm from the bearing cap's inner radius, was taken to be representative of the predicted bearing cap (element 43) temperature in PROMETS. With the low thermal resistance value (R_{th}=0.035 K/W), the film temperature prediction compares well with the experimental measurement but the temperature offset between the film temperature and bearing cap is under predicted (see Figure 64). With the 'baseline' value of thermal resistance the film temperature is more responsive to changes in engine speed and the temperature offset

to the bearing cap element is more representative of measured trends (see Figure 65). A value of 0.07 K/ W was therefore retained for all analyses presented in this thesis. A further indicator of the suitability of the chosen value of thermal resistance, is the observed response of the film temperature to perturbations in the oil feed temperature. This will be discussed in detail in Chapter 6.

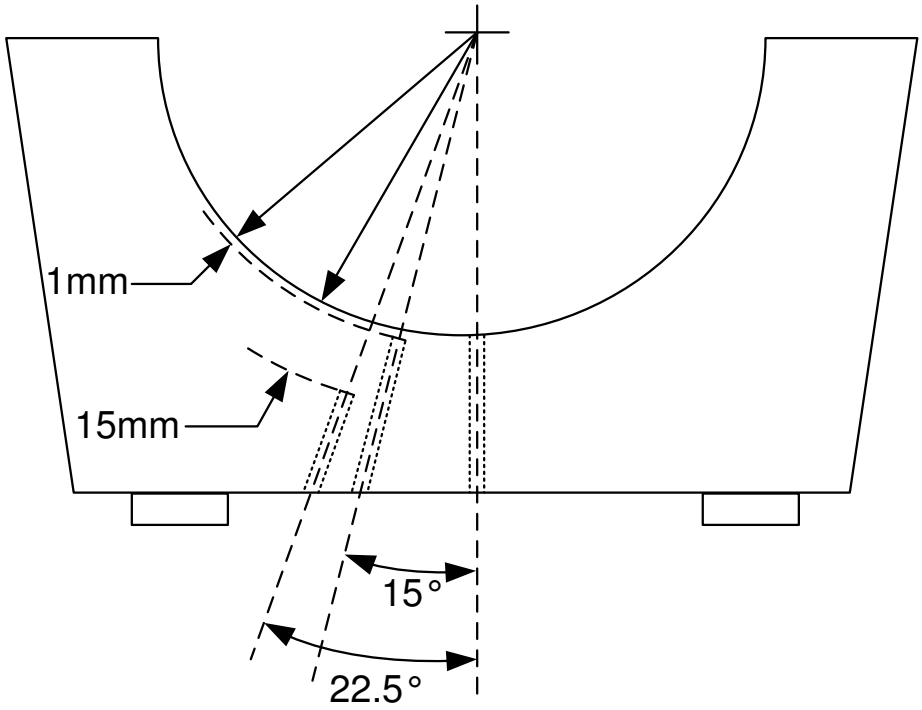

Figure 63 Instrumentation of bearing caps: thermocouple positions to measure oil film temperature and metal temperatures at 1mm and 15mm from the inner surface of the cap

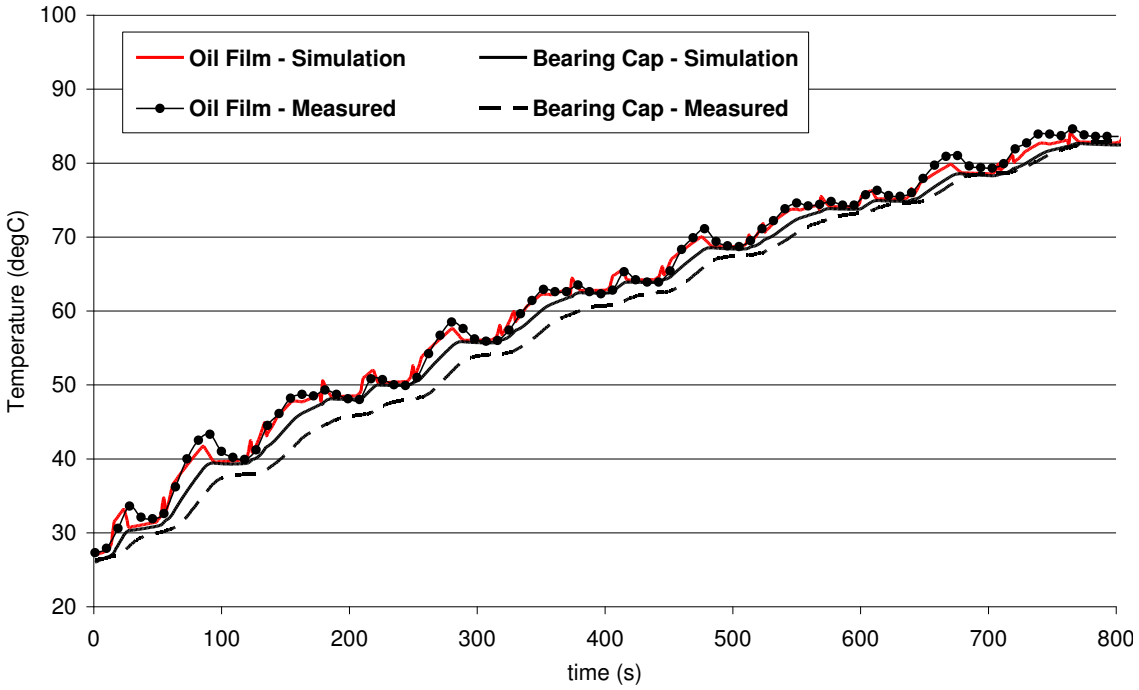

Figure 64 Comparison of measured and predicted oil film and bearing cap temperatures with low R_{th} (0.035 K/ W) over first 800s of NEDC

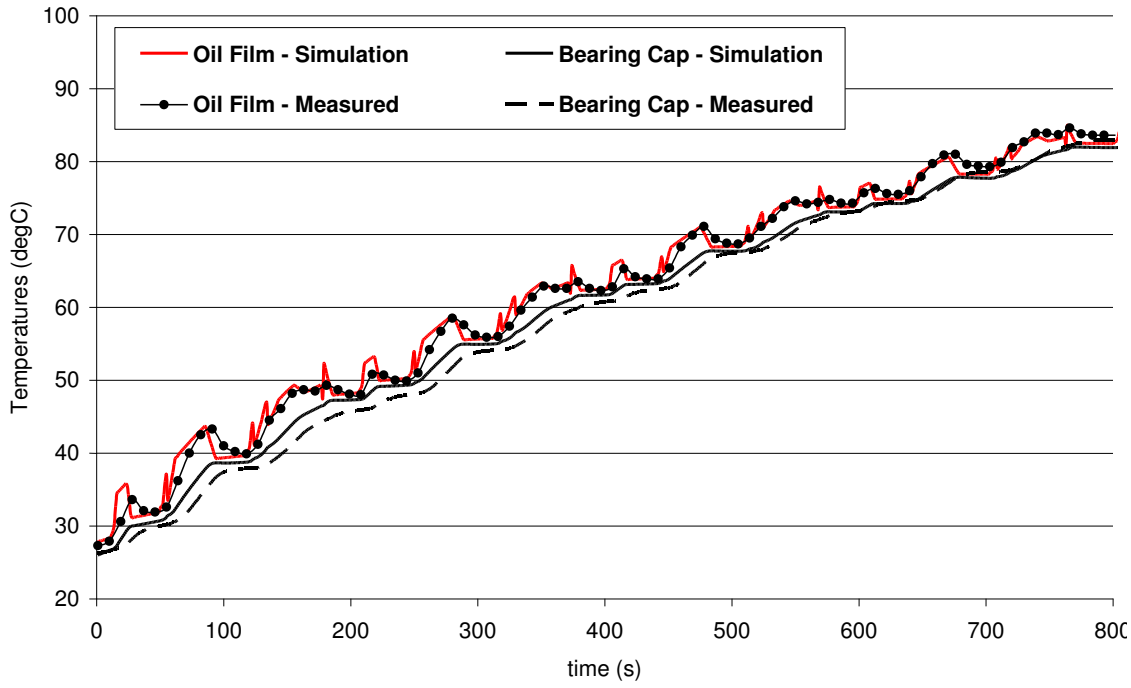

Figure 65 Comparison of measured and predicted oil film and bearing cap temperatures with baseline R_{th} (0.07 K/ W) over first 800s of NEDC

5.4.2. Main Bearing element masses

The effect of changing the assumed mass of the three main bearing elements (elements 42-44) by +/- 50 % on the film and sump oil temperature predictions is illustrated in Figure 66 and Figure 67 respectively. In contrast to changing the thermal resistance between the oil film and bearing elements, changes to the element masses do not change the film temperature rise on start-up. However, a lower thermal capacity of the bearing elements means that their warm-up rate is faster, particularly in the first minute of engine operation. This results in an over-prediction of film temperatures in the order of 3-4 °C throughout most of the warm-up. Increasing the element masses reverses the above trend and results in under-prediction of film temperatures. The general trend is the same for the oil sump temperatures.

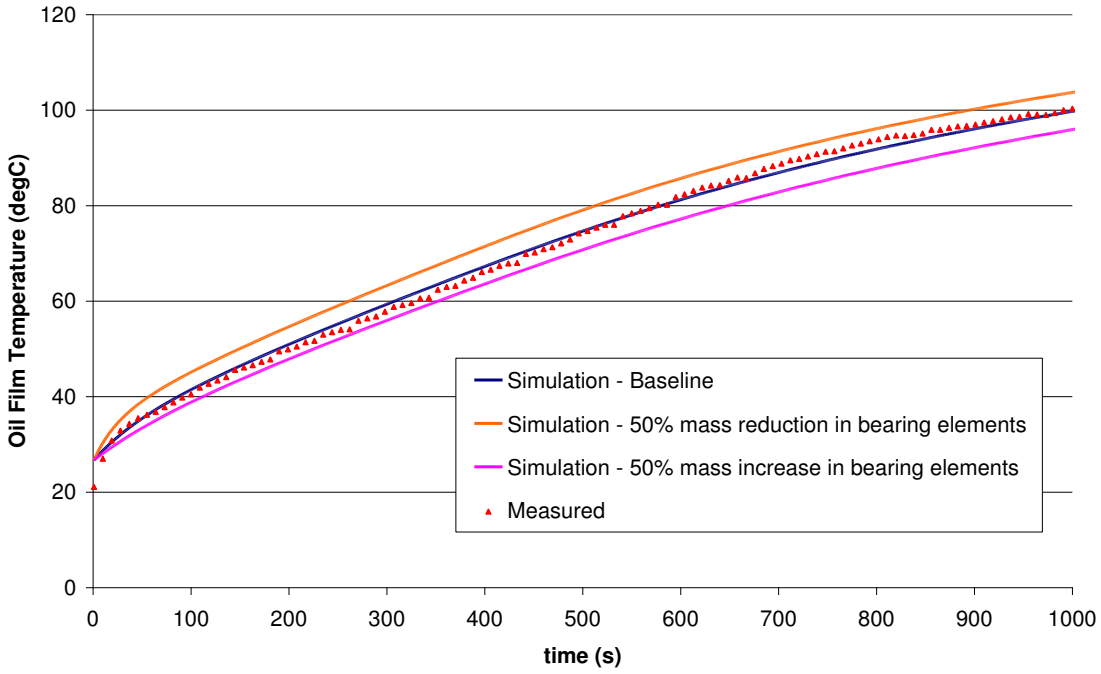

Figure 66 Sensitivity of oil film temperature prediction to +/-50% change in main bearing element masses. Engine operating condition: 2000rev/ min, 3bar BMEP

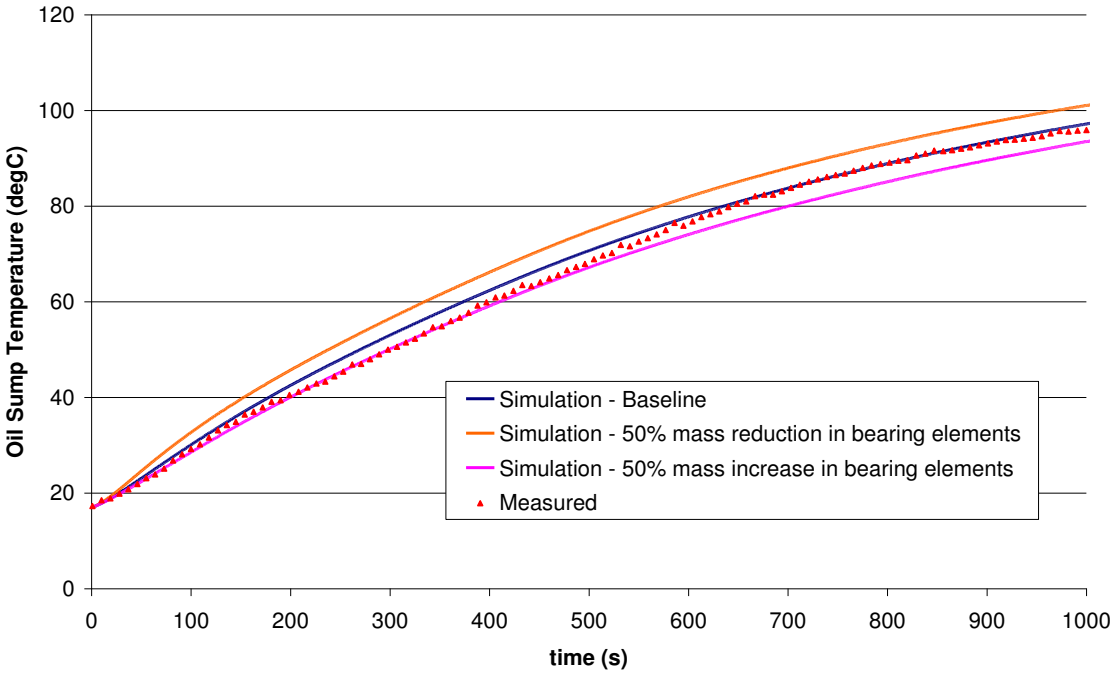

Figure 67 Sensitivity of sump oil temperature prediction to +/-50% change in main bearing element masses. Engine operating condition: 2000rev/ min, 3bar BMEP

5.4.3. Friction Correction Index

Motoring tests by [39] show that the crankshaft friction correction index varied by around 35% across an engine speed range of 200-2000 rev/ min for the engine family used in this investigation. The sensitivity of model predictions to +/-20 % change in the main bearing friction correction index was investigated. On start-up, a larger friction index increases main bearing friction by approximately 18 %. As the oil temperature rises to 70 °C and above, FMEP values are unaffected, Figure 68. Higher friction dissipation increases the temperature rise across the bearing, such that the film temperature in the early phases of the warm-up, is over-predicted by ~2 °C. Heat rejected to the oil circuit from bearing friction increases by around 14 %, so that oil sump temperatures are also higher, by ~1 °C. Fully-warm temperatures are practically identical. The observed sensitivity has implications for the thermal system investigations and predicted friction and fuel savings reported in Chapters 6 & 7. The additional fuel consumption of the cold started engine is largely the result of increased friction losses due to a higher oil viscosity. A higher friction index not only increases the FC penalty of the cold-started engine. The potential to reduce friction from raising oil temperature earlier in the warm-up is also greater, making potential improvements larger.

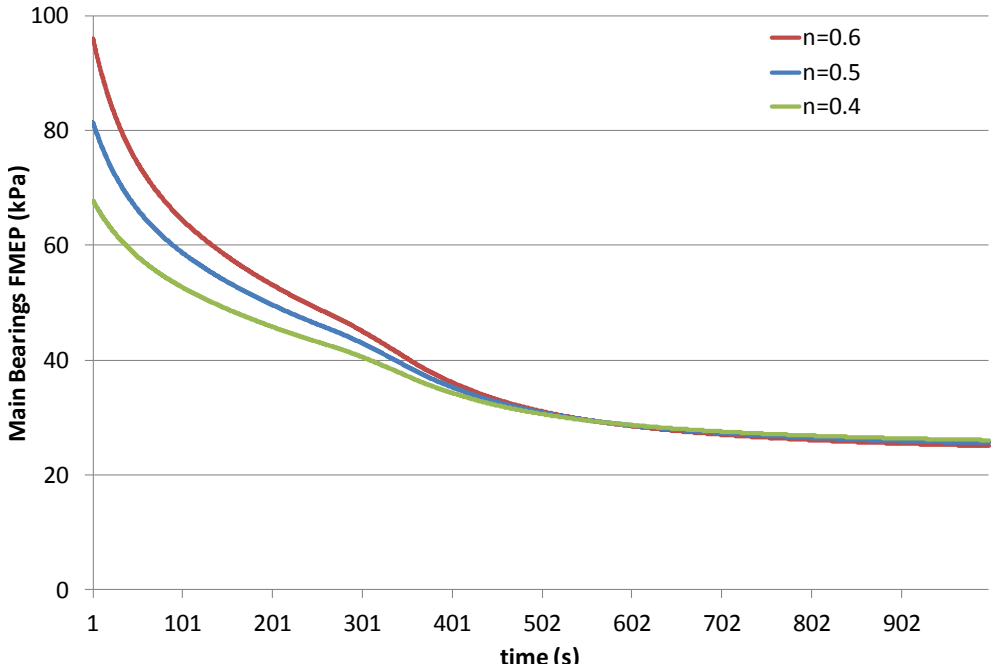

Figure 68 Effect of changing main bearing friction index on main bearing FMEP prediction at 2000rev/ min, 3 bar BMEP (20°C start)

5.5. Results

5.5.1. Main Bearing Heat Flows

Model predictions of heat flows within the bearing oil film from a cold start (Figure 69) illustrate the strong thermal coupling between the film and surrounding metal. At the start of the simulation, the total heat conducted from the oil film to the bearing surfaces accounts for over 85 % of the friction power dissipation. This is split approximately equally between conduction to the crankshaft journal and conduction to the bearing shells. This reflects the model assumption that the thermal resistance to heat transfer between the film and bearing shells is the same as that between the film and journal. As the engine block and crankshaft warm up, the balance of energy transfers rapidly changes. The proportion of friction heat carried away by the oil flow rises to around 20 % in the first 6-8 s after key-on and then increases progressively with time to reach a steady state value of ~75 %. This value agrees well with measured values reported by Dowson [128]. The general trend is also in agreement with the findings of Jarrier [125], Figure 71. The perturbation observed at around 280s in Figure 70 is caused by streaming of coolant into the FCA. In this case the oil feed temperature to the bearing is momentarily raised above that of the bulk oil. In

response to a higher inlet temperature heat transfer to the journal and bearing shells increases limiting the oil temperature rise and change in oil enthalpy flux across the bearing.

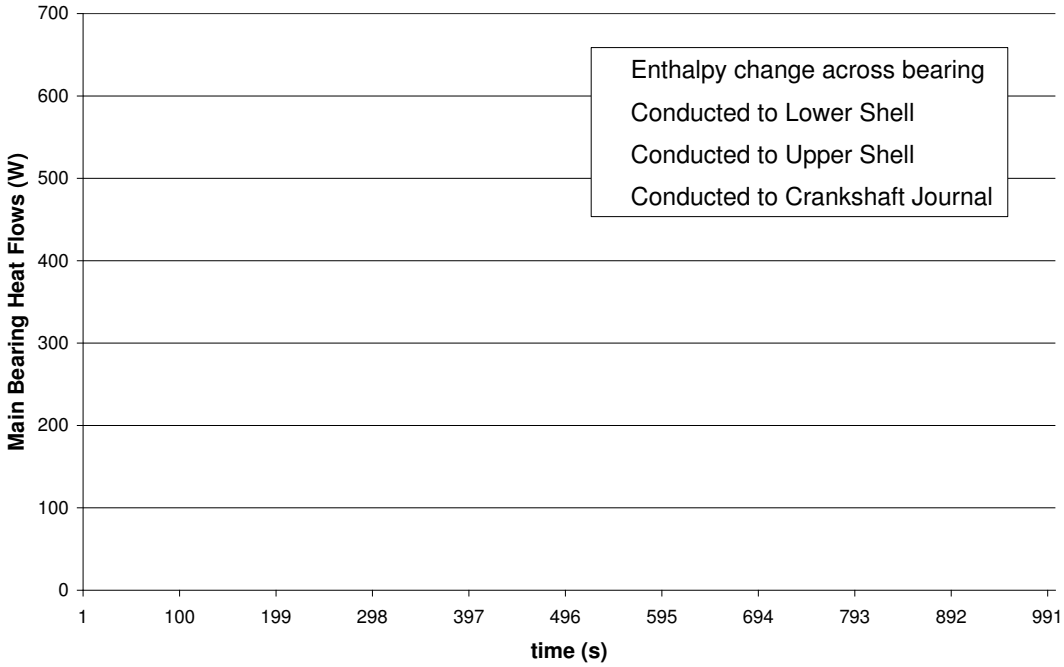

Figure 69 Energy flows (per bearing) within main bearing oil film - 2000 rev/min, 3bar BMEP (20 ºC start)

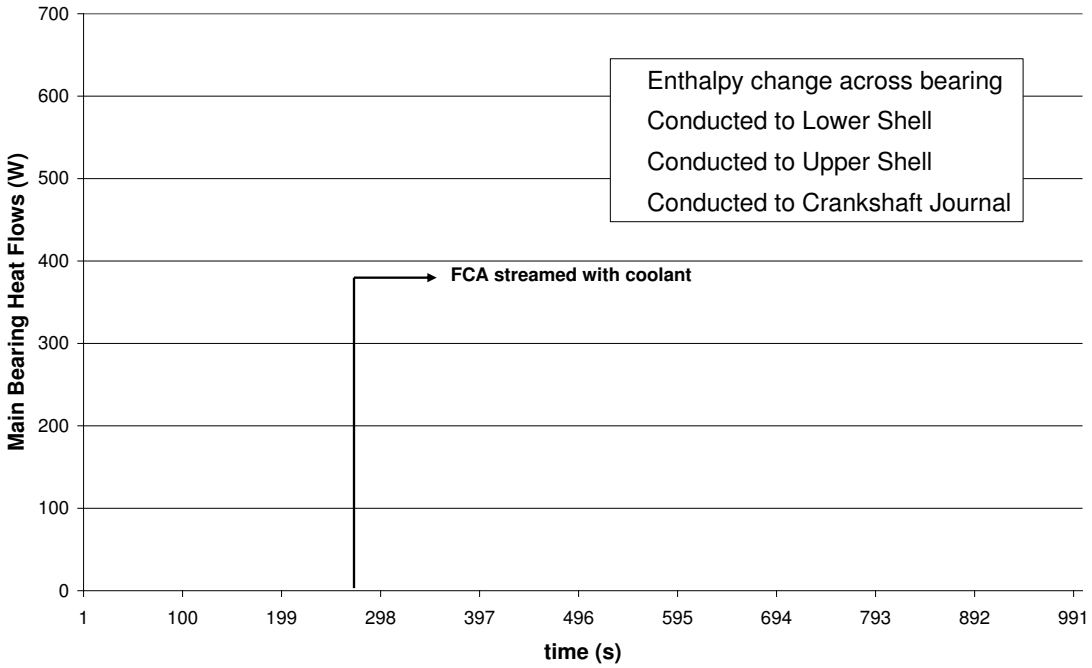

Figure 70 Energy flows (per bearing) within main bearing oil film - 2000 rev/min, 3bar BMEP (20 ºC start). FCA streamed with coolant at 280s

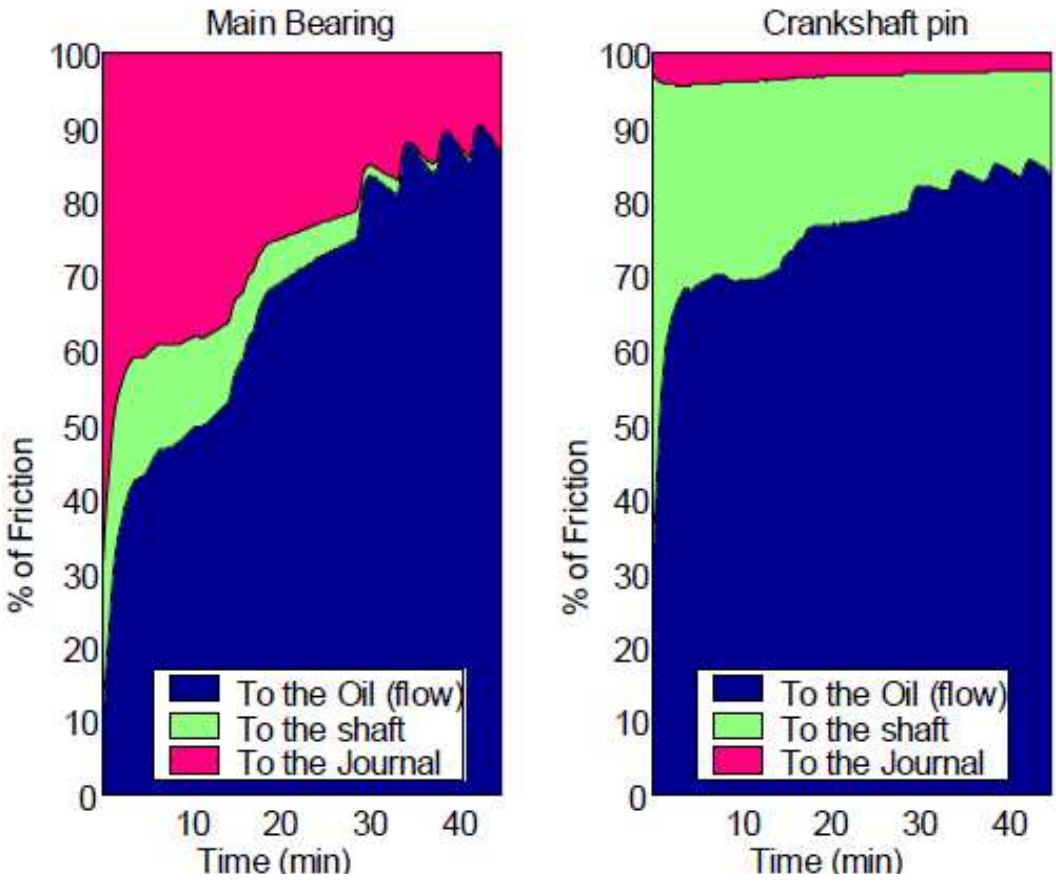

Figure 71 Energy balance within main and big-end bearing oil films during warm-up [126]. In this case the 'Journal' refers to the main bearing housing or connecting rod big-end in the case of the crankshaft pin. Engine operating condition is unspecified.

The proportion of friction heat carried away by the oil flow under fully-warm conditions is a function of engine speed (Figure 72) since this affects the oil flow rate through the bearings. Higher engine speeds promote a larger hydrodynamic flow rate and, through an increase in the feed pressure to the bearings, a higher pressure-fed flow component too. Under fully-warm conditions, main gallery oil pressure is regulated (limited) by the pressure relief valve above 2000 rev/ min. As a result the oil flow rate through the bearings at 2000 rev/ min is more than double that at 1000 rev/ min, but the increase in oil flow rate from 2000 to 3000 rev/ min is just under 40 %. The change in the percentage of friction heat carried away by the oil flow reflects these changes in oil flow rate with engine speed.

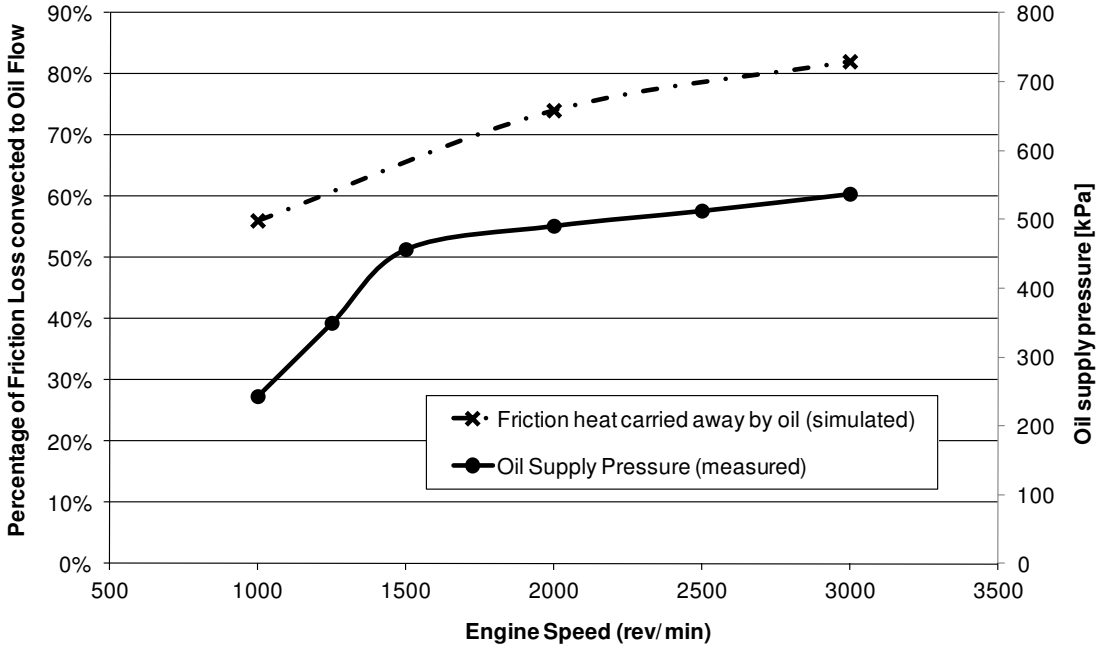

Figure 72 Simulated proportion of friction dissipation carried away by oil flow and measured main gallery oil pressure at different engine speeds under fully-warm conditions

The variations in oil film heat outflows over the NEDC are illustrated in Figure 73, expressed as a percentage of the main bearings total friction power loss. The transient nature of the prediction reflects the rapidly changing engine speed over the NEDC. Changes in engine speed (Figure 74) lead to significant fluctuations in main bearing friction. Also, the resulting changes in oil pump speed cause a variation in the oil flow rate through the bearings. In this case, oil pressure data fed to the bearing model for the calculation of the oil flow rate, was taken from a test engine equipped with a variable flow oil pump [104]. Oil pressure in the main gallery was controlled between a minimum of 1 bar (gauge) during engine idle phases and a maximum of 2 bar for the remaining engine operating points. With the engine idling, the low flow rate results in the oil enthalpy gain across the bearing being the lowest during these phases. In the urban section of the NEDC (0-780s) a large temperature difference is induced between the oil film and bearing surfaces each time the engine speed increases rapidly from the idle condition (Figure 73). These acceleration phases resemble the first seconds of operation in a constant speed test condition. However, over the urban part of the drive cycle, engine speed is not maintained constant long enough for the warm-up rate of the bearing elements and oil film to equilibrate. As a result, the rate of heat conduction to the bearing surfaces remains relatively high for

the majority of the drive cycle, and throughout the urban section doesn't drop below 70% of the bearing friction power loss. The oil enthalpy gain only starts to increase steadily during the prolonged constant engine speed conditions seen in the extra-urban part of the drive cycle (800-1200s). Also, by this point the engine has approached the fully-warm state. The above observations indicate that under low speed, light load operating conditions, the bearings take longer to reach fully-warm temperatures. This in turn increases the potential to reduce friction from changes that promote a faster oil film temperature rise.

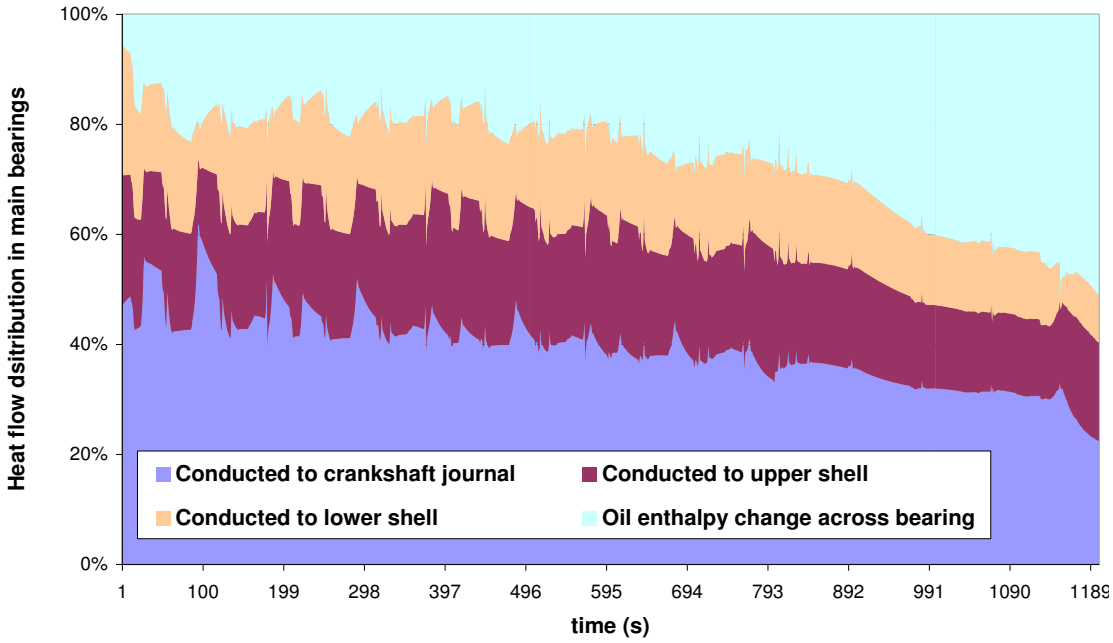

Figure 73 Energy balance within main bearing oil film during a cold start (26°C) NEDC

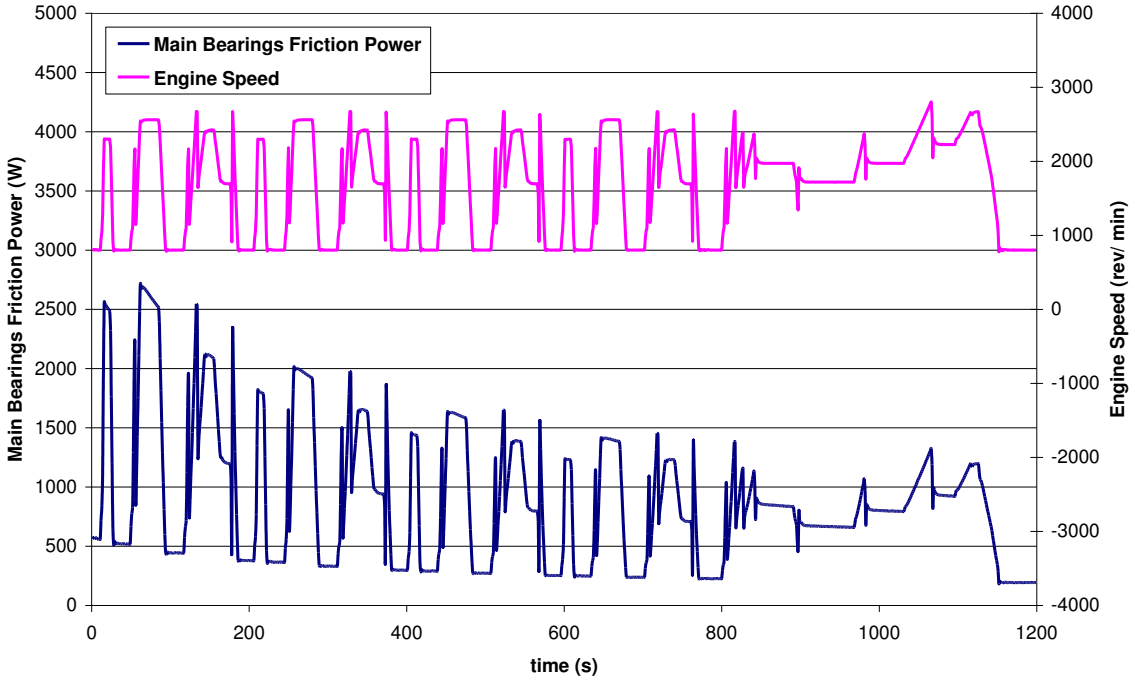

Figure 74 Engine speed variation and predicted main bearings friction power over cold start NEDC

5.5.2. Engine crankcase and crankshaft heat flows

The revised crankcase elemental representation provides a more detailed description of heat flows in this part of the engine structure. The previous section has looked at how heat transfer from the oil film to the bearing shells and crankshaft journal changes throughout warm-up. The section looks at the propagation of heat from the bearing elements (crankshaft journal, bearing cap and part of the bearing support wall) to the surrounding metal structure of the crankcase and the interaction of oil mist with the crankcase elements.

Predicted fully-warm metal temperatures in the crankcase and main bearing assembly are illustrated in Figure 76 for a 2000 rev/ min, 3 bar BMEP running condition. The FCA is streamed with coolant in this case. The main bearing elements are hottest, due to their strong thermal coupling with the oil film. All three elements are within one degree of the film temperature, which is in turn, around 3°C above that in the sump. Heat input from the oil film to the crankshaft journal is marginally greater than that to the remaining bearing elements but is entirely dissipated to the crankcase oil mist. The majority of heat input from the oil film to the bearing cap and bearing support

wall elements, on the other hand, is conducted radially outwards to the crankcase walls (elements 15 and 16) where it is lost to ambient. Heat transfer to the crankcase walls also includes heat input from the oil mist, oil flowing in the main gallery and heat input from the big-end bearings. Of the total heat lost to ambient (from the crankcase surfaces), approximately 40 % is from friction dissipation in the main and big-end bearings. Heat transfer from oil in the main gallery and crank case oil mist accounts for ~50 % of the heat convected to ambient. The heat exchange with the 'upper' parts of the engine (liners and block) is relatively small at 10 %, which is in agreement with the observations of Mason [135]. Extensive metal temperature measurements by Mason on a Ford CVH engine showed that temperatures in the upper engine block and cylinder liners were controlled by the coolant temperature, while crankcase surface temperatures were mainly determined by the oil temperature, with the dominant heat transfer mechanism being a balance between heat input from the oil mist and oil gallery and heat rejection to ambient. The above analysis shows that the contributions from friction dissipation in the main and big-end bearings are just as important as those of the crankcase oil mist and convection in the main gallery. With no coolant streamed through the FCA oil temperatures rise by around 15 °C, as do metal temperatures in the crankcase and main bearing. The overall heat balance however remains largely unchanged except that heat transfer down from the upper parts of the engine structure is reversed; crankcase element temperatures rise above those of the cylinder block and lower liner (which remain similar to when the FCA was enabled, closely coupled to the coolant temperature) and conduct heat up to the upper block.

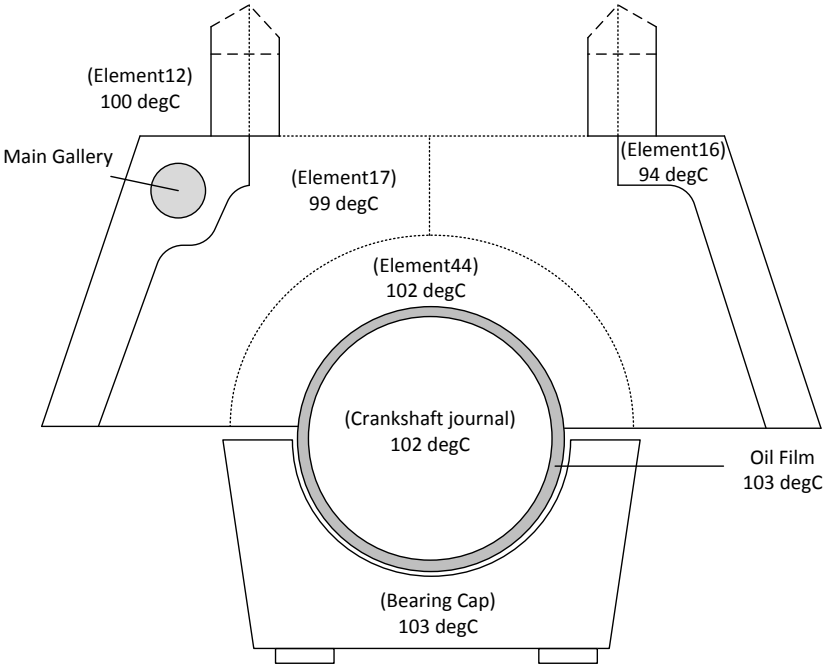

Figure 75 Engine Crank Case Element Temperatures in steady state thermal conditions (FCA streamed with coolant)

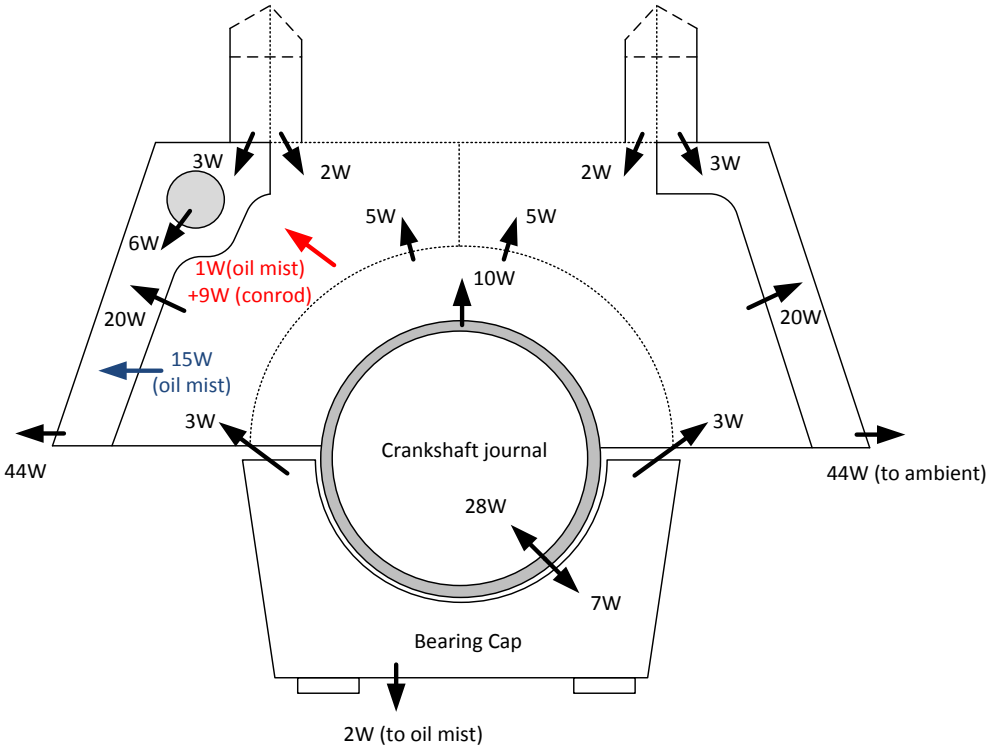

Figure 76 Engine Crankcase Heat Flows in steady state thermal conditions (FCA streamed with coolant)

5.6. Discussion and Conclusions

Revisions to the bearing sub-model have provided a more comprehensive description of thermal-friction conditions in crankshaft main bearings. A key feature of the model is that friction levels are coupled to the oil film temperature rather than that of the bulk oil. Calibration of the main model parameters was based on the comparison of simulated and measured oil film temperatures over steady and transient engine operation. The observed sensitivity of model predictions was also used to quantify the level of uncertainty introduced by the model assumptions, some of which have implications for the investigations reported in the next two chapters.

A strong thermal coupling between the oil film and bearing elements is apparent. This holds the film temperature down following a cold start, resulting in a substantial friction penalty when compared to the fully-warm state. The benefits of reducing the degree of this thermal coupling are explored in the following chapter. Results show that the percentage of friction heat carried away by the oil flow through the bearings increase steadily from under 10% when the structure is cold to around 70-80 % under fully-warm conditions. As a result oil flow rate bears little influence on the film temperature prediction particularly in the first minutes after start up. The fully-warm proportion of friction heat carried away by the oil flow was in turn shown to be dependent on the oil flow rate through the bearings, which is generally strongly related to engine speed.

As part of integrating the bearing model into PROMETS, the assumption on the net proportion of friction heat retained in the oil was revised. Simulations indicate that heat flow from the main and big-end bearings accounts for the greatest majority of the total heat flow to the oil. There is still some uncertainty as to the proportion of piston friction heat retained in the oil; simulations indicate that this is significantly lower than in main bearings such that piston friction can be assumed to be entirely dissipated into the liner. This has been mainly attributed to the low oil flow rates reaching the ring-pack.

In the fully-warm state the temperatures of the oil film, crankshaft journal, bearing cap and bearing support walls are within a degree or two of each other. The temperature of the crankcase components are mainly determined by the oil

temperature in the main gallery and in the main bearing film. This is in good agreement with the findings of [135]. Friction heating in the bearing film, heat transfer from oil in the main gallery and from oil mist to the crankcase walls is ultimately dissipated as heat losses to ambient from the crankcase outer surfaces. Heat transfer to the cylinder liners and block is small in comparison, around 10 % of the total heat flow. The implication of this is that oil is in good thermal coupling with the lower parts of the engine structure which are in turn remote from the gas-side heat source. The large thermal capacity of the crankcase means this warms up slowest in the engine, and more importantly slower than the engine fluids. This is detrimental to the oil warm-up rate as it sinks heat from both the bearing films and bulk oil.

Representing the complex shape of the crankshaft and heat flow patterns within it during warm-up using one lumped mass element, is a simplification done on the basis of keeping the number of variables used in the model to a minimum. Based on comparisons of PROMETS predictions with those from other models reported in the literature [125] [129], this approach has its limitations when modelling the intricate heat flow patterns within the crankshaft. Nonetheless this approach was shown to be suitable to model the film temperature rise both under steady state and transient engine operating conditions while making the model simple to calibrate. Greater focus has been given to the main bearings as their friction contribution is substantially (~40 %) greater than that of the big-ends. Additionally the main conclusions drawn from the exploitation of the model are expected to be directly transferable to the big-end bearings.

Chapter 6 – Reducing Main Bearing Friction during Warm-up

6.1. Introduction

In the following, various measures to minimise the penalty of friction in the crankshaft main bearings are explored, including reducing the bearing oil flow rate through a reduction in feed pressure. Particular focus is given to the effectiveness of heating the oil supply to the main bearings. In this case the computational study was complemented by an experimental investigation. Minimising the thermal coupling of the oil film to the bearing surfaces is shown to be crucial to maximise friction work savings.

6.2. Effect of reducing oil flow rate

The effect of reducing the oil flow rate through the bearings on the film temperature rise has been investigated. For a given enthalpy gain, a lower oil flow rate induces a greater temperature rise across the bearing, through this accelerating the drop in oil viscosity and friction following a cold start. Reducing the oil flow demand of an engine offers further friction savings through a reduction in oil pumping work. Shimura et al. [123] describe modifications to the oil supply groove which successfully reduced oil flow rates through the main bearings by up to 50 % at an engine speed of 2000 rev/ min. This allowed a downsizing of the oil pump reducing oil pump torque by up to 0.3 Nm, while main bearing friction in the fully-warm state was unaffected. A reduction in oil flow rate must, however, be achieved without compromising the cooling and lubrication performance at the rubbing surfaces. These issues will also be discussed in the following chapter.

The bearing oil flow rate calculation was explained in Section 5.2.1 to be the sum of two components. The equation used to calculate the pressure-fed flow component applies to a 180° rectangular supply groove. Different oil groove arrangements will have different flow characteristics and must be modelled using other equations [133]. For a given bearing size and eccentricity, the parameters determining the oil flow rate through the bearing are the radial clearance, supply pressure and oil viscosity. Neglecting pressure and shear rate effects, oil viscosity is coupled to the film

temperature and as such cannot be directly controlled unless the oil grade is changed. Clearance has a strong influence on oil flow, affecting both the hydrodynamic flow requirement of the bearing and the pressure-fed component. Operating with tighter clearances is one way of reducing bearing flow rates [125] but generally leads to higher friction losses [33].

In the following study, the first method of lowering the bearing oil flow rate was to reduce main gallery oil pressure. Model predictions were made with half and a quarter of the baseline oil supply pressure to the bearings, which equate to 2.5 bar and 1.25 bar respectively under fully warm operation at an engine speed of 2000 rev/ min. A minimum pressure of 2bar was operated by Law [20] on the same engine used in this investigation. The quarter pressure case must therefore be considered as a hypothetical case which may not be realisable on the actual engine. The extent of the reduction in main bearing oil flow rate is illustrated in Figure 77 with the associated savings in friction work shown in Figure 78. The latter shows the components of an energy balance within the oil film 10 minutes into the simulation. The total energy is reduced with the lower oil flow rates, consistent with a reduction in friction losses as a result of the higher temperature rise across the bearing. Overall, the benefit in friction from reducing the pressure feed to the bearings is small, ~2 % for the quarter pressure case. The main reason for this is that when cold, heat losses from the film are dominated by conduction to the shells and journal; the proportion of friction heat convected away by the oil flow is small, less than 35 % in the first 2 minutes of operation. Hence oil flow rate has a relatively small influence on the film temperature rise. Moreover, at the start of the run, when the potential reductions in friction are highest, the hydrodynamic flow component accounts for over 60 % of the total flow rate through the bearing and this is unaffected by the oil feed pressure, as illustrated in Figure 77.

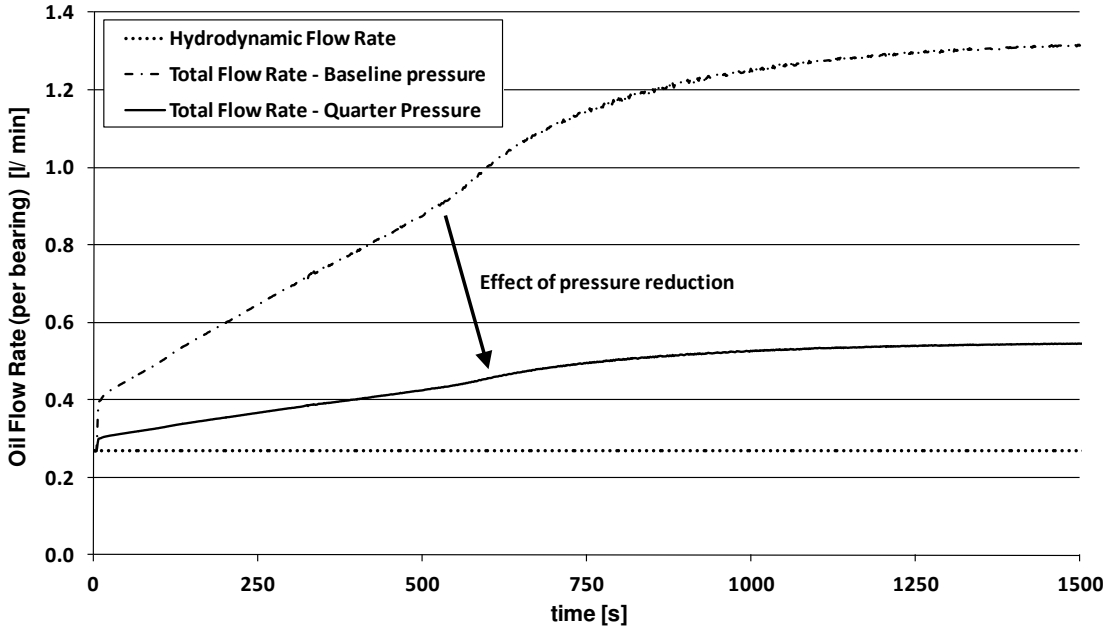

Figure 77 Predicted oil flow rate (per bearing) with baseline and quarter main gallery pressure. Also shown is the hydrodynamic flow component which is unaffected by the oil supply pressure

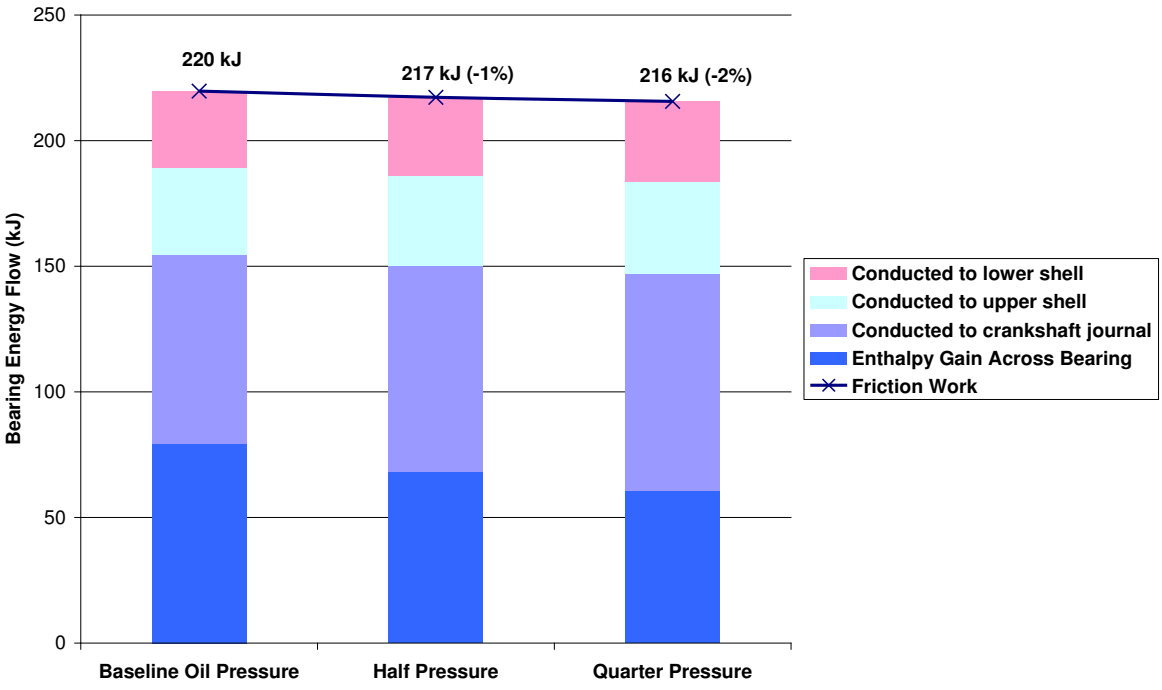

Figure 78 Friction work saving (per bearing) at 10 minutes into the warm-up achieved from reducing the gallery pressure to a half (Case 1) and a quarter (Case 2) of the baseline value

The friction benefit, while small, increases as the oil flow rate through the bearings is reduced. As the pressure feed is reduced to zero, the oil flow rate through the bearings reaches a minimum which is the hydrodynamic flow. For the oil flow rate to drop below this level a restriction must be placed in the oil feed to the bearings. In practice this can be achieved by changing the geometry of the oil supply, for example by switching from a rectangular groove to a circular hole of small diameter. As the flow rate supplied is reduced below its hydrodynamic requirement, the bearing is said to no longer operate in a flooded condition, but is starved [97]. This is illustrated in Figure 79. In the model, cases 3 and 4 simulated the effects of a more severe reduction in oil flow rate than that achieved through a reduction in feed pressure alone. The benefits in friction work are significantly greater in this case, but still relatively small (see Figure 80) because increased heat transfer to the shells and journal limits the film temperature rise associated with the reduction in oil flow rate. Moreover, while a lower oil flow promotes a larger temperature rise across the bearing, heat carried away by the oil is reduced. A lower heat input to the oil flow slows down the rate of temperature rise in the sump such that a higher temperature rise across the bearing is partly offset by a lower feed temperature to the bearing. From Figure 81 it can be seen that in case 4 the absolute increase in oil film temperature relative to the baseline case, is approximately half the additional temperature rise across the bearing. This behaviour agrees well with the experimental observations of Law [20] when a variable flow oil pump was used to reduce main gallery oil pressure on the same engine as used in this study. It also agrees well with the simulated results of Jarrier [125] who also looked at the effect of reducing the oil flow rate through the bearings.

As the fully-warm thermal state is approached, heat convected to the oil flow becomes substantial and accounts for over 70 % of the friction heat generation. Consequently, fully warm oil film temperatures were increased by 2-3 °C for cases in which the oil pressure was reduced, and by 5-9 °C in cases 3 and 4. Changing the oil supply geometry leads to a permanent reduction in the bearing flow rate and may therefore compromise fully-warm operation. However, the feed pressure could be raised when operating fully-warm to provide additional cooling to the bearings.

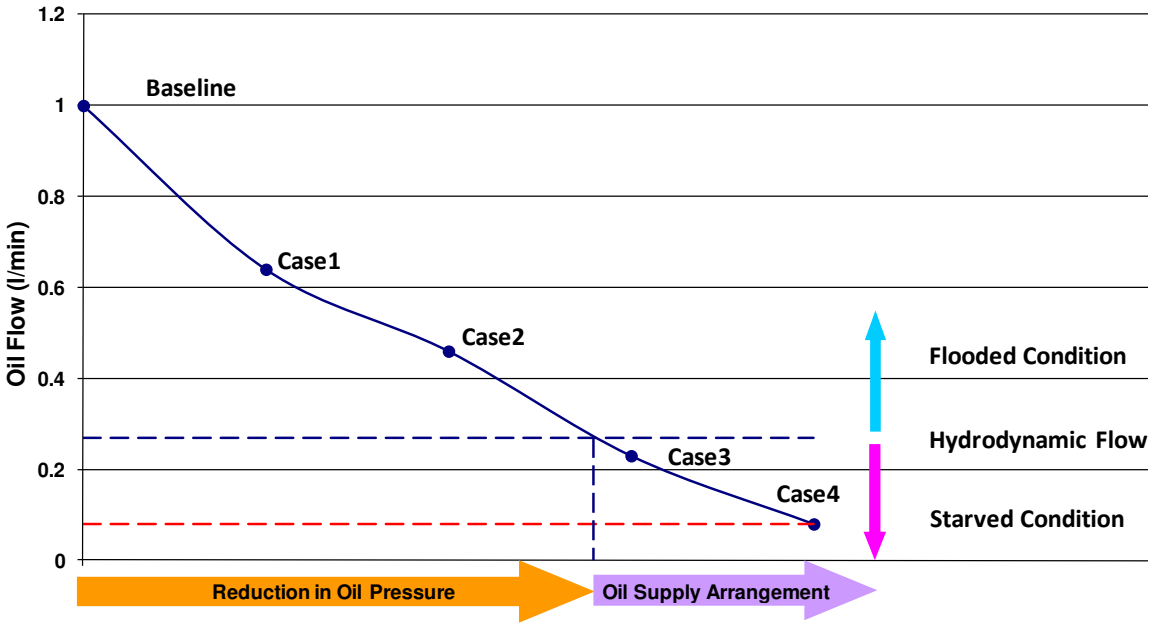

Figure 79 Oil flow rate (per bearing) for different simulated cases at 10 minutes into warm-up.

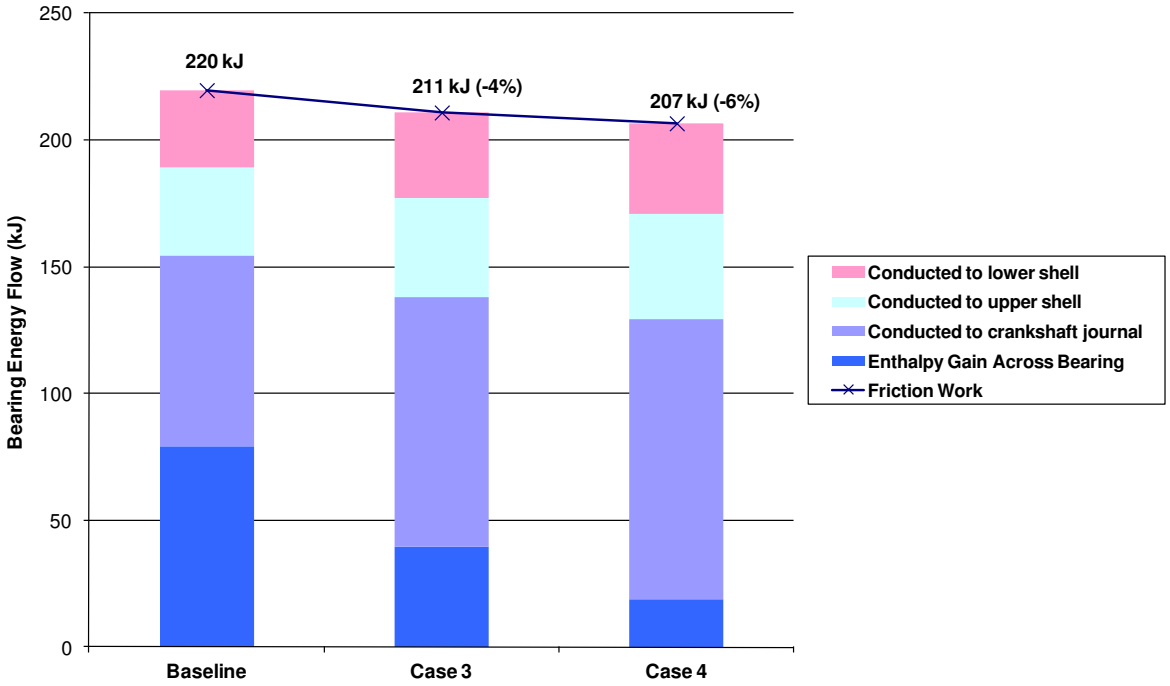

Figure 80 Friction work saving (per bearing) at 10 minutes into the warm-up achieved from oil starvation

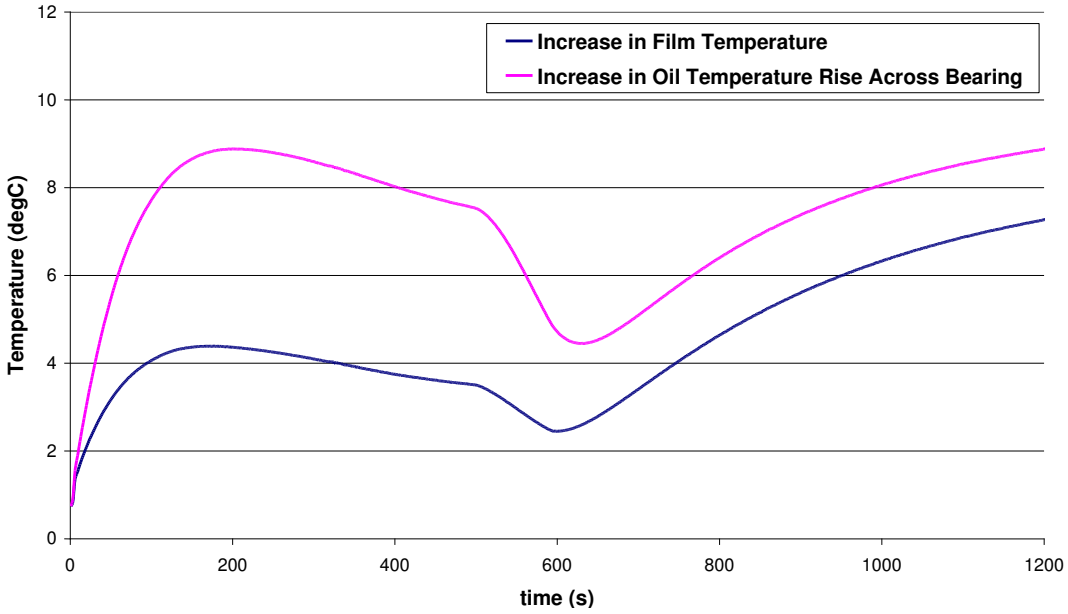

Figure 81 Absolute increase in oil film temperature in case 4 relative to the baseline case. Also shown is the increase in the temperature rise across the bearing.

Simulated cases 3 and 4 are solely intended to show the change in the energy balance within the oil film as a result of severe reductions in oil flow. In reality operating a journal bearing under starved lubrication conditions leads to a number of changes to the oil film which are not accounted for in the bearing model described in this thesis. The effect of oil starvation in steadily loaded bearings has been studied extensively, computationally [136] [137] and experimentally [138]. The most significant change observed is a shortening of the full-film region. As illustrated in Figure 82, the film starts later and terminates earlier than for a fully-flooded bearing.

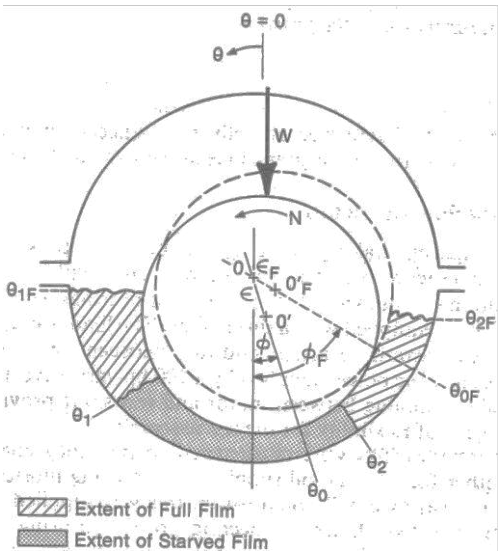

Figure 82 Effect of oil starvation on journal bearing film. $\theta_{1F} - \theta_{2F}$ indicates angular extent of full film (flooded condition), $\theta_1 - \theta_2$ indicates extent of starved film [138]

In terms of changes to the friction power loss, an increase in shaft eccentricity reduces the minimum film thickness. On its own this would result in higher friction dissipation. However, the increase in film temperature as a result of the lower oil flow, together with a shortening of the oil film angular extent, means that overall, friction losses continue to reduce with oil starvation up until ~10 % of the flow required for a flooded condition. Load capacity is not seen to reduce significantly either, until very severe levels of starvation [138]. As the attitude angle of the shaft is reduced, the vertical stiffness of the loaded shaft increases. However, the shortening of the film's angular extent means that horizontal stiffness is compromised and [138] measured an increase in horizontal vibration as a result of this. The implications of this on the performance of dynamically loaded bearings, is uncertain. While the findings of [136] [138] suggest that oil starvation can be managed in steadily loaded bearings to provided friction benefits, its applicability to i.c. engine main bearings may be limited. Moreover, restricting oil flow to the bearings may also lead to a problematic oil delivery; cavitation in the supply channels and groove tend to disrupt the steady flow of oil to the bearings resulting instead in a pulsating type flow which may in turn lead to the periodic failure of hydrodynamic lubrication with subsequent bearing damage [97].

6.3. Effect of pre-heating the oil feed

The effectiveness of using an external heat source to raise the oil temperature in the main gallery and crankshaft bearing films was investigated through experimental investigations and computational modelling. Oil temperature measurements throughout the oil system were used to illustrate the persistence of the temperature rise from the point of heat application to the main bearing film. The bearing model was also used to explore further ways of influencing the film temperature rise during warm-up.

The investigation was carried out on the same 2.4l d.i. diesel engine with instrumented bearing caps, measurements from which were used to validate the bearing model predictions presented in the previous chapter. As the engine was installed on the test bed prior to commencement of this investigation, access to the oil gallery and crankshaft main bearings was greatly restricted. This limited the heating

methods that could be employed. The introduction of swarf into the oil circuit from machining of any kind can be detrimental to engine life. Hence the method employed was to be non-intrusive to the oil circuit. Heating in the oil sump is relatively easy to achieve due to ease of access. In addition heat transfer can take place over a large surface area minimising the chance of oil degradation from local overheating. However, given the observations of Law et al. [70], it is advantageous to heat the oil as close as possible to the bearings to minimise heat losses from oil flowing in the main gallery.

The oil was heated by streaming pre-heated coolant through the FCA. The FCA was disconnected from the main engine coolant circuit and connected to an unpressurised coolant storage tank with an integral 3 kW electric heater (Figure 83). Coolant flow in this auxiliary circuit was driven by a 12 V electric pump. Prior to engine start-up, with valve 2 shut and valve 1 open, the electric heater was switched on to pre-heat the coolant to around 90 °C. The electric pump was switched on circulating coolant from the tank through a bypass loop ensuring that a homogenous water temperature was achieved earlier within the tank. The engine was then started and run at a fixed speed and load condition of 2000 rev/ min, 3 bar BMEP. Once oil temperature warm-up rates in the bearing film, sump and main gallery were established, the electric heater was switched off while simultaneously the positions of valves 1 and 2 were switched. This allowed hot coolant to flow through the FCA. The coolant flow rate through the auxiliary circuit was maintained constant and measured at 3.75 l/min. Coolant temperatures in the hot storage tank and at the inlet and outlet of the FCA were measured. Oil temperatures in the sump, at the inlet and outlet of the FCA, at the feed to the main gallery and in the main bearing films were also recorded.

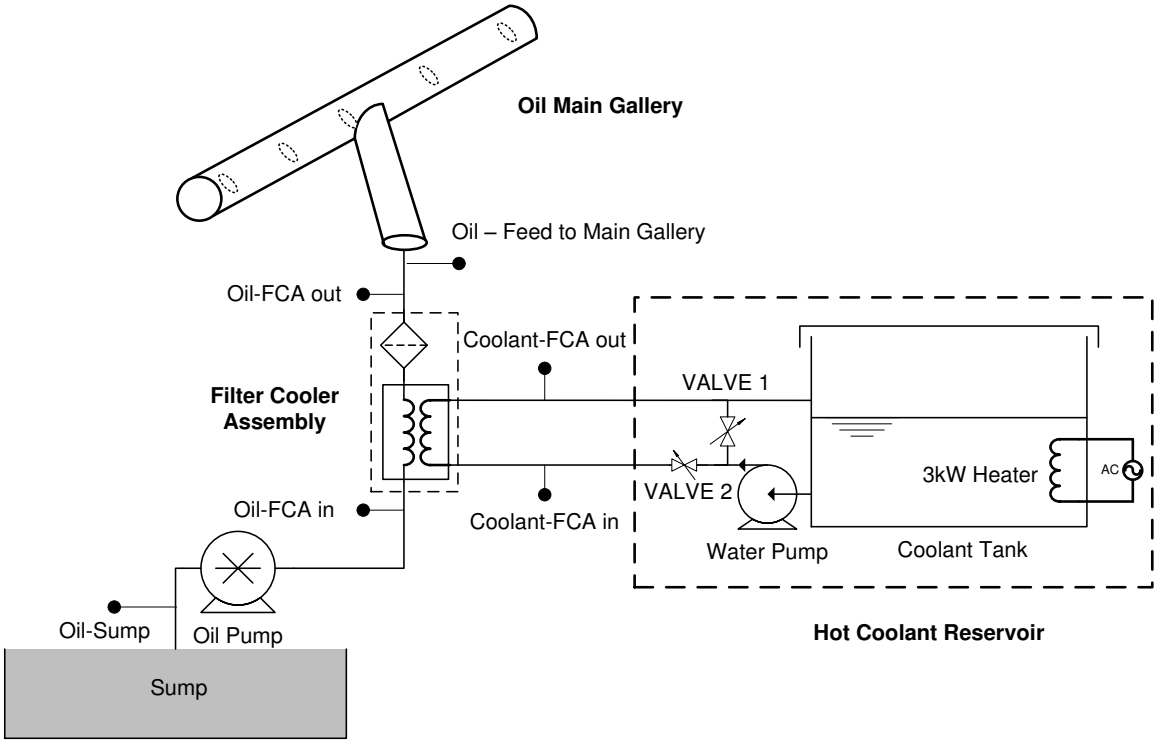

Figure 83 Heat store circuit

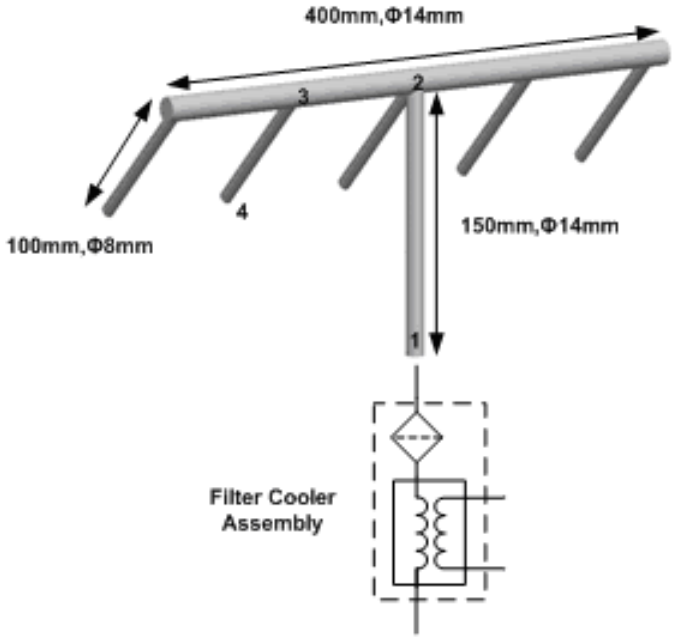

Figure 84 Puma 2.4 Main Gallery Schematic

6.3.1. Response to oil heating

The hot water storage tank was not modelled in PROMETS. Instead, coolant temperature measured at the inlet to the FCA was provided as a model input to calculate the heat transfer rates across the FCA. The oil-to-coolant heat exchanger effectiveness map from Section 3.9 was unmodified. Measured and predicted rates of heat transfer from the hot coolant store to the engine oil are shown in Figure 85. The measured trend was calculated from the enthalpy change on the coolant side of the FCA which was determined from measurements of the temperature drop across the FCA and coolant mass flow rate in the loop. A coolant volume of approximately 300ml resides in the FCA and connecting hoses between the FCA inlet and outlet thermocouple positions. When coolant from the storage tank is first streamed through the FCA, there are large uncertainties in the heat exchange calculation during the few seconds taken for hot fluid to displace the cold coolant in the FCA. Data from this phase of the test has been omitted. However, within a few seconds, heat transfer from the coolant store peaked at close to 4 kW and then dropped to under 1kW over a period of 270s as the oil warmed up, at which point the circulation of heat store coolant was shut down. The model describes this phase of the test well. The total energy transfer over the 270s of FCA activation is 496 kJ. Model predictions for bulk oil and bearing film temperatures, illustrated in Figure 86, compare well with trends measured on the test bed. The difference in film temperature produced by the oil heating in the FCA builds up to approximately 9 ºC while the heating is on. The temperature of oil in the sump reservoir was raised by one or two degrees more, around 11 ºC.

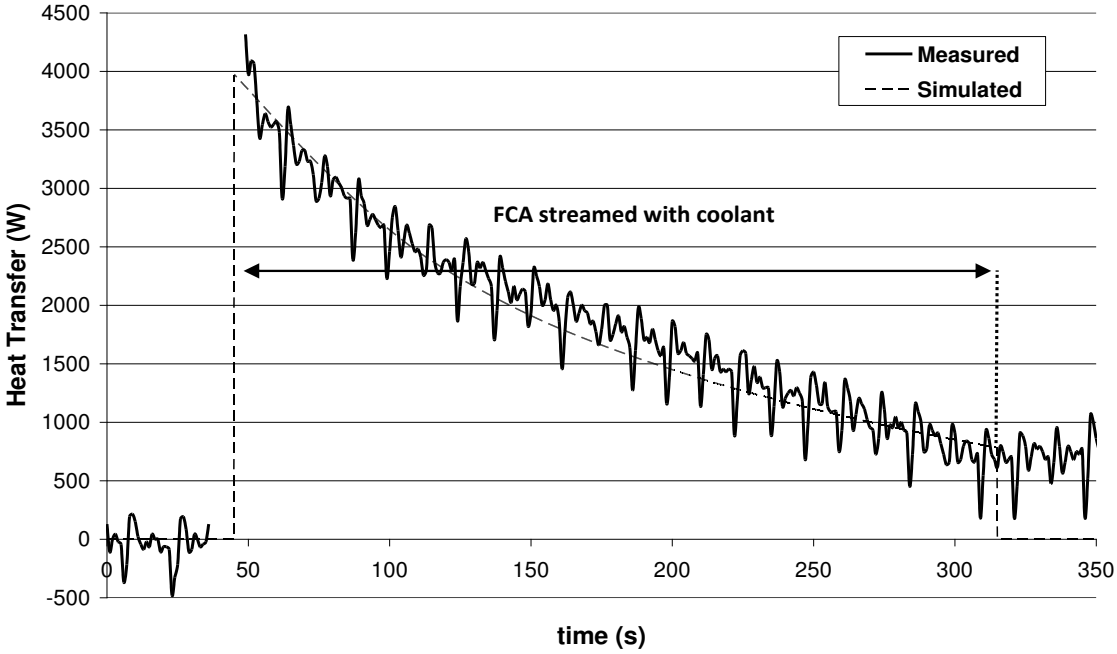

Figure 85 Heat input from heated coolant store to engine lubricant

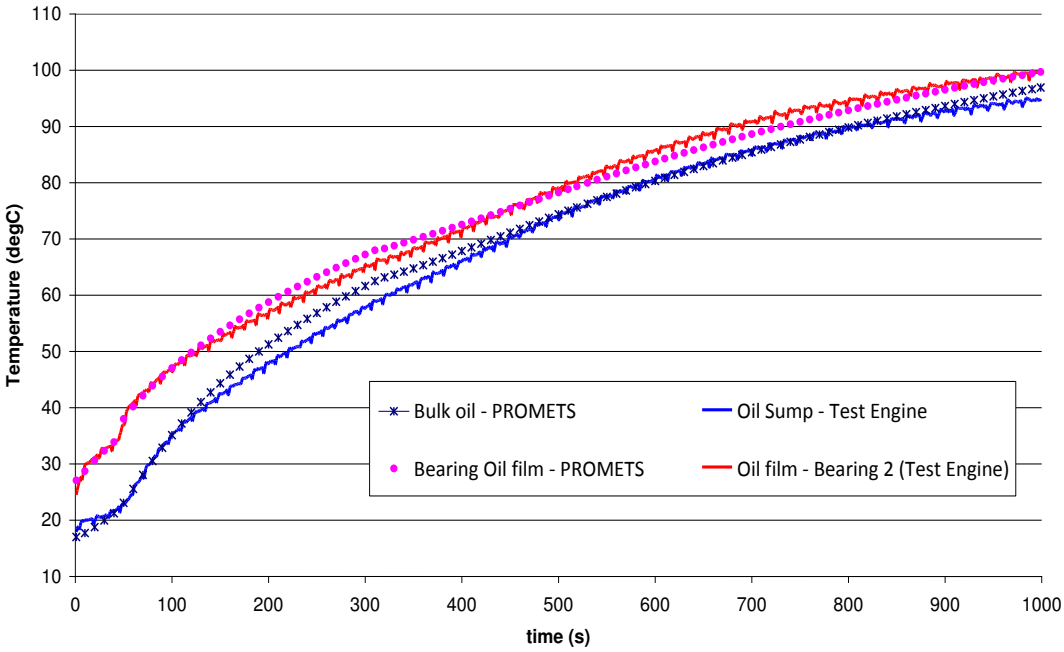

Figure 86 Comparison of predicted and measured sump oil and bearing film warm-up trends with external heat store activated at 45s

At the bearing, the measured temperature response to the rise in oil feed temperature is shown in Figure 87. When hot coolant is streamed through the FCA, a step increase of 20 ºC is observed in the oil outlet temperature. This increase is nearer 15 ºC at the inlet to the main gallery, but only 5 ºC in the bearing oil film. This relatively small increase in film temperature reflects the strong thermal coupling of the film to the shells and journal of the bearing. Before hot coolant heats the oil flow through the FCA, the bearing shell and oil film are at a similar temperature. When the oil feed temperature is raised the film temperature responds, albeit with a modest rise, but the measured temperature of the lower shell shows no immediate change, so the temperature difference between the film and the shell, and the corresponding rate of heat transfer from the film, rises sharply. A similar rise in the rate of heat transfer to the bearing journal will occur at the same time.

Predicted temperatures are in good agreement with the measured temperatures, and are plotted in Figure 88. The corresponding predictions of heat flows into the bearing shells and journal are shown in Figure 89. This clearly shows a sharp increase in heat transfer to both shells and journal, and a sharp reduction in the change in oil enthalpy flux across the bearing when hot store coolant is streamed through the FCA. The combined effect is to limit the deviation of the film temperature from the adjacent metal temperature. Overall, there is a reduction in the total heat flow consistent with a reduction in frictional losses in the bearing, but this is much smaller than the benefits a 15-20 ºC increase in film temperature would yield.

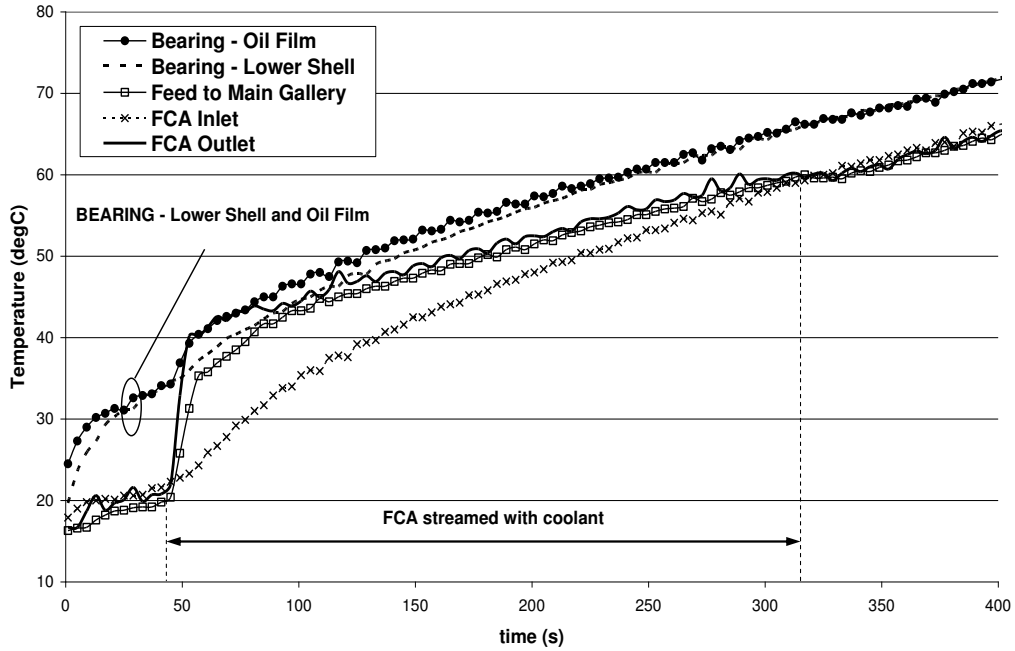

Figure 87 Measured oil temperatures in the sump, at outlet of FCA, in the feed to the main gallery and in the main bearing oil film with oil heating from 45-315s

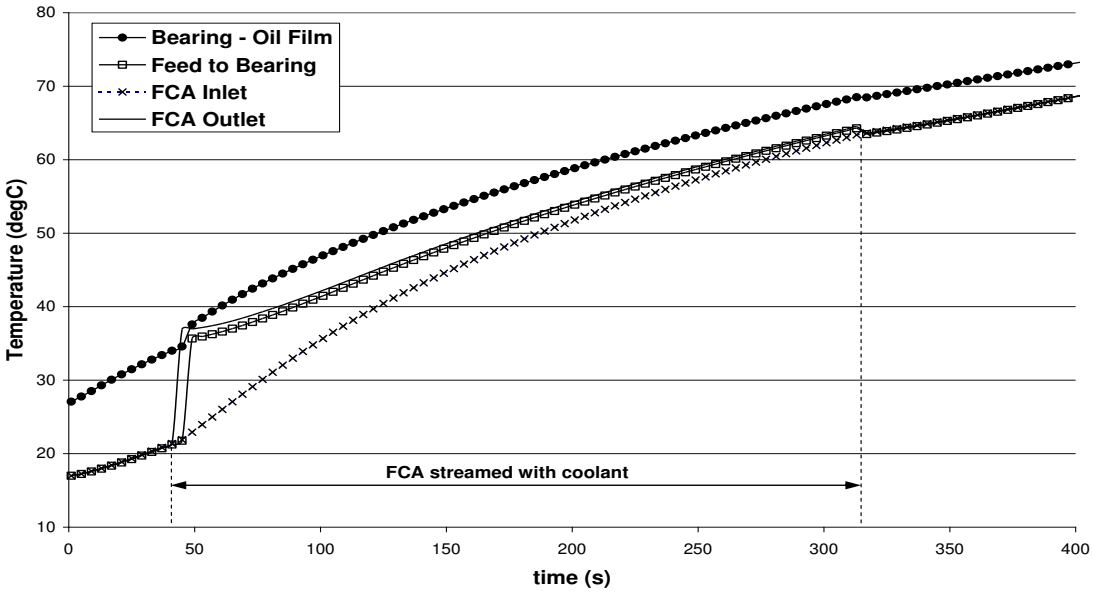

Figure 88 Predicted oil temperatures in the sump, at outlet of FCA, in the feed to the main bearings and in the main bearing oil film with oil heating from 45-315s

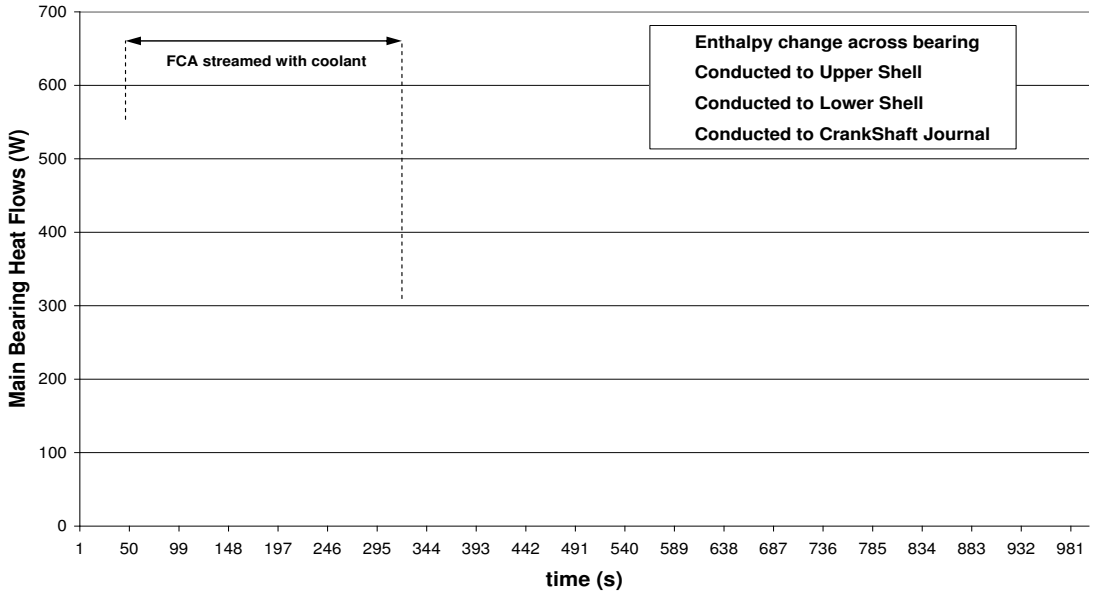

Figure 89 Energy flows (per bearing) in main bearing oil film in response to heat input from heat store

Temperature responses measured in the sump, in the pathway to the main bearings and in the bearing oil film, exemplify the uncertainty introduced when predicting bearing friction using oil temperatures remote from the rubbing surfaces. This is highlighted in Figure 90, which shows the variation in main bearing FMEP evaluated using oil temperature measurements in the sump (green), at the feed to the main gallery (magenta) and in the main bearing film (blue), respectively. The correlations used have been described in Section 3.6.1. Three phases of the test have been considered: Phase I is prior to oil heating, Phase II represents the first 55s of oil heating and Phase III is later on in the heat application period. Up until the point when hot coolant is streamed through the FCA (Phase I), all three FMEP predictions are practically identical. On heating the oil flow a significant divergence is observed between the predicted trends. After 315s into the test, when the flow of hot coolant through the FCA is stopped, all three friction traces are again practically identical. The degree of this divergence can be quantified in terms of a root mean squared error as summarised in Table 14. The 'error' in the predicted friction work is also shown, in Table 15. This has been evaluated for both the sump and feed to main gallery predictions relative to the prediction made using the oil film temperature, as this is assumed to be representative of true conditions in the bearings at all times throughout the warm-up. The temperature change at the feed to the main gallery in response to

oil heating is relatively immediate. Given the oil flow rate and gallery dimensions, it is estimated that it takes less than 0.5s for heated oil to travel through the main gallery to the bearings. As a result the film temperature response is also immediate but is heavily damped in magnitude relative to the change observed at the feed to the main gallery, for reasons explained previously in this section. Due to this, using an oil viscosity correction based on the feed to main gallery temperature, results in an under prediction of main bearing friction work throughout the oil heating phase; the error is significant at ~9 %. The oil sump temperature response shows a considerable time delay of ~8s from the moment oil heating is applied. This can be mainly attributed to hot oil returning and mixing with colder oil in the sump. Also the oil warm-up rate in the sump reflects the net heat transfer to the oil from thermal-friction interactions around the whole lubrication circuit and is therefore different to that in the main gallery and film for up to a minute into the oil heating phase. The overall effect is that an oil viscosity correction based on sump temperature results in an over prediction of main bearing friction during the oil heating phase.

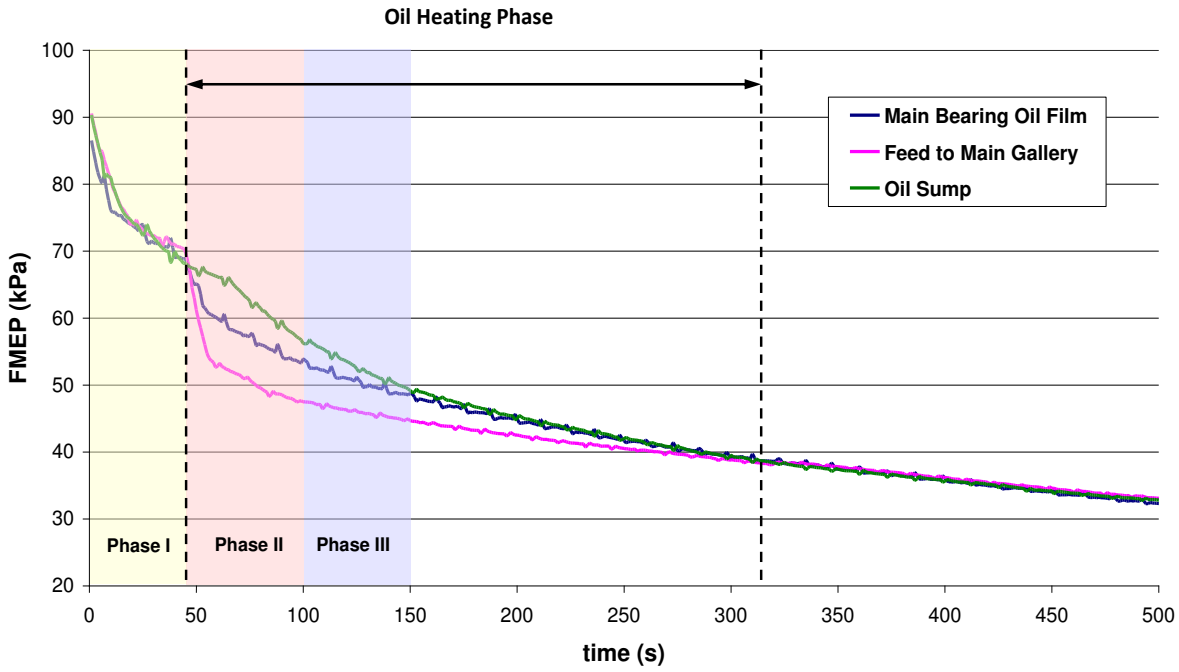

Figure 90 Main Bearings FMEP prediction using oil film, main gallery and oil sump temperature measurements over a warm-up at 2000 rev/ min, 3 bar BMEP

	Phase I	Phase II	Phase III
	kPa	kPa	kPa
$RMS_{feed\ to\ main}$	2.28	6.11	4.67
RMS_{sump}	2.15	5.05	2.38

Table 14 Root mean squared error in FMEP prediction from using oil temperatures in the sump and feed to main gallery to characterise main bearing friction

	Phase I	Phase II	Phase III
	%	%	%
$\Delta W_{f,\ feed\ to\ main}$	2.29	-9.92	-8.91
$\Delta W_{f,\ sump}$	1.53	7.63	4.95

Table 15 Error in predicted main bearing friction work from using oil temperatures in the sump and feed to main gallery to characterise main bearing friction. Prior to oil heating (Phase 1) the error is relatively small at ~2%, but becomes significant (>5%) during the heating phases.

6.3.2. Potential benefit of reducing heat transfer to shells and journal

For the steady speed and brake load conditions examined (2000 rev/min, 3 bar BMEP), simulation results indicate the saving in main bearing friction work to the end of the heat application period (315s into the test) was 68 kJ, or 10 %, as illustrated in Figure 91. Given that the benefit of raising oil temperature in the FCA is limited by the strong thermal coupling of the bearing film to the shells and journal, the effect of insulating parts of the bearing in conjunction with employing the heat store was explored. Various cases of selective insulation were modelled; the first was to perfectly insulate the main oil gallery to eliminate the drop in oil temperature between the FCA outlet and the bearing feed position. The oil flow rate in the main gallery has a Reynolds number in the range 50-3500, and throughout most of the warm-up period, it is at the lower end of the range. The corresponding heat transfer coefficient was calculated from Equation 24 to be 400-700 W/ m^2K. The predicted benefit of eliminating the heat loss in the main gallery was however, relatively small.

For the baseline bearing case the reduction in friction work over the entire duration of the simulation was less than 0.5%.

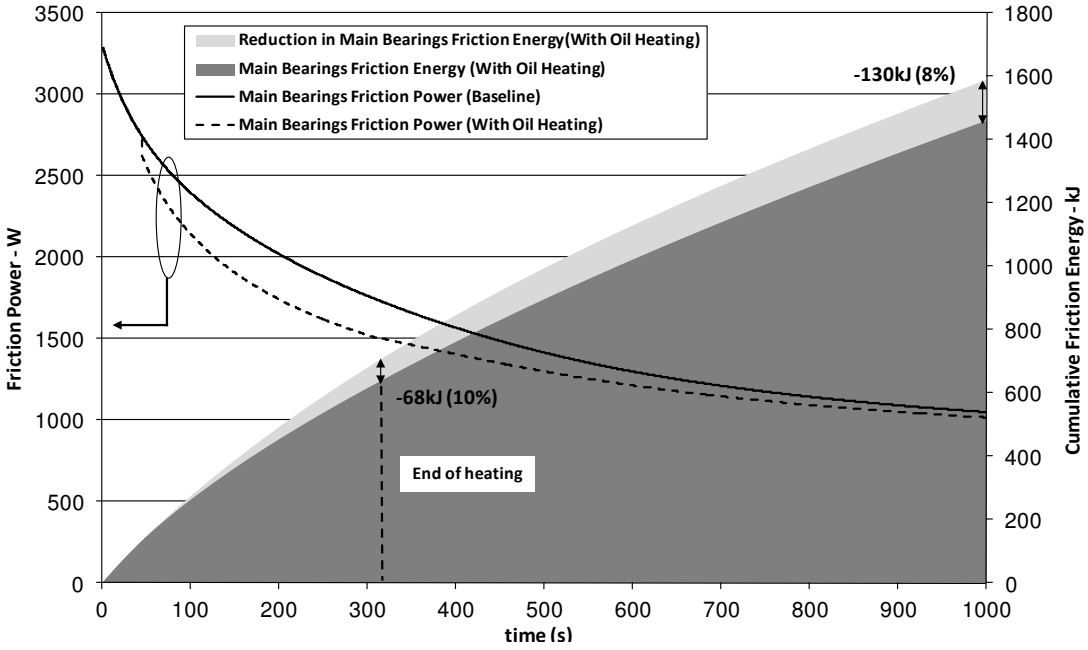

Figure 91 Model Predictions for Main Bearing Friction Loss with and without Oil heating at 2000rpm, 3bar BMEP

The potential benefit of reducing heat transfer from oil in the main bearings is greater. The reductions in friction work depend on the extent of thermal coupling of the oil film across the outer interface with the shells and the inner interface with the journal. Completely isolating the oil film would maximise both the rise in oil temperature across the bearing and the reduction in friction work. The predicted effect of eliminating heat transfer from the oil film to just the bearing shells, just the journal and finally to both the journal and the shells, is shown in Figure 92, for the case when the FCA is streamed with hot coolant to raise the oil feed temperature. Insulating the journal and the shells drops frictional dissipation by 1/3 almost from start up. The saving falls with time as the bulk oil and engine structure warm up, but when the oil is pre-heated in the FCA from 45s into the run, the benefit of the heat input is increased by the bearing insulation. When just the shells or just the bearing journal is insulated, the reduction in friction work is less than half that achieved when both are insulated. This is due to the rise in oil film temperature increasing the temperature difference driving heat transfer in the un-insulated direction. In the

model, the thermal resistances to heat transfer from the oil film to the crankshaft journal and to the bearing shells have been assumed equal. Yet, for up to ~100s into the warm-up, insulating the journal results in a marginally greater reduction in friction than that achieved from insulating the bearing shells. The journal thermal inertia is greater than that attributed to the bearing elements such that early in the warm-up heat transfer to the crankshaft is marginally greater than heat conducted to the bearing elements. However, in the later stages of warm-up, heat transfer from the crankcase oil mist to the 'cold' crankshaft journal slows the warm-up rate of the bulk oil. A lower feed temperature to the bearings therefore partly offsets the benefit of insulating the journal. The journal element influences heat transfer to the crankcase oil mist more than the bearing elements as it is better coupled to the oil mist to account for its rotation. As explained earlier in Section 5.2.2, this observation must be viewed with the simplicity of the crankshaft model in mind. Yet, it is still reasonable to conclude from the above results, that the crankshaft affects the oil temperature rise in two ways: locally in the main bearing films, and in the sump through its interaction with the crankcase oil mist. For the best case, when both the journal and the shells are insulated, the cumulative saving in friction work is shown in Figure 93.

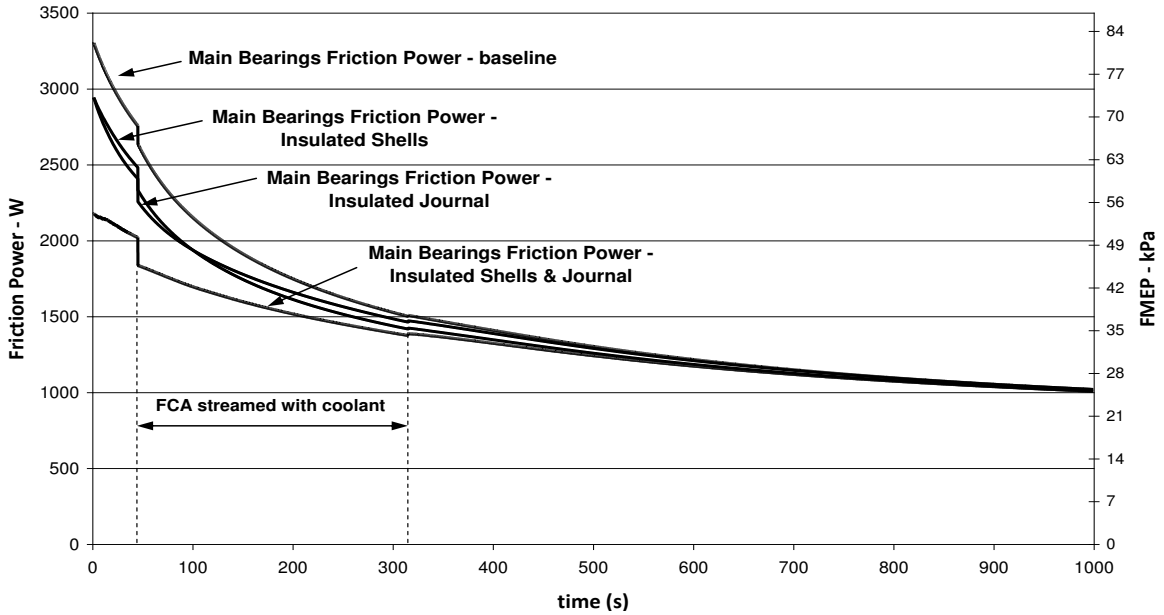

Figure 92 Comparison of Main Bearing Friction Level Predictions for Baseline and Selective Insulation Cases

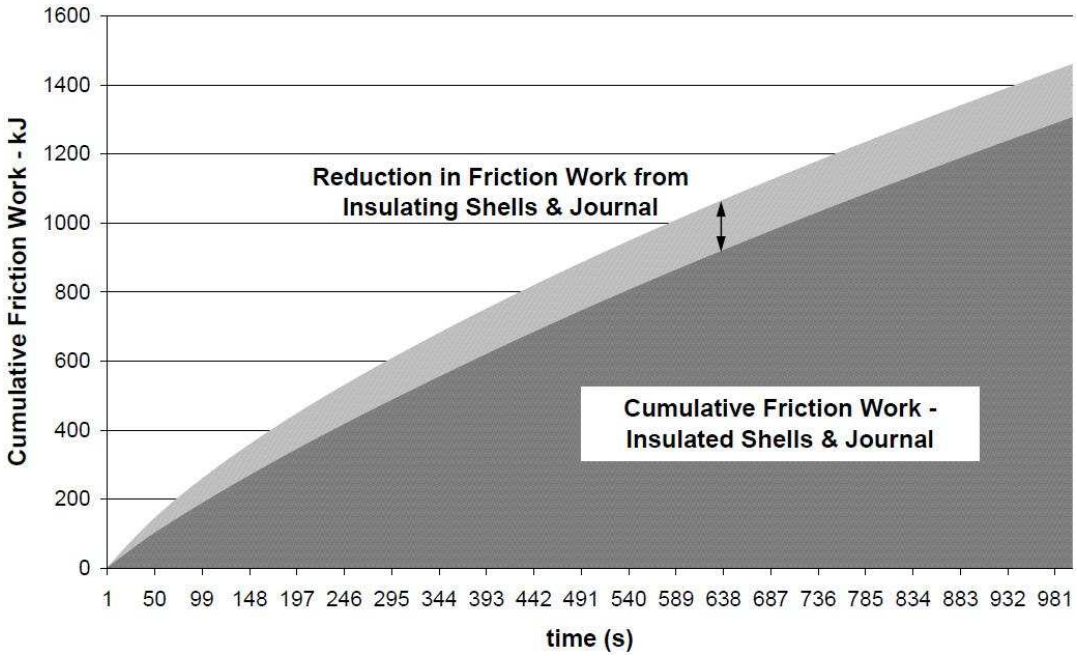

Figure 93 Model Predictions for Main Bearing Friction Energy Dissipation with Oil heating for the baseline and insulated bearing

A summary of the friction work dissipated up to the end of the oil heating phase (315s) and at the end of the simulated run (999s) is given in Table 16. Cases with external oil heating (FCA on) and with no heating (FCA off) are shown. Thermally isolating the oil film from the journal and shells provides a greater benefit in friction work than raising the oil feed temperature to the bearings by external heating. The percentage reduction in main bearing friction work over the duration of the simulation from heating of the oil is 8 % for the baseline case (Case 1 vs. Case 2). With a completely insulated bearing the benefit is lower at 6 % (Case 7 vs. Case 8), since the starting friction levels are lower. However, friction work for the insulated bearing is over 10 % lower than for the baseline case (Case 7 vs. Case 1). With no oil heating the improvement is similar at 12 %. Individual insulation of the journal or bearing shells provides improvements of 5 and 6.2 % respectively with no oil heating. With the heat store activated the improvements are similar at 4 and 5.5 %. The benefit of insulating the bearing is greater at lower engine speeds. Lower friction levels lead to prolonged engine and oil warm-up times and a greater opportunity to reduce losses by raising the film temperature earlier in the warm-up. At 1000 rev/ min, the percentage reduction in friction work at 315s into the warm-up from completely insulating the bearing is roughly double the saving at 2000 rev/ min.

time 't'(s)	Cumulative Main Bearing Friction Work (kJ) at time 't'							
	Baseline		Insulated Journal		Insulated Shells		Insulated Journal & Shells	
	FCA on	FCA off	FCA on	FCA off	FCA on	FCA off	FCA on	FCA off
	Case1	**Case2**	**Case3**	**Case4**	**Case5**	**Case6**	**Case7**	**Case8**
315	638	706	585	642	580	642	514	563
999	1461	1590	1401	1516	1380	1490	1306	1396

Table 16 Main bearings friction work at 315s (end of oil heating phase) and at 999s (end of test)

The predicted friction work savings depend on the assumed value of the friction correction index, (Section 5.4.3). The sensitivity of model predictions to +/- 20 % change in the friction correction index is illustrated in Table 17. A higher friction index not only increases the absolute levels of friction dissipation but also increases the benefit of raising the film temperature earlier in the warm-up. A lower friction correction index, on the other hand, reduces the rise in friction at cold temperatures and therefore the potential friction savings from raising the film temperature. Nonetheless the predicted trends are unchanged in that the friction benefit from thermally isolating the oil film is still clearly greater than that from pre-heating the oil, independent of what the friction correction index is assumed to be. Also shown in Table 17 is a case where oil heating was initiated from start-up (oil heating at 0s). Up to now, cases shown were for when the oil supply to the bearings was heated once thermal conditions in the bearings had stabilised (at ~45s). This was done so as to better isolate the influence of the oil feed temperature on the film temperature rise. However, to maximise friction savings oil heating should be applied as early as possible in the warm-up. Simulated benefits were ~4 % higher when oil heating was initiated from start-up, but still significantly smaller than the friction benefits attained from thermally isolating the bearing film.

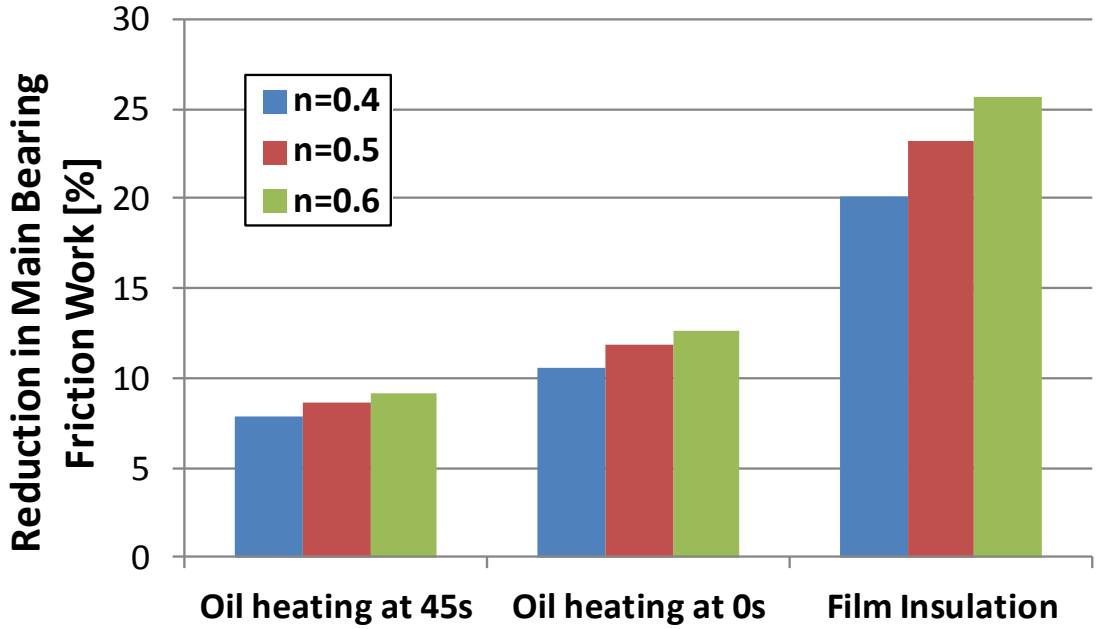

Table 17 Sensitivity of predicted main bearings friction savings to +/- 20% change in the assumed value of friction correction index. Results are shown at 315s into run.

The friction savings from heating the oil supply to the bearings as a function of the heat input to the oil are illustrated in Table 18. The heat inputs vary slightly for different cases; for cases where the oil warms up faster the heat transfer across the FCA is lower. The friction saving to energy input ratio, calculated at the end of the simulation, is similar for all cases, at ~25 %. This is a relatively small return on the energy transferred from the pre-heated coolant stream.

Case	Energy Input from Heat Store Q_{in} (kJ)	Main Bearings Friction Work W_f (kJ)	Friction Work Saving ΔW_f (kJ)	$\frac{\Delta W_f}{Q_{in}}$ (%)
Baseline	496	1461	129	26
Insulated Journal	494	1401	115	23
Insulated Shells	439	1380	110	25
Insulated Journal & Shells	415	1306	90	22

Table 18 Friction Work Reductions expressed as a percentage of the heat input to oil – 2000 rev/ min, 3 bar BMEP. Values quoted are at t=999s

The thermal inertia of the bearing results in the film temperature responding slowly to the heat input; the point of maximum friction saving does not coincide with the highest rate of heat input, but occurs at ~170s, 125s after heating is started (Figure 94). Even after the oil heating phase is terminated, lower bearing friction levels are maintained relative to a warm-up with no oil heating because of the higher film temperature. From Figure 94, it can be seen that the reductions in friction work during the heating phase and from when oil heating is stopped to the end of the simulation, are similar. As a result the friction saving to energy input ratio increases and is much higher at the end of the simulation than at the point when heating of the oil stream is stopped, Figure 95. This is in contrast to when the oil film is insulated from the rubbing surfaces, in which case the maximum friction saving is achieved on start-up. This partly explains why insulating the oil film achieves greater reductions in friction and also why it is even more effective in comparison to heating the oil, if engine operation time is especially short (<5 mins). Simulations in which streaming of the hot coolant was stopped earlier, show that the decision as to which heating strategy is optimal, depends on whether this is based on the absolute benefit in friction work or the ratio of this saving to the heat input. Stopping the heating earlier in the simulation resulted in a lower friction saving, but a higher calculated efficiency, as summarised in Figure 95 and Table 19. If it is assumed that heat input can be achieved with no associated fuel penalty, extending the heating phase to deliver the maximum heat input is most beneficial.

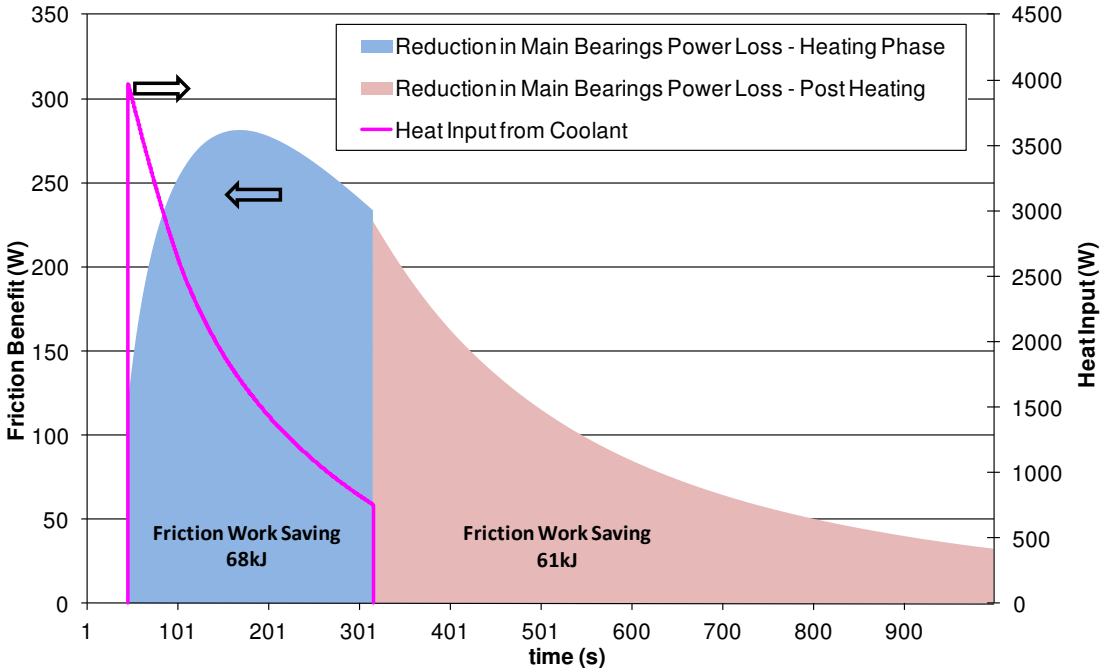

Figure 94 Main bearings friction work saving during and after oil heating phase – baseline bearing (no insulation) case

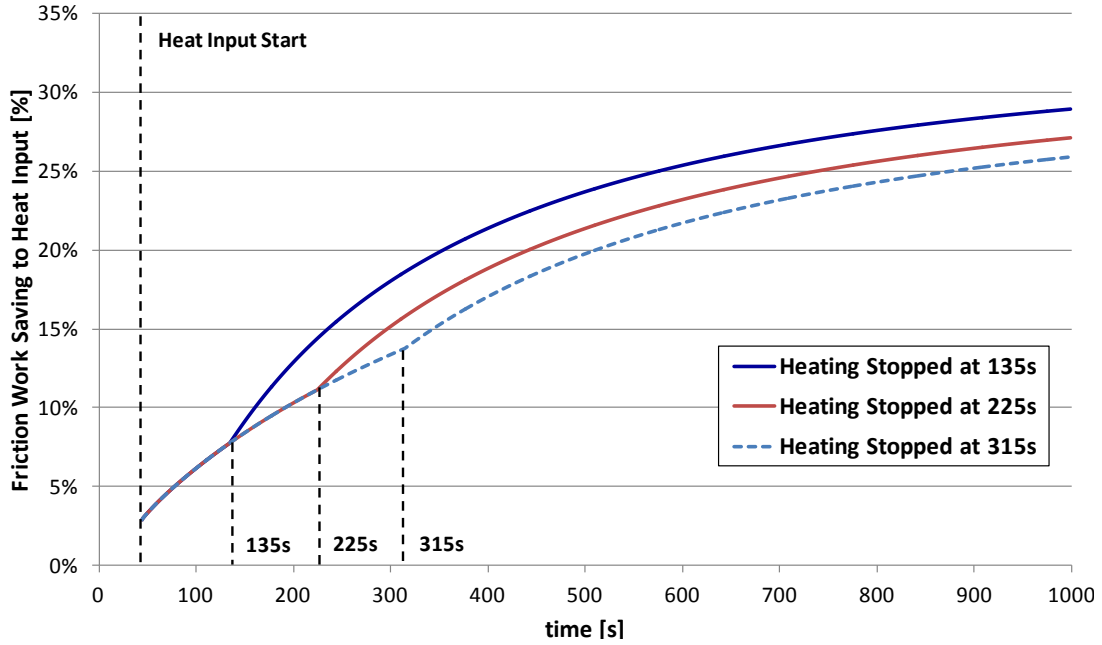

Figure 95 Friction work saving to energy input ratio for different heating durations

Heat Input Duration (s)	Energy Input (kJ)	Friction Work Saving ΔW_f (kJ)		$\frac{\Delta W_f}{Q_{in}}$ (%)	
		End of heating	**End of Run**	**End of heating**	**End of Run**
90	259	20	75	8	29
180	400	45	109	11	27
270	496	68	129	14	26

Table 19 Main bearings friction work saving and friction saving to energy input ratio for different heating durations – Oil heating was initiated at 45s in all cases

6.3.3. Reducing crankshaft journal thermal capacity

Reducing the thermal coupling between the oil film and rubbing surface was shown to offer substantial savings in main bearing friction. While Shayler et al. [4] showed that conduction through the bearing shells could be successfully reduced by increasing the thermal contact resistance between the back of the shells and the engine block, thermal isolation of the crankshaft journal may be harder to achieve. Similar benefits in friction seen from insulating the crankshaft journal could theoretically be achieved by reducing its thermal capacity. Different patents are reported in literature on the manufacturing of hollow crankshafts [139] [140]. To model the effect of a reduction in journal mass of 70 %, the journal was treated as a short cylinder with an internal diameter of 55 mm and the same external diameter, 65mm. The shell elements were treated as insulated as before. Friction levels on start up are 35% higher when compared to the fully insulated bearing case. The initial heat conduction rate to the journal is the same as when the journal is not insulated, but this now falls more rapidly due to the reduced thermal inertia. As a result, at 45 s into the run (initiation of oil heating) the friction penalty has dropped to 12 % (Figure 96). At the start of the oil heating phase, the friction work penalty is around 17 kJ or 18 %, but by the end of the heating phase (315s into the simulation) friction levels for both cases are practically identical and the friction work penalty has dropped to 6 %.

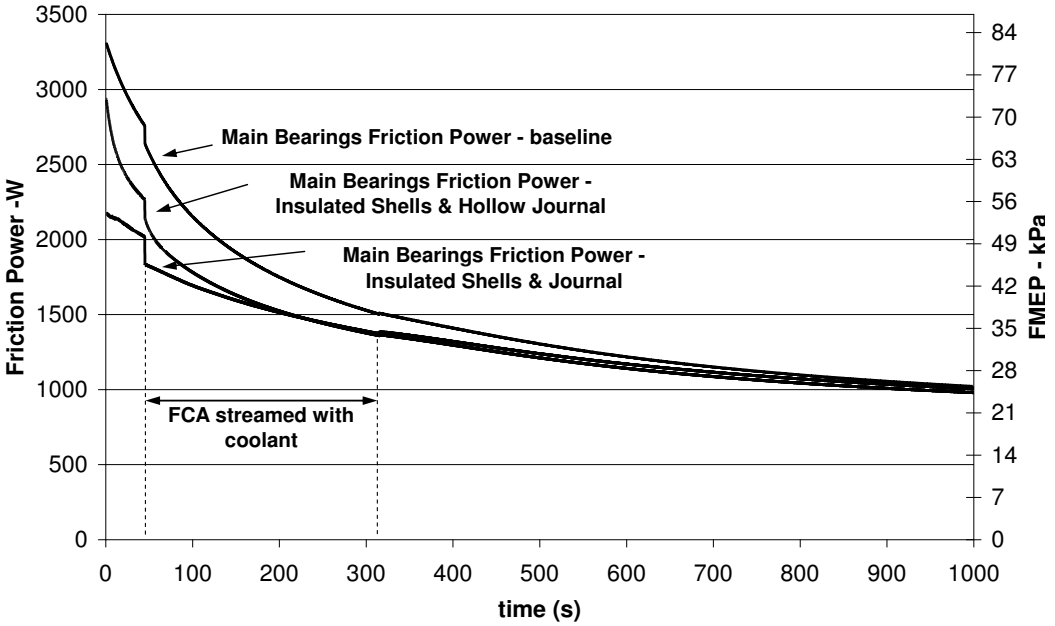

Figure 96 Model Predictions for Main Bearing Friction Work Dissipation with Oil heating for the baseline, fully insulated bearing and hollow journal and insulated shells (2000 rev/min)

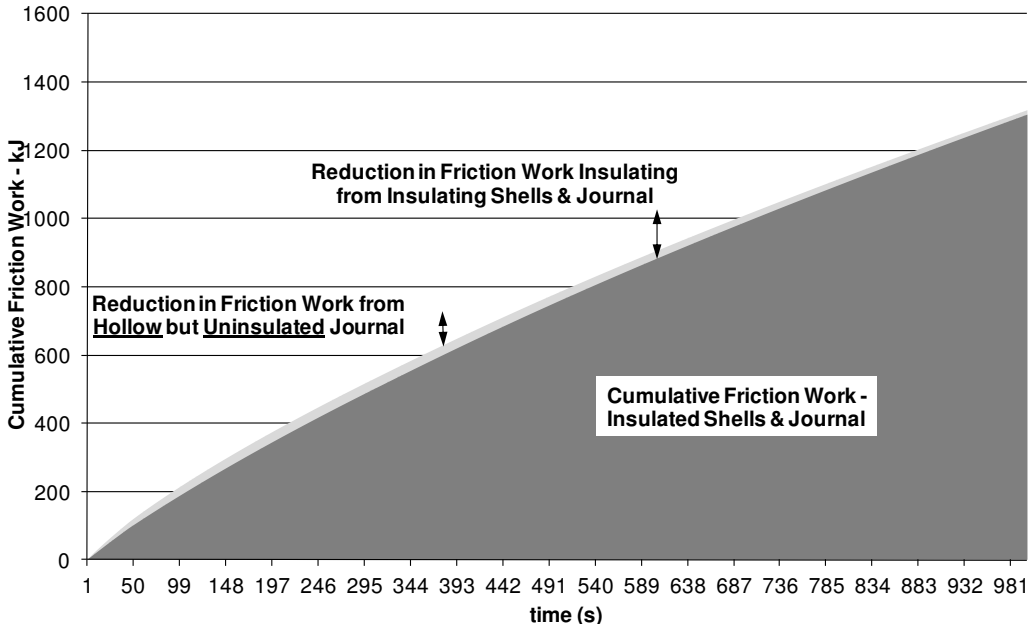

Figure 97 Model Predictions for Main Bearing Friction Energy Dissipation with Oil heating for the baseline, insulated bearing and hollow journal cases

6.3.4. Total Engine Friction Savings

The preceding considers only the effect on main bearing conditions. The benefit of the heat input extends beyond this to the big end bearings, to the temperature of oil discharged through PCJs, and the small rise in bulk oil temperature. These further effects have not been accounted for. In the main bearing sub-model, friction levels are coupled to the oil film temperature. An estimate of the saving in total engine friction work at the end of the oil heating period (315s) based on the improvement in bulk oil temperature indicates savings of approximately 7 %, 8 % and 14 % could be achieved respectively through oil heating alone, insulating the bearing shells and journal alone, and in combination, Table 20.

	Friction Savings Relative to Baseline Build @ 315s	
	Main Bearings	**Total Engine**
Oil Heating	67kJ	182kJ
	9.5%	6.9%
Insulated Shells & Journal	143kJ	222kJ
	20.3%	8.4%
Oil Heating & Insulation	191kJ	373kJ
	27.2%	14.2%

Table 20 Reductions in main bearing & total engine friction work at 315s from oil heating and thermal isolation of the bearing film. Engine operating condition: 2000 rev/min, 3bar BMEP.

Insulating the shells and journal doubles the friction saving in the main bearings achieved from heating the oil supply, but it only slightly increases the saving in total engine friction. In this case, the benefit in main bearing friction accounts for ~65 % of the total friction saving. Inhibiting heat transfer from the oil film bears a direct and strong influence on the film temperature rise and therefore on friction dissipation in the main bearings. It also promotes a faster warm-up rate of the bulk oil, reducing friction at the remaining friction surfaces, but this is only a secondary effect. Heating of the oil supply on the other hand has a bigger influence on bulk oil warm-up rate and as a result has a more global effect on total engine friction. In this case the saving in main bearing friction accounts for ~37 % of the total friction saving.

6.4. Discussion and Conclusions

Experimental and computational investigations have shown that heating the oil feed to the main gallery is one way of reducing friction in crankshaft main bearings during cold operation. However, the effectiveness of this method is limited by the strong thermal coupling of the oil film to the bearing journal, shells and surrounding metal which have a high thermal capacity. In response to a higher feed temperature, heat transfer from the oil film increases and limits the deviation of the film temperature from that of the surrounding metal surfaces. The model was used to simulate the effect of insulating different parts of the bearing. The greatest friction saving was achieved by completely eliminating heat transfer from the oil film to the bearing shells and crankshaft journal. In this case the friction saving was 50-100% greater than that achieved from externally heating the oil supply to the bearings. Individual insulation of the crankshaft journal and bearing shells showed similar savings in friction work, approximately half the saving achieved with the totally insulated case. Thermal isolation does not negate the benefits of an external heat input to the oil feed and a combination of thermal isolation and oil heating results in the maximum benefit: a reduction in friction work of 18% relative to the baseline bearing case with no oil heating.

While other researchers [4] have described an effective way of reducing heat losses from the oil film to the bearing shells, no practical means of insulating the oil film from the crankshaft journal has been identified. A 70% reduction in crankshaft thermal capacity was simulated as an alternative to insulating the journal, but was not as effective. In reality, the permitted reduction in crankshaft mass must be determined according to other engine design considerations such as structural integrity of the crankshaft itself and the NVH quality of the power train. Nevertheless, numerous studies have shown that current crankshaft designs possess a significant potential for mass optimisation from changes to web design and reductions in main bearing diameter [141]. While forged steel crankshafts are generally the preferred choice in automotive applications due to their superior NVH qualities, cast ductile iron crankshafts tend to be lighter, by up to 10 % [142]. Druschitz et al. [143] claim a 50 % reduction in weight from a more extreme design featuring hollow main journals, crankpins and balancing webs.

Results show that while the main bearing friction work saving from insulating the shells and journal is far greater than that achieved from heating the oil supply, the savings in total engine friction are comparable. Ultimately as it is total engine friction savings which translate into fuel economy benefits, supplementary heating remains a valuable way of reducing the cold start fuel consumption penalty. However, the relatively small friction saving to heat input ratio limits the possible heat sourcing methods that can return a net benefit in fuel economy. Generally, electrical heating devices are limited to relatively low power outputs and the efficiency of the charging system (alternator) leads to an overall increase in parasitic losses and fuel consumption. Heat recovery from the exhaust and coolant streams does not incur such a penalty but the available energy is generally limited in the early phases of warm-up. One possible solution is a heat battery [78] used to store energy drawn from the coolant or exhaust streams when the engine is fully-warm, to introduce it into the oil system during a cold start.

For a lower ambient temperature start, friction benefits will be higher than those observed in this investigation, partly because the initial friction levels would be higher, but also because higher rates of heat transfer could be driven from the heat store. The predicted absolute values of friction work dissipated depend on the assumed friction correction index and other model assumptions. However, the friction saving trends observed from pre-heating the oil feed to the bearings or thermally isolating the oil film do not change significantly and the main observations from the above investigations remain valid.

The savings in bearing friction work, from reducing the oil flow rate during warm-up, were shown to be small in comparison to those attainable from thermal isolation of the oil film. The proportion of friction heat carried away by convection in the early stages after a cold start is small. As a result oil flow rate has little influence on the film temperature rise. Reducing feed pressure is less effective still, given that the hydrodynamic flow component dominates early on in the warm-up and this is independent of pressure. Moreover the thermal coupling of the film to the shells and journal limits any film temperature deviation associated with reductions in oil flow. The effect of a more severe reduction in oil flow rate than that achieved through a reduction in oil supply pressure alone was also demonstrated. In this case, a slower

rate of temperature rise in the sump resulted in colder oil being fed to the bearings, partly offsetting the higher temperature rise across the bearing and limiting the absolute increase in film temperature. As for cases where the oil feed to the bearings was pre-heated, this observation also points to the importance of using the film temperature to characterise bearing friction rather than the feed temperature.

The benefits of operating with a lower oil supply pressure extend beyond the small reductions in main bearing friction demonstrated here. Experimental investigations with a variable flow oil pump on an engine of the same family as used in this investigation [144], showed that fuel savings of up to 2 % could be achieved over the NEDC from a reduction in pump delivery pressure and the associated reduction in oil pump torque demand. The extent of the allowable pressure reduction depends on a number of factors. Koch et al. [145] explain that at high engine speeds (>4000 rev/ min) the minimum supply pressure is mainly determined by the need to avoid the formation of air bubbles in the oil supply channel from the main bearings to the connecting rod big-ends. Sufficient oil pressure must also be maintained to allow satisfactory operation of piston cooling jets and, where fitted, VVT components. A reduction in main gallery pressure can be expected to reduce the oil jets flow rate and their cooling effectiveness. Nonetheless, given the typically light engine loads in the urban section of the NEDC, piston cooling is not so critical in the early phases of warm-up. A reduction in main gallery oil pressure could therefore be achieved without the danger of overheating the pistons, while normal operating pressure could be restored under high load conditions as the engine approached the fully-warm state. This would also guarantee sufficient oil cooling to the bearings when fully-warm.

Chapter 7 – Potential to Increase Rate of Oil Warm-Up

7.1. Introduction

In this chapter potential changes to thermal systems to promote faster oil warm-up rates over a cold start NEDC are investigated. The performance of 6 system variants has been ranked by the reduction in friction losses from a baseline case. Each modification/ strategy is firstly investigated and its benefits discussed separately. Where appropriate, combinations were considered to examine if these offer further gains. The results presented here represent the case of the test engine installed in a C class vehicle. The modelling studies carried out by the author made use of experimental data provided by Bath University [104] and Ford Motor Co. [101].

The investigations presented in the first part of this chapter concerned with the effectiveness of cooling the EGR gases with oil and exhaust heat recovery as means of promoting faster oil warm-up rates, were complimented by experimental work carried out at the University of Bath [10] as part of the Low Carbon Vehicle TSB programme. The model was adapted to reflect the experimental setup used for these studies, illustrated in Figure 98. While the core engine model remained unchanged, the internal coolant circuit was modified to include a novel split-EGR cooler element. This includes a diverter valve which can direct EGR gases either to a coolant cooled heat exchanger, as per the baseline engine build specification, or to an oil cooled heat exchanger. Adjustments were also made to account for additional coolant mass in the test setup (needed to instrument the external circuit with ultrasonic flow meters) and increased heat losses to ambient; a blower fan was used on the University of Bath test bed to replicate wind speed conditions of the driven vehicle. The coolant circuit can be considered to be made up of two major sections or loops. Flow to the radiator loop was shut throughout most of the drive cycle until coolant temperature reached ~90 °C. This section of the external circuit is therefore not modelled. The following analysis is instead focused on the coolant branch that is ‘active’ throughout the warm-up phase which includes two main elements of interest: the EGR cooler and oil-to-coolant heat exchanger (FCA). Their influence on engine warm-up and friction will be explored in this chapter. The PCJs were enabled in all simulations presented here. Over the NEDC, the fuel economy penalty as a result of the drop in bulk oil temperature from switching the jets off was predicted to be ~0.6 %.

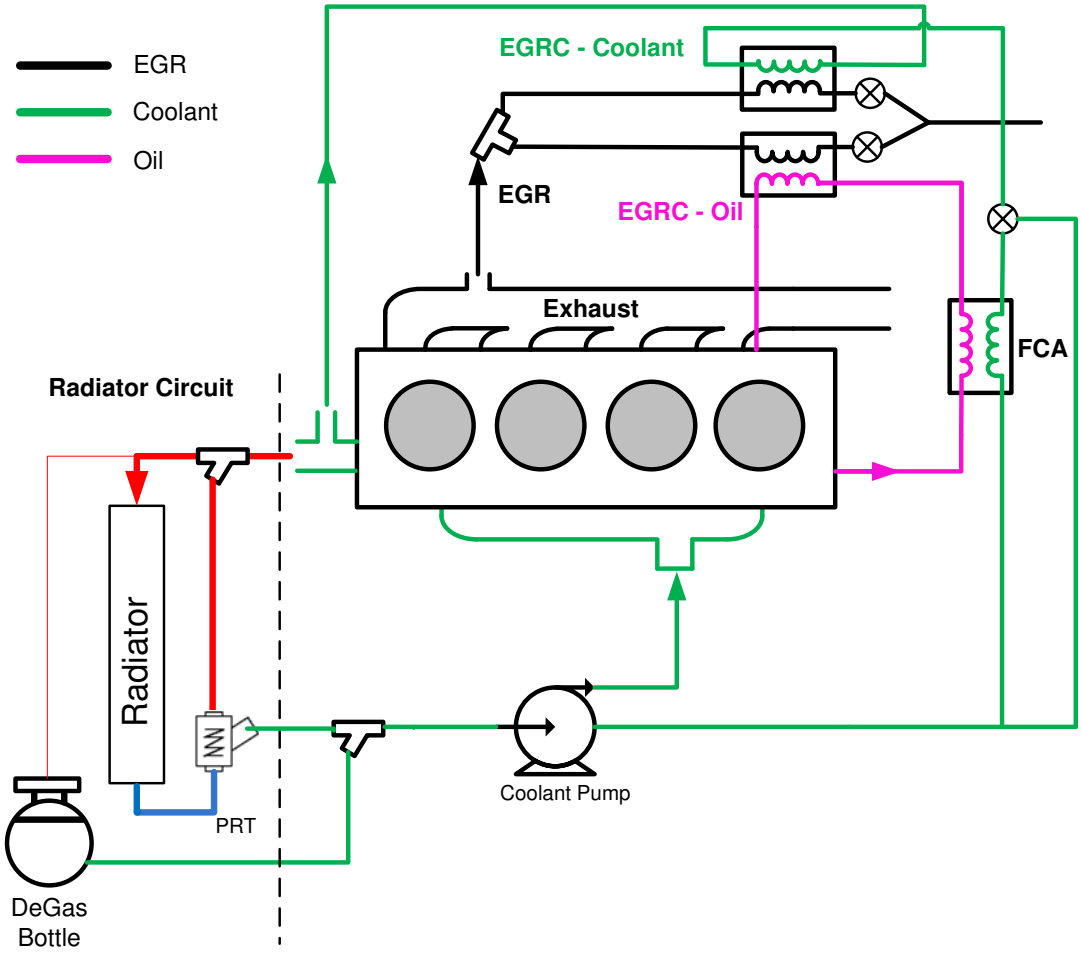

Figure 98 Test engine external circuit as installed at the University of Bath [104]

Heat transfer in the EGR cooler was modelled using a fixed effectiveness value of 30 % (Section 3.9) which was set by comparison of measured and simulated heat transfer rates from the EGR gases to the coolant. Measured heat transfer rates were calculated as the enthalpy change on the coolant side of the EGR cooler, determined from measurements of the temperature rise across the EGR cooler and coolant mass flow rate. Exhaust gas temperatures at the inlet to the EGR cooler were as measured on the test bed. Generally good correlation is observed for both the instantaneous heat exchange (Figure 99) and the cumulative heat energy transfer (Figure 100). The discrepancy between predicted and measured heat transfer rates in the acceleration phases of the drive cycle (**A**), are the result of an over-prediction in EGR mass flow rate. The AFR and EGR rate measurements over the drive cycle are highly transient and subject to different time delays which causes some uncertainty in the EGR mass flow rate calculation. However, overall the effect on the cumulative heat energy transferred is small, as illustrated in Figure 100. Data is only shown prior to main

thermostat opening (850s) as beyond this point coolant temperature is fixed to 90 °C. Up to this point the model under-predicted the cumulative heat energy rejected to coolant by ~8 %. A similar approach was used to set up the second EGR cooler sub-model coupled to the oil circuit.

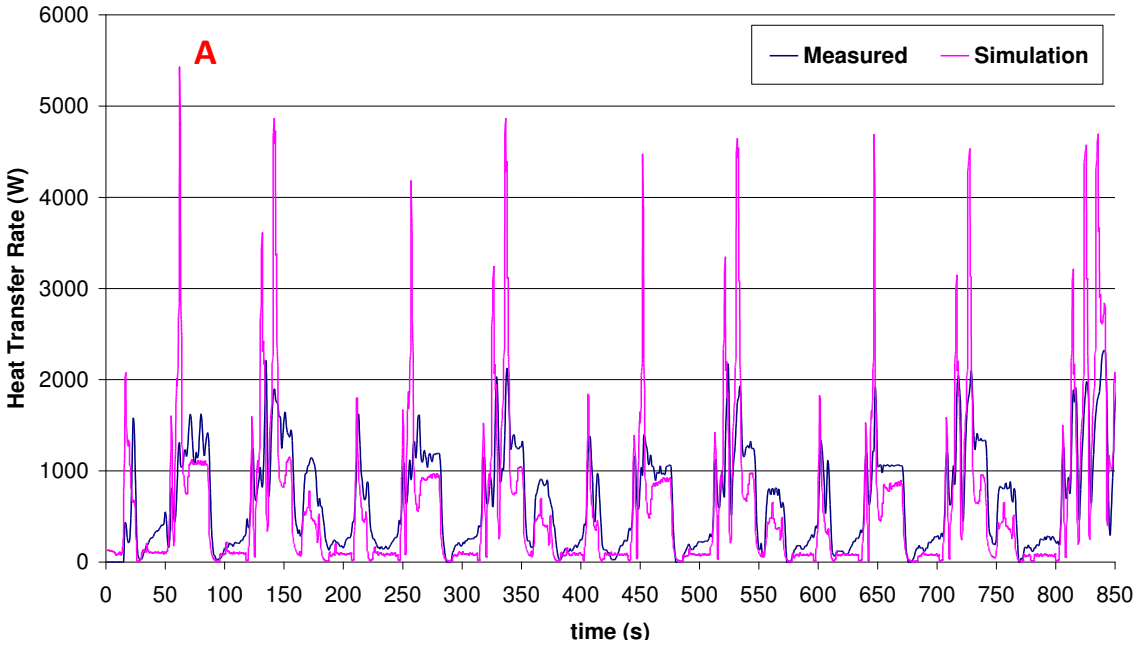

Figure 99 Simulated and measured heat transfer rates from the EGR gases to the coolant over the first 850s of the NEDC

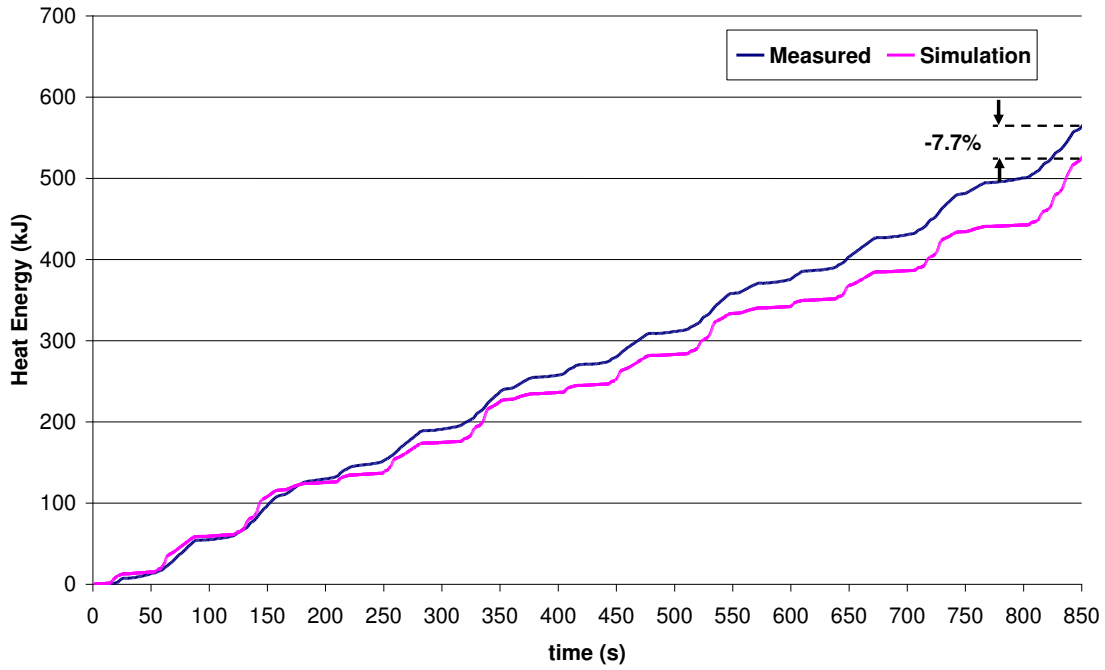

Figure 100 Simulated and measured heat energy transferred from the EGR gases to the coolant over the first 850s of the NEDC

For the investigations presented in this chapter, PROMETS was set up to predict fuel flow rates (Section 3.10). For the baseline engine build (with the EGR cooler streamed with coolant) these were in good agreement with test bed measurements except at points of fuel 'cut off' during the deceleration phases in the drive cycle, Figure 101. This condition is not replicated in the model which predicts a 'zero' load fuel consumption from the moment the fuel demand (pedal position) goes to zero. Zero and negative fuelling levels cause singularities in a number of the sub-model calculations in PROMETS resulting in a loss of accuracy and lengthening of the computational time. The error introduced by this simplification on the total fuel consumed is ~2 %. The investigations in this chapter are concerned with changes in fuel consumption from a baseline case rather than predictions of absolute values. Therefore, given the modelling purposes here, this error was considered acceptable. The cumulative fuel consumption breakdown for a cold start NEDC is shown in Figure 102. The proportion of fuel lost as a result of the engine's thermal efficiency (predominantly heat losses from in-cylinder gases to coolant and exhaust) is greatest at ~60 %. In the urban section of the drive cycle, friction losses are high due to the low oil temperatures and a greater proportion of fuel is used to overcome friction losses than that used to provide useful brake power output. In the extra-urban section of the drive cycle, the higher engine loads result in this trend being reversed. Over the complete drive cycle the brake load accounts for 24 % of the fuel used, while friction losses account for 15 %. The fuel quantity consumed to overcome pumping losses is small at less than 3 % and differences in pumping losses from changes in engine warm-up rate have been neglected. Likewise any penalty associated with cold operation on fuel conversion efficiency is neglected, such that changes in fuel consumption are solely associated with changes in friction dissipation.

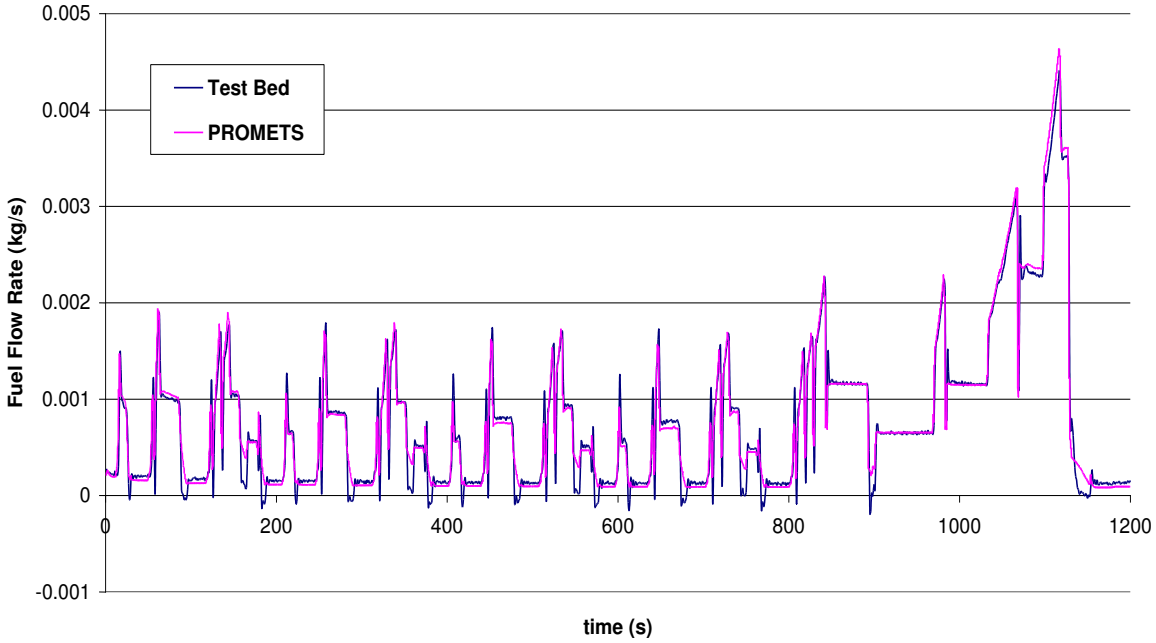

Figure 101 Simulated and measured [104] fuel flow rates over the NEDC.

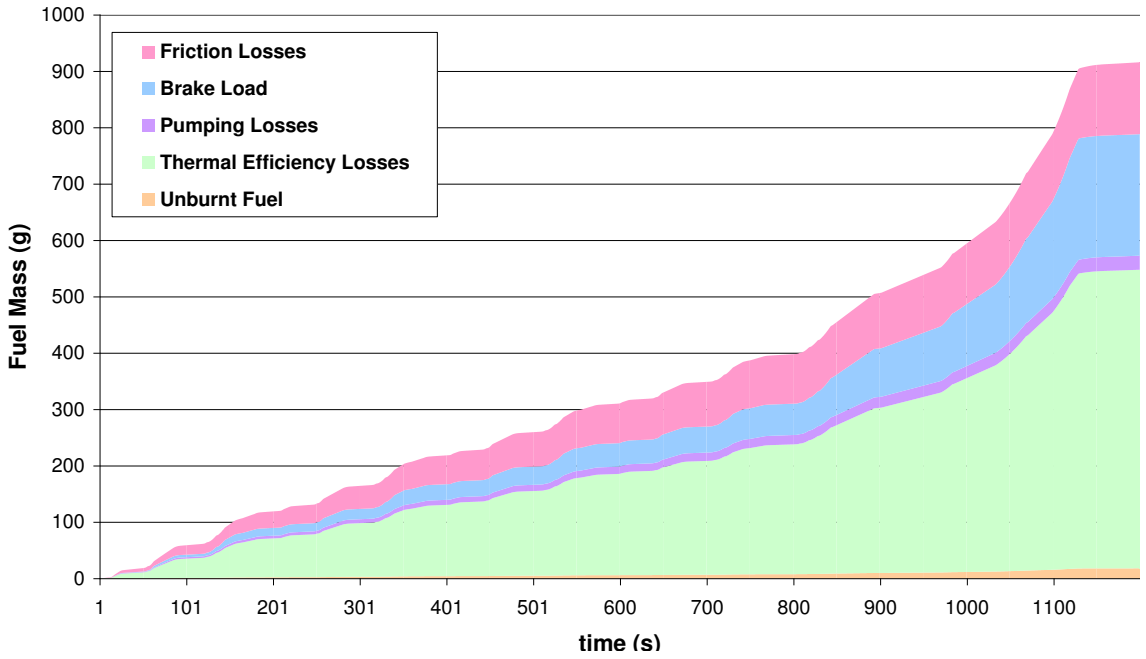

Figure 102 Predicted Fuel Consumption breakdown over a cold start NEDC

7.2. Effect of Switching from coolant to oil cooled EGR and streaming the FCA with coolant

In this section, using engine oil rather than coolant to cool the EGR gases as a way of increasing the rate of oil warm-up, is investigated. Predicted oil and coolant warm-up trends over a cold-started NEDC were in good agreement with variations measured

on the test bed with the EGR heat exchanger streamed with either the coolant (Figure 103) or the oil (Figure 104). The former case is considered as the baseline engine build; Build 3. Oil temperatures were consistently 1-2 °C higher throughout warm-up when the EGR was cooled with oil rather than the coolant. The improvement in fuel economy given by switching the EGR cooler from coolant to oil cooled was consequently small in both the predicted (0.6 %) and measured cases (0.1 %) [104]; the predicted saving of friction work associated with this was 1.9 %.

Predicted warm-up rates for the case when the EGR is cooled by oil and no coolant is streamed through the FCA, are also shown, in Figure 105. In this case the fuel consumption benefit over the baseline engine build is even smaller at 0.3 %. More importantly however, the improvement in fuel consumption achieved by switching from coolant to oil-cooled EGR is a more substantial 1.7 % (case 3 vs. case 4 in Table 21), compared to the predicted 0.6 % benefit for cases when the FCA was streamed with coolant (case 1 vs. case 2). With the coolant temperature leading that of the oil, the FCA acts as an oil heater throughout the majority of the warm-up, Figure 106. Thermal system changes that successfully increase the oil warm-up rate penalize heat transfer from the coolant to the oil across the FCA (due to the smaller temperature difference between the two fluid streams). Simplified oil circuit heat flows for EGR cooling with coolant and oil, Figure 106 and Figure 107 respectively, illustrate this. In the first case, heat input to the oil from the FCA is ~500 kJ at 800s into the warm-up. In the second case, heat input to the oil from the EGR gases is ~400 kJ, but heat transfer from the coolant to the oil in the FCA is reduced to ~200 kJ. Heat input to the oil from the EGR gases is therefore partly offset by a reduced heat transfer in the FCA. The effect of the FCA extends further. Since oil temperatures are generally higher when the FCA is enabled, the potential reduction in friction is also lower. This can be highlighted by comparing the difference in fuel consumption between a cold and hot started engine for cases when the FCA is enabled (5.8 %) and disabled (7.4 %). In essence, streaming the FCA with coolant from key-on represents an effective way of raising oil temperatures during warm-up and makes further improvements in fuel consumption harder to achieve.

A number of other EGR setup variations were simulated and these are summarized in Table 21. For the EGR cooler streamed with either coolant or oil an increase in the

heat exchanger effectiveness gave only small improvements, particularly in the former case. For cases where the EGR coolers were arranged in series, placing the EGR cooler streamed with oil before that streamed with coolant provided the greater fuel consumption benefit but overall cases 6 and 7 gave similar benefits in fuel consumption. This reflects the redistribution of heat between the oil and coolant circuits across the FCA as explained above.

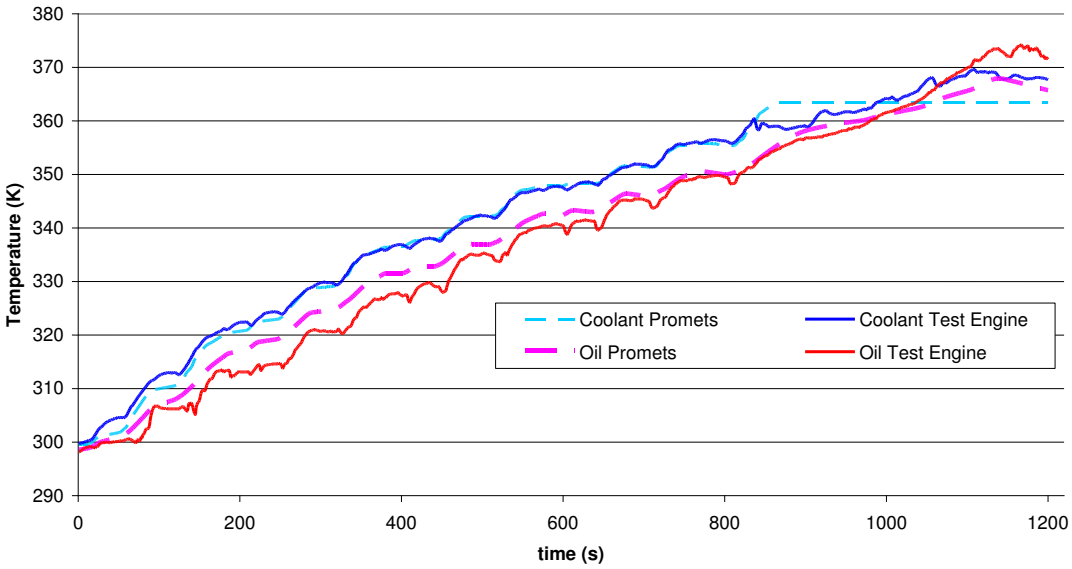

Figure 103 Simulated and measured oil and coolant warm-up rates for the baseline engine build (EGR cooler & FCA streamed with coolant from key-on)

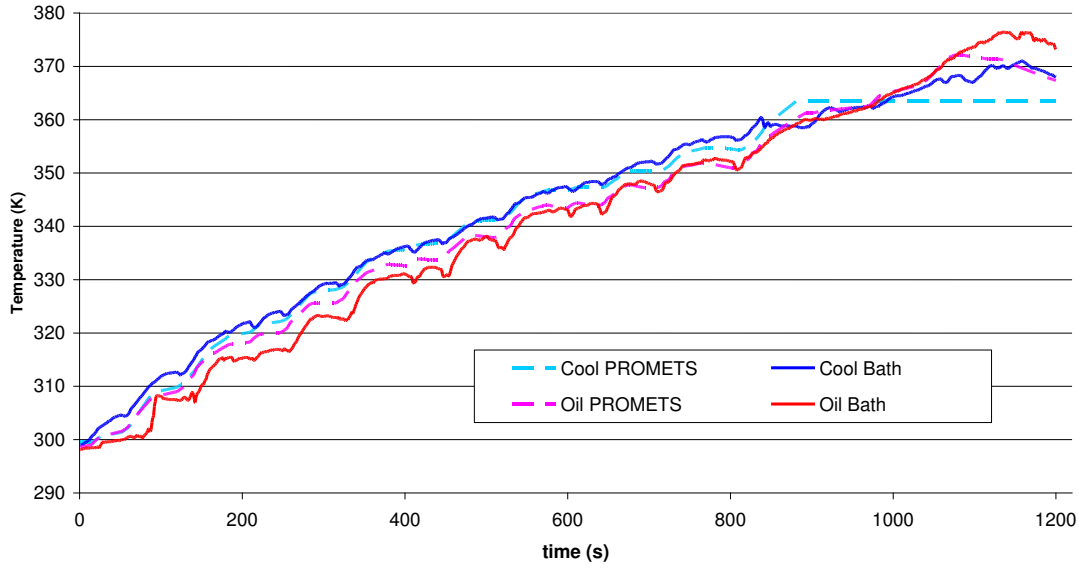

Figure 104 Simulated and measured oil and coolant warm-up rates with the EGR cooler streamed with oil and the FCA streamed with coolant from start up

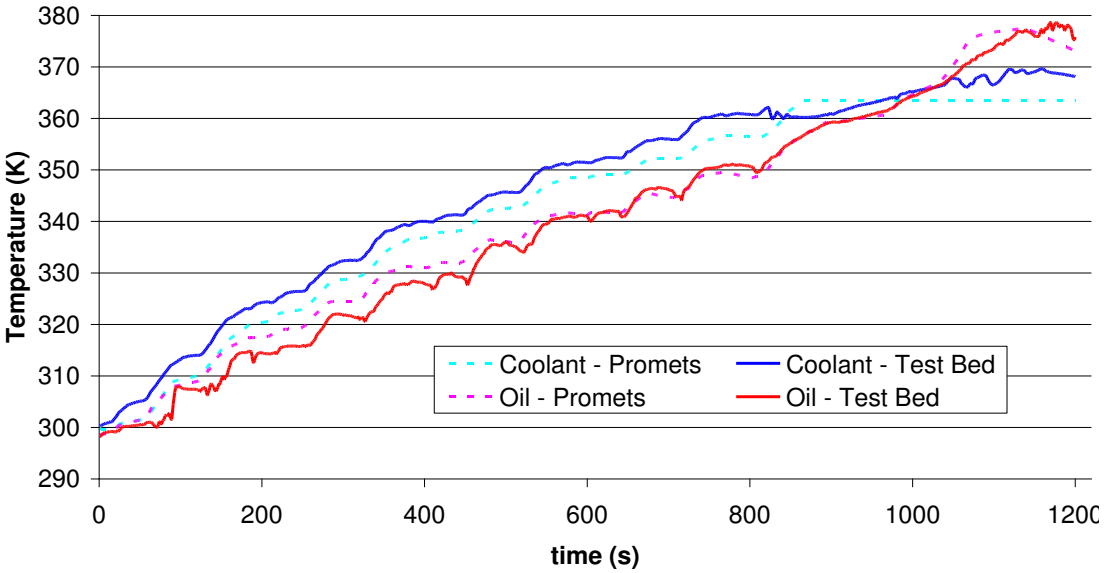

Figure 105 Simulated and measured oil and coolant warm-up rates with the EGR cooler streamed with oil and no coolant streamed through the FCA

Case	Strategy/ Modification	FC reduction (%)
1	Baseline **(Build 3)** – FCA streamed with coolant; EGR to coolant heat exchange	n/a
2	As 1, but with EGR to oil heat exchange	0.63
3	As 2, but with no coolant streamed through FCA	0.34
4	As 1, but with no coolant streamed through FCA	-1.37
5	As 2, but with 50% increase in EGR heat exchange effectiveness	0.88
6	As 1, but with EGR heat exchangers to coolant and then oil arranged in series	0.62
7	As 1, but with EGR heat exchangers to oil and then coolant arranged in series	0.78

Table 21 Simulated fuel consumption benefits of different EGR cooling setups and the effect of streaming coolant through FCA

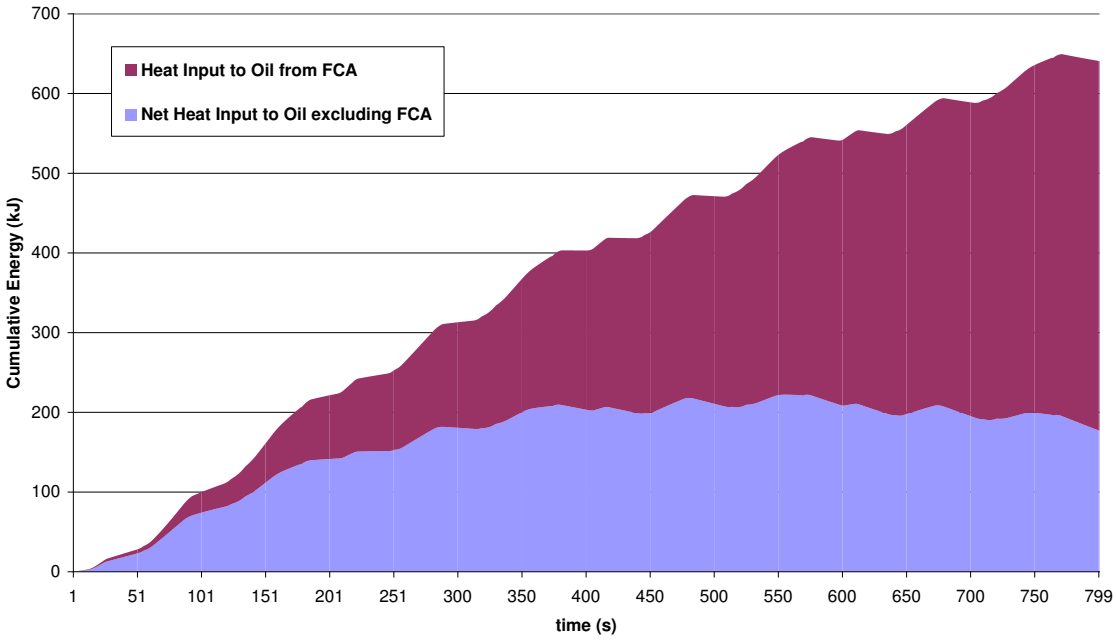

Figure 106 Oil circuit heat flows with the EGR cooler and FCA streamed with coolant. Purple area shows net heat input to oil excluding heat input from FCA. This is shown separately by the burgundy area.

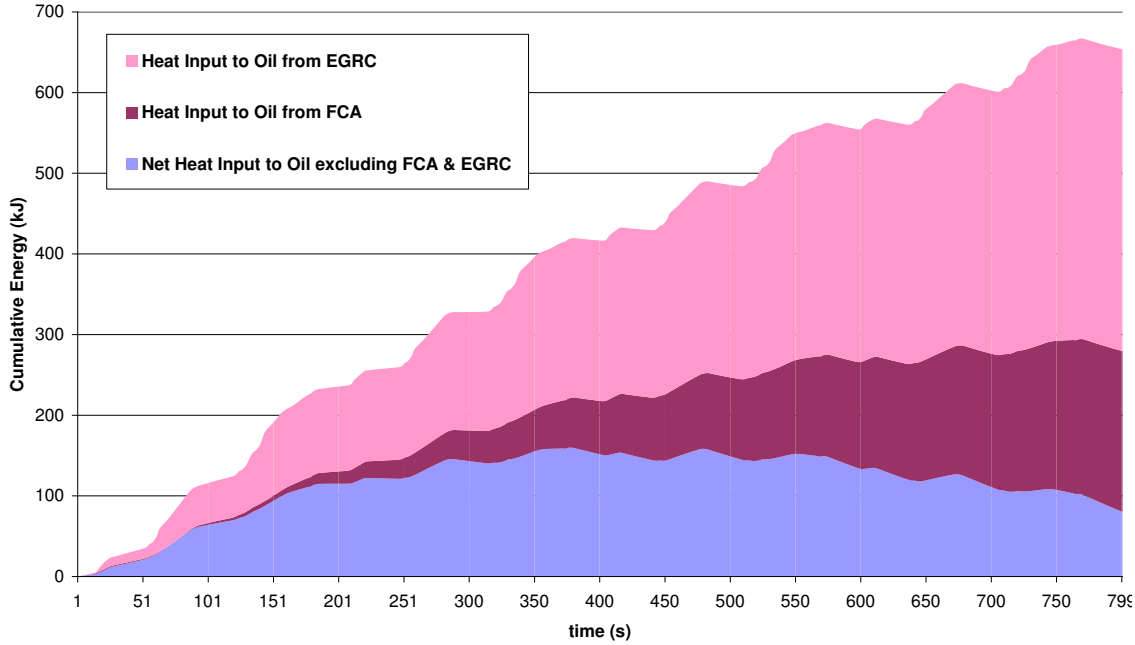

Figure 107 Oil circuit heat flows with the EGR cooler streamed with oil. Additional heat input from the EGR gases to the oil is shown by the pink area. Heat input from FCA is reduced when compared to Figure 106.

7.3. Supplementary Heating (Effect of Heat Transfer Rate) &Thermal Energy Storage

The predicted heat energy recovered by the oil-cooled EGR cooler over the NEDC is 744 kJ which, if averaged over the duration of the NEDC, represents an additional 0.6 kW heat input to the oil circuit over the baseline case (with coolant cooled EGR). The same energy was introduced into the oil circuit at three different power ratings over the first 200, 400 and 600s of the NEDC respectively. In all cases the EGR was cooled by the engine coolant and the FCA was only enabled whenever the coolant temperature was above that of the oil, so as to further promote higher oil temperatures. The results are summarized in Table 22.

Case	Build Description	FC saving relative to Build3 (%)
S1	**3.7kW heat input over 200s**	**1.78**
S2	1.86kW heat input over 400s	1.45
S3	1.24kW heat input over 600s	1.14

Table 22 Predicted FC benefit from supplementary heat input (744kJ) to the bulk oil at three power ratings. In all cases EGR was cooled by the coolant.

The results above show that the fuel saving becomes larger as the heat input rate is increased, and therefore point to the potential of thermal energy storage, given that the available energy is generally limited during warm-up. Assuming the NEDC is truly representative of real world customer driving, the thermal store's energy should be available at every cold start. Further simulations were therefore carried out in which heat energy input at the start of the drive cycle was recovered at the end of the drive cycle (to simulate recharging of the energy store). For these simulations, only the highest power rating (3.7 kW) was considered and it was assumed that the store can be re-charged at the same rate as it is discharged. The effect of transferring heat to the coolant circuit rather than the oil was also investigated as was the effect of

EGR cooling by either the coolant or oil streams. Savings in fuel consumption are summarized in Table 23. Predicted oil and coolant warm-up rates for Supp Build 2 and Supp Build 4 are also illustrated, in Figure 108.

Build Name	Build Description	EGR Valve	Supplementary Heat Input	FC saving relative to Case1 (Build 3) (%)
Supp Build 1	3.7kW Heat Input (with recovery)	Coolant	Oil	1.43
Supp Build 2	**3.7kW Heat Input (with recovery)**	**Oil**	**Oil**	**2.19**
Supp Build 3	3.7kW Heat Input (with recovery)	Coolant	Coolant	0.64
Supp Build 4	3.7kW Heat Input (with recovery)	Oil	Coolant	1.22
Supp Build 5*	**3.7kW Heat Input (with recovery)**	**Oil**	**Oil**	**5.70**

***Supp Build 5 - supplementary heat input combined with minimised heat loss from the oil circuit: no heat transfer in the main gallery, to the crankcase (see Section 7.7), sump walls and the crankshaft mass**.

Table 23 Predicted fuel consumption benefit from supplementary heat input (744kJ) with recovery. For all cases FCA was streamed with coolant when $T_{oil} < T_{coolant}$.

The penalty of recovering heat at the end of the drive cycle is small, < 0.4% (Supp Build 1 vs. Case S1 in Table 22). This reflects the reduced sensitivity of oil viscosity to temperature changes at the higher temperatures; the friction penalty from the oil temperature drop at the end of the drive cycle as the thermal store is recharged is far smaller than the friction benefit from the oil temperature rise at the beginning of the drive cycle. The greatest benefit in fuel consumption is achieved through supplementary heat input to the oil circuit, coupled to oil cooling of the EGR stream (Supp Build 2). In this case, oil temperature is above that of the coolant for up to 500s into the drive cycle (see Figure 108) and decoupling the two fluid streams is beneficial to retain heat in the oil circuit. Using the energy store in combination with suppressing heat losses from the oil circuit (in the main gallery, to the crankcase and sump walls and the crankshaft mass), achieved a 5.7 % improvement in fuel consumption (Supp Build 5), which is close to the reduction achieved by starting the

engine fully warm. In this case the oil reached 90 °C 255s after the start-up and was limited by means of the FCA to a maximum temperature of ~110 °C. Cases where supplementary heat was directed to the coolant circuit, also resulted in fuel consumption savings as the FCA redistributes heat from the coolant to the oil circuit. The benefits were however not as great as those achieved by direct heat input to the oil circuit but would be favoured if cabin comfort requirements preceded fuel saving requirements.

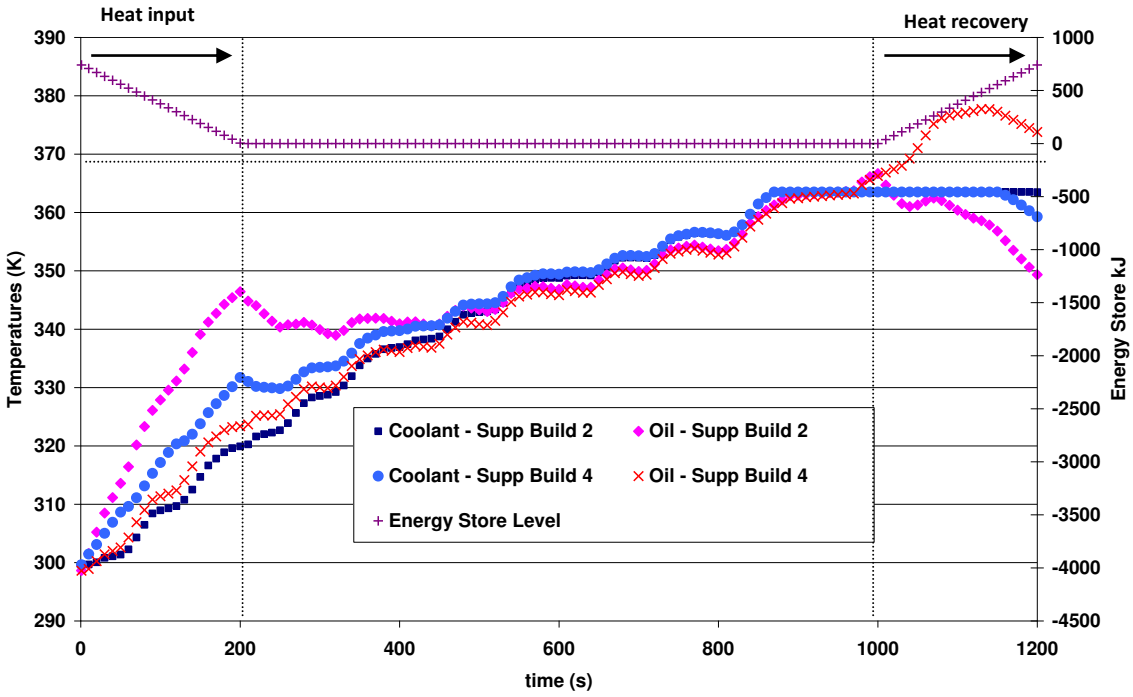

Figure 108 Simulated Oil and Coolant Temperatures for Supp Build 2 & 4. Also shown is the energy store level – discharged in the first 200s of the NEDC with heat recovery in the final 200s.

7.4. Exhaust Heat Recovery: Effect on engine warm-up

Generally, exhaust enthalpy accounts for between 22-35 % of the fuel energy released from combustion in a diesel engine [2]. Various measures to recover part of this energy have been reported in the literature, from turbo-compounding [146] [147] to different thermodynamic cycles [148]. In a turbocharged engine, as used throughout this work, some energy is recovered across the turbine. However, exhaust temperatures leaving the turbine are still high, and as a result so is the available enthalpy. In the following, reductions in fuel consumption from shortening the engine warm-up time using an exhaust heat exchanger have been investigated. Investigations

with coolant-to-exhaust heat exchangers have been reported to provide fuel consumption benefits [149] [6] while Morgan [34] simulated the effect of an oil-to-exhaust heat exchanger. The latter setup was not considered here as it is expected to result in a substantial oil pumping work penalty from the need to pump high viscosity oil around the heat exchanger circuit. Due to strict emission legislations, catalyst light off times must not be compromised by such installations and heat recovery must therefore occur post-catalyst. Given the typical position of the engine bay and after treatment systems in relation to each other, the installation of the exhaust gas heat exchanger is generally remote from the engine, Figure 109. This compromises the installation in two ways. Firstly, during warm-up, heat losses to the exhaust system and the thermal capacity of the after treatment system, result in a significant temperature drop from the exhaust manifold to the inlet of the exhaust gas heat exchanger. Also, relatively long coolant hoses must be used to connect the heat exchanger to the engine coolant system. This constitutes additional thermal inertia in the system which may reduce or even outweigh the potential benefits of heat recovery. In the following, this trade-off was investigated by simulating two different heat exchanger installations, experimental data for which was provided by the University of Bath [104].

7.4.1. Exhaust Heat Exchanger in loop with FCA

In the first setup the FCA was disconnected from the engine coolant circuit and connected directly to the exhaust gas heat exchanger. An electric pump was used to drive coolant flow in this loop. The oil side of the FCA was unmodified. This setup is illustrated in Figure 109. Measured exhaust gas temperature at the inlet to the heat exchanger was used as a model input. The effectiveness of the heat exchanger was set to 60% by comparing simulated and measured exhaust gas temperature drops across the heat exchanger. The total mass of coolant and hose pipes in the heat exchanger circuit was estimated to be 3.3 kg. In the model it was assumed that the hose pipes are at coolant temperature at all times and their mass was hence lumped into the coolant volume which was set at 4 L. On the test bed, changes in coolant flow rate through the heat exchanger showed negligible effect on the heat recovered. Simulated results shown here are for a coolant flow of 10 l/ min.

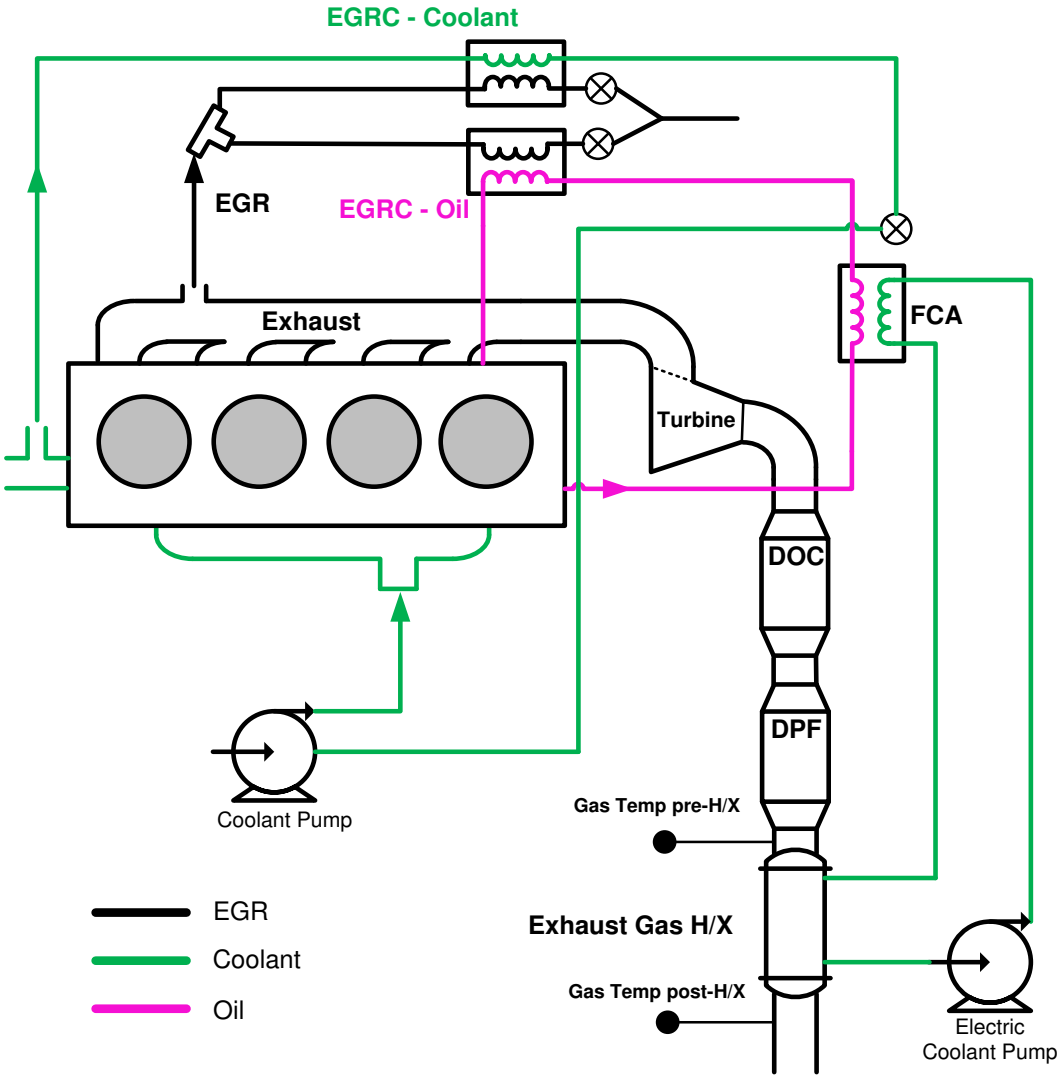

Figure 109 Exhaust gas heat exchanger connected to FCA.
(DOC - diesel oxidation catalyst, DPF - diesel particulate filter)

Predictions of oil and coolant temperatures throughout the warm-up compare well with variations measured on the test bed, as illustrated in Figure 110. When compared to the baseline engine build (Build 3), the rate of coolant warm-up in the engine circuit is higher due to the elimination of heat losses from the coolant to oil across the FCA. However, more importantly, oil warm-up is slower. Due to its high thermal capacity, coolant temperature in the heat exchanger circuit is lower than that of the engine oil until around 400s into the test and heat transfer in the FCA is in the reverse direction to that intended (Figure 111). Up to ~700s into the test, the cumulative energy recovered from the exhaust gases is equal to the energy stored in the coolant, implying that there was no net heat transfer to the oil circuit. The coolant energy has been calculated relative to the ambient start temperature of 26 ºC. Even at

the end of the test the heat stored in the coolant accounts for 70 % of the total energy recovered from the exhaust. The energy input to the oil system is around 545 kJ but overall the system incurs a fuel consumption penalty of 0.4 % when compared to the baseline build (with coolant cooled EGR and no exhaust heat recovery).

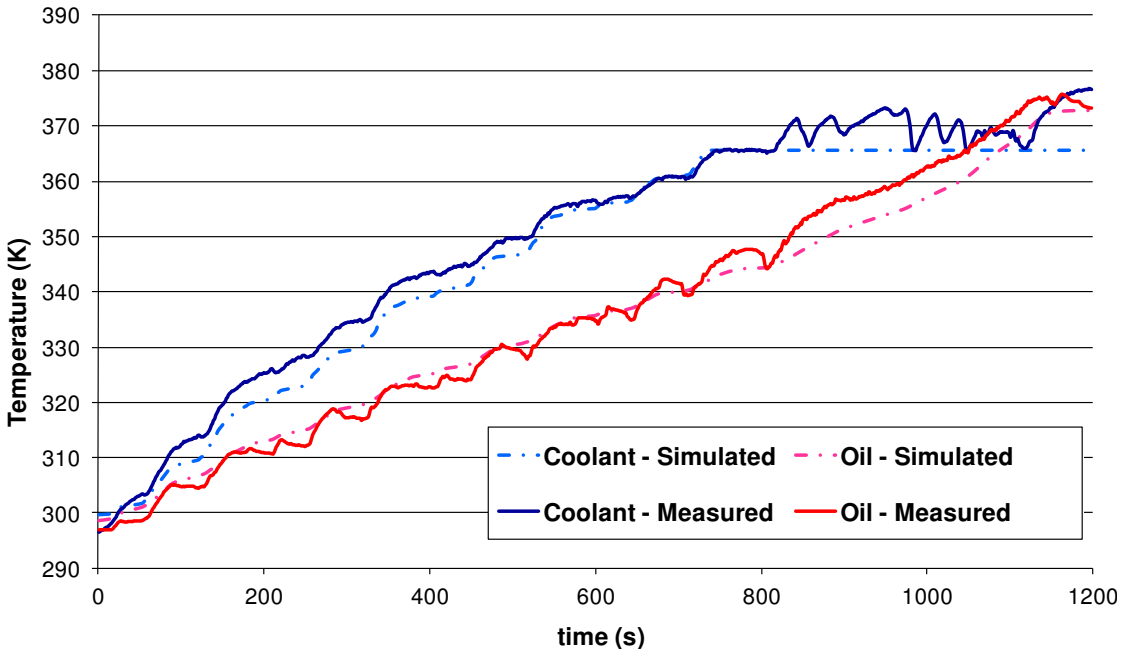

Figure 110 Comparison of simulated and measured oil and coolant warm-up rates with exhaust heat exchanger in loop with FCA

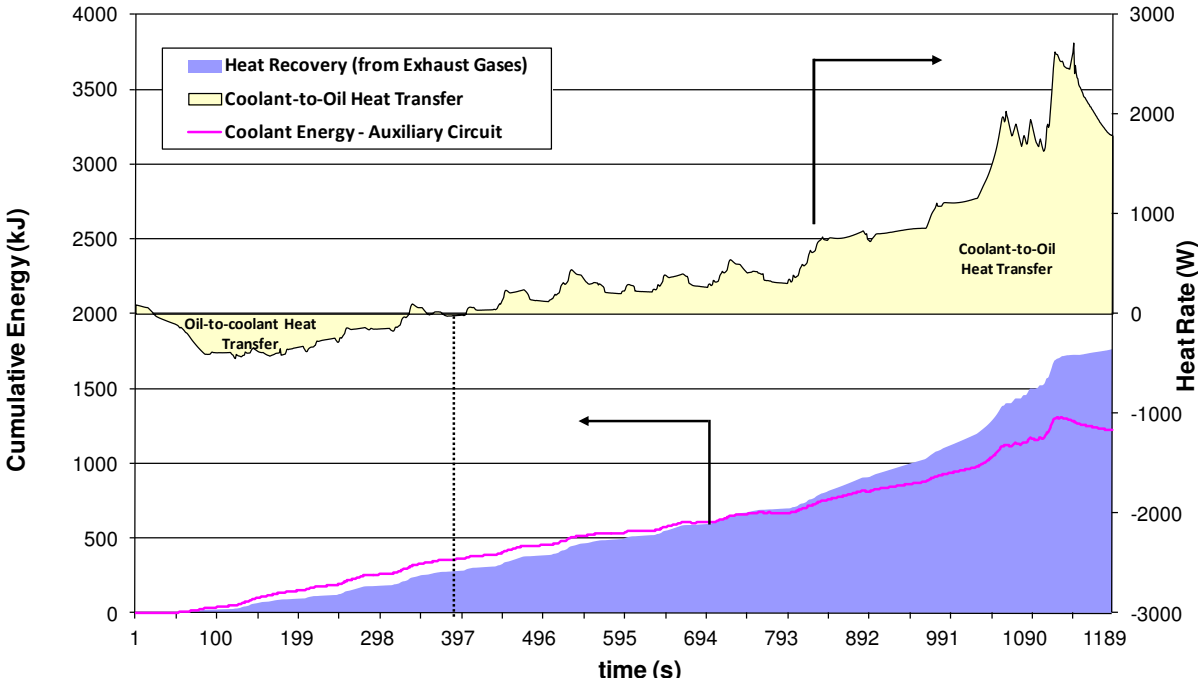

Figure 111 Coolant to oil heat transfer rates with exhaust heat exchanger in loop with FCA. Also shown is energy recovered from exhaust and that retained in coolant

7.4.2. Exhaust Heat Exchanger in main engine coolant circuit

In the second setup the exhaust gas heat exchanger was installed in the main engine coolant circuit (Figure 112), as was the FCA. The aim in this case was for heat recovery from the exhaust gases to raise coolant temperature and increase heat transfer to the oil across the FCA. By comparing simulated and measured oil and coolant temperatures over the warm-up, the additional coolant volume in this case was adjusted to 2 L, half that used in the previous build. The predicted benefit in fuel consumption was still negligible at 0.05 %. Assuming that no additional coolant is required by the heat exchanger installation, the simulated fuel consumption benefit was greater but still small at 0.3 %. This implies that the small improvement in fuel economy is not solely the result of the additional thermal inertia of the coolant system. A significant temperature drop occurs from the exhaust manifold up to the exhaust heat exchanger inlet as illustrated in Figure 113. This is due to the exhaust system's thermal inertia and heavily compromises the recovery potential of the heat exchanger. Compared to the EGR cooler, the benefit of a higher exhaust mass flow is outweighed by lower exhaust gas temperatures, particularly in the early phases of the drive cycle and leads to lower heat recovery rates than those achieved across the EGR cooler.

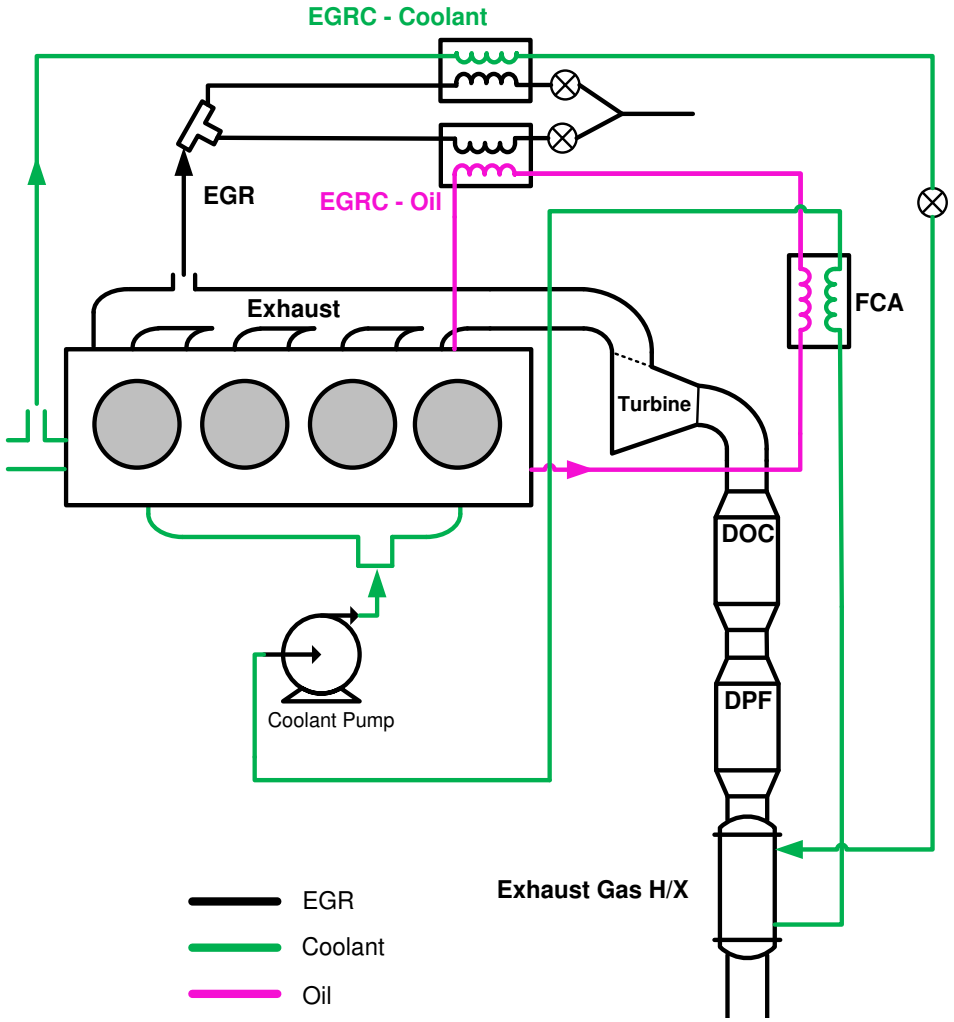

Figure 112 Exhaust gas heat exchanger included in main engine coolant circuit

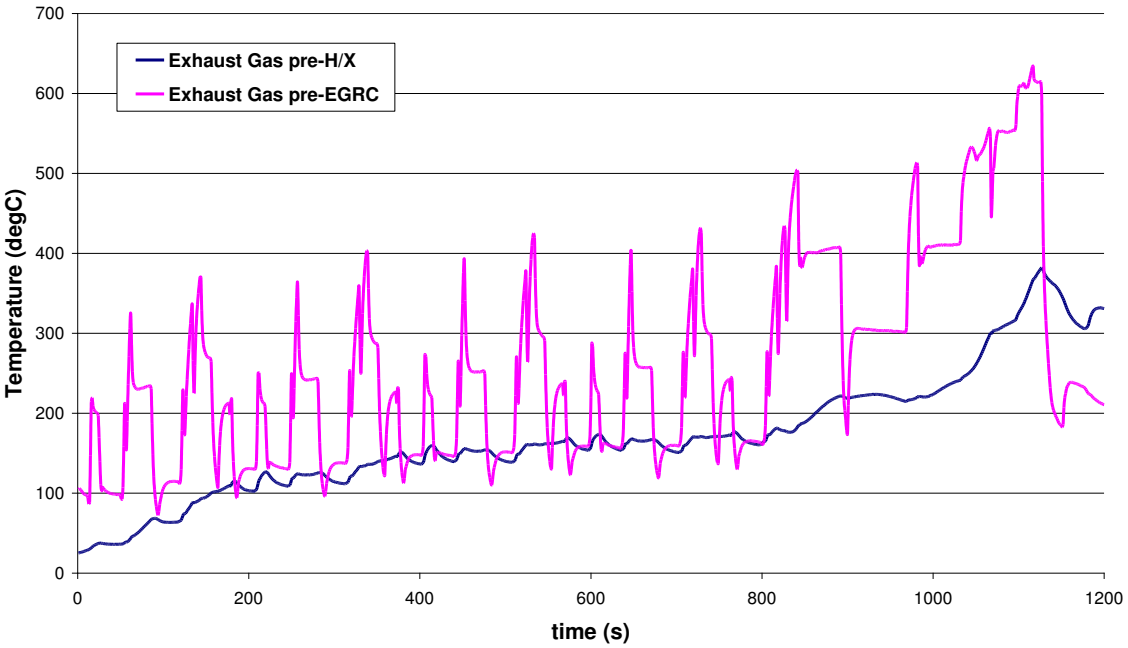

Figure 113 Measured exhaust gas temperatures at the inlet to the EGR cooler (exhaust manifold) and exhaust heat exchanger (post after-treatment)

7.4.3. Exhaust Heat Recovery with Thermal Storage

Exhaust gas heat recovery showed little or no benefit in engine fuel economy due to the additional coolant thermal inertia incurred by both systems described above. However, the additional coolant volume could theoretically be used for thermal energy storage. Once the engine has reached fully-warm operating temperature, coolant in the heat exchanger circuit could be stored in a thermally insulated vessel extending its cool down time in preparation for the next cold engine start. For this investigation the setup described in Section 7.4.1was considered. The coolant volume in the heat exchanger loop was initialized at 90 °C, while the engine structure, oil and coolant in the main engine circuit were started as normal from an ambient temperature of 26 °C. In this case high rates of heat transfer to the oil are achieved from key on (Figure 114). The rate of heat transfer drops sharply as the oil warms up. A higher initial coolant temperature also means that heat recovery from the exhaust stream cannot start until about two minutes into the simulation. High engine loads in the extra urban (EUDC) section of the NEDC result in high exhaust mass flow rates and high gas temperatures such that the coolant temperature can be raised well above its starting temperature of 90 °C. The maximum energy recovered will obviously be limited by the need to avoid boiling of the coolant. An exhaust diverter valve could be used to bypass the exhaust heat exchanger once heat recovery is no longer desired. However, more importantly, this shows that the thermal store could be fully re-charged to its initial energy level by the end of the drive cycle. The fuel consumption benefit from using the heat exchanger in combination with the heat store was calculated to be substantial at 1.3 %.

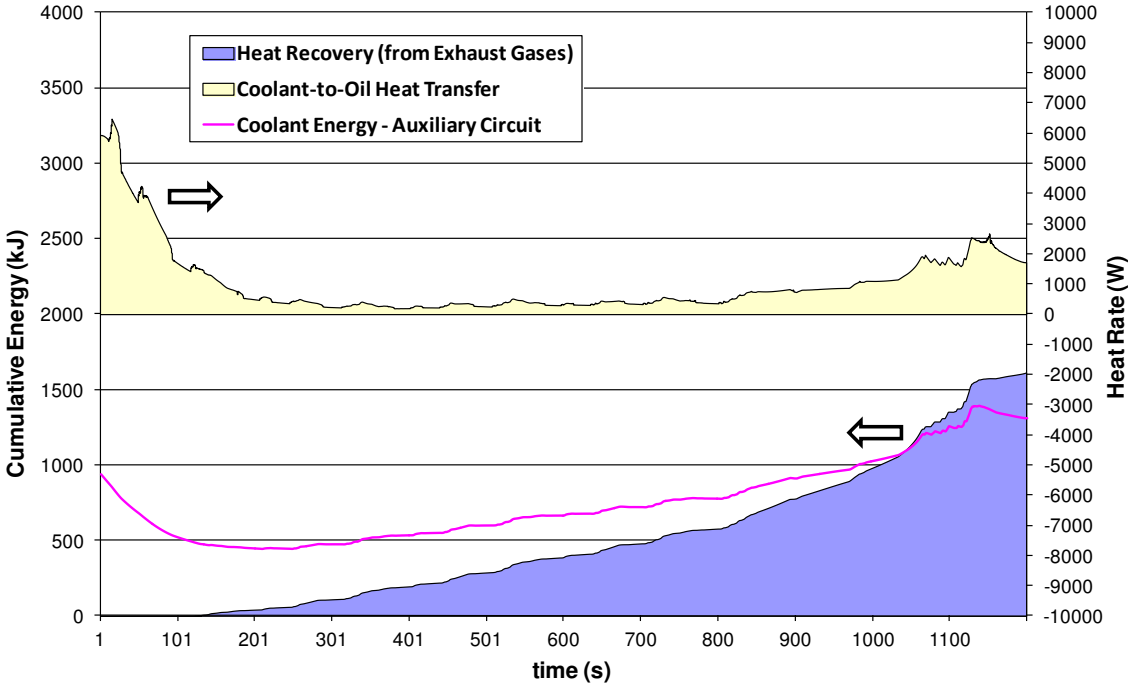

Figure 114 Coolant to oil heat transfer rates with coolant in heat exchanger-FCA loop initiated at 90°C. Also shown is energy recovered from exhaust and that retained in coolant

7.5. Reducing Ambient Heat Losses

Ambient heat losses from the engine are mainly due to convective heat transfer from the oil sump, engine block and cylinder head walls. The total engine surface area exposed to ambient is taken to be 0.58 m^2 of which a quarter is accounted for by the oil sump. In this section, the effect of reducing and completely eliminating heat losses from the oil sump and other engine surfaces is explored. A possible modification to the sump construction to achieve this and its effectiveness are discussed.

The surface area of the major engine parts and the potential saving in fuel consumption from perfectly insulating each part in turn is illustrated in Figure 115. The benefit from a complete insulation of the entire engine surface is also shown. The convective heat transfer coefficient was assumed to be uniform at 60 W/ m^2K for all engine surfaces. While there is a correlation between the insulated area and potential fuel saving, the mechanism by which the insulation of different engine surfaces affects the warm-up characteristic is different. The crankcase and oil sump affect heat losses from the oil directly and therefore bear the greatest influence on friction and fuel consumption. The cylinder block and cylinder head have an indirect

influence, in that they promote a faster coolant warm-up rate which then redirects part of the retained heat to the oil circuit via the FCA. The oil sump is the most efficient in terms of a fuel saving to insulated area ratio, even when compared to the crankcase. The reason for this is the large thermal capacity of the crankcase elements which holds their temperature down in the first minutes after start-up. As a result, while the area exposed to ambient is greater, early in the drive cycle, heat losses from the crankcase are lower than losses from the sump.

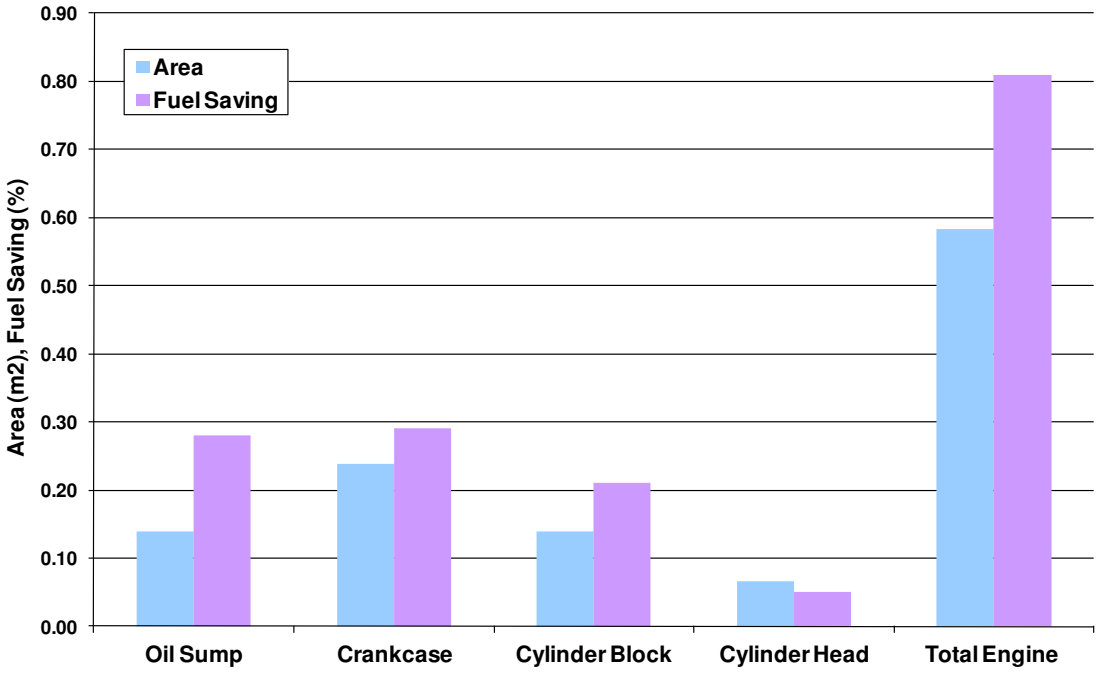

Figure 115 Exposed surface area & FC saving from completely eliminating heat losses from the various engine exposed surfaces (HTC=60W/m^{2}K)

The effect of replacing the original pressed steel sump with a fibre reinforced plastic one of 3mm wall thickness was simulated as one possible way of reducing heat losses from the sump. The calculated wall thermal resistance in this case is higher at 0.0857 K/ W as a result of a lower material thermal conductivity (0.25 W/ mK [135] versus 43 W/ mK for steel) and a thicker wall section. Taking the convective heat transfer coefficient to ambient as 60 W/ m^{2}K, the new combined thermal resistance can be converted to an equivalent convective heat transfer coefficient of 35 W/ m^{2}K. The predicted benefit in fuel consumption over the NEDC from using a fibre reinforced plastic sump was small at just over 0.1%, which is around a third of the benefit from completely eliminating heat losses from the sump. Overall, heat losses from the sump

have a small effect on fuel consumption as they only become significant late in the drive cycle; up to 200s into the drive cycle, heat losses from the sump account for less than 22 % of the total heat outflow from the bulk oil. Changes in the oil warm-up rate from insulating the sump only become discernible after ~200s into the drive cycle, at which point the oil temperature has risen to 44 ºC and the potential for friction reduction has already dropped significantly. At this temperature, oil viscosity has dropped by 55 % relative to that at the start and friction levels are only 40% higher than when fully warm, compared to 150 % higher on start up. Experimental investigations by [150] also show that lagging the oil sump had little effect on oil warm-up rate. Nonetheless, it will be shown later in this chapter, that heat losses from the sump become important and bear greater influence on oil warm-up rate if the other major routes of heat transfer out of the oil are inhibited.

A thermally severe vehicle operating condition, generally referred to as an uphill trailer tow, was also simulated to examine any adverse effects of inhibiting heat losses from the sump. An uphill trailer tow is characterised by a highly loaded engine operating condition but reduced cooling capacity as a result of a low vehicle speed. The engine running condition chosen was 2000 rev/ min and 12 bar BMEP while the ambient heat transfer coefficient was assumed to be 35 W/m^2K, representative of a 35 mph vehicle speed. With PCJs on and the FCA streamed with coolant, fully-warm oil temperature was just under 112 °C and heat losses from the sump 420W. Inhibiting heat losses from the sump raised the oil temperature in the sump by only 3°C. Heat transfer across the FCA to the coolant was increased by 220 W (11 %) while total heat rejection to coolant increased by just under 2 %. These results indicate that overall heat losses from the sump bear little influence on engine thermal behavior both during warm-up and under fully-warm operation; insulation of the sump can carried out without the danger of excessively high oil temperatures or the need for a major increase in the coolant system's heat rejection capacity.

7.6. Reducing Engine Thermal Capacity

The warm-up rate of an engine is determined by the net rate of heat transfer and the cumulative thermal capacity of its structure, lubricant and coolant volumes. The thermal capacity is defined by the product of the structure and fluid volumes, and

their respective densities and specific heat capacities. The thermal capacity of the structure can hence be varied in different ways. The first involves a reduction in material volume, which for given material properties reduces the structural mass. In reality this would require a re-design of the engine structure with features such as thinner wall sections in the crankcase and cylinder liner regions. However, with advances in CAE modeling, engine design has already reached a high level of optimisation such that further removal of material without compromising block stiffness, durability and noise vibration harshness (NVH) qualities has become increasingly difficult.

The second way of achieving a reduction in thermal capacity involves using different construction materials of either lower density and specific heat capacity (SHC) or superior strength. In the case of diesel engines for example, replacing a cast iron block with one constructed from compacted graphite iron (CGI) can offer a weight saving of up to 10 % [151], with a similar reduction in thermal capacity. Aluminium and magnesium designs offer even greater weight savings but are generally limited to gasoline engines which typically operate at lower peak cylinder pressures than diesel engines [152]. Moreover, the specific heat capacity of aluminium is around double that of cast iron, such that a reduction in mass does not necessarily translate into a reduction in thermal capacity. A study was conducted to investigate the improvement in fuel consumption that could be obtained from reductions in engine structural thermal capacity. The thermal capacity of the structure was reduced by a total of 20 % in steps of 5 %, by reducing the element densities. Simulations with a reduced time step of 0.05s (the baseline time-step is 0.1s) showed that results were independent of the time-step size used. The element volumes and thermal conductivities were unchanged so as not to change the thermal conductance paths between elements and also, to ensure that the Biot number criterion was satisfied (Section 3.3). In reality, changes in material thermal conductivity would affect the propagation of heat and therefore the warm-up characteristic of the structure which could add or detract to the benefit of a reduction in thermal capacity. Table 24 provides a summary of the element thermal properties. The reduction in mass per cylinder and improvement in fuel consumption is shown in Table 25, which is around 0.2 % for every 5 % reduction in the mass. This compares well with comparable simulation results by [153].

Engine Part	Material	Elements	ρ (kg/ m^3)	C_s (J/kg. K)	Mass (kg)
Cylinder Liner & Block	**Cast Iron**	1-14	7570	470	7.33
Crankcase & Crankshaft	**Cast Iron**	15-18, 42-44	7570	470	9.21
Cylinder Head & Piston	**Aluminium**	19-27	2660	910	7.39
Valves	**Alloy Steel**	28-39	8036	440	0.2
Total (per cylinder)	/	/	/	/	**24.13**

Table 24 Summary of baseline element material properties

Case Number	Case Description (Reduction in density)	Mass -per cylinder (kg)	FC benefit (%)
M1	0% (Baseline)	24.13	n/a
M2	5%	22.93	0.22%
M3	10%	21.72	0.45%
M4	15%	20.52	0.68%
M5	20%	19.31	0.92%

Table 25 Fuel consumption benefit from reduction in engine thermal capacity

Different engine components may have a greater weight reduction potential than others. Typically the crankcase accounts for around a quarter of the total engine mass, and is also the component with the greatest weight reduction potential, 10-12 % for cast-iron versions [152]. Having defined the benefit from a uniform reduction in engine thermal capacity, further simulations were conducted to quantify whether bigger benefits could be obtained if the reduction in mass is achieved from the 'upper' end of the engine structure (cylinder block and head) versus the 'lower' regions (crankcase and crankshaft). A rough description of the mass reduction scheme adopted in each case is depicted in Figure 116. In each case a total 10 % reduction in mass was simulated. In general, the thermal capacity of the upper parts of the engine structure, have a strong influence on the coolant rise time while the oil rise time is more dependent on the warm-up rate of the lower parts of the structure. However, when coolant is streamed through the FCA, the oil and coolant temperatures are strongly coupled together. As a result, Figure 117 shows that for cases when the FCA is streamed with coolant, the benefit in fuel consumption is the same, irrelevant of where the reduction in engine mass is made. In fact for a

reduction in mass from the top end, coolant warm-up is promoted but so is heat transfer across the FCA from the hotter coolant to the oil. However, when the FCA is disabled, this redistribution of heat between the coolant and oil is weaker. In this case the greatest benefit in fuel consumption is achieved by promoting a faster oil warm-up through a reduction in mass from the engine's lower regions.

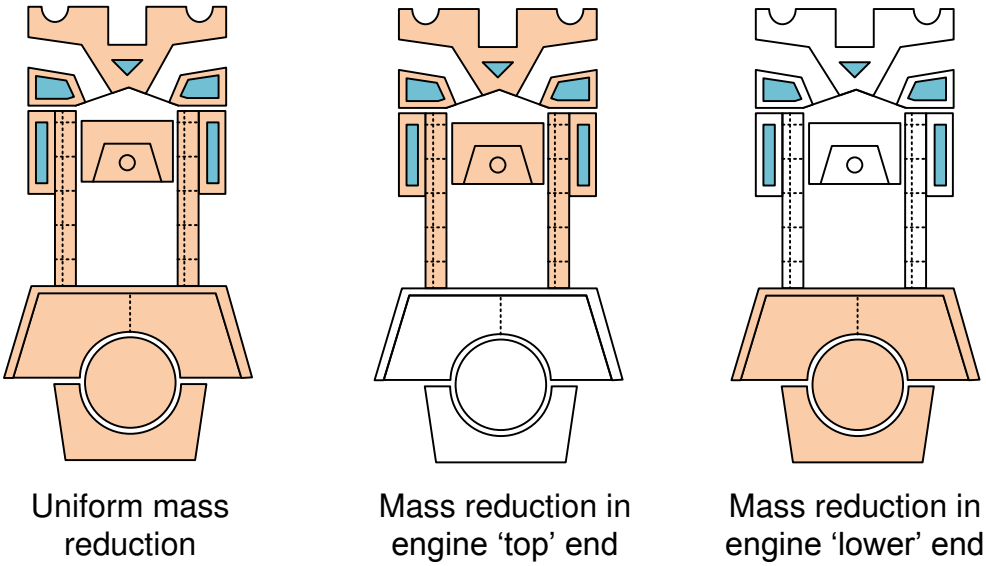

Figure 116 Different areas of the engine structure targeted for mass reduction

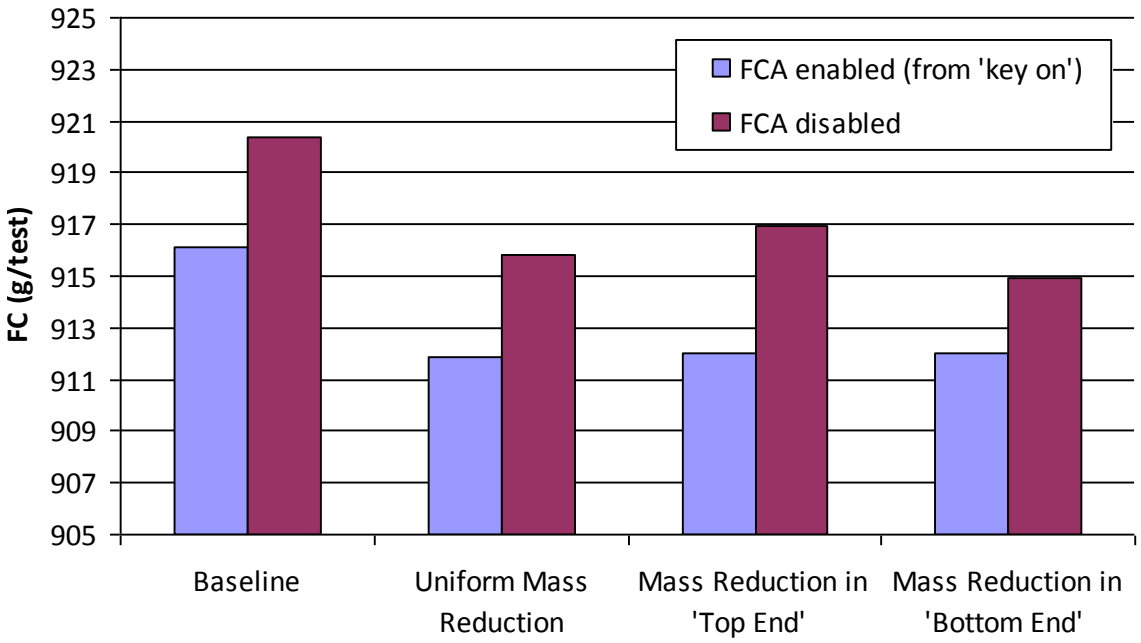

Figure 117: Fuel consumption for baseline engine, a 10% uniform reduction in mass and two cases of selective mass reduction. Cases with and without coolant streamed through the FCA are shown.

7.7. Oil Circuit Heat Losses: Main gallery relocation and the influence of crankcase oil mist heat losses

The elemental representation of the engine crankcase in PROMETS has been reviewed in Chapter 5. Regions of the crankcase remote from the main bearings are represented by elements 15-18 and these generally warm up considerably slower than both the coolant and oil, mainly due to their high thermal capacity. As illustrated in Figure 119, during the first 200s of the drive cycle, heat transfer to the lower engine structure accounts for 67 % of the gross heat losses from the bulk oil. Specifically 42 % of these losses are from oil mist to the crankcase walls and when the oil gallery is located in element 15 (Figure 118), 25 % is convective heat loss from oil flowing in the main gallery. The effect of perfectly insulating the main oil gallery was simulated as an illustration of the maximum benefit of reducing heat losses from oil flowing in the gallery. The fuel economy benefit was small but still noticeable at around 0.2 % when the EGR was cooled with oil. A further solution to eliminating heat losses from oil flowing in the main gallery is to relocate the gallery to a different part of the engine structure which warms up at a faster rate than the oil. In this case the direction of heat flow can be reversed such that the oil is heated rather than cooled as it flows within the main gallery. In PROMETS one possible location is in proximity to element 13 which represents part of the engine block wall surrounding the outer coolant passages (Figure 118). The effect of this modification on the major heat outflows from the oil circuit is shown in Figure 120.

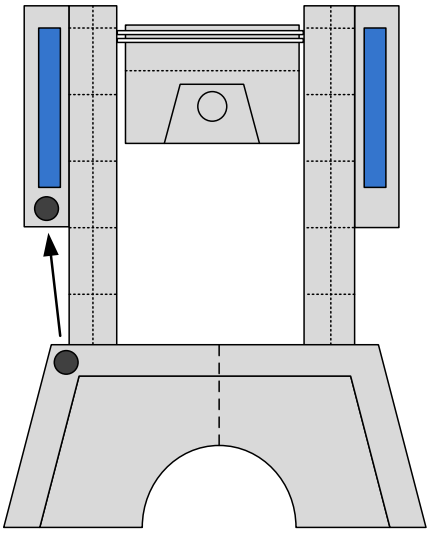

Figure 118 Oil gallery relocation from crankcase to engine block

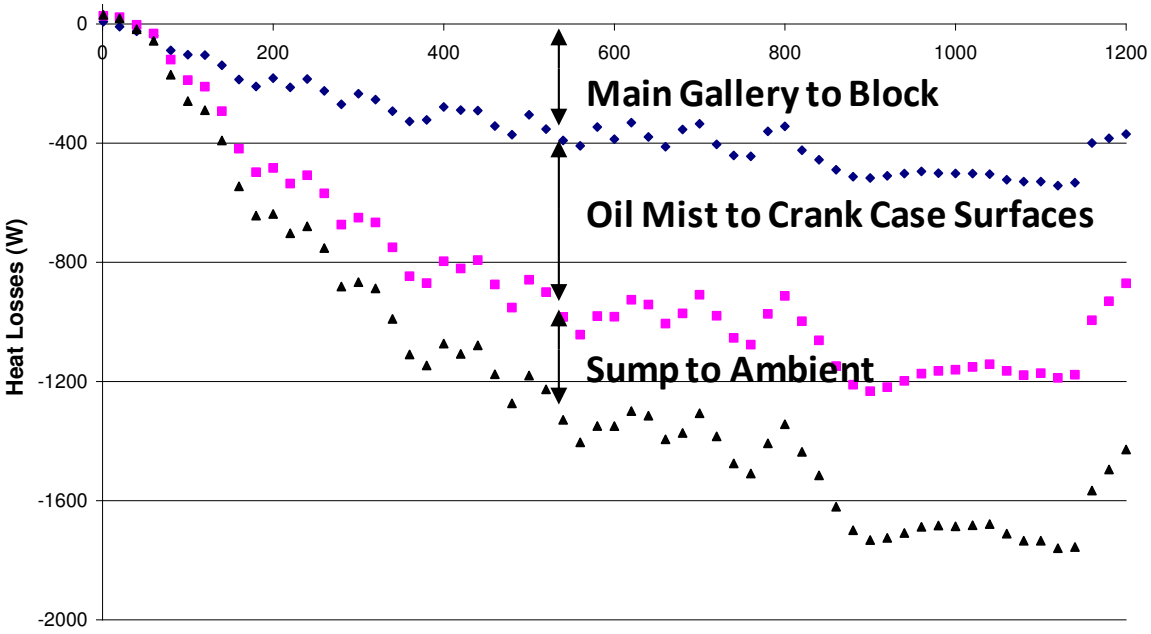

Figure 119 Predicted oil circuit heat outflows over NEDC: Main gallery located in element 15

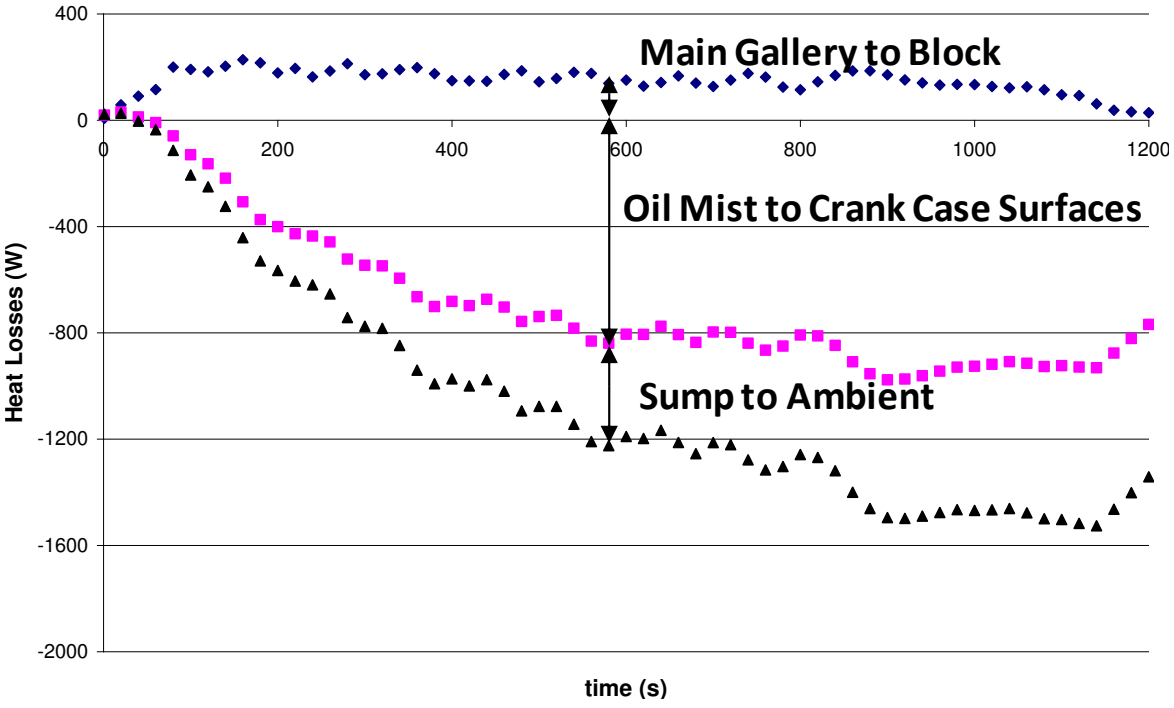

Figure 120 Predicted oil circuit heat outflows over the NEDC: Main gallery located in element 13

The fuel economy benefit from relocating the oil gallery is 0.37 %, around double that achieved from a perfect insulation of the gallery (see Table 26). Relocating the oil gallery to element 13 puts the oil in better thermal coupling with the coolant. As a result, the increase in oil warm-up rate is dependent on whether the FCA is streamed with coolant or not, since the former case already provides a strong thermal coupling between the coolant and oil. With no coolant streamed through the FCA, relocating the gallery improves fuel consumption by a more substantial 0.94 % (Case 3 vs. Case 7in Table 26). However, absolute fuel consumption is still worse by 0.25 % relative to the baseline case with the gallery located in Element 15 and coolant streamed through the FCA; therefore relocating the oil gallery closer to the coolant jacket is not as effective as streaming the FCA with coolant in terms of raising oil temperature.

Case	Gallery location	FCA streamed with coolant	Oil mist to crankcase heat losses	FC benefit
1	**Element 15**	**Yes**	**Enabled**	**n/a**
2	Element 15	Yes	Disabled	0.51%
3	Element 15	No	Enabled	-1.20%
4	Element 15	No	Disabled	-0.31%
5	**Element 13**	**Yes**	**Enabled**	**0.37%**
6	Element 13	Yes	Disabled	1.15%
7	Element 13	No	Enabled	-0.25%
8	Element 13	No	Disabled	1.15%

Table 26: Fuel consumption benefit from eliminating crankcase oil mist heat transfer and relocating the main gallery. Fuel consumption benefit is calculated relative to Case 1 which is the baseline build (Build 3 - FCA streamed with coolant and EGR to coolant heat exchange). Negative values indicate a fuel consumption penalty.

With the gallery located in element 13, the interaction between the oil mist and crankcase walls becomes the major route for heat transfer out of the oil, accounting for 65-80 % of the total heat outflow from the oil circuit. As a result the sensitivity of the oil warm-up rate to mist heat losses is dependent on the location of the oil gallery, but also on whether the FCA is streamed with coolant or not. The greatest improvement in fuel consumption achieved from preventing oil mist heat losses is for an oil gallery situated in element 13 and the FCA disabled (Case 7 vs. Case 8). In this case a reduction in friction of 4.28 % translates to a fuel consumption saving of 1.4

%. The predicted friction benefit from eliminating heat losses to the crankcase is in good agreement with the modelling results of Jarrier [59]. The oil mist heat transfer is least influential for cases when the oil gallery is situated in element 15 and the FCA enabled (Case 1 vs. Case 2). In this case the friction reduction is 1.57 % and the fuel consumption improvement only 0.5%. Relocation of the oil gallery to element 13 coupled to elimination of oil mist heat losses, results in the oil temperature closely tracking that of the coolant. The heat transfer across the FCA as a result is very low and disabling the FCA in this case incurs no fuel consumption penalty (Case 6 vs. Case 8). This also represents the best case in terms of fuel economy, a saving of 1.2 % over the baseline.

7.8. Discussion and Conclusions

A further model extension has been described in the form of a 'split-EGR cooler' able to demonstrate the effect of re-directing EGR heat from the coolant to the oil circuit. Heat input from the EGR cooler was successful at raising oil temperature. However, reduced heat transfer to the oil across the FCA partly outweighed this such that the net change in heat input to the oil from switching to oil cooled EGR was small, around 1% at the end of the ECE. Consequently, the predicted benefit in fuel consumption was also small, at 0.6%. However, the ability to cool EGR gases using the oil stream offers added flexibility, such as when coolant flow through the engine block is stalled during the first minutes of engine operation [154]. In this case heat transfer to the coolant is reduced in favour of raising cylinder liner temperatures, with an associated reduction in piston friction and lower ancillary (water pump) losses. However, heat transfer from the coolant to the oil across the FCA is penalized or unavailable altogether, which leads to colder oil temperatures and higher frictional losses in the crankshaft bearings. In this case, oil-cooled EGR provides an alternative means to cool the EGR gases while making up for the oil heating deficit at the FCA.

Substantial benefits (>1.5 %) were seen from using a thermal energy store to recover heat in the final phases of the drive cycle when the engine is fully warm, and release it into the engine fluids on key-on. While the energy input was similar to that recovered from the EGR gases, the benefits observed were greater as the heat transfer rates were substantially higher in the case of the thermal store. This reflects the

increased sensitivity of oil viscosity to changes in temperature at cold temperatures and points to the importance of introducing supplementary heat into the oil circuit as early as possible after start-up when the potential for friction reduction is highest.

Eliminating ambient heat losses from the engine surfaces in isolation showed small improvements in fuel consumption, ~0.3 %. Likewise, a reduction in oil volume also showed small benefits in fuel consumption, on the order of 0.2 % for a 20 % reduction in oil mass. The strong thermal coupling to the engine structure means that during warm-up the apparent thermal capacity of the oil is much greater than that associated solely with its mass; reductions in oil volume achieve only small reductions in the overall thermal inertia of the oil system. Relocating the oil gallery closer to the cooling jacket eliminated heat losses from oil flowing in the block, but the improvement in fuel consumption was small for cases where the FCA was streamed with coolant (<0.4 %). Moreover relocating the gallery was not as effective as streaming coolant through the FCA in terms of raising oil temperature. Heat transfer from the oil mist to the crankcase surfaces is shown to be the greatest heat sink from the oil. A hypothetical elimination of this heat loss coupled to a relocation of the oil gallery can provide substantial fuel consumption savings (>1 %). In this case the warm-up rate of the oil matched that of the coolant such that streaming the FCA with coolant provides no additional benefit in fuel consumption.

Investigations, in which an ‘idealised’ thermal store was used to heat the oil, showed that the oil temperature could, under certain conditions, be raised above that of the coolant. In this case de-coupling the oil and coolant circuits (by not streaming coolant through the FCA) is beneficial so as to retain as much heat as possible in the oil. Also, relocating the gallery closer to the coolant jacket isn’t sufficient to eliminate heat transfer from oil flowing in the block. A perfectly insulated gallery would be more beneficial in these cases. In practice, one way of insulating the main gallery would be to bore the gallery oversize and insert a PTFE tube. The potential reduction in heat losses from doing so can be estimated from the increase in thermal resistance between the oil and engine block. Assuming a 3mm pipe wall thickness, a 65 % reduction in the overall heat transfer coefficient was calculated while Styrofoam practically achieves perfect insulation. The suitability of the insulating material

would also have to consider further criteria such as a low reactivity and high temperature resistance.

The exhaust gas stream provides a greater energy recovery potential than the EGR stream. However, the additional coolant thermal inertia incurred by the installation of an exhaust-to-coolant heat exchanger nullified any potential benefit in friction and fuel economy. Neglecting the additional coolant volume, predicted benefits were still small at 0.3 %. The thermal inertia of the after-treatment system and the light engine loads in the ECE section of the drive cycle, mean that exhaust temperatures at the inlet to the heat exchanger are too low to achieve significant heat recovery. High rates of heat transfer are only achieved late in the drive cycle when the potential for reducing frictional losses is small. Exhaust heat recovery is however a good candidate for recharging thermal stores. Such a setup was simulated and in this case the benefit in fuel economy was substantial at ~1.3 %.

Fuel economy improvements scaled linearly with a reduction in engine structural thermal capacity, ~0.2 % reduction in fuel consumption for every 5 % reduction in mass. With the FCA streamed with coolant, there was no appreciable difference between cases of selective mass reduction. The effects of using different engine construction materials to achieve a reduction in thermal capacity may extend beyond the warm-up rate. Changes in the thermal expansion characteristics for example, may lead to changes in piston and main bearing operating clearances. These could add or detract to the friction benefit of a faster warm-up but have not been accounted for in the analysis presented in this chapter.

The model uncertainties discussed in previous chapters have implications for the results of the thermal analysis investigations conducted here. A higher friction correction index increases both the friction penalty of the cold started engine and the benefits of a faster warm-up. However, while this changes the absolute values of fuel consumption and fuel saving predictions, the trends outlined above remain valid. Likewise, fuel consumption improvements for cases where the crankcase walls were thermally isolated from the oil mist depend on the assumed thermal capacity and exposed surface area of the crankcase elements. As expected, engine designs with a heavier crankcase structure will benefit more from reducing the interaction of oil mist

with the crankcase walls. In this chapter, assessment of strategies to reduce friction losses during warm-up was conducted over the NEDC from a 26 °C ambient temperature start. Lower starting temperatures would potentially increase the calculated benefits because friction conditions are more severe at colder temperatures.

The fuel savings from the various measures explored in this chapter have been ranked in order of magnitude in Table 27. The potential maximum improvement in fuel consumption, given by starting the drive cycle with a fully warm engine, is 5.8 %. None of the modifications individually or in combinations achieved more than half of this theoretical maximum. In a number of cases the benefit from a single modification in isolation was small to insignificant, but yielded significant improvement when used in conjunction with other changes, e.g. exhaust heat recovery with thermal storage. The main conclusions from this study are:

- An oil-cooled EGR cooler provides only small benefits in fuel consumption when the FCA is streamed with coolant, but would be an effective replacement oil heater if a FCA is not installed.

- Given an available source of thermal energy which can be transferred to the oil over a chosen time, simulations indicate that a higher power input over a shorter period is most beneficial.

- The benefit of reducing heat losses from the oil increases as the oil temperature is raised through various means. The benefit of reducing heat transfer from the sump, main gallery and crankcase oil mist in combination is greater than the summation of the benefits from doing each in isolation.

- Given the availability of a 3.7 kW heat source over the first 200 seconds of the NEDC, the fuel consumption savings can be close to that achieved by starting the engine fully warm if heat losses from the oil in the lower parts of the engine (sump, crankcase, main gallery) can be eliminated.

Case		Strategy/ Modification	FC reduction (%)
D		**Engine started fully warm with coolant and oil at 90 °C @ t=0s**	**5.8**
C3	**Supplementary Heat Input & Thermal Energy Storage**	3.7kW heat input to oil, EGR to oil heat exchange and heat losses from oil suppressed	**5.7**
C2		3.7kW heat input to oil and EGR to oil heat exchange	**2.19**
C1		As A1, with exhaust heat recovery and thermal energy storage	**1.3***
B6	**Additional benefit from reducing thermal capacity and heat losses from oil**	As A3, with oil mist to crankcase heat transfer suppressed, main oil gallery insulated & insulated sump	**2.34**
B5		As A3, with oil mist to crankcase heat transfer suppressed	**1.14**
B4		As A3, but with 10% reduction in engine thermal capacity	**1.08**
B3		As A3, with insulated sump	**0.94**
B2		As A3, with main oil gallery insulated	**0.84**
B1		As A3, with 20% reduction in sump oil mass	**0.83**
A4	**EGR cooing with oil and streaming FCA with coolant**	As A1, but with EGR heat exchangers to oil and then coolant arranged in series	**0.78**
A3		As A1, but with EGR to oil heat exchange	**0.63**
A2		EGR to oil heat exchange, no coolant streamed through FCA	**0.34**
A1		**Baseline – FCA streamed with coolant; EGR to coolant heat exchange**	**n/a**

Table 27 Simulated Fuel Consumption Savings Summary – Case A1 represents the baseline case with EGR cooled by the coolant stream and the FCA streamed with coolant. Not streaming the FCA with coolant results in a fuel economy penalty of ~1.4% (not shown here).

*Ranked according to technology not fuel economy benefit

Chapter 8: Discussion and Conclusions

8.1. Discussion

Raising engine oil temperature to its fully-warm value as soon as possible is key to minimising frictional losses following a cold start [3] [4]. Determining the numerous heat flow paths into and out of the oil is challenging due to measurement difficulties and uncertainties. A version of PROMETS has been revised and applied in conjunction with engine testing to try and quantify the major thermal-friction interactions between the engine structure, oil and coolant circuits. Based on these findings a number of potential improvements from re-designing the oil system and the implementation of various other measures have been outlined. Results indicate that while supplementary heat input to the oil is one way of promoting higher oil temperatures, minimizing heat transfers out of the oil system is even more crucial.

The large thermal capacity of the crankshaft and crankcase has been shown to be detrimental to the oil warm-up rate and the ability to decouple the oil from these structural elements may allow reductions in friction to be achieved and fuel consumption benefits in the region of 1-1.5 %. In the first minutes after engine start-up, heat transfer from the crankcase oil mist constitutes a significant heat loss from the bulk oil. Oil flow into the crankcase is made up of side-leakage flow from main and big-end bearings, piston cooling jet oil return from the piston crown galleries and oil return from the cylinder head. The rotation of the crankshaft results in oil being flung out onto the crankcase walls and lower regions of the liner. The large area results in high rates of heat transfer early in the warm-up. Different approaches could be taken to minimize these losses such as coating the inner surfaces of the crankcase with thermally isolative material or better managing oil flow (and splash) within the crankcase. Reducing oil flow into the crankcase is one way of reducing the quantity of oil entrained in the crankcase air but cannot be completely eliminated given that lubrication of the piston depends on it. Computational investigations showed that small benefits in main bearing friction could also be achieved through a reduction in bearing oil flow rate. In the case of the PCJs, too great a reduction in oil jet flow rate is expected to reduce their effectiveness, resulting in increased piston temperatures and a lower heat input to the oil flow. Hence, while a lower oil flow rate may be one

way of reducing heat losses to the crankcase it also reduces heat input to the oil from other sources. From the point of view of raising oil temperature during warm-up, a more effective approach would be to better manage oil return into the sump; ideally hotter oil from the bearings and PCJs should not be allowed to run onto the crankshaft webs but rather be collected and directed to the sump or oil pump inlet. The tight packaging of engine components within the crankcase however makes this difficult to achieve. Oil windage trays installed below the crankshaft are commonplace to shield the sump oil surface from the crankshaft's air motion and oil droplets thrown off it, helping to reduce oil aeration. Similarly, baffles placed above the crankshaft could reduce oil 'throw' onto the crankcase walls and lower liner while simultaneously collecting hot oil returning from the PCJs. However, the typically tight clearance between the crankshaft balancing webs and piston skirt when this is at BDC must be accounted for. Additionally, restricting airflow beneath the piston may lead to higher windage losses which could outweigh the benefits of raising the oil temperature.

The benefits of a lower oil flow rate extend beyond the oil warm-up rate. Experimental investigations with a variable flow oil pump on an engine of the same family as used in this investigation [144], showed fuel savings of up to 2 % over the NEDC. In this case, throughout most of the warm-up, sump oil temperature was around 5-8 °C lower than when the oil pump was set to deliver its maximum flow. This suggests that the benefit of a lower oil pump torque demand outweighed the penalty of higher friction losses at the rubbing surfaces as a result of the colder oil temperature and illustrates that the merit of reducing the engine oil demand cannot be judged solely on its effect on oil temperature. Reducing the oil entrained within the crankcase air also leads to lower crankshaft windage losses at high engine speeds [122], more typical of spark ignition rather than diesel engines.

Oil flowing in the main gallery also loses heat to the lower parts of the engine block. Locating the gallery closer to the coolant jacket was shown to be one way of minimizing or even reversing heat losses from the oil. Putting the oil in better thermal coupling with the coolant is not only beneficial during warm-up but also from the viewpoint of controlling fully-warm oil temperatures. If the thermal coupling between the oil and coolant provided through the engine structure is strong enough,

the oil-to-coolant heat exchanger can be removed from the internal circuit altogether with an associated cost saving to the vehicle manufacturer. While the main gallery can be positioned close to the coolant jacket, oil pathways to the main bearings must still be routed through the bearing support walls, distant from the combustion heat source. In this case thermally isolating the oil from the metal walls is most beneficial.

In Chapter 5 it was shown that the strong thermal coupling between the oil and engine structure extends to the rubbing surfaces. In crankshaft main bearings the oil film temperature is governed by the temperature of the local metal surfaces; upper and lower shells and the crankshaft journal. Computational investigations showed that substantial reductions in bearing friction could be achieved from a cold start by perfectly insulating the oil film from the metallic surfaces. The thermal inertia of the film is negligible such that friction dissipation in the bearing is sufficient to raise the film temperature rapidly following a cold start, as long as heat transfer out of the film is inhibited. In practice the actual benefits will depend on the degree of insulation attainable. Increasing the contact resistance between the back of the shells and engine block through the creation of an air gap was shown [4] to provide a convenient way of reducing heat transfer to the engine block and bearing caps. For performance and reliability however, the elasto-hydrodynamic behaviour of the bearing must be considered and the thermal resistance to heat transfer from the film would have to be raised through other means, possibly by coating the rubbing surfaces with an insulating material. When operating fully-warm, the proportion of friction heat carried away by the oil flow dominates over conduction to the metal surfaces such that thermal isolation of the oil film can be carried out without the danger of overheating the bearings. When cold, the proportion of friction heat convected away by the oil flow is small. Consequently, the friction benefits from reducing the oil flow rate were also shown to be small in comparison to those achieved from thermally isolating the film.

Heating the oil supply to the bearings is another method to raise oil film temperatures during warm-up but the effectiveness of this method is greatly limited by the strong thermal coupling of the oil film to the rubbing surfaces which limits the deviation of the film temperature from that of the surrounding metal surfaces. While thermal isolation of the bearing film may be more effective at reducing friction in the

bearings, oil heating has a strong impact on global (total) engine friction. As a result over a cold start NEDC, the fuel economy benefit from thermally isolating the bearing films (~1.5 %) is comparable to a heat input of around 750 kJ at an average rate of ~ 1.9 kW. A number of factors may determine which technology is better suited to a given vehicle application from cost considerations, packaging constraints but also driving conditions. For example, if the vehicle travel length is too short for the engine to achieve fully-warm operating conditions, then it may be difficult to recharge the heat store. In this case insulation of the bearing surfaces is a more effective solution.

Various ways of re-distributing heat from the coolant to the oil circuit have been identified. The FCA and EGR cooler are two of these elements. A FCA is commonly found on production vehicles and streaming the FCA with coolant from key-on was shown to be an effective way of raising the oil temperature in practically all cases. Only when a heat store was used to raise the oil temperature above that of the coolant, was it beneficial to decouple the two engine fluids. The benefit of streaming the EGR cooler with oil rather than coolant was small, but does offer alternative oil heating if heat transfer across the FCA is unavailable, such as when coolant flow through the engine block is 'stalled' in the early phases of warm-up [154].

The oil jets were shown to offer a further way of redirecting a larger proportion of combustion heat transfer from the piston crown to the oil circuit. Redistribution of heat to the structure, particularly from the crankcase oil mist and oil flow in the main gallery, means that the net increase in heat input to the oil is significantly less than the heat carried away by the oil jets. Simulations and measurement [113] both show the influence on overall coolant heat rejection to be small. Over the NEDC, enabling the PCJs resulted in a predicted fuel saving of just over 0.6 %. However, a hypothetical increase of 50 % in the piston crown oil gallery heat transfer coefficient provided only a small increase in the fuel saving (~0.1 %). The predicted benefits in friction have been based solely on the rise in bulk oil temperature. The effect of the oil jets on changes to the liner oil film thickness and the implication of this on piston friction remains uncertain, as is the influence of lower piston temperatures on the ring film temperatures. Lower piston bowl temperatures from enabling the PCJs are expected to increase thermal losses in the cylinder leading to a lower indicated

thermal efficiency. This may reduce or even nullify the predicted benefits in friction and associated fuel saving. Measurements by Luff et al. [113] also show that a small reduction in gaseous emissions of NO_x and a small increase in CO occurred when the PCJs were enabled. Ultimately the prime purpose of the PCJs is to cool the piston at high power operating conditions. It is unclear whether there is any real benefit from disabling them at lower engine loads. From the viewpoint of raising the oil temperature however, enabling the PCJs is always beneficial.

The potential to reduce friction is highest in the first minutes after engine start up as oil viscosity drops rapidly hereafter. The benefits of exhaust heat recovery were shown to be heavily compromised by the additional coolant volume required by the installation of the heat exchanger. This, coupled to low exhaust gas temperatures as a result of the after-treatment system's thermal inertia, meant that heat input from the exhaust stream was small and only became significant later in the drive cycle. Exhaust gases in spark-ignition engines are significantly hotter than in diesel engines due to higher equivalence ratios and lower cylinder expansion ratios [2]. Therefore the potential benefits of employing exhaust heat recovery on a spark ignition engine may be greater than those seen in this investigation. Moreover, the benefits of exhaust heat recovery extend further beyond the warm-up phase and represent a prime way of increasing overall power-train efficiency under vehicle cruise conditions (motorway driving) by providing an alternative means of powering engine ancillaries or supplementary tractive power [83].

Thermal energy stores [78] [77] have been shown to be effective in shortening engine warm-up times because they make available high rates of heat input from key-on. One example of such an energy store is the hot coolant reservoir used to pre-heat the oil feed to the crankshaft bearings. The total energy transfer from the hot coolant to the oil was estimated to be around 500 kJ, with peak rates of 4 kW. In this case the energy transfer was limited by the diminishing temperature difference between the hot coolant and engine oil as the engine warmed up. A large coolant volume, in excess of 12l, was used on the test bed to minimize the drop in coolant temperature. Achieving this on a production vehicle is challenging due to weight and packaging restrictions. Schatz [78] describes a latent heat store designed specifically for automotive applications. The heat storage mass in this case was based on a barium

hydroxide salt and featured greater energy density, around 30 % higher, than the hot coolant reservoir tested here. It was also capable of substantially higher heat rates than those reported in this work; between 50-100 kW in the first 10s of operation, and over 10 kW for up to 1 minute after start up. However, these were achieved at starting temperatures of around -20 ºC, significantly colder than the typical laboratory ambient conditions (~20 ºC) considered in this work. The FCA, which was used in this investigation as an oil heater, is designed to limit oil temperatures under fully-warm conditions and may therefore not be ideally suited to maximize heat transfer to the oil, particularly when the oil is cold and its viscosity high. Also, in the case of [78] heat input from the energy store was to the engine coolant. Heat transfer to oil may be inherently disadvantaged when compared to heat transfer to coolant due to the increase in oil viscosity at cold temperatures. Electric heating may offer the advantage of better control over the heat rates that are delivered, but peak rates of heat transfer are generally limited by the alternator power rating. It also increases the engine parasitic load demand leading to an overall fuel consumption penalty. Thermal energy input from heat stores on the other hand can be achieved without any fuel cost as they rely on engine waste heat energy to recharge. Investigations presented in this thesis show that heat recovery from the exhaust gas stream can be one way of recharging a heat store over the NEDC. Heat losses from the heat store are reported by Schatz to be in order of 3 W at -20 °C. For a 2.8 MJ heat store this means an overall efficiency of well over 90 % is maintained 15 hours after charging.

The investigations presented here have been limited to the effects of supplementary heat input to the engine fluids. If the available energy is small however, Janowski [27] reports, that it is more beneficial to heat other elements in the vehicle power-train rather than the engine. For heat rates below ~4 kW heating the final drive unit (differential) is more beneficial than heating either the engine or transmission oil. This reflects the small thermal capacity of the final drive unit in comparison to that of the engine and transmission.

A number of the measures described above do not require changes to the core engine structure and can be thought of as ‘bolt-on’ technology that can be applied to existing engine designs. The challenge of implementing thermal energy storage and exhaust heat recovery lies more in satisfying the vehicle’s packaging constraints. As a result

such devices may be better suited to larger, high-end vehicles, given also that the weight and cost penalty will be smaller in this case. On the other hand, changing the internal engine heat flows by for example, re-locating the oil gallery or better managing oil flow into the crankcase, may require a substantial engine re-design and must be integrated early on in the design process. Features like external oil galleries may simplify the engine block design possibly compensating for the cost of additional assembly and parts. The benefit of reducing engine block mass explored in Chapter 7 extends beyond shortening the warm-up phase and may lead to further fuel economy benefits from an overall reduction in vehicle weight. Traditionally, diesel engines operate at higher peak cylinder pressures making them heavier than their spark ignition counterparts. However, the recent launch of the low compression ratio Mazda 'Skyactiv–D' engine [155], suggests that this discrepancy between engine types may reduce in the future. By operating at lower in-cylinder pressures, Mazda claim a 25 kg weight saving over a conventional diesel engine by switching to an aluminium block construction, and a further reduction of 3 kg from using thinner wall sections in the cylinder head. As for the pistons, their weight was reduced by 25 %. Similarly, smaller main journal diameters resulted in a 25 % reduction in crankshaft mass while rubbing friction was reduced to levels comparable to those of the average gasoline engine. This suggests that a significant weight reduction potential exists in current engine designs, but achieving these reductions will depend on the design direction taken.

The fuel economy improvements reported in Chapter 7 depend on the assumed oil viscosity-temperature relationship. Oil formulations with a higher viscosity index and therefore a 'flatter' viscosity-temperature characteristic will reduce the friction penalty of the cold started engine and as a result reduce the scope for raising oil temperature earlier in the warm-up. Reducing oil viscosity is the prime way of lowering friction losses given that the major engine friction contributions (crankshaft and piston assemblies) operate in the hydrodynamic regime. This is particularly true for the engine considered in this study as the valve-train was actuated via roller followers. For engines with direct acting tappets the contribution of boundary lubricated components is greater. In this case the benefit of reducing oil viscosity will be smaller while greater friction benefits can be had from the addition of friction modifiers [156].

The fuel economy improvements from shortening the warm-up phase also depend on the driving conditions considered. The urban section of the NEDC, as considered in this study, is characterized by very light engine loads which prolong the engine warm-up phase. Drive cycles requiring higher power train loads from start up will lead to shorter warm-up times reducing the cold start fuel consumption penalty. This was demonstrated by simulating a modified drive cycle in which the city-cycle and EUDC sections were swapped round. In this case the time to reach thermostat opening temperature was around 5 minutes, compared to 13 minutes in the conventional NEDC. Oil temperature reached a temperature of 90 °C 4 minutes earlier and the cold start fuel consumption penalty was reduced by 30 %. Longer drive cycles such as the FTP [79] will also benefit less from rapid warm-up measures since the warm-up phase will be constitute a smaller percentage of the total drive cycle duration.

8.2. Future Work

The main bearing model in PROMETS was revised to characterize bearing friction using oil film temperature. This offers improved accuracy when modelling changes local to the rubbing surfaces that perturb the film temperature from that of the bulk oil. There is considerable interest in extending this approach to the piston friction model given that the piston assembly represents the largest contributor to total engine friction. However, the analysis of the piston-liner contact is inherently more complex than that of a journal bearing. While main bearings predominantly operate in the hydrodynamic lubrication regime, fluctuations in piston velocity and side-thrust forces over an engine cycle, lead to variations in oil film thickness moving the piston-liner contact into different lubrication regimes. There is also uncertainty in modelling the oil flow patterns through the ring-pack. Unlike main bearings, which are supplied from a pressurized oil gallery, oil delivery to the liner is generally from oil splash in the crankcase and from the PCJs. There is a need for a better understanding of the oil transport mechanism and residence time of oil within the ring-pack. This in turn could also provide a better insight into the net heat transfer rates between the cylinder liner and oil. Determining whether oil film temperature at the piston-liner interface equilibrates to that of the liner also has important implications on modelling piston

friction. In this case, piston liner friction will be governed more by the cylinder liner temperature rather than that of the bulk oil.

There is increased interest in variable flow oil pumps due to the potential fuel savings they offer. The oil pump friction model currently in PROMETS is representative of a fixed displacement pump and was calibrated from motoring tests in which the oil supply pressure was controlled according to the standard pressure relief valve. An extension of the model is required to account for the dependency of pump torque on delivery pressure. Further model development is also required to account for the effect of lower flow rates on the oil warm-up rate. In PROMETS, a number of heat transfer coefficients and empirical constants governing heat transfer into and out of the oil circuit have been historically assumed to be independent of oil flow rate. Due to this, there is some uncertainty with regards to the sensitivity of the oil temperature prediction to changes in oil flow rate. The effect of flow rate on heat transfer between the crankcase oil mist and engine structure (crankcase, liners and piston underside) is one area of particular interest, but is hard to quantify given the measurement difficulties. Similarly, the correlation derived for the piston crown oil gallery heat transfer coefficient, has no dependency on oil jet flow rate. The effect of flow rate on the oil jets' effectiveness would be worth further investigation given the jets' influence on oil warm-up rates but also on piston temperatures.

The revised bearing model presented in Chapter 5 is representative of thermal conditions in and around the main journal. While this proved suitable to model film temperatures during warm-up and in steady state, additional lumped mass nodes could provide further detail on the more intricate heat flow patterns within a real crankshaft. Of particular interest would be a more realistic representation of heat redistribution between the crankcase oil mist and crankshaft.

8.3. Conclusions

The main conclusions of the investigations presented in this thesis are:

Engine Thermal Behaviour and Modelling

- External heat input to the oil is a relatively inefficient way to raise oil temperature at the rubbing surfaces. The strong thermal coupling between the oil and engine structure, in particular in the crankcase and crankshaft bearings, results in a substantial redistribution of any 'additional' heat input to the oil. The oil's apparent thermal capacity is much greater than that attributed solely to its actual mass.

- While the temperature in the sump reflects the general thermal state of the oil circuit, friction is better characterized by film temperatures at the rubbing surfaces which are in turn closely coupled to the local metal temperatures.

Piston Heat Transfer

- Without piston cooling jets, conduction through the piston rings accounts for at least 80 % of the total heat outflow. The remainder is transferred to the crankcase oil mist. With piston cooling jets, the heat flow split between conduction through the rings and heat transfer to the oil mist and oil jets is roughly 50:50.

- The piston cooling jets always produce an increase in bulk oil warm-up rate; with the piston cooling jets on, oil temperatures are typically 6-10 ºC higher during warm-up at a given time and engine rubbing friction is ~5 % lower.

- With the engine in a fully-warm state, switching the PCJs does not alter the total heat rejection to coolant. With the PCJs on, a lower heat rejection across the engine block is offset by increased heat transfer from the oil to the coolant across the FCA. Predicted trends are consistent with experimental data.

Crankshaft main bearings

- The benefit of raising the oil temperature in the main gallery is reduced substantially by the thermal coupling of the oil film to the bearing surfaces. In response to a step rise in oil temperature of ~15 °C at the feed, the film temperature rise was only 5 °C.

- Simulations show that thermally isolating the oil film from the crankshaft journal and bearing shells would provide between 50-100 % greater benefit in friction work dissipation than heating the feed temperature. A combined thermal isolation and oil heating results in the maximum friction work saving of 18 % relative to the baseline case.

- Insulating the bearing oil film from the crankshaft journal and bearing shells was the most effective strategy for promoting friction reduction in the bearings during warm-up. Insulating one or the other gave approximately half the benefit of insulating both. Reducing the thermal capacity of the journal by 70 % in combination with insulating the bearing shells was less effective.

- The predicted saving in bearing friction work from reducing the oil flow rate during warm-up was shown to be approximately half the benefit attainable from thermal isolation of the film. Reducing feed pressure is less effective still, given that hydrodynamic flow dominates early on in the warm-up and this is independent of the feed pressure.

Optimising engine warm-up

- Streaming the FCA with coolant from the time of engine start up promotes higher oil temperatures during warm-up. Over a cold start NEDC, the fuel economy improvement associated with streaming coolant through the FCA is ~1.4 %. It is always beneficial to stream the FCA with coolant unless a thermal store is used to raise oil temperature above that of the coolant.

- Coupling the EGR cooler to the oil circuit rather than the coolant, improved fuel economy by 0.6% when the FCA was streamed with coolant and by 1.7 % when the FCA was disconnected from the coolant. However, the absolute

fuel economy improvement in the latter case was ~0.3 % less than in the former.

- The benefits of isolating the oil from the engine structure extend beyond the rubbing surfaces. The high thermal capacity of structural elements in the crankcase holds the bulk oil temperature down during warm-up. The main heat losses are from the crankcase oil mist and oil flowing in the main gallery.

- Positioning the oil gallery close to the cooling jacket is beneficial and is one way of eliminating and reversing heat losses from oil flowing in the main gallery. In this case heat transfer from the crankcase oil mist becomes the dominant heat outflow mechanism from the oil and inhibiting it provides fuel economy improvements in the region of 1 %.

- Heat losses to ambient only become significant late in the drive cycle when the engine has approached fully warm operation. Inhibiting heat losses from the sump is most effective in terms of a fuel saving to insulated area ratio. The fuel saving from eliminating sump heat losses was still relatively small at 0.28 %. Ambient heat losses become more important if oil temperature is raised earlier in the warm-up through various means or if the other heat transfer routes out of the oil are suppressed.

- Over a cold start NEDC, a 0.45 % reduction in fuel consumption was predicted for every 10 % reduction in engine mass. With the FCA streamed with coolant, reductions in mass from the upper and lower regions of the engine structure showed similar benefits in fuel consumption. With no coolant streamed through the FCA, reducing mass from the lower regions of the engine structure is more effective at promoting higher oil temperatures.

- Given an available source of thermal energy simulations indicate that a higher power input over a shorter period is most beneficial. Simulations suggest that the fuel consumption saving achieved from heating the oil using a thermal store can be very close to that achieved by starting the engine fully warm if heat losses to the lower engine structure (sump, crankcase, main gallery) can be eliminated. This equates to ~6% improvement in fuel economy.

References

1. http://www.innas.com/HD_fuel_NEDC.html (accessed September 2012).
2. **Heywood, J.B.** Internal Combustion Engine Fundamentals. McGraw-Hill, 1988. ISBN 0-07-100499-8.
3. **Andrews, G.E., Harris, J.R. and Ounzain, A.** SI Engine Warm-Up: Water and Lubricating Oil Temperature Influences. SAE 892103, 1989.
4. **Shayler, Paul J., Baylis, Warren S. and Murphy, M.** Main Bearing Friction and Thermal Interaction During the Early Seconds of Cold Engine Operation. ASME Journal of Engineering for Gas Turbines and Power, Vol. 127 pp.197-205, 2005.
5. **Farrant, P.E., Robertson, A., Hartland, J. and Joyce, S.** The Application of Thermal Modelling to an Engine and Transmission to Improve Fuel Consumption Following a Cold Start. SAE 2005-01-2038, 2005.
6. **Andrews, G. E, Ounzain, A; Li, H, Bell, MC, Tate, JE and Ropkins, K.** The Use of a Water/Lube Oil Heat Exchanger and Enhanced Cooling Water Heating to Increase Water and Lube Oil Heating Rates in Passenger Cars for Reduced Fuel Consumption and CO2 Emissions During Cold Start. SAE 2007-01-2067, 2007.
7. **Revereault, P., Rouaud, C. and Marchi, A.** Fuel Economy and Cabin Heating Improvements Thanks to Thermal Management Solutions Installed in a Diesel Hybrid Electric Vehicle. SAE 2010-01-0800, 2010.
8. **Andre, M.** In Actual Use Car Testing: 70000 Kilometres and 10000 Trips by 55 French Cars under Real Conditions. SAE 910039, 1991.
9. **Shayler, P.J., Christian, S.J. and Ma, T.** A Model for the Investigation of Temperature, Heat Flow and Friction Characteristics During Engine Warm-up. SAE 931153, 1993.
10. **Burke, R.D., Brace, C.J., Lewis, A., Cox, A.and Pegg, I.** Analysis of energy flows in engine coolant, structure and lubricant during warm-up. IMechE/ SAE Int Conf VTMS 10, 2011.
11. **Zammit, J.P., Shayler, P.J. and Pegg, I.** Thermal Coupling and Energy Flows between Coolant, Engine Structure and Lubricating Oil during Engine Warm Up. IMechE/ SAE Int Conf VTMS 10, C1305/053, 2011.
12. **Zammit, J., Shayler, P., Gardiner, R. and Pegg, I.** Investigating the Potential to Reduce Crankshaft Main Bearing Friction During Engine Warm-up by Raising Oil Feed Temperature. SAE Int. J. Engines 5, SAE 2012-01-1216, 2012.
13. **UnitedNations.** Kyoto Protocol to the united nations framework convention on climate change. s.l. : United Nations, 1998.
14. http://ec.europa.eu/clima/policies/transport/vehicles/cars/index_en.htm (accessed September 2012).
15. **Nieuwenhuis, P.** Car CO2 reduction feasibility assessment; is 130g/ km possible? s.l. : Centre for Automotive Industry Research & Cardiff University, 2007.
16. **Zervas, E. and Lazarou, C.** CO2 benefit from the increasing percentage of diesel passenger cars in Sweden. International Journal of Energy Research, Vol. 31, pp192-203, 2007.
17. **Sullivan, J.L., Baker, R.E., Boyer, B.A., Hammerle, R.H., Kennedy, T.E., Muniz, L. and Wallington, T.J.** CO2 Emission Benefit of Diesel (versus Gasoline) Powered Vehicles. Environmental Science & Technology, Vol. 38,pp. 3217-3223, 2004.
18. **Bishop, J., Nedungadi, A., Ostrowski, G., Surampudi, B., Armiroli, P. and Taspinar, E.** An Engine Start/ Stop System for Improved Fuel Economy. SAE 2007-01-1777, 2007.

19. **Ventker, K., Maassen, F., Lang, O. and Weinowski, R.** Short Term Measures of the Reduction of Fuel Consumption of Spark Ignition Engines- Objectives in the Areas of Thermodynamics, Engine Mechanics, and Calibration. International Conference INSA de Strasbourg, France, 2007.
20. **Law, T.** The Effects of Lubrication System Modifications on Engine Friction and Thermal Behaviour. PhD Thesis, University of Nottingham, 2007.
21. **Tomaselli, L. and Alexandre, A.** Fuel and pollution decreasing of thermal motor cars by cooling system optimisation. Entropie no 41, 2002.
22. **Bassett, M.** Investigation of Technologies to Improve Drive-cycle Fuel Economy. Retrieved from Lotus Engineering Software: http://www.lesoft.co.uk/files/Hyb_Veh_2005.pdf.
23. **Hoag, K.L.** Vehicular Engine Design - Powertrain. s.l. : Springer Wien New York, 2006. ISSN 1613-6349.
24. **Seider, G., Bet, F., Heid, T., Hess, U., Klein, T. and Sauer, J.** A Numerical Simulation Strategy for Complex Automotive Cooling Systems. SAE 2001-01-1722, 2001.
25. **Noda, Y., Mamiya, N., Sometani, S., Hosoya, M. and Koide, K.** Development of an Engine Oil Temperature Prediction Method Using 3D Model Simulation. SAE 2005-01-1881, 2005.
26. **Burke, J. and Haws, J.** Vehicle Thermal Systems Modelling using FLOWMASTER 2. SAE 2001-01-1696, 2001.
27. **Janowski, P., Shayler, P.J., Robinson, S. and Goodman, M.** The effectiveness of heating parts of the powertrain to improve vehicle fuel economy during warm-up. VTMS 10, 2011.
28. **Dris, A., Farid, M., Shayler, P., Caine, J., Helle-Lorentzen, R. and Rose, D.** Engine warm-up modelling for real time simulation. IMechE Paper C640/007/2007,Proc. of SAE/IMechE Int. Conf VTMS8, Nottingham, May 2007.
29. **Shayler, P.J., Chick, J.P. and Ma, T.** Correlation of Engine Heat Transfer for Heat Rejection and Warm-Up Modelling. SAE 971851, 1997.
30. **Christian, S.J.** A Spark Ignition Engine Model for Heat FLow and Friction Characterisitics. PhD Thesis, University of Nottingham, 1992.
31. **Yuen, H.C.R.** An Investigation of Thermal Conditions in Spark Ignition Engines. PhD Thesis, University of Nottingham, 1995.
32. **Chick, J.P.** The Modelling of Engine Thermal Systems. PhD Thesis, University of Nottingham, 1998.
33. **W.S.Baylis.** An Investigation of Heat Transfer and Friction in Turbocharged Diesel Engines. PhD Thesis, University of Nottingham, 1999.
34. **Morgan, T. J.** The Modelling of Internal Combustion Engine Thermal Systems and Behaviour. PhD Thesis, University of Nottingham, 2003.
35. **Taylor, C.F.** The Internal Combustion Engine in Theory and Practice. Volume 2: Combustion, Fuels, Materials, Design. s.l. : MIT Press, 1985.
36. **Millington, B.W. and Hartles, E.R.** Frictional Losses in Diesel Engines. SAE 680590, 1968.
37. **Taylor, R.I.** Tribology & energy efficiency. London : Presented as the Donald Julius Groen Prize Lecture, 3rd December, 2008.
38. **Skjoedt, M., Butts, R., Assanis, D. N. and Bohac, S. V.** Effects of oil properties on spark-ignition gasoline engine friction. Tribology International Vol. 41, pp. 556-563, 2008.
39. **Leong, D.K.** Investigations of Friction Losses in Automotive Internal Combustion Engines. PhD Thesis, University of Nottingham, 2004.

40. **Burrows, J. A.** An Investigation into the Cold Start Performance of Automotive Diesel Engines. PhD Thesis, University of Nottingham, 1998.
41. **Monaghan, M.L.** Engine Friction - A change in emphasis: A new approach which may result in significant fuel consumption gains. Industrial Lubrication and Tribology, Vol. 40 Iss: 2, pp. 4-11, 1988.
42. **Goenka, P.K., Paranjpe, R.S. and Y.R.** FLARE: An Integrated Software Package for Friction and Lubrication Analysis of Automotive Engines-Part 1: Overview and Applications. SAE 920487, 1992.
43. **Rezeka, S.F. and Henein, N.A.** A New Approach to Evaluate Instantaneous Friction and Its Components in Internal Combustion Engines. SAE 960357, 1996.
44. **Kouremenos, D.A., et al.** Development of a Detailed Friction Model to Predict Mechanical Losses at Elevated Maximum Combustion Pressures. SAE 2001-01-0333, 2001.
45. **Thring, R.H.** Engine Friction Modelling. SAE 920482, 1992.
46. **Miura, A. and Shiraishi, K.** Investigation of Main Bearing Friction in a Diesel Engine. SAE 890140, 1989.
47. **Luff, D., Cheng, K. Y., Leong, D., Law, T. and Shayler, P.J.** Diesel Engine Cold Start - Progress Report 47. 2003. ME EG: DCS47/03.
48. **Owen, N. J., Gilbert, I.P. and Jackson, N. S.** Firing Friction Breakdown of a Ford 1.8L IDI Diesel Engine. Ricardo, 1989.
49. **Livanos, G. and Kyrtatos, N.P.** A Model of the Friction Losses in Diesel Engines. SAE 2006-01-0888, 2006.
50. **Hirani, H., Athre, K. and Biswas, S.** Dynamically Loaded Finite Length Journal Bearings: Analytical Method of Solution. ASME Journal of Tribology, vol. 121 (4), pp. 844-852, 1999.
51. **Zweiri, Y.H., Whidborne, J.F. and Seneviratne, L.D.** Instantaneous frictin components model for transient engine operation. Proc. Inst. Mech. Engrs., Journal of Automobile Engineering, Vol. 214, 1999.
52. **Ma, Q., Rajagopalan, S.S.V., Yurkovich, S. and Guezenec, Y. G.** A High Fidelity Starter Model for Engine Start Simulations. American Control Conference, pp.4423-4427, Portland 2005.
53. **Ciulli, E.** A Review of Internal Combustion Engine Losses - Part 1: Specific Studies on the Motion of Pistons, Valves and Bearings. Proc. Instn. Mech. Engrs., Part D, Journal of Automobile Engineering. No. 206, pp223-236, 1992.
54. **Winterborne, D.E. and Tennant, D.W.H.** The Variation of Friction and Combustion Rates During Diesel Engine Transients. SAE 810339, 1981.
55. **Bishop, I.N.** Effect of Design Variables on Friction and Economy. SAE Paper 812A, 1964.
56. **Patton, Kenneth J., Nitschke, Ronald G. and Heywood, John B.** Development and Evaluation of a Friction Model for Spark – Ignition Engines. SAE 890836, 1989.
57. **Sandoval, D. and Heywood, J.B.** An Improved Friction Model for Spark-Ignition Engines. SAE 2003-01-0725, 2003.
58. **Shayler, P.J., Leong, D.K. and Murphy, M.** Friction Teardown Data from Motored Engine Tests in Light Duty Automotive Diesel Engines at Low Temperatures and Speeds. ASME Fall Technical Conference, Erie, 2003.
59. **Jarrier, L., Champoussin, J.C., Yu, R. and Gentile, D.** Warm-Up of a D.I. Diesel Engine: Experiment and Modelling. SAE 2000-01-0299, 2000.
60. **Barnes-Moss, H.W.** A Designer's Viewpoint. IMechE, Conf. Publ. 19, C343/73, 1973.

61. **Finol, C.A. and Robinson, K.** Thermal Profile of a Modern Passenger Car Diesel Engine. SAE 2006-01-3409, 2006.
62. **Torregrosa, A., Olmeda, P., Degraeuwe, B.,and Reyes, M.** A concise wall temperature model for DI Diesel engines. Applied Thermal Engineering 26: 1320-1327, 2006.
63. **Holman, J.P.** Heat Transfer. New York : McGraw-Hill, 1990. ISBN 978-007-126769-4.
64. **Veshagh, A. and Chen, C.** A Computer Model for Thermofluid Analysis of Engine Warm-up Process. SAE 931157, 1993.
65. **Torregrosa, A.J., Broatch, A., Olmeda, P. and Romero, C.** Assessment of the Influence of Different Cooling System Configurations on Engine Warm-up, Emissions and Fuel Consumption. International Journal of Automotive Technology, Vol. 9, No. 4, pp. 447−458, 2008.
66. **Woschni, G.** A universally applicable equation for the instantaneous heat transfer coefficient in the internal combustion engine. SAE 670931, 1967.
67. **Zoz, S., Strepek, S., Wiseman, M.and Qian, C.** Engine Lubrication System Model for Sump Oil Temperature Prediction. SAE 2001-01-1073, 2001.
68. **Trapy, J.D. and Damiral, P.** An Investigation of Lubricating System Warm-up for the Improvement of Cold Start Efficiency and Emissions of S.I. Automotive Engines. SAE 902089, 1992.
69. **Kaplan, J.A. and Heywood, J.B.** Modelling the Spark Ignition Engine Warm-Up Process to Predict Component Temperatures and Hydrocarbon Emissions. SAE 910302, 1991.
70. **Law, T., Shayler, P.J. and Pegg, I.** Investigations of sump design to improve thermal management of oi temperature during warm-up. IMechE Paper 640/044/2007,Proc. SAE/IMechE Int. Conf VTMS8, Nottingham, May 2007.
71. **Kajiwara, H., Fujioka, Y. and Negishi, H.** Prediction of Temperatures on Pistons with Cooling Gallery in Diesel Engines using CFD Tool. SAE 2003-02-0986, 2003.
72. **Varghese, M.B., Goyal, S.K. and Agarwal, A.K.** Numerical and Experimental Investigation of Oil Jet Cooled Piston. SAE 2005-01-1382, 2005.
73. **Pan, J., Nigro, R. and Matsuo, E.** 3-D Modeling of Heat Transfer in Diesel Engine Piston Cooling Galleries. SAE 2005-01-1644, 2005.
74. **Metzger, D.E., Cummings, K.N. and Ruby, W.A.** Effects of Prandtl Number on Heat Transfer Characteristics of Impinging Liquid Jets. Proc. of the 5th International Heat Transfer Conference, Vol.2, pp.20-24,1974.
75. **Stevens, J. and Webb, B.W.** Local Heat Transfer Coefficient Under an Axi-Symmetric, Single Phase, Liquid Jet. ASME Journal of Heat Transfer Vol.113, pp.71-78, 1991.
76. **Bush, J. E. and London, A.L.** Design Data for 'Cocktail Shaker' Cooled Pistons and Valves. SAE 650727, 1965.
77. **Kuze, Y., Kobayashi, H., Ichinose, H. and Otsuka, T.** Development of New Generation Hybrid System (THS II) - Development of Toyota Coolant Heat Storage System. SAE 2004-01-0643, 2004.
78. **Schatz, O.** Cold Start Improvement by use of Latent Heat Stores. SAE 921605, 1992.
79. http://www.dieselnet.com/standards/cycles/ftp75.php (accessed September 2012).
80. **Diehl, P., Haubner, F., Klopstein, S. and Koch, F.** Exhaust Heat Recovery System for Modern Cars. SAE 2001-01-1020, 2001.

81. **Vetrovec, J.** Engine Cooling System with a Heat Load Averaging Capability. SAE 2008-01-1168, 2008.
82. **Hughes, C.A.V. and Wiseman, M.W.** Feasibility of Intelligent Control Strategies to Reduce Cooling System Size. SAE 2001-01-1759, 2001.
83. http://www.greencarcongress.com/2005/12/bmw_developing_.html (accessed September 2012).
84. http://www.greencarcongress.com/2008/02/honda-researchi.html (accessed September 2012).
85. **Crane, D., Jackson, G. and Holloway, D.** Towards Optimization of Automotive Waste Heat Recovery Using Thermoelectrics. SAE 2001-01-1021, 2001.
86. **Pang, H.H. and Brace, C.J.** Review of engine cooling technologies for modern engines. Proc. Inst. Mech. Engrs., Part D-Journal of Automobile Engineering, Vol 218, pp.1209-1215, Nov 2004.
87. **Finlay, I.C., Tugwell, W., Biddulph, T.W. and Marshall, R. A.** The influence of coolant temperature on the performance of a four cylinder 1100cc engine employing a dual circuit cooling. SAE 880263, 1988.
88. **Kobayashi, H., Yoshimura, K. and Hirayama, T.** A Study on Dual Circuit Cooling for Higher Compression Ratio. SAE 841294, 1984.
89. **Robinson, K., Campbell, N.A.F., J.G.Hawley and D.G.Tilley.** A Review of Precision Engine Cooling. SAE 1999-01-0578.
90. **Clough, M. J.** Precision cooling of a four valve per cylinder engine. SAE 931123, 1993.
91. **Brace, C.J., Slipper-Burnham, H., Wijetunge, R.S., Vaughan, N. D., Wright, K. and Blight, D.** Integrated Cooling Systems for Passenger Vehicles. SAE 2001-01-1248, 2001.
92. **Taylor, C. F. and Toong, T.Y.** Heat Transfer in intercal-combustion engines. ASME paper 57-HT-17, 1957.
93. **Bohao, S., Baker, D.M. and Assanis, D.N.** A Global Model for Steady State and Transient SI Engine Heat Transfer Studies. SAE 960073, 1996.
94. **Annand, W.J.D.** Heat Transfer in the cylinders of reciprocating internal combustion engines. Proc. Instn Mech. Engrs, 1963, 177(36), 973-990.
95. **LeFuevre, T., Myers, P.S. and Uyehara, O.A.** Experimental instantaneous heat fluxes in a diesel engine and their correlation. SAE 690464, 1969.
96. **Imabeppu, S., et al.** Development of a Method for Predicting Heat Rejection to the Engine Coolant. SAE 931114, 1993.
97. **Stachowiak, G.W. and Batchelor, A.W.** Engineering Tribology. Amsterdam : Elsevier, 1993. ISBN 0-7506-7304-4.
98. **Cameron, A.** Basic Lubrication Theory. Chicester, UK : Ellis Horwood Limited, 1981. ISBN: 085312177x.
99. **Taylor, R.I., et al.** The Influence of Lubricant Rheology on Friction in the Piston Ring-Pack. SAE 941981, 1994.
100. **Taylor, C.F.** Internal Combustion Engines in Theory and Practice, Volume 1: Thermodynamics, Fluid Flow, Performance, Second Edition. s.l. : MIT Press, 1996. ISBN 0-262-70026-3.
101. **I.Pegg.** Personal Communication, Ford Motor Co. 2007.
102. **Bancroft, T.G., Sapsford, S.M. and Butler, D.J.** Underhood Airflow Prediction Using VECTIS Coupled to a 1-D System Model. In Proceedings of 5th Ricardo Software International Users Conference, Shoreham-by-Sea, UK, 2000.
103. **K.T.Lan and K.Srinivasan.** Influences of Free Stream Conditions on Vehicle Thermal Management - An Analytical Study. SAE 2009-01-1152, 2009.

104. **Burke, R.** Personal Communication. University of Bath, 2011.
105. http://www.engineeringtoolbox.com/thermal-conductivity-d_429.html (accessed September 2012).
106. **Collier, J.G. and Thome, J.R.** Convective Boiling and Condensation, 3rd Edition. Oxford Engineering Science Series, 1996, ISBN-0-19-8562829.
107. **Chen, J.C.** Correlation for Boiling Heat Transfer to Saturated Fluids in Convective Flow. Ind. Engng Chem. Proc. Des. Dev. 5, 322-329, 1966.
108. **Hawley, J.G., Wallace, F.J., Cox, A., Horrocks, R.W. and Bird, G.L.** Reduction of Steady State NOx Levels from an Automotive Diesel Engine Using Optimised VGT/ EGR Schedules. SAE 1999-01-0835, 1999.
109. **Jun, J.H., et al.** Comparison of NOx Level and BSFC for HPL EGR and LPL EGR System of Heavy-Duty Diesel Engine. SAE 2007-01-3451, 2007.
110. **Ladommatos, N., Abdelhaim, S.M., Zhao, H. and Z.Hu.** The Effects of Carbon Dioxide in Exhaust Gas Recirculation on Diesel Engine Emissions. Proc. of IMechE, Part D, Journal of Automobile Engineering, Vol. 212, pp 25-42, 1998.
111. **W.Wu and M.Ross.** Modelling of Direct Injection Diesel Engine Fuel Consumption. SAE 971142, 1997.
112. **Brace, C.J., Hawley, G., Akehurst, S., Piddock, M. and I.Pegg.** Cooling system improvements - assessing the effects on emissions and fuel economy. Proceedings of the Institution of Mechanical Engineers, Part D: Journal of Automobile Engineering, vol. 222, pp. 579-591, 2008.
113. **Luff, D.C., Law, T. and Shayler, P.J.** The Effect of Piston Cooling Jets on Diesel Engine Piston Temperatures, Emissions and Fuel Consumtpion. SAE 2012-01-1212, 2012.
114. **Leites, J. M. M.** Heat Flow in an Articulated Piston. SAE 891896, 1989.
115. **Furuhama, S. and Suzuki, H.** Temperature Distribution of Piston Rings and Piston in High Speed Diesel Engine. Bulletin of JSME, Vol. 22, No. 174, Pg. 1788-1795, 1979.
116. **Li, C-H.** Piston Thermal Deformation and Friction Considerations. SAE 820086, 1982.
117. **Sitkei, G.** Heat Transfer and Thermal Loading in Internal Combustion Engines. Akademiai Kaido:Budapest, 1974, ISBN 9630500973.
118. **Parker, D.A., Ettles, C.M. McC and J.W.Richmond.** The AEconoguide Low Friction Feature - Analysis and Further Running Experience. IMechE C70/85 pp. 51-65, 1985.
119. **Mierbach, A. and Duck, G. E.** Heat Flow Through Piston Rings and Its Influence on Shape. SAE 831283, 1983.
120. **Manganiello, E.J.** Piston Temperatures in an Air-Cooled Engine for Various Operating Conditions. National Advisory Committee for Aeronautics, Report 698, 1942.
121. **Dembroski, T. J.** Piston Heat Transfer in an Air Cooled Engine. University of Wisconsin-Madison, 2002.
122. **Ogawa, T., Suzuki, T., Ezaki, S., Kikuchi, T.Suzuki. T., Harada, K. and Kataoka, T.** Reduction of Friction Losses in Crankcase at High Engine Speeds. SAE 2006-01-3350, 2006.
123. **Shimura, T., Kikuchi, T., Hikita, Y. and Yamazaki, M.** Reducing the Amount of Lubricating Oil by Using a New Crankshaft Bearing with Eccentric Oil Groove. SAE 2004-01-3048, 2004.

124. **Suzuki, Y., Shimano, K., Enomoto, Y., Emi, M. and Yamada, Y.** Direct heat loss to combustion chamber walls in a direct-injection diesel engine: evaluation of direct heat loss to piston and cylinder head. IMechE Int. J. Eng. Res. Vol. 6, 2005.
125. **Jarrier, L., Gyan, Ph. and Champoussin, J.C.** Thermo-Hydraulic Oil Loop Modeling for I.C.E. Warm-Up Investigation. SAE 2002-01-2197, 2002.
126. **Dowson, D. and March, C.N.** A Thermohydrodynamic Analysis of Journal Bearings. Proc. I. Mech. E., Vol. 181, Part 30, 1966–1967, pp. 117–126.
127. **Paranjpe, R.S.** A Study of Dynamically Loaded Engine Bearings Using a Transient Thermohydrodynamic Analysis. Tribology Transactions, Vol. 39, pp. 636-644, 1996.
128. **Dowson, D., Hudson, J.D., Hunter, B. and March, C. N.** An Experimental Investigation of the Thermal Equilibrium of Steadily Loaded Bearings. Proc. IMechE Vol. 181 Pt. 3b, pp. 70-80, 1967.
129. **Conway-Jones, J.M. and Tarver, N.** Refinement of Engine Bearing Design Techniques. SAE 932901, 1993.
130. **Wilcock, D.F. and Booser, E.R.** Bearing Design and Application,. s.l. : McGraw-Hill Book Co., 1957, ISBN: 9780070701977.
131. **Han, T. and Paranjpe, R.S.** A Finite Volume Analysis of the Thermo-hydrodynamic Performance of Finite Journal Bearings. Journal of Tribology, Vol. 112, 1990.
132. **Pinkus, O. and Wilcock, D.J.** Thermal Effects in Fluid Film Bearings. Proc. of the 6th Leed-Lyon Symposium on Tribology, IMechE, London, pp3-23, 1980.
133. **Marint, F. A. and Lee, C. S.** Feed-Pressure Flow in Plain Journal Bearings. Transactions of the ASLE, Vol 26, 3, pp381-392, 1983.
134. **Shimada, A., Harigaya, Y. and Suzuki, M.** An Analysis of Oil Film Temperature, Oil Film Thickness and Heat Transfer on a Piston Ring of Internal Combustion Engine: The Effect of Local Lubricant Viscosity. SAE 2004-32-0024, 2004.
135. **Mason, B.R.** Thermal Analysis of S.I. Engines with High Reinforced Plastic Content. PhD Thesis, University of Nottingham, 1990.
136. **Vijayaraghavan, D., Jr, T.G. Keith and Brewe, D.E.** Effect of Lubricant Supply Starvation on the Thermohydrodynamic Performance of a Journal Bearing. Tribology Transactions Vol.39, pp. 645-653, 1996.
137. **Artiles, A. and Heshmat, H.** Analysis of Starved Journal Bearings Including Temperature and Cavitation Effects. Journal of Tribology (ASME) Vol.107, 1985.
138. **Heshmat, h. and Pinkus, O.** Performance of Starved Journal Bearings With Oil Ring Lubrication. Journal of Tribology, Vol. 107, pp. 23-31, 1985.
139. **Shibano, M., Tsuchida, T. and Hayama, K.** Cast hollow crankshaft and manufacturing method of the same. 2007/0193405 A1 United States, 23 August 2007.
140. **Pathak, V., et al.** Hollow Crankshaft for IC Engines. WO/2011/121611 6 October 2011.
141. **Cevik, M. Cagri, Rebbert, M. and Maassen, F.** Weight and Friction Optimized Cranktrain Design Supported by Coupled CAE Tools. SAE 2009-01-1452, 2009.
142. **Druschitz, Alan P., Warrick, Robert J., Grimley, Peter R., Towalski, Craig R., Killion, David L. and Marlow, Richard.** Influence of Crankshaft Material and Design on the NVH Characteristic of a Modern, Aluminium Block, V-6 Engine. SAE 1999-01-1225, 1999.
143. **Druschitz, Alan P., Fitzgerald, David C. and Hoegfeldt, Inge.** Lightweight Crankshafts. SAE 2006-01-0016, 2006.

144. **Burke, R.D., Brace, C.J., Hawley, J.G. and Pegg, I.** Systems approach to the improvement of engine warm-up behaviour. IMechE, J Auto Eng, Poc IMechE Vol 224, Pt D, 2011.
145. **Koch, F., Haubner, G.H. and Orlowsky, K.** Lubrications and Ventilation System of Modern Engines - Measurements, Calculations and Analysis. SAE 2002-01-1315, 2002.
146. **Hountalas, D.T., Katsanos, C.O. and Lamaris, V.T.** Recovering Energy from the Diesel Engine Exhaust Using Mechanical and Electrical Turbocompounding. SAE 2007-01-1563, 2007.
147. **Patterson, A.T.C., Tett, R.J. and McGuire, J.** Exhaust Heat Recovery using Electro-Turbogenerators. SAE 2009-01-1604, 2009.
148. **Ringler, J., Seifert, M. and Guyotot, V. and Hubner, W.** Rankine Cycle for Waste Heat Recovery of IC Engines. SAE 2009-01-0174, 2009.
149. **Kay, D., Davies, M., Caine, J., McCabe, R. and Theis, J.** Application of a gas-to-coolant exhaust heat exchanger: fuel economy and emissions benefits. VTMS 8 -Vehicle Thermal Management Systems Conference and Exhibition, Nottingham, United Kingdom, 2007, pp. 379-388.
150. **G.E.Andrews, Harris, J.R. and Ounzain, A.** The Influence of External Heat Losses on the Transient SFC and Emissions During Warm-up Period of an SI Engine. Engine Transient Performance, IMechE, 1990.
151. **Dawson, S.** Compacted Graphite Iron: New Opportunities for Engine Design. SAE 952226, 1995.
152. **Schoffmann, W., Beste, F. and Marquard, R.** Lightweight Engine Design Strategies. SAE 2000-01-1546, 2000.
153. **Green, N.** Personal Communication. Jaguar Land Rover, 2011.
154. **Samhaber, C., Wimmer, A. and Loibner, E.** Modeling of Engine Warm-Up with Integration of Vehicle and Engine Cycle Simulation. SAE 2001-01-1697, 2001.
155. http://www.mazda.com/mazdaspirit/skyactiv/engine/skyactiv-d.html (accessed September 2012).
156. **Taylor, R.I. and Coy, R.C.** Improved Fuel Efficiency by Lubricant Design: A Review. Proc. Instn. Mech. Engrs., Vol 214, Part J, 1999, pp: 1-15.

Appendices

A. Test Engine Specification

Engine Name	Ford ZSD-424 'Puma'
Type	In-line, 4-cylinder, 16V DOHC
Rated Power (kW/ rpm)	92/ 3800
Fuel Delivery	Rotary Pump, Mechanical Injector, Direct injection
Induction	Turbocharged, Intercooled with water cooled EGR
Lubrication	Oil-to-coolant cooler with Piston Cooling Jets
Capacity (cm^3)	2402
Bore (mm)	89.9
Stroke (mm)	94.6
Compression Ratio	19
Number of big-end bearings	4
Big-eng Bearing Length (mm)	53
Big-end Bearing Diameter (mm)	24.3
Number of main bearings	5
Main Bearing Length (mm)	22
Main Bearing Diameter (mm)	65
Valve Actuation	Roller finger follower, Hydraulic Lifter with chain drive
Number of Camshaft bearings	10
Intake Valve Diameter (mm)	29.8
Exhaust Valve Diameter (mm)	25.8

Table 28 Ford Puma 2.4l specification

B. Friction Model

Crankshaft Assembly	$C_{cb}\left(\frac{N^{0.6}D_b^3L_bn_b}{B^2Sn_c}\right)\left(\frac{\mu}{\mu_{ref}}\right)^n + C_{cs}\left(\frac{D_b}{B^2Sn_c}\right)$	
Piston Assembly	$\left(C_{pb}\left(\frac{N^{0.6}D_b^3L_bn_b}{B^2Sn_c}\right) + C_{ps}\left(\frac{V_p^{0.5}}{B}\right) + C_{pr}\left(\frac{V_p^{0.5}}{B^2}\right)\right)\left(\frac{\mu}{\mu_{ref}}\right)^n$	
Valve Train	$\left(C_{vb}\left(\frac{N^{0.6}n_b}{B^2Sn_c}\right) + C_{v,oh}\left(\frac{L_v^{1.5}N^{0.5}n_v}{BSn_c}\right)\right)\left(\frac{\mu}{\mu_{ref}}\right)^n + C_{v,om}\left(2+\frac{10}{5+\mu N}\right)\frac{L_vn_v}{Sn_c} + C_{vs} + (\text{cam / follower})$	
	Cam/follower	$\text{fmep}_{\text{flatfollower}} = C_{v,ff}\left(2+\frac{10}{5+\mu N}\right)\frac{n_v}{Sn_c}$ $\text{fmep}_{\text{flatfollower}} = C_{v,rf}\left(\frac{Nn_v}{Sn_c}\right)$
Auxiliary Components	$\alpha + \left(\beta N + \gamma N^2\right)\left(\frac{\mu}{\mu_{ref}}\right)^n$	

Table 29 Summary of modified PNH engine friction formulation

Engine Component		**Index n**
Crankshaft Assembly		0.4
Piston Assembly		0.3
Valve Train		0.7
Auxiliary Components	Oil Pump	0.3
	Water Pump	0.7
	FIE	0.5

Table 30 Index n values for engine friction sub-assemblies

Crankshaft Assembly		Units	
Main Bearing	C_{cb}	kPa-min$^{0.6}$/rev$^{0.6}$-mm	0.0279
Oil Seal	C_{cs}	kPa-mm^2	93600
Piston Assembly			
Piston Skirt	C_{ps}	kPa-(mm-s)$^{0.5}$	13.3
Piston Ring	C_{pr}	kPa-mm$^{1.5}$-s$^{0.5}$	2559
Big-end bearing	C_{pb}	kPa-min$^{0.6}$/rev$^{0.6}$-mm	0.0202
Valve Train			
Camshaft bearing	C_{vb}	kPa-mm^3-min$^{0.6}$/rev$^{0.6}$	6720
Oil Seal	C_{vs}	kPa	1.2
Cam/ roller follower	$C_{v,rf}$	kPa-mm-min/rev	0.0151
Oscillating Hydrodynamic	$C_{v,oh}$	kPa-(mm-min/rev)$^{0.5}$	0.5
Oscillating Mixed	$C_{v,om}$	kPa	21.4
Auxiliary Components			
Oil Pump	α	kPa	2.55
	β	kPa-min/rev	0.0063
	γ	kPa-min^2/rev^2	-8.4x10^{-7}
Water Pump	α	kPa	0.13
	β	kPa-min/rev	0.002
	γ	kPa-min^2/rev^2	3x10^{-7}
FIE Pump	α	kPa	1.72
	β	kPa-min/rev	
	γ	kPa-min^2/rev^2	1.2x10^{-7}

Table 31 Modified PNH model coefficients